THE PHYSICAL REVIEW

A journal of experimental and theoretical physics established by E. L. Nichols in 1893

Published by the American Institute of Physics for the

AMERICAN PHYSICAL SOCIETY

Officers

President

F. W. Loomis
University of Illinois
Urbana, Illinois

Vice-President

I. I. Rabi
Columbia University
New York, New York

Secretary

K. K. Darrow
Bell Telephone Laboratories
Office:
Columbia University
New York 27, New York

Treasurer

G. B. Pegram
Columbia University
New York 27, New York

Local Secretary for the Pacific Coast

J. Kaplan
University of California at Los Angeles
Los Angeles, California

Managing Editor

John T. Tate
University of Minnesota
Minneapolis, Minnesota

BOARD OF EDITORS

Editor — John T. Tate

Assistant Editor — J. W. Buchta

Associate Editors

H. A. Bethe — S. A. Goudsmit — W. E. Lamb, Jr.
L. A. Ellenbogen — E. M. Purcell — R. G. Herb
W. H. Zachariasen — V. F. Weisskopf — J. Barnett

Manuscripts for publication should be submitted to John T. Tate, University of Minnesota, Minneapolis, Minnesota. The authors' institutions are requested to pay a publication charge of $4 per page which, if honored, entitles them to 100 free reprints. Instructions will be sent with galley proofs.

Proof and all correspondence concerning papers in the process of publication should be addressed to the Publication Manager, American Institute of Physics, 57 East 55 Street, New York 22, New York.

Subscription Price

United States and Canada $15.00
Elsewhere $16.50

Back Numbers[1]

Yearly back number rate when complete year is available: $20.00.
Single copies: $2.00 each, prior to July, 1929;
$1.00 each, July, 1929–December, 1941;
$2.00 each, January, 1942–December, 1946.
Current issues: $3.00 each.
General index, 1893–1920: $4.00.

Subscriptions and orders for back numbers should be addressed to Prince and Lemon Streets, Lancaster, Pennsylvania, or to the American Institute of Physics, 57 East 55 Street, New York 22, New York.

Changes of address in the case of members of the American Physical Society should be addressed to the Treasurer; in the case of other subscribers to the Subscription Manager, American Institute of Physics.

[1] Bethe Section 1 Physics Department, Cornell University, Ithaca, New York.

The Physical Review is published [illegible] at Prince and Lemon Streets, Lancaster, Pennsylvania.

Entered as second-class matter March 8, 1917, at the Post Office at Lancaster, Pennsylvania, under the Act of March 3, 1879.

Acceptance for mailing at special rate of postage provided for in paragraph 4, section 538, P. L. & R., authorized January 27, 1933.

THE
PHYSICAL REVIEW

A journal of experimental and theoretical physics established by E. L. Nichols in 1893

SECOND SERIES, VOL. 75, NO. 11 JUNE 1, 1949

On the Analysis of Nucleon-Nucleon Scattering Experiments

GEOFFREY F. CHEW AND MARVIN L. GOLDBERGER
Radiation Laboratory, University of California, Berkeley, California
(Received January 17, 1949)

A method of perturbation calculation, especially adapted to nucleon-nucleon scattering problems, is described. Any contribution to the energy of the system which is relatively small where the nuclear potential is large may be treated as the perturbation. Two principal examples are discussed. (1) Energy as the perturbation: An expansion of the phase shifts in powers of the energy is written down which extends earlier results of Schwinger, Blatt, and Jackson. (2) The Coulomb field as the perturbation in the proton-proton problem: Expansions are given which relate the nuclear phase shifts in a combined nuclear and Coulomb field to the corresponding phase shifts for a purely nuclear problem. Attention is confined to central forces throughout.

I. INTRODUCTION

THE study of nucleon-nucleon scattering has long been recognized as a source of direct information about the nature of nuclear forces. In the absence of a detailed theory of nuclear forces, the procedure commonly adopted in the past has been to describe the interaction phenomenologically by a short range potential of some particular shape. Calculations of scattering cross sections were carried out and comparisons made with experimental data, with varying degrees of success depending on the energy region in question.

In the low energy region (<10 Mev) it was found that no potential was obviously superior to any other.[1] The underlying reason for this lack of discrimination was recently explained quantitatively by Schwinger.[2] The reason is that the scattering characteristics of a given potential shape may be described, in this limited energy region, by only two parameters. These may be chosen as the scattering length at zero energy[3] and the so-called effective range.[4] Since there are only two parameters to be fitted, it is evident that any shape potential is suitable provided the proper choice of range and depth is made.

Schwinger's analysis, which has been confined thus far to central forces, is based on an expansion of the quantity, $k\cot\delta$, in powers of k^2. k is the wave number and δ is the S phase shift for neutron-proton scattering.

$$k\cot\delta = A_0 + A_1k^2 + A_2k^4 + \cdots. \qquad \text{(A)}$$

For *any* positive (or negative) definite short range potential, A_2 turns out to be so small that the third term cannot be noticed experimentally at low energies. This, of course, is the underlying reason for the well shape independence of low energy cross sections. It is not clear from Schwinger's procedure, however, why the quantity $k\cot\delta$ should be representable by a rapidly convergent power series in the energy. In fact, the appropriate quantity to expand in the case of proton-proton scattering is considerably more complicated. In this paper we derive a general expression for that quantity which in a particular problem can be expected to have a convergent power series representation. The actual determination of any number of the terms in the expansion can be carried out in a straightforward way, and the form of these terms is, in general, simpler in appearance than that given by Schwinger's variational method. The higher terms in the energy expansions are of physical interest because of the information they give about the shape of the nuclear potential, but we shall not discuss this aspect of the

[1] Breit, Condon, and Present, Phys. Rev. **50**, 825 (1936).
[2] Julian Schwinger, Phys. Rev. **72**, 742 A (1947); Hectographed Notes on Nuclear Physics, Harvard (1947).
[3] E. Fermi and L. Marshall, Phys. Rev. **71**, 66 (1947).
[4] John M. Blatt, Phys. Rev. **74**, 92 (1948).

problem. Blatt and Jackson[5] have made a detailed investigation of the coefficient A_2, using the variational principle. They discuss the physical implications in detail.

The expansion (A) will also be generalized to an arbitrary angular momentum. The possibility of making analogous expansions in parameters other than the energy is pointed out, and in particular the case of the Coulomb field as a perturbation is discussed in considerable detail. The usefulness of the various expansions will be discussed in Section V.

We shall confine ourselves, for simplicity, to central forces. The generalization to tensor forces has been made by R. S. Christian and will be published by him.

II. THE GENERAL METHOD

The problem to be solved is the determination of the asymptotic form of the regular solution of the following differential equation:

$$\{L+f\}u(x) = -\epsilon g(x)u(x), \tag{1}$$

where

$$L = (d^2/dx^2)+q(x), \tag{2}$$

f is a short range self-adjoint operator, ϵ is a parameter of smallness, $q(x)$ is an arbitrary function no more singular at the origin than $1/x^2$ and $g(x)$ another function no more singular than $1/x$.

Equation (1) is therefore a general form for the radial Schrödinger equation for an arbitrary angular momentum. The choice of $q(x)$, ϵ, and $g(x)$ will vary from problem to problem. The asymptotic form of $u(x)$ shall be called $X(x)$; i.e., $X(x)$ is an irregular solution of the equation

$$LX(x) = -\epsilon g(x)X(x). \tag{3}$$

Since an expansion in powers of ϵ is the object here, we define explicitly the limiting forms of $u(x)$ and $X(x)$ as ϵ approaches zero. Thus $v_R(x)$ is the regular solution of the equation

$$\{L+f\}v_R(x) = 0, \tag{4}$$

and $Y_I(x)$ is the asymptotic form of $v_R(x)$, being in turn an irregular solution of the equation

$$LY_I(x) = 0. \tag{5}$$

It is convenient also to define at this time an irregular solution of Eq. (4) and the regular solution of Eq. (5). These will be designated as $v_I(x)$ and $Y_R(x)$, respectively, and chosen so that

$$\left.\begin{aligned} W_x(v_I, v_R) &= 1 \\ W_x(Y_I, Y_R) &= 1 \end{aligned}\right\} \text{for all } x, \tag{6}$$

and so that asymptotically $v_I(x)$ approaches $-Y_R(x)$. The notation $W_x(f, g)$ means the Wronskian $[f(x)dg(x)/dx - g(x)df(x)/dx]$. These conditions can be achieved by a proper choice of the constant in the following representation of $v_I(x)$:

$$v_I(x) = v_R(x)\left\{-\int^x \frac{dx'}{v_R^2(x')} + \text{constant}\right\}. \tag{7}$$

We now derive the fundamental identity from which all subsequent results can be obtained. From Eqs. (1) and (4), one sees that

$$W_{x_0}(v_R, u) = W_{x_1}(v_R, u) + \epsilon\int_{x_0}^{x_1} g(x)v_R(x)u(x)dx. \tag{8}$$

Similarly from Eqs. (3) and (5)

$$W_{x_0}(Y_I, X) = W_{x_1}(Y_I, X) + \epsilon\int_{x_0}^{x_1} g(x)\,Y_I(x)X(x)dx. \tag{9}$$

The difference of these equations gives

$$W_{x_0}(Y_I, X) - W_{x_0}(v_R, u) = W_{x_1}(Y_I, X) - W_{x_1}(v_R, u) + \epsilon\int_{x_0}^{x_1} g(x)[Y_I(x)X(x) - v_R(x)u(x)]dx.$$

Now pass to the limit $x_1\to\infty$, $x_0\to 0$. We obtain

$$\lim_{x_0\to 0} W_{x_0}(Y_I, X) = \lim_{x_0\to 0}\epsilon\int_{x_0}^{\infty} g(x)[Y_I(x)X(x) - v_R(x)u(x)]dx, \tag{10}$$

since the Wronskian of the two regular functions $u(x)$ and $v_R(x)$ must vanish at the origin. Henceforth the limiting process, $x_0\to 0$, will be implied wherever x_0 is written.

Later examples will show that $W_{x_0}(Y_I, X)$ is a measure of the influence of the term $\epsilon g(x)$ on the scattering characteristics of the system. It is evident that $W_{x_0}(Y_I, X)$ can be represented by a rapidly convergent power series in ϵ whenever the functions, $u(x)$ and $X(x)$, can be so represented *in the region where the nuclear potential is important.* This, in turn, will be the case if $\epsilon g(x)$ is relatively small in the region where f is effective.

It should be noted that Eq. (10) is homogeneous, i.e., it is independent of the normalization of $v_R(x)$ and $u(x)$. This follows from the fact that if v_R or u is multiplied by a constant factor, the corresponding asymptotic form must be multiplied by the same factor. In subsequent examples the normalization will be chosen for convenience.

A procedure is now set up by which any number

[5] J. M. Blatt and J. D. Jackson, Phys. Rev. **75**, 341 (1949). We are indebted to Drs. Blatt and Jackson for an advance copy of their more detailed paper.

of terms in the required expansion can be obtained. The expansions of $u(x)$ and $X(x)$, if they exist, can be obtained by the iteration method which follows.[6]

The differential equation (1), together with its boundary conditions, may be replaced by the following integral equation,

$$u(x)=W_{x_1}(v_I,u)v_R(x)+\epsilon\Big\{v_I(x)\int_0^x g(x')v_R(x')u(x')dx'+v_R(x)\int_x^{x_1} g(x')v_I(x')u(x')dx'\Big\}. \quad (11)$$

If we choose x_1 sufficiently large to be outside the range of f, then

$$W_{x_1}(v_I,u)=W_{x_1}(-Y_R,X)=-W_0(Y_R,X)+\epsilon\int_0^{x_1} g(x')Y_R(x')X(x'). \quad (12)$$

Thus

$$u(x)=-W_0(Y_R,X)v_R(x)+\epsilon\Big\{v_I(x)\int_0^x g(x')v_R(x')u(x')dx'-v_R(x)\int_0^x g(x')v_I(x')u(x')dx'+v_R(x)\int_0^{x_1} g(x')[Y_R(x')X(x')+v_I(x')u(x')]dx'\Big\}.$$

It is obvious now that x_1 may just as well be taken as $+\infty$, and one can always adjust the relative normalizations so that

$$W_0(Y_R,X)=-1.$$

Assuming this to be done and defining

$$H_{12}(x)=Y_R(x)X(x)+v_I(x)u(x), \quad (13)$$

we arrive at the final integral equation

$$u(x)=v_R(x)+\epsilon\Big\{v_I(x)\int_0^x g(x')v_R(x')u(x')dx'-v_R(x)\int_0^x g(x')v_I(x')u(x')dx'+v_R(x)\int_0^\infty g(x')H_{12}(x')dx'\Big\}. \quad (14)$$

[6] Ince, *Ordinary Differential Equations* (Longmans Green and Company, London, 1926), Chapter XI.

The corresponding equation for $X(x)$ is

$$X(x)=Y_I(x)+W_{x_0}(Y_I,X)Y_R(x)+\epsilon\Big\{Y_I(x)\int_0^x g(x')Y_R(x')X(x')dx'-Y_R(x)\int_{x_0}^x g(x')Y_I(x')X(x')dx'\Big\}. \quad (15)$$

The three equations (10), (14), and (15) may now be used to find the desired expansion of $W_{x_0}(Y_I,X)$:

$$W_{x_0}(Y_I,X)=\epsilon\sum_{n=0}^{\infty}W_n\epsilon^n. \quad (16)$$

Designate the corresponding expansions of $u(x)$ and $X(x)$ as follows:

$$u(x)=\sum_{n=0}^{\infty}u_n(x)\epsilon^n, \quad (17)$$

$$X(x)=\sum_{n=0}^{\infty}X_n(x)\epsilon^n. \quad (18)$$

It is convenient to define

$$h_{11}(x)=Y_I^2(x)-v_R^2(x),$$
$$h_{22}(x)=Y_R^2(x)-v_I^2(x),$$
$$h_{12}(x)=Y_R(x)Y_I(x)+v_R(x)v_I(x).$$

The zeroth-order terms are written down at once.

$$u_0(x)=v_R(x),\quad X_0(x)=Y_I(x),\quad W_0=\int_{x_0}^\infty g(x)h_{11}(x)dx. \quad (19)$$

To obtain W_1, we must substitute in (10) $u_0+\epsilon u_1$ for u and $X_0+\epsilon X_1$ for X. X_1 is written down from (15),

$$X_1(x)=W_0Y_R(x)+Y_I(x)\int_0^x g(x')Y_R(x')Y_I(x')dx'-Y_R(x)\int_{x_0}^x g(x')Y_I^2(x')dx',$$

and u_1 from (14)

$$u_1(x)=v_I(x)\int_0^x g(x')v_R^2(x')dx'-v_R(x)\int_0^x v_I(x')v_R(x')\times dx'+v_R(x)\int_0^\infty g(x')h_{12}(x')dx'.$$

This leads to

$$W_1=2\int_{x_0}^{\infty}g(x)h_{11}(x)dx\int_0^x g(x')\,Y_R(x')\,Y_I(x')dx'$$
$$-2\int_{x_0}^{\infty}g(x)h_{12}(x)dx\int_0^x g(x')v_R{}^2(x')dx'. \quad (20)$$

This procedure may obviously be continued to give any number of terms which may be desired. We write down only one more, since the complication is rapidly increasing and there is as yet not sufficient experimental information to permit conclusions about the size of higher terms, in the energy expansion at least.

$$W_2=\int_{x_0}^{\infty}dxg(x)\Big\{2h_{11}(x)\Big[\int_0^x g(x')\,Y_I(x')\,Y_R(x')dx'\Big]^2+h_{22}(x)\Big[\int_0^x g(x')v_R{}^2(x')dx'\Big]^2$$
$$-2Y_R{}^2(x)\Big[\int_0^x g(x')v_R{}^2(x')dx'\Big]\Big[\int_x^{\infty}g(x'')h_{11}(x'')dx''\Big]+Y_R{}^2(x)\Big[\int_x^{\infty}g(x')h_{11}(x')dx'\Big]^2$$
$$-v_R{}^2(x)\Big[\int_x^{\infty}g(x')h_{12}(x')dx'\Big]^2-2h_{12}(x)\Big[\int_0^x g(x')\,Y_I(x')dx'\Big]\Big[\int_0^x g(x'')v_R{}^2(x'')dx''\Big]$$
$$-2v_I(x)v_R(x)\Big[\int_0^x g(x')v_R{}^2(x')dx'\Big]\Big[\int_x^{\infty}g(x'')h_{12}(x'')dx''\Big]$$
$$-2v_R{}^2(x)\Big[\int_0^x g(x')\,Y_I(x')\,Y_R(x')dx'\Big]\Big[\int_x^{\infty}g(x'')h_{12}(x'')dx''\Big]\Big\}. \quad (21)$$

Applications of the expansion (16) will now be given.

III. NEUTRON-PROTON SCATTERING

(a) Low energies

The chief motivation for this investigation was to find a systematic scheme for determining the coefficients in the expansion (*A*). The differential equation in question is that for an *S* state of the *n-p* system:

$$\Big\{\frac{d^2}{dx^2}+f\Big\}u^0(x)=-\kappa^2u^0(x), \quad (22)$$

where the unit of length has been taken to be the range of the nuclear potential, f, and κ is the relative wave number of the incident proton in these units. As usual, $u(x)$ is r times the radial wave function. We wish to treat the energy as a perturbation, so that in terms of our general notation, $q(x)=0$, $g(x)=1$, and $\epsilon=\kappa^2$.

Let us first determine the meaning of $W_{x_0}(Y_I, X)$. Write

$$X^0(x)=\kappa\cot\delta^0\frac{\sin\kappa x}{\kappa}+\cos\kappa x, \quad (23)$$

where δ^0 is the *S* phase shift. A possible way of writing $Y_I(x)$ is

$$Y^0{}_I(x)=1+\frac{x}{a^0}, \quad (24)$$

where a^0 is the scattering length. It follows immediately that

$$W_{x_0}(Y_I, X)=\kappa\cot\delta^0-\frac{1}{a^0}, \quad (25)$$

and we have from (16)

$$\kappa\cot\delta^0-\frac{1}{a^0}=\kappa^2W^0{}_0+\kappa^4W^0{}_1+\kappa^6W^0{}_2+\cdots, \quad (26)$$

where $W^0{}_0$, $W^0{}_1$, $W^0{}_2$, $\cdots$ are given by the expressions (19), (20), (21)$\cdots$ in which $v_R(x)$ is taken as the zero energy solution of Eq. (22), normalized to (24) at infinity, and $v_I(x)$ is the irregular solution, normalized to $-Y^0{}_R(x)=-x$.

In (26), the coefficient $W^0{}_0$ is half the effective range, as defined by Schwinger,[2,4] and the coefficient $W^0{}_1$ has been obtained by Blatt and Jackson[5] by a variational method. Their method, however, does not introduce explicitly the irregular zero energy solution, $v_I(x)$, and consequently leads to a more complicated expression. $W^0{}_2$ has not previously been given. From a practical point of view, the introduction of $v^0{}_I(x)$ is justified because it can always be constructed from its representation (7) in terms of $v^0{}_R(x)$, once the latter is known.

The expansion (26) is correct for both singlet and triplet *S* states of the *n-p* system. In the triplet case, however, it is desirable to relate the scattering length, a^0, to the binding energy of the deuteron. The relation may be obtained at once from the above formalism.

The radial equation for the bound state of the deuteron is

$$\left\{\frac{d^2}{dx^2}+f\right\}u_D(x)=\alpha^2 u_D(x). \tag{27}$$

($\alpha r_0=(MB/\hbar^2)^{\frac{1}{2}}$, with r_0 the range of the force, B the binding energy of the deuteron.)

The boundary condition is that $u_D(x)$ approach zero for large x. We must set $\epsilon=-\alpha^2$, $q(x)=0$, and $g(x)=1$. Then $v_R(x)$, $v_I(x)$, $Y_R(x)$, $Y_I(x)$ will be the same functions as above. If we choose

$$X_D(x)=e^{-\alpha x},$$

then

$$W_0(Y_I, X)=W_0[1+(x/a^0), e^{-\alpha x}]=-\alpha-(1/a^0),$$

so that

$$1/a^0=-\alpha+\alpha^2 W^0{}_0-\alpha^4 W^0{}_1+\alpha^6 W^0{}_2+\cdots. \tag{28}$$

The coefficients in (28) are the same as in (26), so that we may rewrite the latter for the triplet case as

$$\kappa\cot\delta^0=-\alpha+(\kappa^2+\alpha^2)W^0{}_0+(\kappa^4-\alpha^4)W^0{}_1 +(\kappa^6+\alpha^6)W^0{}_2+\cdots. \tag{29}$$

The coefficients here are defined in terms of zero-energy *scattering* functions, not the deuteron functions, as is sometimes done.

(b) High Energies

If the value of $\kappa\cot\delta$ is known at some energy other than zero, say at κ'^2, then the energy dependence in the neighborhood of this value is given by the identity (10). The generalization of the procedure in (*a*) is obvious. The result is

$$\kappa\cot\delta^0=\kappa'\operatorname{ctn}\delta_0'+(\kappa^2-\kappa'^2)W^0{}_0' +(\kappa^2-\kappa'^2)W^0{}_1'+\cdots, \tag{30}$$

where the coefficients $W^0{}_n'$ are defined in terms of the regular and irregular solutions at the energy κ'^2 and $\delta^{0\prime}$ is the corresponding phase shift.

(c) Higher Angular Momenta

We next generalize Eq. (22) to

$$\left[\frac{d^2}{dx^2}-\frac{l(l+1)}{x^2}+f\right]u^0{}_l(x)=-\kappa^2 u^0{}_l(x), \tag{31}$$

still treating κ^2 as the perturbation. Choose

$$X^0(x)=\kappa^{2l+1}\cot\delta^0{}_l\frac{j_l(x)}{\kappa^{l+1}}+\kappa^l n_l(x),$$

and

$$Y^0{}_l(x)=\frac{(2l)!}{2^l l!}x^{-l}+\frac{1}{a^0{}_l}\frac{2^l l!}{(2l+1)!}x^{l+1},$$

where $j_l(x)$ and $n_l(x)$ are, respectively, $(\pi\kappa x/2)^{\frac{1}{2}}\times J_{l+\frac{1}{2}}(\kappa x)$ and $(-1)^l(\pi\kappa x/2)^{\frac{1}{2}}J_{-l-\frac{1}{2}}(\kappa x)$. Asymptotically,

$$j_l(x)\to\sin\left(\kappa x-\frac{l\pi}{2}\right),\quad n_l(x)\to\cos\left(\kappa x-\frac{l\pi}{2}\right).$$

Then

$$W_{x_0}(Y_I, X)=\kappa^{2l+1}\cot\delta^0{}_l -\frac{1}{a^0{}_l}-\frac{(2l)!}{2^l l!}W_{x_0}(x^{-l}, \kappa^l n_l). \tag{32}$$

The last term on the right-hand side will in general become infinite as x_0 approaches zero, but reference to (10) shows that this will be exactly compensated by terms on the right-hand side of that equation. This fact is guaranteed by the identity (9). Therefore let us define a series

$$-\frac{(2l)!}{2^l l!}W_{x_0}(x^{-l}, \kappa^l n_l)=\kappa^2\sum_{n=0}^{l}D_{l,n}(\kappa^2)^n$$

and write out the expansion (16) as

$$\kappa^{2l+1}\cot\delta^0{}_l-\frac{1}{a^0{}_l}=(W^0{}_{l,0}-D_{l,0})\kappa^2 +(W^0{}_{l,1}-D_{l,1})\kappa^4+\cdots, \tag{33}$$

where the $W^0{}_{l,n}$ are defined in terms of the zero energy solutions of Eq. (31).

For potentials without a "tail," such as the square well, the expansion (33) converges equally well for all l. The criterion for convergence stated in II shows us, however, that if a small tail is important in producing the phase shift in question the perturbation approach fails as soon as the energy is comparable to the strength of the tail. Since the phase shifts for higher l have a strong tail dependence, the convergence of (33) will become rapidly poorer as l increases.

It is quite feasible, however, to use the analog of (30) to investigate the effect on any phase shift of small *fractional* changes in the energy.

IV. PROTON-PROTON SCATTERING

(a) Low Energies

Proton-proton scattering may be treated in much the same way as above. The radial equation for the S state in this case is

$$\left[\frac{d^2}{dx^2}-\frac{\beta}{x}+f\right]u(x)=-\kappa^2 u(x), \tag{34}$$

where $\beta=r_0/(h/Mc^2)$, with r_0 the range of the nuclear potential and M the proton mass. For low

energies, we again identify κ^2 with ϵ to obtain the expansion analogous to (26). Choose

$$X(x)=C_0^2\kappa\cot\delta\frac{F_0(x)}{C_0\kappa}+C_0G_0(x), \tag{35}$$

where $F_0(x)$ and $G_0(x)$ are the regular and irregular solutions in a repulsive Coulomb field defined by Breit, Wheeler, and Yost.[7]

$$F_0=C_0\kappa x\left\{1+\frac{\beta x}{2}-\frac{1}{6}\kappa^2x^2+\frac{\beta^2x^2}{12}+\cdots\right\},$$

$$G_0=\frac{1}{C_0}\Big[1-\frac{\kappa^2x^2}{2}+\frac{3}{4}\beta^2x^2 +\beta x\{\ln\gamma^2\beta x-1+Q\}+\cdots\Big], \tag{36}$$

$$F_0\underset{\text{as.}}{\longrightarrow}\sin(\kappa x+\delta_c),$$

$$G_0\underset{\text{as.}}{\longrightarrow}\cos(\kappa x+\delta_c),$$

where

$$C_0^2=2\pi\alpha/(e^{2\pi\alpha}-1),$$

$$\delta_c=\arg\Gamma(1+i\alpha)-\alpha\ln 2\kappa x,$$

$$\alpha=\beta/2\kappa,$$

$$Q=\left\{\text{Real Part}\frac{\Gamma'(-i\alpha)}{\Gamma(-i\alpha)}\right\}-\ln\alpha,$$

$$\ln\gamma=\text{Euler's constant}=0.5772\cdots.$$

The zero-energy asymptotic form is taken as

$$Y_I=K(x)+I(x)/a, \tag{37}$$

where

$$I(x)=1/\beta(\beta x)^{\frac{1}{2}}I_1(2(\beta x)^{\frac{1}{2}}),$$
$$K(x)=2(\beta x)^{\frac{1}{2}}K_1(2(\beta x)^{\frac{1}{2}}), \tag{38}$$

and a might be called a dimensionless "Coulomb scattering length." $I_1(x)$ and $K_1(x)$ are the modified Bessel functions of the second kind of pure imaginary argument as defined by Watson.[8] The behavior of $I(x)$ and $K(x)$ near the origin is

$$I(x)\sim x+\beta x^2/2,\quad K(x)\sim 1+\beta x\{\ln\gamma^2\beta x-1\},$$

allowing us to calculate

$$W_0(Y_I,X)=C_0^2\kappa\cot\delta-1/a+\beta Q. \tag{39}$$

The required expansion is, therefore

$$C_0^2\kappa\cot\delta+\beta Q=1/a+\kappa^2W_0+\kappa^4W_1+\kappa^6W_2, \tag{40}$$

where the W_n are defined in terms of the appropriately normalized zero energy solutions of Eq. (34). Here again the coefficients W_0 and W_1 have been obtained and discussed by Schwinger and others. We believe that the method of approach given here is simpler and makes the relation between the *n-p* and *p-p* expansions clearer.

It is obvious that the results of III(b) and III(c) can be generalized to the *p-p* case. The formulas become quite complicated, so we shall write down only a single special case, one that might be of interest in the near future. This case is the p phase shift for triplet proton-proton scattering. The appropriate expansion turns out to be

$$(1+\alpha^2)C_0^2\kappa^3\cot\delta_1+\beta\kappa^2(Q_1-2)+\beta^3Q_1/4-1/a_1 =\kappa^2(W_0-\beta\ln\gamma^2\beta x_0-1/x_0) +\kappa^4W_1+\kappa^6W_2+\cdots, \tag{41}$$

where

$$Q_1=\text{R.P.}\frac{\Gamma'(2-i\alpha)}{\Gamma(2-i\alpha)}-\ln\alpha$$

and the W_n are defined in terms of the solutions of the equation

$$\left\{\frac{d^2}{dx^2}-\beta/x-2/x^2+f\right\}\begin{Bmatrix}v_R\\ v_I\end{Bmatrix}=0$$

normalized at infinity to

$$Y_I=\beta(\beta x)^{\frac{1}{2}}K_3(2(\beta x)^{\frac{1}{2}})+\frac{1}{a_1}\frac{2}{\beta}\left(\frac{x}{\beta}\right)^{\frac{1}{2}}I_3(2(\beta x)^{\frac{1}{2}}),$$

and

$$Y_R=-\frac{2}{\beta}\left(\frac{x}{\beta}\right)^{\frac{1}{2}}I_3(2(\beta x)^{\frac{1}{2}}).$$

(b) A Treatment of the Coulomb Field as a Perturbation

Up to this point we have consistently had $g(x)=1$ in all applications. As was pointed out in the introduction, there is no reason why this must be done. One might, for instance, investigate the effect of small changes in the nuclear potential itself. We describe here an application, in which the Coulomb term, β/x, is considered as small. This is possible even though outside the range of the nuclear force, the Coulomb term may represent the main contribution to the total energy. The point is that the integrand on the right-hand side of Eq. (10) fails to vanish only within the range of the nuclear force. What the perturbation may do to the function $u(x)$ outside the range, therefore, does not affect the value of the integral. The only requirement is that its relative effect *inside* the range is small. This condition is clearly satisfied by the Coulomb field, even when the kinetic energy of the incident proton is small.

[7] Breit, Wheeler, and Yost, Phys. Rev. **49**, 174 (1936).
[8] G. N. Watson, *Bessel Functions* (Cambridge University Press, New York, 1944).

Let us consider Eq. (34) again, therefore, this time regarding $-\beta/x$ as the perturbation, i.e., $\epsilon=-\beta$, $g\doteq 1/x$. X is again given by (35) but Y_I is now to be

$$Y_I=\kappa\cot\delta^0\frac{\sin\kappa x}{\kappa}+\cos\kappa x,$$

where δ^0 is the phase shift produced by the nuclear field alone. We calculate

$$W_{x_0}(Y_I, X)=C_0^2\kappa\cot\delta-\kappa\cot\delta^0+\beta\ln\gamma^2\beta x_0+\beta Q. \quad (42)$$

The expansion (16) becomes

$$C_0^2\kappa\cot\delta+\beta Q=\kappa\cot\delta^0-\beta(W_0+\ln\gamma^2\beta x_0)+\beta^2W_1-\beta^3W_2, \quad (43)$$

where the coefficients W_n are defined in terms of the *purely nuclear* wave functions at the energy in question. Since β is always of the order $\frac{1}{10}$ or less, the series converges rapidly and we have a method for computing Coulomb phase shifts without actual recourse to the complicated and only incompletely tabulated hypergeometric functions. The corresponding relation for the p phase shift is

$$(1+\alpha^2)C_0^2\kappa^3\cot\delta_1+\beta\kappa^2(Q_1-2)+\beta^3Q_1/4-\kappa^3\cot\delta^0{}_1=-\beta[W_0+\ln\gamma^2\beta x_0-(1/2)x_0^2]+\beta^2[W_1-(1/2)x_0]-\beta^3[W_2+\tfrac{1}{4}\ln\gamma^2\beta x_0+\tfrac{3}{8}]+\beta^4W_3+\cdots, \quad (44)$$

where the W_n are defined in terms of the purely nuclear p-wave functions at the energy κ^2 normalized as in III(c).

(c) Coulomb Field Plus Energy as Perturbation

The last application of the identity (10) to be given here is provided by the case in which the energy term and the Coulomb term are simultaneously considered as perturbations. We restrict our attention to S scattering. In Eq. (34), therefore, we regard $\kappa^2-\beta/x$ as $\epsilon g(x)$. Here we use (35) for $X(x)$ and (24) for $Y_I(x)$. This leads to

$$W_{x_0}(Y_I,X)=C_0^2\kappa\cot\delta+\beta Q+\beta\ln\gamma^2\beta x_0-\frac{1}{a^0},$$

and thus to

$$C_0^2\kappa\cot\delta+\beta Q=\frac{1}{a^0}+\int_{x_0}^{\infty}(\kappa^2-\beta/x)(Y^0{}_I{}^2-v^0{}_R{}^2)dx-\beta\ln\gamma^2\beta x_0+2\int_{x_0}^{\infty}dx(\kappa^2-\beta/x)\times\left[h^0{}_{11}(x)\int_0^x Y^0{}_I(x')\,Y^0{}_R(x')(\kappa^2-\beta/x')dx'-h^0{}_{12}(x)\int_0^x v^0{}_R{}^2(x')(\kappa^2-\beta/x')dx'\right]. \quad (40')$$

A comparison of (40′) with (40) allows us to express the Coulomb scattering length and effective range in terms of the corresponding purely nuclear quantities. Thus

$$\frac{1}{a}=\frac{1}{a_0}-\beta\left[\int_{x_0}^{\infty}\frac{1}{x}(Y^0{}_I{}^2(x)-v^0{}_R{}^2(x))dx+\ln\gamma^2\beta x_0\right]+2\beta^2\left[\int_{x_0}^{\infty}dx\frac{h^0{}_{11}(x)}{x}\int_0^x\frac{dx'}{x'}Y^0{}_I(x')\,Y^0{}_R(x')-\int_{x_0}^{\infty}dx\frac{h^0{}_{12}(x)}{x}\int_0^x\frac{v^0{}_R{}^2(x')}{x'}dx'\right]+0(\beta^3), \quad (45)$$

$$W_0=W^0{}_0-2\beta\int_{x_0}^{\infty}dx\left[h^0{}_{11}(x)\int_0^x\frac{Y^0{}_I(x')\,Y^0{}_R(x')}{x'}dx'+\frac{h^0{}_{11}(x)}{x}\int_0^x Y^0{}_I(x')\,Y^0{}_R(x')dx'-h^0{}_{12}(x)\int_0^x\frac{v^0{}_R{}^2(x')}{x'}dx'-\frac{h^0{}_{12}(x)}{x}\int_0^x v^0{}_R{}^2(x')dx'\right]+0(\beta^2). \quad (46)$$

These last two formulas are of considerable practical use, because the best way of analyzing low energy p-p data at present is to plot the left-hand side of (40) *versus* energy (or κ^2) and then read off (in dimensional units of course) the intercept and slope of the resulting straight line. The problem is then to find out what these two numbers, the Coulomb scattering length and the effective range, imply about the nuclear potential which is acting. A definition of $1/a$ and W_0 in terms of a purely nuclear zero-energy wave function is much easier to interpret than one which involves the combined nuclear and Coulomb field. The terms actually written above give sufficient accuracy for the available data, the residual error in each expansion being less than 1 percent.

DISCUSSION

The advantages of analyzing nucleon-nucleon scattering data via expansions in powers of the energy have been mentioned in the introduction and are discussed in great detail by Blatt and Jackson.[5] Unfortunately the data available at present make this a completely practical procedure only for singlet-S proton-proton scattering. Higher angular momenta and n-p scattering in general still require the direct computation of phase shifts from an assumed potential for at least part of the analysis. We believe that in many cases expansions such as presented in this paper afford the most

convenient means of making such computations. It is necessary to determine a wave function, in general by numerical integration, and then to evaluate various definite integrals involving this function. Once these integrals are known, the behavior of the phase shifts over a considerable region of variation of the parameter in question is also known. We give a few typical examples.

(1) *Energy Dependence of Phase Shifts*—A knowledge of $W^0{}_0$ and $W^0{}_1$ in the expansion (26) will yield the *n-p* singlet-*S* phase shift with an accuracy of 1 percent up to an energy of 40 Mev. A similar situation exists in expansion (40) for the *p-p* singlet *S* phase shift. In the expansions (33) and (41) a knowledge of the coefficient of κ^2 yields δ_1 to 2 percent up to energies of 30 Mev for wells without tails.

Triplet phase shifts are given with a comparable accuracy. The triplet *S* is an especially favorable case because of the nearness to 90° during much of the interesting range.

(2) *Modification of the Nuclear Phase Shift due to the Coulomb Field*—Expansion (43), keeping only terms proportional to β, may be used at all energies with roughly the same accuracy. At 32 Mev the error in the phase shift is about 0.2°. The accuracy of the formulas in Section IV(c) has already been discussed.

We have been purposely vague about the nature of the potential, *f*. The only requirements that need be made are that it be a short range, self adjoint operator. Professor Breit has pointed out in this connection that an operator of the form

$$f\psi(r)=\int dr'\,V(r,r')\psi(r'),$$

with $V(r,r')=V(r',r)$ may be treated by this method.

ACKNOWLEDGMENTS

We are indebted to Professor Serber who first pointed out to us the possibility of obtaining the expansions by a straightforward non-variational procedure and who contributed helpful advice at many points. Thanks are also due R. S. Christian for the scheme of including boundary conditions in the integral equation (11) and for many enlightening discussions on the general scattering problem.

Work described in this report was performed under the auspices of the AEC.

Notes added in proof.—(1) Professor Bethe[9] has derived Eq. (10) for $g(x)$, a constant, and has demonstrated explicitly the extreme smallness of W_1 in this case. Further investigation shows, however, that higher terms (i.e., W_2, $W_3\cdots$) are not correspondingly smaller if the well has a tail. For practical purposes there is, then, a radius of convergence at about $2\kappa W_0=1$. Our statements in paragraph (1) of the discussion, therefore, apply only to wells with sharp boundaries.

(2) Dr. Jackson has pointed out a more concise method of writing the formula (21), namely as

$$W_2=\int_{x_0}^{\infty} g(x)[X_1{}^2(x)-u_1{}^2(x)]dx.$$

From the computational standpoint, it is easier to evaluate the functions X_1 and u_1 numerically and substitute into this formula than to use the cumbersome (21).

[9] H. A. Bethe, Phys. Rev. (to be published).

PHYSICAL REVIEW VOLUME 75, NUMBER 11 JUNE 1, 1949

The Charge Density and Magnetic Moments of the Nucleons*

MURRAY SLOTNICK
Columbia University, New York, New York,

AND

WALTER HEITLER
Dublin Institute for Advanced Studies, Dublin, Eire

(Received January 24, 1949)

Using pseudoscalar meson theory, the behavior of a single-nucleon system in an electric field is studied. From the electrostatic interaction, the interaction between neutrons and electrons is computed. From the spin-orbit interaction, the magnetic moments of neutron and proton are computed. The calculation is carried out relativistically, with nucleon and pseudoscalar meson fields both subjected to second quantization. The Hamiltonian of the nucleon-meson system is diagonalized to second order in the coupling parameters by two canonical transformations, and transitions induced by the electric field between single-nucleon states are investigated. For pseudoscalar coupling of 282 e.m. mesons, estimating the coupling constants for charge-symmetric theory from the observed singlet neutron-proton scattering length (using static nuclear forces), it is found that the volume integral of the neutron-electron interaction potential is about -14 kev $\times(4\pi/3)(e^2/mc^2)^3$, and that μ_P and μ_N are about 1.7 and -5 nuclear magnetons respectively. Results are also given for pure charged theory. Pseudovector coupling is compared to pseudoscalar coupling, and is found to give the same magnetic moments, but a logarithmically divergent neutron-electron interaction. The influence of the contact interaction term is discussed.

The results are compared with those of "non-relativistic" methods and with experimental values, and the neutron-electron interaction is computed approximately for several types of mesons with an improved non-relativistic method. Charge renormalization and the approximate distribution of the charge cloud around a neutron are discussed. The pseudoscalar meson contribution to the Lamb Shift of the $2S$ hydrogen level is estimated as $+0.08$ Mc.

I. INTRODUCTION

A MESON field coupled to nucleons modifies the behavior of the nucleons in electromagnetic fields. It had thus been hoped that meson theory would provide an explanation of the anomalous magnetic moments and other properties of neutrons and protons, as it does indeed qualitatively.[1] Unfortunately, quantitative investigation of the magnetic moments[2] and charge clouds[3] led to divergent results with the ordinary weak-coupling theory that necessitated the introduction of ad hoc cut-offs, while other theories[4] led to incorrect results. This, together with the failure of meson theories to yield nuclear forces free from objectionable singularities was considered to limit severely the value of the theory.

However, in the calculations with weak-coupling theory cited above,[2,3] the divergences may have been introduced by the following assumptions made there:

(1) The nucleon was taken to be infinitely heavy. If nucleon recoil is taken into account, certain energy denominators occurring in the calculations will be large for high momentum virtual states and may decrease the degree of divergence.

(2) Hole theory was not used, and it is conceivable that negative-energy processes might cancel part of the divergences of positive-energy processes, as is the case for electron self-energy, etc.

Moreover, recent advances in quantum electrodynamics suggest how divergences due to mass effects can be separated from true divergences in relativistic calculations. It was thus thought worth while to reinvestigate the divergent results relativistically.

On the other hand, experimental evidence has very recently been obtained by Havens, Rabi, and Rainwater,[5] and Fermi and Marshall[6] that indicates a weak attraction between neutrons and electrons that is not a spin effect. Improved experiments by Rainwater, Rabi, and Havens are in progress;[7] the earlier experiment[5] suggesting a value of minus several kev for the quantity $U_0 \equiv$ Volume integral of interaction $\div(4\pi/3)(e^2/mc^2)^3$, which is called the "neutron-electron interaction." This is of the sign and order of magnitude expected qualitatively from meson theory,[6] so that a detailed investigation is of considerable interest.

The two forms of weakly coupled meson theory that have proved most useful are the pseudoscalar and vector theories, and we will restrict our attention principally to the former. We will investigate the behavior of a single nucleon in an electric field. The interaction between the neutron charge cloud and the electric field of an electron will be used to

* Publication assisted by the Ernest Kempton Adams Fund for Physical Research of Columbia University.

[1] W. Heitler, Nature **148**, 680 (1941); H. Fröhlich and W. Heitler, Nature **141**, 37 (1938).

[2] Fröhlich, Heitler, and Kemmer, Proc. Roy. Soc. **A166**, 127 (1938).

[3] Fröhlich, Heitler, and Kahn, Proc. Roy. Soc. **A177**, 269 (1939); W. E. Lamb, Jr. and L. I. Schiff, Phys. Rev. **53**, 651 (1938).

[4] See G. Wentzel, Rev. Mod. Phys. **19**, 1 (1947).

[5] Havens, Rabi, and Rainwater, Phys. Rev. **72**, 634 (1947).

[6] Fermi and Marshall, Phys. Rev. **72**, 1139 (1947).

[7] See Rainwater, Rabi, and Havens, Phys. Rev. **75**, 1295 (1949).

compute the neutron-electron interaction, while the magnetic moments can be computed from the spin-orbit interaction of the nucleon in an electric field.[8] By dealing only with electric fields, we avoid use of the more complicated vector potentials and current density operators.

It should also be stressed that exact quantitative agreement with experiment can hardly be expected from pseudoscalar meson theory alone, since it fails in other respects[4] (high singularity of tensor force), and because the solution will be carried only to second order in the coupling parameter. It is also likely that mesons of mass 700–1000 e.m. will add contributions.

II. METHOD OF COMPUTATION

Lagrangian and Hamiltonian

The nucleons will be described by a doubly quantized Fermi-Dirac field, with 8-component field operators $\psi=\begin{pmatrix}\psi_P\\ \psi_N\end{pmatrix}$, where ψ_P and ψ_N are 4-component Dirac operators for proton and neutron respectively. We define the charge operators

$$\tau=\begin{pmatrix}0&1\\0&0\end{pmatrix},\quad \tau^\dagger=\begin{pmatrix}0&0\\1&0\end{pmatrix},\quad \tau^0=\begin{pmatrix}1&0\\0&-1\end{pmatrix},$$

$$\tau_P=\begin{pmatrix}1&0\\0&0\end{pmatrix},\quad \tau_N=\begin{pmatrix}0&0\\0&1\end{pmatrix}, \tag{1}$$

where τ changes neutrons to protons, $\tau^\dagger$ protons to neutrons, and τ_P and τ_N respectively single out the proton and neutron parts of ψ. ψ^* is the Hermitian conjugate of ψ.

The mesons are described by a doubly quantized Einstein-Bose field with pseudoscalar field operators Ψ and its Hermitian conjugate $\Psi^\dagger$ for charged mesons and $\Psi^0=\Psi^{0\dagger}$ for neutral mesons. $\hbar$ and c will be taken as unity throughout and the summation convention will be used. We use the Schrödinger representation with time-independent operators.

The Lorentz- and gauge-invariant Lagrangian density of the system of mesons and nucleons in the external field is:

$$\mathfrak{L}=-\{d_\nu^\dagger\Psi^\dagger d_\nu\Psi+\mu^2\Psi^\dagger\Psi\}-\frac{1}{2}\left\{\frac{\partial\Psi^0}{\partial x_\nu}\frac{\partial\Psi^0}{\partial x_\nu}+\mu^2\Psi^{02}\right\}+i\psi^\dagger\left\{\gamma_\nu\left(\frac{\partial}{\partial x_\nu}-ie\tau_P A_\nu\right)+M\right\}\psi+(4\pi)^{\frac{1}{2}}g(B\Psi+B^\dagger\Psi^\dagger)$$
$$+(4\pi)^{\frac{1}{2}}g_0B^0\Psi^0-\frac{(4\pi)^{\frac{1}{2}}}{\mu}f(B_\nu d_\nu\Psi+B_\nu^\dagger d_\nu^\dagger\Psi^\dagger)-\frac{(4\pi)^{\frac{1}{2}}}{\mu}f_0B_\nu^0\frac{\partial\Psi^0}{\partial x_\nu}+s\frac{4\pi}{\mu^2}f^2B_\nu^\dagger B_\nu+\frac{t}{2}\frac{4\pi}{\mu^2}f_0^2B_\nu^0B_\nu^0 \tag{2}$$

where the following notation is employed:

$\psi^\dagger=i\psi^*\beta$ is the "adjoint" operator of ψ;

$$d_\nu=\frac{\partial}{\partial x_\nu}-ieA_\nu;\quad d_\nu^\dagger=\frac{\partial}{\partial x_\nu}+ieA_\nu;$$

$A_\nu=(\mathbf{A}(\mathbf{r}),\ iV(\mathbf{r}))$ = 4-potential of external electromagnetic field;

μ = meson mass (assumed equal for charged and neutral mesons);

M = neutron mass = proton mass (the mass difference is neglected);

$B=(\psi^\dagger\gamma_5\tau\psi)$; $B^\dagger=(\psi^\dagger\gamma_5\tau^\dagger\psi)$; $B^0=(\psi^\dagger\gamma_5\tau^0\psi)$;

$\gamma_5=\gamma_1\gamma_2\gamma_3\gamma_4$;

$B_\nu=(\psi^\dagger\gamma_5\gamma_\nu\tau\psi)$; $B_\nu^\dagger=(\psi^\dagger\gamma_5\gamma_\nu\tau^\dagger\psi)$;

$B_\nu^0=(\psi^\dagger\gamma_5\gamma_\nu\tau^0\psi)$;

s and t are arbitrary constants to be discussed later;

g, g_0 are "pseudoscalar coupling" constants for charged and neutral mesons, respectively;

f, f_0 are "pseudovector coupling" constants for charged, neutral mesons.

The Hamiltonian density is given by

$$\mathfrak{H}(\mathbf{r})=\Pi^\dagger\Pi+\nabla\Psi^\dagger\cdot\nabla\Psi+\mu^2\Psi^\dagger\Psi+\tfrac{1}{2}\{\Pi^{02}+(\nabla\Psi^0)^2+\mu^2\Psi^{02}\}+\psi^*\left[\boldsymbol{\alpha}\cdot\frac{\nabla}{i}+\beta M\right]\psi-(4\pi)^{\frac{1}{2}}g(B\Psi+B^\dagger\Psi^\dagger)$$
$$-(4\pi)^{\frac{1}{2}}g_0B^0\Psi^0+\frac{(4\pi)^{\frac{1}{2}}}{\mu}f(\mathbf{B}\cdot\nabla\Psi+\mathbf{B}^\dagger\cdot\nabla\Psi^\dagger)+\frac{(4\pi)^{\frac{1}{2}}}{\mu}f(\Pi^\dagger B_0+\Pi B_0^\dagger)+\frac{(4\pi)^{\frac{1}{2}}}{\mu}f_0(\mathbf{B}^0\cdot\nabla\Psi^0)$$
$$+\frac{(4\pi)^{\frac{1}{2}}}{\mu}f_0\Pi^0B_0^0-s\frac{4\pi f^2}{\mu^2}\mathbf{B}^\dagger\cdot\mathbf{B}+(1+s)\frac{4\pi f^2}{\mu^2}B_0^\dagger B_0-\frac{t}{2}\frac{4\pi f_0^2}{\mu^2}\mathbf{B}^{02}+\frac{(1+t)}{2}\frac{4\pi f_0^2}{\mu^2}B_0^{02}$$
$$+ie\{V(\Pi^\dagger\Psi^\dagger-\Pi\Psi)+\Psi^\dagger\mathbf{A}\cdot\nabla\Psi-\Psi\mathbf{A}\cdot\nabla\Psi^\dagger\}+e^2\mathbf{A}^2\Psi^\dagger\Psi+eV\psi^*\tau_P\psi-e\mathbf{A}\cdot(\psi^*\boldsymbol{\alpha}\tau_P\psi)$$
$$+ie\frac{(4\pi)^{\frac{1}{2}}}{\mu}f\{\Psi^\dagger\mathbf{A}\cdot\mathbf{B}^\dagger-\Psi\mathbf{A}\cdot\mathbf{B}\} \tag{3}$$

[8] We are indebted to Professor H. A. Bethe for pointing out this fact.

where Π, $\Pi^\dagger$, and Π^0 are the momenta conjugate to Ψ, $\Psi^\dagger$, and Ψ^0, and

$$B=(\psi^*\alpha_1\alpha_2\alpha_3\beta\tau\psi),\qquad B^\dagger=(\psi^*\alpha_1\alpha_2\alpha_3\beta\tau^\dagger\psi),$$
$$B^0=(\psi^*\alpha_1\alpha_2\alpha_3\beta\tau^0\psi),$$
$$\mathbf{B}=(\psi^*\boldsymbol{\sigma}\tau\psi),\qquad \mathbf{B}^\dagger=(\psi^*\boldsymbol{\sigma}\tau^\dagger\psi),$$
$$\mathbf{B}^0=(\psi^*\boldsymbol{\sigma}\tau^0\psi),$$
$$B_0=-i(\psi^*\alpha_1\alpha_2\alpha_3\tau\psi),\quad B_0^\dagger=-i(\psi^*\alpha_1\alpha_2\alpha_3\tau^\dagger\psi),$$
$$B_0^0=-i(\psi^*\alpha_1\alpha_2\alpha_3\tau^0\psi).$$

In (3), the first line refers to the pure meson and nucleon fields, the second to the meson-nucleon interaction, the third to a self-energy and a contact or "δ-function" interaction between two nucleons that will be discussed later, and the fourth line to the interaction between mesons and nucleons and the electromagnetic field. Putting $f_0=g_0=0$ gives pure charged theory, while $g_0=g/\sqrt{2}$, $f_0=f/\sqrt{2}$ gives symmetrical meson theory. More generally, the neutral meson need not have the mass μ and τ^0 can be any diagonal charge-operator, but we will deal only with pure charged and symmetrical theory.

We transform to momentum representation by

$$\Psi(\mathbf{r})=\sum_{\mathbf{k}}(2\epsilon_kL^3)^{-\frac{1}{2}}\{q_{+\mathbf{k}}\exp(i\mathbf{k}\cdot\mathbf{r})+q_{-\mathbf{k}}^\dagger\exp(-i\mathbf{k}\cdot\mathbf{r})\}$$
$$\Psi^0(\mathbf{r})=\sum_{\mathbf{k}}(2\epsilon_kL^3)^{-\frac{1}{2}}\{q_{0\mathbf{k}}\exp(i\mathbf{k}\cdot\mathbf{r})+q_{0\mathbf{k}}^\dagger\exp(-i\mathbf{k}\cdot\mathbf{r})\}$$
$$\Pi(\mathbf{r})=\sum_{\mathbf{k}}i(\epsilon_k/2L^3)^{\frac{1}{2}}\{q_{+\mathbf{k}}^\dagger\exp(-i\mathbf{k}\cdot\mathbf{r})-q_{-\mathbf{k}}\exp(i\mathbf{k}\cdot\mathbf{r})\}$$
$$\Pi^0(\mathbf{r})=\sum_{\mathbf{k}}i(\epsilon_k/2L^3)^{\frac{1}{2}}\{q_{0\mathbf{k}}^\dagger\exp(-i\mathbf{k}\cdot\mathbf{r})-q_{0\mathbf{k}}\exp(i\mathbf{k}\cdot\mathbf{r})\}$$
$$\psi(\mathbf{r})=\sum_{\mathbf{p}}L^{-\frac{1}{2}}a_{\mathbf{p}}u_{\mathbf{p}}\exp(i\mathbf{p}\cdot\mathbf{r}),\tag{4}$$

and the conjugate equations. Here, L is the length of the cubic enclosure in which we imagine our system, $\epsilon_k=(\mathbf{k}^2+\mu^2)^{\frac{1}{2}}$, and $u_{\mathbf{p}}$ is a normalized 8-component Dirac spinor for which we have omitted subscripts for spin direction, sign of energy, and charge. The commutation relations are in this representation:

$$[q_{+\mathbf{k}}^\dagger,\,q_{+\mathbf{k}'}]=[q_{-\mathbf{k}}^\dagger,\,q_{-\mathbf{k}'}]=[q_{0\mathbf{k}}^\dagger,\,q_{0\mathbf{k}'}]=\delta_{\mathbf{k}\mathbf{k}'};$$
$$[a_{\mathbf{p}}^\dagger,\,a_{\mathbf{p}'}]=\delta_{\mathbf{p}\mathbf{p}'}.\tag{5}$$

Other commutators involving q's and anticommutators involving a's are zero.

The Hamiltonian $H=\int\mathfrak{H}d\tau$ then becomes (we restrict ourselves to the case $\mathbf{A}(\mathbf{r})=0$):

$$H=H^m+H^n+H^i+H^e+H^\delta,\tag{6}$$

where

$$H^m=\sum_{\mathbf{k}}\epsilon_k(N_{+\mathbf{k}}+N_{-\mathbf{k}}+N_{0\mathbf{k}}),\quad H^n=\sum_{\mathbf{p}}E_{\mathbf{p}}N_{\mathbf{p}},$$

$$H^i=\sum_{\mathbf{p}\mathbf{p}'\mathbf{k}}a_{\mathbf{p}'}^\dagger a_{\mathbf{p}}(2\pi/\epsilon_kL^3)^{\frac{1}{2}}\Big(u_{\mathbf{p}'}^*\Big\{\Big[(q_{+\mathbf{k}}\tau+q_{-\mathbf{k}}\tau^\dagger)\Big(-g\alpha_1\alpha_2\alpha_3\beta-\frac{f}{\mu}\epsilon_k\alpha_1\alpha_2\alpha_3+\frac{if}{\mu}\boldsymbol{\sigma}\cdot\mathbf{k}\Big)$$
$$+q_{0\mathbf{k}}\tau^0\Big(-g_0\alpha_1\alpha_2\alpha_3\beta-\frac{f_0}{\mu}\epsilon_k\alpha_1\alpha_2\alpha_3+\frac{if_0}{\mu}\boldsymbol{\sigma}\cdot\mathbf{k}\Big)\Big]\delta_{\mathbf{p}',\mathbf{p}+\mathbf{k}}$$
$$+\Big[(q_{+\mathbf{k}}^\dagger\tau^\dagger+q_{-\mathbf{k}}^\dagger\tau)\Big(-g\alpha_1\alpha_2\alpha_3\beta+\frac{f}{\mu}\epsilon_k\alpha_1\alpha_2\alpha_3-\frac{if}{\mu}\boldsymbol{\sigma}\cdot\mathbf{k}\Big)$$
$$+q_{0\mathbf{k}}^\dagger\tau^0\Big(-g_0\alpha_1\alpha_2\alpha_3\beta+\frac{f_0}{\mu}\epsilon_k\alpha_1\alpha_2\alpha_3-\frac{if_0}{\mu}\boldsymbol{\sigma}\cdot\mathbf{k}\Big)\Big]\delta_{\mathbf{p}',\mathbf{p}+\mathbf{k}}\Big\}u_{\mathbf{p}}\Big)$$

$$H^e=H^{em}+H^{en}$$
$$=\frac{e}{2L^3}\int d\tau V(\mathbf{r})\sum_{\mathbf{k}\mathbf{k}'}(\epsilon_k\epsilon_{k'})^{-\frac{1}{2}}\{(q_{+\mathbf{k}'}^\dagger q_{+\mathbf{k}}-q_{-\mathbf{k}'}^\dagger q_{-\mathbf{k}})(\epsilon_k+\epsilon_{k'})\exp(i(\mathbf{k}-\mathbf{k}')\cdot\mathbf{r})$$
$$+q_{-\mathbf{k}'}q_{+\mathbf{k}}(\epsilon_k-\epsilon_{k'})\exp(i(\mathbf{k}+\mathbf{k}')\cdot\mathbf{r})-q_{+\mathbf{k}'}^\dagger q_{-\mathbf{k}}^\dagger(\epsilon_k-\epsilon_{k'})\exp(-i(\mathbf{k}+\mathbf{k}')\cdot\mathbf{r})\}$$
$$+\frac{e}{L^3}\int d\tau V(\mathbf{r})\sum_{\mathbf{p}\mathbf{p}'}a_{\mathbf{p}'}^\dagger a_{\mathbf{p}}(u_{\mathbf{p}'}^*\tau_Pu_{\mathbf{p}})\exp(i(\mathbf{p}-\mathbf{p}')\cdot\mathbf{r})$$

$$H^\delta=-\Big(\frac{4\pi f^2}{\mu^2L^3}\Big)\sum_{\mathbf{p}\mathbf{p}'\mathbf{p}_0\mathbf{p}_0'}\delta_{\mathbf{p}+\mathbf{p}',\mathbf{p}_0+\mathbf{p}_0'}a_{\mathbf{p}}^\dagger a_{\mathbf{p}_0'}a_{\mathbf{p}'}^\dagger a_{\mathbf{p}_0}\{(1+s)(u_{\mathbf{p}}^*\alpha_1\alpha_2\alpha_3\tau^\dagger u_{\mathbf{p}_0})(u_{\mathbf{p}'}^*\alpha_1\alpha_2\alpha_3\tau u_{\mathbf{p}_0'})$$
$$+s(u_{\mathbf{p}}^*\boldsymbol{\sigma}\tau^\dagger u_{\mathbf{p}_0'})\cdot(u_{\mathbf{p}'}^*\boldsymbol{\sigma}\tau u_{\mathbf{p}_0})\}$$
$$-\Big(\frac{4\pi f_0^2}{2\mu^2L^3}\Big)\sum_{\mathbf{p}\mathbf{p}'\mathbf{p}_0\mathbf{p}_0'}\delta_{\mathbf{p}+\mathbf{p}',\mathbf{p}_0+\mathbf{p}_0'}a_{\mathbf{p}}^\dagger a_{\mathbf{p}_0'}a_{\mathbf{p}'}^\dagger a_{\mathbf{p}_0}\{(1+t)(u_{\mathbf{p}}^*\alpha_1\alpha_2\alpha_3\tau^0u_{\mathbf{p}_0'})(u_{\mathbf{p}'}^*\alpha_1\alpha_2\alpha_3\tau^0u_{\mathbf{p}_0})$$
$$+t(u_{\mathbf{p}}^*\boldsymbol{\sigma}\tau^0u_{\mathbf{p}_0'})\cdot(u_{\mathbf{p}'}^*\boldsymbol{\sigma}\tau u_{\mathbf{p}_0})\}.\tag{7}$$

Here, $E_\mathbf{p}=(u_\mathbf{p}^*[\boldsymbol{\alpha}\cdot\mathbf{p}+\beta M]u_\mathbf{p})$, and is $\pm(\mathbf{p}^2+M^2)^{\frac{1}{2}}$ while $N_\mathbf{p}=a_\mathbf{p}^\dagger a_{\mathbf{p}0}$, $N_{+\mathbf{k}}=q_{+\mathbf{k}}^\dagger q_{+\mathbf{k}}$, $N_{-\mathbf{k}}=q_{-\mathbf{k}}^\dagger q_{-\mathbf{k}}$, $N_{0\mathbf{k}}=q_{0\mathbf{k}}^\dagger q_{0\mathbf{k}}$.

It should be mentioned that the nucleon charge density operator used above, namely, $e\psi^*\tau_P\psi$ (see (3)), gives a negative infinite expectation value for the total charge in the vacuum state. This can be avoided by using Heisenberg's symmetrized charge density $e/2(\psi^*\tau_P\psi-\psi\tau_P\psi^*)$. However, only off-diagonal elements of the charge density will be encountered, and by virtue of the commutation relations, the two definitions give identical results for such elements.

The Canonical Transformations

The representation in which $N_\mathbf{p}$, $N_{+\mathbf{k}}$, $N_{-\mathbf{k}}$, $N_{0\mathbf{k}}$, and hence $H^0=H^m+H^n$ is diagonal will be used as the unperturbed representation. The state in which all N's are zero, except that the $N_\mathbf{p}$'s for negative-energy states are unity, is the vacuum state. A single-nucleon state of momentum $\mathbf{p}$ is one that differs from the vacuum state only in that for this one positive-energy state, $N_\mathbf{p}=1$.

If a canonical transformation $\exp(-iS)$ is applied to H to diagonalize the part $H^0+H^i+H^\delta$ not containing the electric field, the unperturbed single-nucleon states are transformed into the true single-nucleon states in zero field. The transformed electrical part $\exp(-iS)H^e\exp(iS)$ has matrix elements between the zero-field single-nucleon states that determine the properties of single nucleons in external fields. Actually, however, the diagonalization will only be carried to second order in the coupling parameters, and an unknown error will thus be introduced into the final results.

Before proceeding, account must be taken of the self-energies, which have the effect of causing a mass change δM for the nucleons and $\delta\mu$ for the mesons. (δM diverges logarithmically for pseudoscalar and quadratically for pseudovector coupling.[9]) We write the Hamiltonian as follows:

$$H=(H^0+\delta H)+(H^i+H^\delta-\delta H)+H^e$$

where

$$\delta H=\int d\tau\{\delta M\psi^*\beta\psi+\delta\mu^2\Psi^\dagger\Psi+\tfrac{1}{2}\delta\mu_0{}^2\Psi^{02}\}.$$

The term in the first parenthesis in H is simply H^0 for the nucleon mass $M+\delta M$, charged meson mass $\mu+\delta\mu$, and neutral meson mass $\mu+\delta\mu_0$. These, however, are the experimentally measured masses, and in a correct theory would presumably differ only by a second-order quantity from the inertial masses. The Hamiltonian could then be written, at least to second order, in the form

$$H=H^0+(H^i+H^\delta-\delta H)+H^e, \tag{8}$$

where H^0, etc., are all given by (7), but with M and μ standing for the experimental masses, and δH chosen so that it just cancels the self-energy parts of H^i+H^δ. The form (8) will be used hereafter despite the fact that it is not strictly applicable. It is very reasonable to suppose that any convergent results so obtained will agree to second order with those of the "correct" theory. Divergences, however, should really be treated with refined methods, such as Feynman's relativistic cut-off[10] before it can decisively be stated that they are not really "mass effects."

We note the formula:

$$\exp(-iS)H\exp(iS)=H+(-i)[S,H]+\frac{(-i)^2}{2!}[S,[S,H]]+\cdots. \tag{9}$$

Then, to second order, we have from (8):

$$\begin{aligned}H_I\equiv&\exp(-iS)H\exp(iS)\\&=H^0-i[S,H^0]-\tfrac{1}{2}[S,[S,H^0]]\\&\quad+H^i-i[S,H^i]+H^\delta-\delta H+H^e\\&\quad-i[S,H^e]-\tfrac{1}{2}[S,[S,H^e]].\end{aligned} \tag{10}$$

To eliminate first-order terms, put $-i[S,H^0]+H^i=0$, so that

$$\begin{aligned}H_I=&H^0-(i/2)[S,H^i]+H^\delta-\delta H+H^e\\&-i[S,H^e]-\tfrac{1}{2}[S,[S,H^e]]\end{aligned} \tag{11}$$

with the elements of S between states e and a of energies $E(e)$ and $E(a)$, given by

$$S_{ea}=iH_{ea}{}^i/(E(e)-E(a)). \tag{12}$$

We next apply a transformation $\exp(-iT)$ to eliminate second-order terms from H_I. Then

$$\begin{aligned}H_{II}\equiv&\exp(-iT)H_I\exp(iT)\\&=H^0-i[T,H^0]-(i/2)[S,H^i]\\&\quad+H^\delta-\delta H+H^e-i[T,H^e]\\&\quad-i[S,H^e]-\tfrac{1}{2}[S,[S,H^e]].\end{aligned} \tag{13}$$

"Self-energy transitions" are those for which either initial and final states are identical or (because of the β in δH) those where a nucleon has merely changed the sign of its energy. For such transitions, the matrix elements of $(-(i/2)[S,H^i]+H^\delta-\delta H)$ are zero by our choice of δH. Then

$$T_{ea}=0 \quad \text{(self-energy transitions)}. \tag{14a}$$

Otherwise, we put $T=T^i+T^\delta$, with

$$T_{ea}{}^i=\frac{iH_{ez}{}^iH_{za}{}^i}{2(E(e)-E(a))}\left[\frac{1}{E(e)-E(z)}-\frac{1}{E(z)-E(a)}\right];$$

$$T_{ea}{}^\delta=\frac{iH_{ea}{}^\delta}{E(e)-E(a)}$$

(non-self-energy transitions) (14b)

[9] N. Kemmer, Proc. Roy. Soc. **A166**, 127 (1938).

[10] R. P. Feynman, Phys. Rev. **74**, 1430 (1948).

giving

$$H_{II}=H^0+H^e-i[S, H^e]$$
$$-i[T, H^e]-\tfrac{1}{2}[S, [S, H^e]]. \quad (15)$$

In (15), H^0 has no off-diagonal matrix elements, all transitions being induced by the field. The H^e term has the same matrix elements between single-nucleon states as it would have had if there were no mesons; zero for neutrons and the customary Dirac value for protons. The $[S, H^e]$ term is not diagonal in the number of mesons, and hence has no elements between single-nucleon states. The operator of interest is thus $K=K^i+K^\delta$, where

$$K^i=-i[T^i, H^e]-\tfrac{1}{2}[S, [S, H^e]],$$
$$K^\delta=-i[T^\delta, H^e]. \quad (16)$$

Then, from (12) and (14), we have

$$K_{ea}{}^i=\frac{H_{ew}{}^iH_{wz}{}^iH_{za}{}^e}{(E(e)-E(w))(E(e)-E(z))}$$
$$+\frac{H_{ew}{}^eH_{wz}{}^iH_{za}{}^i}{(E(w)-E(a))(E(z)-E(a))}$$
$$-\frac{H_{ew}{}^iH_{wz}{}^eH_{za}{}^i}{(E(e)-E(w))(E(z)-E(a))},$$

$$K_{ea}{}^\delta=-\frac{H_{ew}{}^\delta H_{wa}{}^e}{E(w)-E(e)}+\frac{H_{ew}{}^eH_{wa}{}^\delta}{E(a)-E(w)},$$

(non-self-energy transitions), (17a)

except that in case the transition $e\to z$ in the first term of K^i or $w\to a$ in the second term are self-energy transitions, we must make respectively the substitutions

$$\frac{H_{ew}{}^iH_{wz}{}^iH_{za}{}^e}{(E(e)-E(w))(E(e)-E(z))}\to$$
$$\frac{H_{ew}{}^iH_{wz}{}^iH_{za}{}^e}{2(E(e)-E(w))(E(w)-E(z))};$$

$$\frac{H_{ew}{}^eH_{wz}{}^iH_{za}{}^i}{(E(w)-E(a))(E(z)-E(a))}\to$$
$$\frac{H_{ew}{}^eH_{wz}{}^iH_{za}{}^i}{2(E(w)-E(z))(E(z)-E(a))}. \quad (17b)$$

In K^δ, only non-self-energy elements of H^δ should be taken. Equation (17) is our basic formula.

III. NEUTRON IN ELECTRIC FIELD: CONVERGENCE INVESTIGATION

The Matrix Element

The matrix element due to the electric field for a transition from a single-neutron state of momentum $\mathbf{p}_0$ to a single-neutron state of momentum $\mathbf{p}$ (not equal to $\mathbf{p}_0$), $K_{\mathbf{p}\mathbf{p}_0}$ will now be examined. In the following table of processes contributing to $K_{\mathbf{p}\mathbf{p}_0}$, which will be seen to be exhaustive, μ^+ and μ^- stand for positive and negative mesons, N^+ and N^- for positive- and negative-energy neutrons, and P^+ and P^- for protons. The momentum of each particle is written immediately after the symbol for the particle, and the term in the Hamiltonian causing the transition indicated by arrows is written in square parentheses.

1. Processes contributing to $K_{\mathbf{p}\mathbf{p}_0}{}^i$ due to H^{em}:

(a) $N^+(\mathbf{p}_0)$ destroyed before $N^+(\mathbf{p})$ created:

(α) $N^+(\mathbf{p}_0)[H^i]\to P^+(-\mathbf{k})+\mu^-(\mathbf{b})$; $\mu^-(\mathbf{b})[H^e]\to\mu^-(\mathbf{a})$; $P^+(-\mathbf{k})+\mu^-(\mathbf{a})[H^i]\to N^+(\mathbf{p})$
(β) $[H^e]\to\mu^+(-\mathbf{b})+\mu^-(\mathbf{a})$; $N^+(\mathbf{p}_0)+\mu^+(-\mathbf{b})[H^i]\to P^+(-\mathbf{k})$; $P^+(-\mathbf{k})+\mu^-(\mathbf{a})[H^i]\to N^+(\mathbf{p})$
(γ) $N^+(\mathbf{p}_0)[H^i]\to P^+(-\mathbf{k})+\mu^-(\mathbf{b})$; $P^+(-\mathbf{k})[H^i]\to N^+(\mathbf{p})+\mu^+(-\mathbf{a})$; $\mu^-(\mathbf{b})+\mu^+(-\mathbf{a})[H^e]\to$.

(b) $N^+(\mathbf{p})$ created before $N^+(\mathbf{p}_0)$ destroyed:

(α) $P^-(-\mathbf{k})[H^i]\to N^+(\mathbf{p})+\mu^+(-\mathbf{a})$; $\mu^+(-\mathbf{a})[H^e]\to\mu^+(-\mathbf{b})$; $N^+(\mathbf{p}_0)+\mu^+(-\mathbf{b})[H^i]\to P^-(-\mathbf{k})$
(β) $P^-(-\mathbf{k})[H^i]\to N^+(\mathbf{p})+\mu^+(-\mathbf{a})$; $N^+(\mathbf{p}_0)[H^i]\to P^-(-\mathbf{k})+\mu^-(\mathbf{b})$; $\mu^+(-\mathbf{a})+\mu^-(\mathbf{b})[H^e]\to$
(γ) $[H^e]\to\mu^+(-\mathbf{b})+\mu^-(\mathbf{a})$; $P^-(-\mathbf{k})+\mu^-(\mathbf{a})[H^i]\to N^+(\mathbf{p})$; $N^+(\mathbf{p}_0)+\mu^+(-\mathbf{b})[H^i]\to P^-(-\mathbf{k})$.

2. Processes contributing to $K_{\mathbf{p}\mathbf{p}_0}{}^i$ due to H^{en}:

(a) $N^+(\mathbf{p}_0)$ destroyed before $N^+(\mathbf{p})$ created:

(α) $N^+(\mathbf{p}_0)[H^i]\to P^+(\mathbf{b})+\mu^-(-\mathbf{k})$; $P^+(\mathbf{b})[H^e]\to P^+(\mathbf{a})$; $P^+(\mathbf{a})+\mu^-(-\mathbf{k})[H^i]\to N^+(\mathbf{p})$
(β) $P^-(\mathbf{b})[H^e]\to P^+(\mathbf{a})$; $N^+(\mathbf{p}_0)[H^i]\to P^-(\mathbf{b})+\mu^-(-\mathbf{k})$; $P^+(\mathbf{a})+\mu^-(-\mathbf{k})[H^i]\to N^+(\mathbf{p})$
(γ) $N^+(\mathbf{p}_0)[H^i]\to P^+(\mathbf{b})+\mu^-(-\mathbf{k})$; $P^-(\mathbf{a})+\mu^+(-\mathbf{k})[H^i]\to N^+(\mathbf{p})$; $P^+(\mathbf{b})[H^e]\to P^-(\mathbf{a})$.

(b) $N^+(\mathbf{p})$ created before $N^+(\mathbf{p}_0)$ destroyed:

(α) $P^-(\mathbf{a})[H^i]\to N^+(\mathbf{p})+\mu^+(\mathbf{k})$; $P^-(\mathbf{b})[H^e]\to P^-(\mathbf{a})$; $N^+(\mathbf{p}_0)+\mu^+(\mathbf{k})[H^i]\to P^-(\mathbf{b})$
(β) $P^-(\mathbf{a})[H^i]\to N^+(\mathbf{p})+\mu^+(\mathbf{k})$; $N^+(\mathbf{p}_0)+\mu^+(\mathbf{k})[H^i]\to P^+(\mathbf{b})$; $P^+(\mathbf{b})[H^e]\to P^-(\mathbf{a})$
(γ) $P^-(\mathbf{b})[H^e]\to P^+(\mathbf{a})$; $P^+(\mathbf{a})[H^i]\to N^+(\mathbf{p})+\mu^+(\mathbf{k})$; $N^+(\mathbf{p}_0)+\mu^+(\mathbf{k})[H^i]\to P^-(\mathbf{b})$.

3. Processes contributing to $K_{\mathbf{p}\mathbf{p}_0{}^\delta}$ due to H^{en}:

(a) $P^-(\mathbf{b})[H^e]\rightarrow P^+(\mathbf{a})$; $N^+(\mathbf{p}_0)+P^+(\mathbf{a})[H^\delta]\rightarrow N^+(\mathbf{p})+P^-(\mathbf{b})$
(b) $P^-(\mathbf{a})+N^+(\mathbf{p}_0)[H^\delta]\rightarrow N^+(\mathbf{p})+P^+(\mathbf{k})$; $P^+(\mathbf{b})[H^e]\rightarrow P^-(\mathbf{a})$.

Here,

$$\mathbf{a}=\mathbf{k}+\mathbf{p},\quad \mathbf{b}=\mathbf{k}+\mathbf{p}_0, \tag{18}$$

and we note that none of these processes are self-energy processes (since $\mathbf{p}\neq\mathbf{p}_0$), so that (17a) should be used.

Using (5), (7), (8), and (17a), as well as properties of Dirac matrices and the usual projection operator tricks,[11] one obtains:

$$K_{\mathbf{p}\mathbf{p}_0}=a_{\mathbf{p}}{}^\dagger a_{\mathbf{p}_0}(-\pi e/2L^6)\left\{\int d\tau\, V(\mathbf{r})\exp(i(\mathbf{p}_0-\mathbf{p})\cdot\mathbf{r})\right\}(u_{\mathbf{p}}{}^*\mathfrak{M}u_{\mathbf{p}_0}), \tag{19}$$

where for general pseudovector and pseudoscalar coupling:

$$\mathfrak{M}=\frac{f^2}{\mu^2}F,\quad F\equiv F^i+F^\delta\equiv\sum_{\mathbf{k}}(F_{\mathbf{k}}{}^i+F_{\mathbf{k}}{}^\delta),\quad F^i\equiv F^{im}+F^{in}\equiv\sum_{\mathbf{k}}(F_{\mathbf{k}}{}^{im}+F_{\mathbf{k}}{}^{in}) \tag{20a}$$

$$\begin{aligned}F_{\mathbf{k}}{}^{im}=&(\epsilon_a+\epsilon_b)\frac{(1+\mathfrak{A})(1+K')(1+\mathfrak{B})}{(\epsilon_a-E_p+E)(\epsilon_b-E_{p0}+E)}-(\epsilon_a-\epsilon_b)\frac{(1+\mathfrak{A})(1+K')(1-\mathfrak{B})}{(\epsilon_a-E_p+E)(\epsilon_a+\epsilon_b-E_p+E_{p0})}\\&+(\epsilon_a-\epsilon_b)\frac{(1-\mathfrak{A})(1+K')(1+\mathfrak{B})}{(\epsilon_a+\epsilon_b-E_{p0}+E_p)(\epsilon_b-E_{p0}+E)}+(\epsilon_a+\epsilon_b)\frac{(1-\mathfrak{A})(1-K')(1-\mathfrak{B})}{(\epsilon_a+E_p+E)(\epsilon_b+E_{p0}+E)}\\&-(\epsilon_a-\epsilon_b)\frac{(1-\mathfrak{A})(1-K')(1+\mathfrak{B})}{(\epsilon_a+E_p+E)(\epsilon_a+\epsilon_b+E_p-E_{p0})}+(\epsilon_a-\epsilon_b)\frac{(1+\mathfrak{A})(1-K')(1-\mathfrak{B})}{(\epsilon_a+\epsilon_b+E_{p0}-E_p)(\epsilon_b+E_{p0}+E)}\end{aligned} \tag{20m}$$

$$\begin{aligned}F_{\mathbf{k}}{}^{in}=&-\epsilon(1+\mathfrak{K})\left\{\frac{(1+A)(1+B)}{(E_a-E_p+\epsilon)(E_b-E_{p0}+\epsilon)}-\frac{(1+A)(1-B)}{(E_a-E_p+\epsilon)(E_a+E_b-E_p+E_{p0})}\right.\\&\left.-\frac{(1-A)(1+B)}{(E_a+E_b+E_p-E_{p0})(E_b-E_{p0}+\epsilon)}\right\}(1+\mathfrak{K})\\&-\epsilon(1-\mathfrak{K})\left\{\frac{(1-A)(1-B)}{(E_a+E_p+\epsilon)(E_b+E_{p0}+\epsilon)}-\frac{(1-A)(1+B)}{(E_a+E_p+\epsilon)(E_a+E_b+E_p-E_{p0})}\right.\\&\left.-\frac{(1+A)(1-B)}{(E_a+E_b-E_p+E_{p0})(E_b+E_{p0}+\epsilon)}\right\}(1-\mathfrak{K})\end{aligned} \tag{20n}$$

$$\begin{aligned}F_{\mathbf{k}}{}^\delta=&-2\frac{(1+s)(1+A)(1-B)-s\boldsymbol{\alpha}(1+A)\cdot(1-B)\boldsymbol{\alpha}}{E_a+E_b-E_p+E_{p0}}-2\frac{(1+s)(1-A)(1+B)-s\boldsymbol{\alpha}(1-A)\cdot(1+B)\boldsymbol{\alpha}}{E_a+E_b+E_p-E_{p0}}\\&+\left(\frac{2f_0{}^2}{f^2}\right)\left(\frac{-4ti\boldsymbol{\sigma}\cdot\mathbf{a}\times\mathbf{b}}{E_aE_b}\right)\left(\frac{1}{E_a+E_b-E_p+E_{p0}}+\frac{1}{E_a+E_b+E_p-E_{p0}}\right).\end{aligned} \tag{20δ}$$

Here,

$$\begin{array}{lll}E_a=+(\mathbf{a}^2+M^2)^{\frac{1}{2}},\ \epsilon_a=+(\mathbf{a}^2+\mu^2)^{\frac{1}{2}},\text{ etc.}, & (E\equiv E_k,\ \epsilon\equiv\epsilon_k); & \rho=\mu g/f;\\ A=(\boldsymbol{\alpha}\cdot\mathbf{a}-\beta M)/E_a, & B=(\boldsymbol{\alpha}\cdot\mathbf{b}-\beta M)/E_b, & K=(\boldsymbol{\alpha}\cdot\mathbf{k}-\beta M)/E;\\ A'=-(\boldsymbol{\alpha}\cdot\mathbf{a}+\beta M)/E_a, & B'=-(\boldsymbol{\alpha}\cdot\mathbf{b}+\beta M)/E_b, & K'=-(\boldsymbol{\alpha}\cdot\mathbf{k}+\beta M)/E;\\ \mathfrak{A}=-(\boldsymbol{\alpha}\cdot\mathbf{a}+\beta\rho)/\epsilon_a, & \mathfrak{B}=-(\boldsymbol{\alpha}\cdot\mathbf{b}+\beta\rho)/\epsilon_b, & \mathfrak{K}=+(\boldsymbol{\alpha}\cdot\mathbf{k}-\beta\rho)/\epsilon.\end{array} \tag{21}$$

For pseudoscalar coupling alone ($f=0$),

$$\mathfrak{M}=g^2G,\quad G=G^m+G^n=\sum_{\mathbf{k}}(G_{\mathbf{k}}{}^m+G_{\mathbf{k}}{}^n) \tag{22a}$$

[11] See W. Heitler, *The Quantum Theory of Radiation* (Oxford University Press, London, 1947), p. 150.

$$G_{\mathbf{k}}^{m}=\frac{(1+K)}{\epsilon_a\epsilon_b}\Bigg\{\frac{\epsilon_a+\epsilon_b}{(\epsilon_a-E_p+E)(\epsilon_b-E_{p0}+E)}+\frac{\epsilon_a-\epsilon_b}{(\epsilon_a-E_p+E)(\epsilon_a+\epsilon_b-E_p+E_{p0})}$$
$$-\frac{\epsilon_a-\epsilon_b}{(\epsilon_a+\epsilon_b+E_p-E_{p0})(\epsilon_b-E_{p0}+E)}\Bigg\}+\frac{(1-K)}{\epsilon_a\epsilon_b}\Bigg\{\frac{\epsilon_a+\epsilon_b}{(\epsilon_a+E_p+E)(\epsilon_b+E_{p0}+E)}$$
$$+\frac{\epsilon_a-\epsilon_b}{(\epsilon_a+E_p+E)(\epsilon_a+\epsilon_b+E_p-E_{p0})}-\frac{\epsilon_a-\epsilon_b}{(\epsilon_a+\epsilon_b-E_p+E_{p0})(\epsilon_b+E_{p0}+E)}\Bigg\} \quad (22\text{m})$$

$$G_{\mathbf{k}}^{n}=-\frac{1}{\epsilon}\Bigg\{\frac{(1+A')(1+B')}{(E_a-E_p+\epsilon)(E_b-E_{p0}+\epsilon)}-\frac{(1+A')(1-B')}{(E_a-E_p+\epsilon)(E_a+E_b-E_p+E_{p0})}$$
$$-\frac{(1-A')(1+B')}{(E_a+E_b+E_p-E_{p0})(E_b-E_{p0}+\epsilon)}\Bigg\}-\frac{1}{\epsilon}\Bigg\{\frac{(1-A')(1-B')}{(E_a+E_p+\epsilon)(E_b+E_{p0}+\epsilon)}$$
$$-\frac{(1-A')(1+B')}{(E_a+E_p+\epsilon)(E_a+E_b+E_p-E_{p0})}-\frac{(1+A')(1-B')}{(E_a+E_b-E_p+E_{p0})(E_b+E_{p0}+\epsilon)}\Bigg\}. \quad (22\text{n})$$

In (20) and (22), the terms are listed in the same order as in the table of processes, so that for instance 2 (a β) contributes the second term of (20n). (In (20δ), the first and second lines come from the charged and neutral mesons, respectively.) We note too that the contribution of every (b) process is the same as that of the analogous (a) process, except that the signs of α, β, $E_{\mathbf{p}}$, and $E_{\mathbf{p}0}$ are reversed. The $a_{\mathbf{p}}^{\dagger}a_{\mathbf{p}0}$ in (19) stands for the matrix element of this operator between the two neutron states in question, and is $+1$ or -1, depending on the ordering of the states. It is not important physically (when $K_{\mathbf{p}\mathbf{p}_0}$ is squared to compute transition probabilities, it has no effect at all) and will not be carried further.

Charge Conservation and Ambiguity of the Integrals

Since $\sum_{\mathbf{k}}\sim(L/2\pi)^3\int dk_x dk_y dk_z$, and the operators (21) are all of order of magnitude unity (or less) for large $\mathbf{k}$, F can diverge no worse than quadratically; G no worse than logarithmically. In fact, the quadratically divergent terms of $\sum_{\mathbf{k}}F_{\mathbf{k}}$ are from processes 1 (a α) and 1 (b α), which contribute $\sim+2/k$ each to $F_{\mathbf{k}}^{im}$, and 2 (a α) and 2 (b α), which contribute $\sim-2/k$ each to $F_{\mathbf{k}}^{in}$. Thus, in both the meson and nucleon contributions, positive- and negative-energy processes contribute terms of the same sign that diverge with equal strength. (For $\sum_{\mathbf{k}}G_{\mathbf{k}}$, the situation is the same: 1 (a α) and 1 (b α) contribute $\sim(1/2k^3)$ each, while 2 (a α) and 2 (b α) contribute $\sim-1/(2k^3)$.) This contradicts the conjecture made initially that negative-energy processes would help the convergence.

The effect of negative-energy processes found here is to be expected intuitively. If, for instance, the total meson charge in a single-neutron state is considered, it is seen that this differs from the meson charge in vacuum for two reasons:

(1) The single neutron can make transitions to a proton-negative meson state, causing a net negative meson charge.

(2) Certain transitions (from negative-energy protons to positive meson+the neutron in question) that would take place in vacuum are now excluded, decreasing the positive meson charge and effectively providing a further negative meson charge. Thus, instead of canceling most of the negative meson charge, the negative-energy processes increase it.

The case with nucleon charge is exactly similar: (1) causes a positive nucleon charge while (2), preventing "dissociation" of negative-energy protons, further increases the positive nucleon charge.

A convergent matrix element is thus possible only if the meson and nucleon charge clouds, which are of opposite sign, give contributions that cancel to a sufficient extent. In fact, it will now be shown that charge-conservation implies that (19) is zero for $\mathbf{p}=\mathbf{p}_0$. Thus, the leading divergences of $F_{\mathbf{k}}$ and $G_{\mathbf{k}}$, which are independent of $\mathbf{p}$ and $\mathbf{p}_0$, must cancel. (This already guarantees the convergence of G.)

The formal statement of charge conservation is that the Hamiltonian and contact transformations are all diagonal in the total charge; i.e., they commute with the total charge operator

$$Q=e\sum_{\mathbf{k}}(N_{+\mathbf{k}}-N_{-\mathbf{k}})+e\sum_{\substack{\text{Proton}\\ \text{states only}}}N_{\mathbf{p}}. \quad (23)$$

(Note that since we will consider only changes of total charge, use of the simple charge operator rather than Heisenberg's symmetrized operator is immaterial.) By (7), H^e becomes identical to Q if $V(\mathbf{r})=1$, so that $K_{\mathbf{p}\mathbf{p}_0}$ for this $V(\mathbf{r})$ gives the change in charge due to the canonical transformations, which must be set equal to zero. Now if $\mathbf{p}=\mathbf{p}_0$, the (b) processes in the tabulation cannot occur, and (17b)

must be used for processes where H^e occurs first or last—and these give a zero contribution, as may be seen from the numerators of the corresponding terms in (20). The result is that

$$\sum_{\mathbf{k}}\left(u_{\mathbf{p}_0}^*\left[2\epsilon_b\frac{(1+\mathfrak{B})(1+K')(1+\mathfrak{B})}{(\epsilon_b-E_{p_0}+E)^2}-\epsilon\frac{(1+\mathfrak{K})(1+B)(1+B)(1+\mathfrak{K})}{(E_b-E_{p_0}+\epsilon)^2}\right]u_{\mathbf{p}_0}\right)=0. \quad (24)$$

Since the same equation holds true if $-\boldsymbol{\alpha}$, $-\boldsymbol{\beta}$, $-E_{\mathbf{p}_0}$ are substituted for $\boldsymbol{\alpha}$, $\boldsymbol{\beta}$, $E_{\mathbf{p}_0}$ in (24) (see the Appendix), it is seen that (19) is zero as asserted for $\mathbf{p}=\mathbf{p}_0$.

It is very difficult to prove (24) by direct calculation. This is connected with the naming of the momenta that has heretofore been used, which was chosen so that the electric field scatters momenta of magnitude $|\mathbf{a}|$ and $|\mathbf{b}|$ in both nucleon and meson cases, which suggests itself rather naturally. If, however, we substitute *in* $F_{\mathbf{k}}^{im}$ *and* $G_{\mathbf{k}}^{n}$ *only*

$$-(\mathbf{k}+\tfrac{1}{2}\boldsymbol{\Delta}) \text{ for } \mathbf{a}; \quad -(\mathbf{k}-\tfrac{1}{2}\boldsymbol{\Delta}) \text{ for } \mathbf{b};$$

$$-\left(\mathbf{k}+\frac{\mathbf{s}}{2}\right)=-\left(\mathbf{a}+\frac{\boldsymbol{\Delta}}{2}\right)=-\left(\mathbf{b}-\frac{\boldsymbol{\Delta}}{2}\right) \text{ for } \mathbf{k}, \quad (25)$$

where

$$\mathbf{s}=\mathbf{p}_0+\mathbf{p}, \quad \boldsymbol{\Delta}=\mathbf{p}_0-\mathbf{p} \quad (25a)$$

it can immediately be seen for $\mathbf{p}_0=\mathbf{p}$, that not only is (24) satisfied, but that $F_{\mathbf{k}}$ and $G_{\mathbf{k}}$ are identically zero. If the meson and nucleon integrals converged individually, such changes of variable would certainly be admissible. However, especially for a quadratic divergence, such a change can alter the results essentially, so that both choices of variable should be examined to verify that the results are not ambiguous. (If they were, the results obtained using the substitution (25) would be preferred, since it is known that charge conservation would then be satisfied practically as well as formally.)

We note that the substitution (25) could just as well have been made in the nucleon terms only, but this will be seen to give the same results.

Degree of Divergence and Effect of Contact Interaction

To determine whether $K_{\mathbf{p}\mathbf{p}_0}$ converges, (20) must be expanded in a power series in k^{-1}. Only the three leading terms (in k^{-1}, k^{-2}, and k^{-3}) give divergent contributions to F, so that all quantities appearing in (20) need be expanded to second order only. One then obtains for finite, but not necessarily small, $\mathbf{p}$ and $\mathbf{p}_0$, after averaging over the possible angles of the vector $\mathbf{k}$,

$$F_{\mathbf{k}}^{i}\sim[2\boldsymbol{\Delta}^2-\tfrac{2}{3}(E_{p_0}-E_p)^2+2i\boldsymbol{\sigma}\cdot\mathbf{p}_0\times\mathbf{p}]\cdot k^{-3} \quad +\text{terms in } k^{-4} \text{ etc.}$$

$$F_{\mathbf{k}}^{\delta}\sim\left[-\left(\frac{5-4s}{3}\right)\boldsymbol{\Delta}^2+\left(\frac{1-4s}{3}\right)(E_{p_0}-E_p)^2 -2i\boldsymbol{\sigma}\cdot\mathbf{p}_0\times\mathbf{p}\right]\cdot k^{-3}+\text{terms in } k^{-4} \text{ etc.}$$

$$F_{\mathbf{k}}\sim\left(\frac{1+4s}{3}\right)[\boldsymbol{\Delta}^2-(E_{p_0}-E_p)^2]\cdot k^{-3} \quad +\text{terms in } k^{-4} \text{ etc.} \quad (26)$$

The lengthy algebra used to derive (26), which made use of the substitutions listed in the Appendix, will not be reproduced here.

If the substitution (25) is made in (20), precisely the same result (26) is obtained, so that any ambiguity is unlikely. In fact, if $F_{\mathbf{k}}^{im}$ is expanded in the original notation, and then $-(\mathbf{k}+\frac{1}{2}\mathbf{s})$ is substituted for $\mathbf{k}$ (before the averaging over the angles of $\mathbf{k}$), further expanded, and then averaged over angles, only the terms in $\mathbf{s}^2$ and $\boldsymbol{\sigma}$ can be changed. The former is, however, zero by charge conservation or direct computation, while the spin term is found to be actually unchanged. Moreover, it is immaterial whether (25) is used on the meson or nucleon contributions to $F_{\mathbf{k}}$.

The absence of a term in ρ^2 (or even ρ) in (26) again verifies the convergence of the pseudoscalar coupling contribution. Moreover, since the divergence of G^m and G^n is only logarithmic, a change of variables such as (25) is very unlikely to change the value of the matrix element.

We note that $F_{\mathbf{k}}$ has a relativistically invariant form, which would seem to indicate that relativistic invariance has not been lost due to divergences. It is important that if $F_{\mathbf{k}}^{\delta}$ were neglected, the result would not have an invariant form. Also, the spin-dependent term, which will be seen in Section IV to represent the magnetic moment, diverges if $F_{\mathbf{k}}^{\delta}$ is neglected. However, if the contact term is consistently handled, the magnetic moment is seen to converge for any value of s, i.e., regardless of whether or not any invariant contact term is added to the Lagrangian. This convergence has been noticed for the special choice $s=-1$ by Case.[12]

However, the matrix element F will diverge unless we choose $s=-\frac{1}{4}$. On the other hand, the physical significance of the contact terms is rather dubious, so that results critically dependent on them, including the convergence of the magnetic

[12] K. M. Case, thesis, Harvard University (1948); Phys. Rev. 74, 1884 (1948).

moments, must be accepted with great caution. In this connection, note that the neutral meson part of (20δ) sums to zero, at least if $E_p=E_{p0}$, as is most easily seen by using (25). It should also be mentioned that the choice $s=-\frac{1}{3}$ has sometimes been recommended to remove contact terms from the static nuclear potentials, but this is a very questionable procedure.

Comparison of Pseudoscalar and Pseudovector Couplings

Dyson has shown rather generally[13] that the pseudoscalar and pseudovector couplings give equivalent results, at least to first order. This may be seen directly from (7), which gives for the matrix element for a transition from a nucleon of momentum $\mathbf{p}_0$ to a meson of momentum $\mathbf{k}$ and nucleon of momentum $\mathbf{p}=\mathbf{p}_0-\mathbf{k}$ the value

$$(2\pi/\epsilon L^3)^{\frac{1}{2}}\{-g(u_p{}^*\alpha_1\alpha_2\alpha_3\beta u_{p0}) + (f/\mu)(u_p{}^*[\epsilon\alpha_1\alpha_2\alpha_3-i\boldsymbol{\sigma}\cdot\mathbf{k}]u_{p0})\}$$

and similarly for absorption. If both nucleons have positive energy, it follows from the Appendix that this is just

$$\left(\frac{2\pi}{\epsilon L^3}\right)^{\frac{1}{2}}\left\{\left(-\frac{g}{2M}\right)\left(u_p{}^*i\boldsymbol{\sigma}\cdot\left[-\mathbf{k}+\left(\frac{E_{p0}-E_p}{E_{p0}+E_p}\right)(\mathbf{p}+\mathbf{p}_0)\right]u_{p0}\right) + \left(\frac{f}{\mu}\right)\left(u_p{}^*i\boldsymbol{\sigma}\cdot\left[-\mathbf{k}+\frac{\epsilon}{E_{p0}+E_p}(\mathbf{p}+\mathbf{p}_0)\right]u_{p0}\right)\right\}. \quad (27)$$

Thus, apart from the second term in each square bracket, which is negligible for low momentum processes, the couplings behave identically; a pseudovector coupling of strength f behaving like a pseudoscalar coupling

$$g=-(2M/\mu)f. \quad (28)$$

In many calculations (such as of static nuclear forces, where only positive-energy processes are considered and only in non-relativistic approximation) the two couplings give rise to the same result. Although this has frequently been overlooked, one need only put $(f-\mu g/2M)$ for f to rectify the omission of pseudoscalar coupling. (Note that from (28) a g^2 of 30 is no more "strongly coupled" than an f^2 of about 0.2.)

It may thus seem surprising that pseudovector coupling can give a divergent interaction while pseudoscalar does not. However, a closer inspection of (27) for high momentum processes ($|\mathbf{k}|\gg M$ or $|\mathbf{p}_0|$) shows that the square bracket of the g term approaches $-\mathbf{k}+\mathbf{k}$, while that of the f term approaches $-\mathbf{k}-\mathbf{k}$, so that the pseudoscalar coupling matrix elements are less divergent. Moreover, many matrix elements between nucleons of different energy signs occur in the calculations, and here the couplings differ considerably.

It is very instructive to extend Dyson's proof to our problem. We define H_f and H_g to be the Hamiltonians (6) with $g=0$ and $f=0$ respectively. We also omit the neutral meson field—which we have seen makes no difference in the neutron scattering element—and set $s=0$ for simplicity. If a unitary transformation $\exp(iR)$ of H_f is carried out, with $R=(4\pi)^{\frac{1}{2}}(f/\mu)\int d\tau(B_0\Psi+B_0{}^\dagger\Psi^\dagger)$, we obtain to second order for the transformed H_f, after considerable reduction, $\exp(iR)H_f\exp(-iR)=H_g+H'$, where

$$H'=(4\pi f^2/\mu^2)\int d\tau\Big\{\tfrac{1}{2}(B_0{}^\dagger B_0-B_0B_0{}^\dagger) + \frac{i}{2}[(\psi^*\tau^0\psi)(\Pi\Psi-\Pi^\dagger\Psi^\dagger) + (\psi^*\boldsymbol{\alpha}\tau^0\psi)\cdot(\Psi\boldsymbol{\nabla}\Psi^\dagger-\Psi^\dagger\boldsymbol{\nabla}\Psi)] - (\psi^*\beta M\psi)(\Psi^\dagger\Psi+\Psi\Psi^\dagger)\Big\},$$

and in H_g, g is given by (28). (It is convenient to perform the reduction in coordinate representation.)

In diagonalizing the non-electrical part of H_f, we may first carry out the transformation $\exp(iR)$, and we then obtain for the neutron scattering element precisely the value for pseudoscalar coupling with an additional term K_{ea}' given by (cf. (17a)):

$$K_{ea}'=\frac{H_{ew}'H_{wa}{}^e}{E(e)-E(w)}+\frac{H_{ew}{}^eH_{wa}'}{E(a)-E(w)}.$$

Only two transition schemes give non-zero contributions:

1. $[H^e]\rightarrow\mu^+(\mathbf{a})+\mu^-(-\mathbf{b})$; $\mu^+(\mathbf{a})+\mu^-(-\mathbf{b})+N^+(\mathbf{p}_0)[H']\rightarrow N^+(\mathbf{p})$.
2. $N^+(\mathbf{p}_0)[H']\rightarrow N^+(\mathbf{p})+\mu^+(-\mathbf{a})+\mu^-(\mathbf{b})$; $\mu^+(-\mathbf{a})+\mu^-(\mathbf{b})[H^e]\rightarrow$.

One obtains finally for the contribution to $F_{\mathbf{k}}$ of (20a):

$$F_{\mathbf{k}}'=\left(\frac{\epsilon_b-\epsilon_a}{\epsilon_a\epsilon_b}\right)\left[\frac{(\epsilon_b-\epsilon_a)+\boldsymbol{\alpha}\cdot(\mathbf{a}+\mathbf{b})}{\epsilon_a+\epsilon_b+(E_{p0}-E_p)} + \frac{(\epsilon_b-\epsilon_a)-\boldsymbol{\alpha}\cdot(\mathbf{a}+\mathbf{b})}{\epsilon_a+\epsilon_b-(E_{p0}-E_p)}\right].$$

If $E_p=E_{p0}$, $F_{\mathbf{k}}'$ becomes $2(\epsilon_b-\epsilon_a)^2/[\epsilon_a\epsilon_b(\epsilon_a+\epsilon_b)]$, which is rigorously spin-independent. Thus H' gives

[13] F. J. Dyson, Phys. Rev. **73**, 929 (1948).

zero contribution to the magnetic moment, so that —to second order at least—pseudoscalar and pseudovector couplings give exactly the same neutron magnetic moment. Investigation of the term proportional to s in (20) shows it to be spin-independent, so this equality of the magnetic moments holds even for non-zero s. The arguments may also be extended to the case of the proton moment.

However, $\sum_{\mathbf{k}} F_{\mathbf{k}}'$ itself diverges logarithmically, since it is easily verified that asymptotically, $F_{\mathbf{k}}' \sim \frac{1}{3}[\boldsymbol{\Delta}^2-(E_{p0}-E_p)^2]k^{-3}$. Since H_θ gives no divergent contribution, $F_{\mathbf{k}}'$ is the only term giving rise to a divergence, and $F_{\mathbf{k}}$ itself $\sim\frac{1}{3}[\boldsymbol{\Delta}^2-(E_{p0}-E_p)^2]k^{-3}$. This agrees exactly with (26) (since we have here put $s=0$), which was computed entirely independently. We note that H' has self-energy terms corresponding to an infinite mass renormalization, but as is to be expected (cf. Section VI), it contains no "charge renormalization" terms.

It thus seems that the pseudovector element diverges genuinely (except for the special choice of s mentioned). On the other hand, Case, using the newer methods, has recently reported that pseudovector and pseudoscalar couplings are exactly equivalent to second order insofar as scattering in an electric field is concerned.[14] The reason for this discrepancy is not known to us at present. If it is not spurious, it may prove to be of great interest.

In any case, the greater simplicity of the pseudoscalar coupling, its freedom from questionable contact interactions, its apparently stronger convergence, and its equivalence to pseudovector coupling in the theory of nuclear forces, are arguments for its exclusive use in the present preliminary stage of the theory. Only pseudoscalar coupling will be considered in Sections IV and V.

IV. THE NEUTRON-ELECTRON INTERACTION AND MAGNETIC MOMENT OF THE NEUTRON

Determination from Matrix Element

In a static electric field, only energy-conserving processes are of interest; i.e., we may take $E_p=E_{p0}$. In this case, G^m, etc., may be written, after using the Appendix, in terms of the following scalars:

$$\mathbf{p}^2=\mathbf{p}_0^2,\quad \mathbf{p}\cdot\mathbf{p}_0,\quad \boldsymbol{\sigma}\cdot\mathbf{p},\quad \boldsymbol{\sigma}\cdot\mathbf{p}_0,\quad \boldsymbol{\sigma}\cdot\mathbf{p}\times\mathbf{p}_0,$$

which (apart from the masses) are the only independent ones available. As may easily be verified, $\boldsymbol{\sigma}$ enters only in triple products involving a cross-product of two other vectors, which either vanishes when averaged over angles, or takes the form $\boldsymbol{\sigma}\cdot\mathbf{p}\times\mathbf{p}_0$. Thus the expressions will take the form (using charge conservation):

$$\begin{aligned}
G^m/L^3&=C_0+(\mathbf{s}^2/M^2)C_s+(\boldsymbol{\Delta}^2/M^2)C_\Delta{}^m\\
&\quad+(i\boldsymbol{\sigma}\cdot\mathbf{p}_0\times\mathbf{p}/M^2)C_\sigma{}^m\\
G^n/L^3&=-C_0-(\mathbf{s}^2/M^2)C_s+(\boldsymbol{\Delta}^2/M^2)C_\Delta{}^n\\
&\quad+(i\boldsymbol{\sigma}\cdot\mathbf{p}_0\times\mathbf{p}/M^2)C_\sigma{}^n\\
G/L^3&=(\boldsymbol{\Delta}^2/M^2)(C_\Delta{}^m+C_\Delta{}^n)\\
&\quad+(i\boldsymbol{\sigma}\cdot\mathbf{p}_0\times\mathbf{p}/M^2)(C_\sigma{}^m+C_\sigma{}^n)\qquad(29)
\end{aligned}$$

where $C_0(\mu/M)$ is a logarithmically divergent integral and C_s, $C_\Delta{}^m$, $C_\Delta{}^n$, $C_\sigma{}^m$, $C_\sigma{}^n$ are dimensionless functions of (μ/M), $(\mathbf{s}^2/M^2)$, and $(\boldsymbol{\Delta}^2/M^2)$. (Since $\mathbf{p}$ and $\mathbf{p}_0$ of interest are $\ll M$, the C's will be computed for $\boldsymbol{\Delta}^2/M^2=\mathbf{s}^2/M^2=0$; i.e., only the first non-vanishing terms of an expansion in $\mathbf{p}$ and $\mathbf{p}_0$ will be used.) The matrix element for a transition between the two single-neutron states in the electric field is then, by (19),

$$\begin{aligned}
K_{\mathbf{pp}_0}=\left(-\frac{\pi e g^2}{2L^3}\right)&\left\{\int d\tau V(\mathbf{r})\exp(i\boldsymbol{\Delta}\cdot\mathbf{r})\right\}\\
&\times\left(u_{\mathbf{p}}{}^*\left[\frac{\boldsymbol{\Delta}^2}{M^2}(C_\Delta{}^m+C_\Delta{}^n)\right.\right.\\
&\left.\left.+\frac{i\boldsymbol{\sigma}\cdot\mathbf{p}\times\mathbf{p}_0}{M^2}(C_\sigma{}^m+C_\sigma{}^n)\right]u_{\mathbf{p}_0}\right).\qquad(30)
\end{aligned}$$

On the other hand, a magnetic dipole moment $\boldsymbol{\mu}$ is associated with the spin-orbit interaction energy $-\boldsymbol{\mu}\cdot(-\nabla V)\times[-(i/M)\nabla]$ ($-i\nabla$ is the momentum operator), which has a matrix element for the transition in question of

$$\begin{aligned}
\int(L^{-\frac{1}{2}}u_{\mathbf{p}}{}^*\exp(-i\mathbf{p}\cdot\mathbf{r}))&\left(-\boldsymbol{\mu}\cdot\nabla V\times\frac{i}{M}\nabla\right)\\
&\times(L^{-\frac{1}{2}}u_{\mathbf{p}_0}\exp(i\mathbf{p}_0\cdot\mathbf{r}))d\tau.
\end{aligned}$$

This is seen to be, apart from a neglected surface integral,

$$(\mu_N e/2M^2L^3)\left\{\int d\tau V(\mathbf{r})\exp(i\boldsymbol{\Delta}\cdot\mathbf{r})\right\}(u_{\mathbf{p}}{}^*i\boldsymbol{\sigma}\cdot\mathbf{p}\times\mathbf{p}_0u_{\mathbf{p}_0})$$

where we have put $\boldsymbol{\mu}=\mu_N(e/2M)\boldsymbol{\sigma}$; μ_N being the neutron moment in nuclear magnetons. Comparing the above expression with (30), we obtain for the neutron moment

$$\mu_N=-\pi g^2(C_\sigma{}^m+C_\sigma{}^n).\qquad(31)$$

(Note that as in the Schwinger calculation of radiative corrections to the electron spin-orbit interaction, no Thomas factor must be used.)

In the neutron scattering experiments from which the neutron-electron interaction is determined,[5,7] spin-dependent effects are not detected because of lack of polarization of both neutron beam and

[14] K. M. Case, Phys. Rev. 75, 1306 (1949).

scattering sample, which averages out interference between spin-dependent neutron-electron and neutron-nucleus scattering. Thus only the C_Δ part of (30) is to be compared with these experiments, which may be done, for instance, by inserting the effective atomic for $V(\mathbf{r})$ in (30).

Alternately, the experimental result may be given in terms of a neutron-electron potential $U(\mathbf{r})$. This would give, for an electron bound to a fixed position (taken as the origin), a matrix element between the two neutron states of

$$\int d\tau (L^{-\frac{1}{2}} u_{\mathbf{p}}^* \exp(-i\mathbf{p}\cdot\mathbf{r}))\, U(\mathbf{r})\, (L^{-\frac{1}{2}} u_{\mathbf{p}_0} \exp(i\mathbf{p}_0\cdot\mathbf{r})).$$

If $U(\mathbf{r})$ has a range short compared to the neutron wave-lengths—a condition well satisfied—this reduces to $\{L^{-3}\int d\tau U(\mathbf{r})\}(u_p^* u_{p0})$. Comparing this to (30) after noting that $\nabla^2 \exp(i\boldsymbol{\Delta}\cdot\mathbf{r}) = -\boldsymbol{\Delta}^2 \exp(i\boldsymbol{\Delta}\cdot\mathbf{r})$, using Green's theorem and then discarding the surface integral, and using $\nabla^2 V = -4\pi\rho(\mathbf{r}) = +4\pi e\delta(\mathbf{r})$ for an electron fixed at the origin, the expression

$$\int U(r)d\tau \equiv U_0 V_e = (2\pi^2 e^2 g^2/M^2)(C_\Delta{}^m + C_\Delta{}^n) \quad (32)$$

is obtained, where by convention $V_e = 4\pi/3(e^2/mc^2)^3$.

Computation for Pseudoscalar Coupling

Using the Appendix, (22) can be written as a multiple of the unit operator plus the scalar product of $\boldsymbol{\sigma}$ and a vector. The spin-dependent term, which contains the magnetic moment, converges even before averaging over angles, so transformations, as (25), do not change the magnetic moment.

If the part of $G_\mathbf{k}$ not involving $\boldsymbol{\sigma}$ is expanded in a series in $\mathbf{p}$ and $\mathbf{p}_0$ (or $\mathbf{s}$ and $\boldsymbol{\Delta}$), one obtains a logarithmically divergent term in $\mathbf{k}$ alone, plus converging terms. If (25) is used, the term in $\boldsymbol{\Delta}^2$ is not influenced at all, while the $\mathbf{s}^2$ term, which is of no interest, is changed in form but integrates to zero in either case.

The results are:

$$C_\sigma{}^m = \int_0^\infty \frac{dk}{2\pi^2}\frac{4k^2}{R^2}\left[\frac{1}{E}+\frac{1}{\epsilon}-\frac{2k^2}{3\epsilon^2}\left(\frac{2}{E}+\frac{1}{2\epsilon}+\frac{2}{ER}\right)\right] = \int_0^\infty \frac{dk}{2\pi^2}\frac{16k^4(E+\epsilon)^2}{3E^2\epsilon R^3}\left(1+\frac{\epsilon R}{4E(E+\epsilon)^2}\right) \quad (33m)$$

$$C_\sigma{}^n = \int_0^\infty \frac{dk}{2\pi^2}\frac{4k^2}{R^2E^4}\left[2E+\epsilon+\frac{4E}{3R}+\frac{R}{2E}\right] \quad (33n)$$

$$C_\Delta{}^m = -\int_0^\infty \frac{dk}{2\pi^2}\frac{k^2}{R^2}\left\{\frac{2}{E}+\frac{1}{2\epsilon}+\frac{k^2}{2\epsilon^3}\left(2-\frac{k^2}{3\epsilon^2}\right)+\left(\frac{\epsilon^2+k^2}{\epsilon}+\frac{2k^2}{E}\right)\left[\frac{2E}{\epsilon R}\left(1-\frac{k^2}{3\epsilon^2}\right)-\frac{4k^2(E+\epsilon)^2}{3\epsilon^2R^2}\right]\right\} \quad (34m)$$

$$C_\Delta{}^n = -\int_0^\infty \frac{dk}{2\pi^2}\frac{k^2}{R^2}\left\{\left(\frac{R}{\epsilon}-\frac{2}{E}\right)\left[\frac{4k^2(E+\epsilon)^2}{3E^2R^2}-\frac{2\epsilon}{ER}\left(1-\frac{k^2}{3E^2}\right)\right]\right.$$
$$\left.+\frac{k^2(2E+\epsilon)}{3E^3\epsilon}\left(\frac{R}{E^2}-1\right)-\frac{k^2}{E^3}\left(1+\frac{1}{3E^2}\right)+\frac{2k^2}{3E^4\epsilon}\right\} \quad (34n)$$

where

$R=(E+\epsilon)^2-1$ and $E=(k^2+1)^{\frac{1}{2}}$, $\epsilon=[k^2+(\mu/M)^2]^{\frac{1}{2}}$,

which differs slightly from previous notation. The second form of $C_\sigma{}^m$ is obtained with (25), and was used as a check.

We note that (33m) and (33n), taken together with (43c) and (43s) below, agree exactly with the results of a recent calculation of the magnetic moments by J. M. Luttinger, who used an entirely different method.[15]

[15] J. M. Luttinger, Helv. Phys. Acta **21**, 483 (1948), especially Eqs. (12), (23), and (25), after correcting some misprints. Note that his μ_p and g^2 correspond to our μ_p-1 and $g^2/2$. Unfortunately, Luttinger substituted for his g^2 twice the experimental value for symmetrical theory and four times the experimental value for pure charged theory, and made some additional numerical errors in his final substitution. He points out that the integrals corresponding to our (33) are elementary and may be brought to familiar form by introducing the variable $Z=(E+\epsilon)^2$. This is also true for (34).

Equations (33) and (34), integrated graphically for $\mu/M=0.154$ corresponding to a meson mass of 282 e.m., give

$$2\pi^2 C_\sigma{}^m = 0.343; \quad 2\pi^2 C_\sigma{}^n = 0.477;$$
$$2\pi^2 C_\Delta{}^m = -0.520; \quad 2\pi^2 C_\Delta{}^n = -0.001. \quad (35)$$

Using (31) and (32), it follows that

$$\mu_N = -0.128g^2; \quad U_0 = -0.340g^2 \text{ kev}. \quad (36)$$

Further discussion of the behavior of the integrands at low momenta, variation with μ/M, etc., will be left to Section VI.*

V. THE MAGNETIC MOMENT OF THE PROTON

The matrix element for the transition from a single-proton state of momentum $\mathbf{p}_0$ to one of mo-

* For $\mu/M=0.50$, (918 e.m.), $2\pi^2 C_\Delta{}^m = -0.118$, $2\pi^2 C_\Delta{}^n = -0.010$, $U_0 = -0.0834g^2$ kev.

mentum $\mathbf{p}$ in an electric field is given by the ordinary Dirac term plus $K_{\mathbf{pp_0}}$ as defined by (17). The Dirac term, as is well known, gives a spin-orbit interaction corresponding to one nuclear magneton (with a Thomas factor of $\frac{1}{2}$) when a reduction to two-component wave functions is made. The anomalous part of the proton moment, μ_P-1 nuclear magnetons, is given in analogy to (31) by

$$\mu_P-1=-\pi g^2(D_\sigma{}^m+D_\sigma{}^n). \tag{37}$$

Here, $D_\sigma{}^m$ and $D_\sigma{}^n$ are the coefficients, exactly analogous to $C_\sigma{}^m$ and $C_\sigma{}^n$ in (29), in the expansion of the operators G^{+m} and G^{+n}, where $\mathfrak{M}$ in (19) is given by

$$\mathfrak{M}\equiv g^2G^+\equiv g^2(G^{+m}+G^{+n}). \tag{37a}$$

Discussions and interpretations will be considered in Section VI.

Charged Meson Contribution

The processes that contribute to the meson part G^{+m} of G^+ are precisely those under (1) in the tabulation of Section III, except that the P's and N's must be interchanged, as well as the signs of all the meson charges. It is easily seen from (7) that this change does not alter any of the matrix elements, except those involving H^e, where it always reverses the sign. Thus, as was to be expected intuitively, we obtain

$$G_{\mathbf{k}}{}^{+m}=-G_{\mathbf{k}}{}^m; \quad D_\sigma{}^m=-C_\sigma{}^m. \tag{38}$$

For the nucleon contribution, none of the processes (2) of Section III, or slight modifications, can be used. For instance, if the initial proton state changes to a virtual neutron plus positive meson state, the neutron cannot interact with the field. However, the following processes are now possible:

1. $P^+(\mathbf{p_0})[H^i]\rightarrow N^+(\mathbf{b})+\mu^+(-\mathbf{k})$; $P^-(\mathbf{p_0})[H^e]\rightarrow P^+(\mathbf{p})$; $N^+(\mathbf{b})+\mu^+(-\mathbf{k})[H^i]\rightarrow P^-(\mathbf{p_0})$.
2. $P^-(\mathbf{p_0})[H^i]\rightarrow N^+(\mathbf{a})+\mu^+(-\mathbf{k})$; $P^+(\mathbf{p_0})[H^e]\rightarrow P^-(\mathbf{p})$; $N^+(\mathbf{a})+\mu^+(-\mathbf{k})[H^i]\rightarrow P^+(\mathbf{p})$.
3. (a) $P^+(\mathbf{p_0})[H^e]\rightarrow P^+(\mathbf{p})$; $P^+(\mathbf{p})[H^i]\rightarrow N^+(\mathbf{a})+\mu^+(\mathbf{k})$; $N^+(\mathbf{a})+\mu^+(-\mathbf{k})[H^i]\rightarrow P^+(\mathbf{p})$.
   (b) $P^+(\mathbf{p_0})[H^e]\rightarrow P^+(\mathbf{p})$; $N^-(\mathbf{b})[H^i]\rightarrow P^+(\mathbf{p_0})+\mu^-(\mathbf{k})$; $P^+(\mathbf{p_0})+\mu^-(\mathbf{k})[H^i]\rightarrow N^-(\mathbf{b})$.
4. (a) $P^-(\mathbf{p_0})[H^e]\rightarrow P^+(\mathbf{p})$; $P^+(\mathbf{p_0})[H^i]\rightarrow N^+(\mathbf{b})+\mu^+(-\mathbf{k})$; $N^+(\mathbf{b})+\mu^+(-\mathbf{k})[H^i]\rightarrow P^-(\mathbf{p_0})$.
   (b) $P^-(\mathbf{p_0})[H^e]\rightarrow P^+(\mathbf{p})$; $N^-(\mathbf{b})[H^i]\rightarrow P^-(\mathbf{p_0})+\mu^-(\mathbf{k})$; $P^+(\mathbf{p_0})+\mu^-(\mathbf{k})[H^i]\rightarrow N^-(\mathbf{b})$.
5. (a) $P^+(\mathbf{p_0})[H^i]\rightarrow N^+(\mathbf{b})+\mu^+(-\mathbf{k})$; $N^+(\mathbf{b})+\mu^+(-\mathbf{k})[H^i]\rightarrow P^+(\mathbf{p_0})$; $P^+(\mathbf{p_0})[H^e]\rightarrow P^+(\mathbf{p})$.
   (b) $N^-(\mathbf{a})[H^i]\rightarrow P^+(\mathbf{p})+\mu^-(\mathbf{k})$; $P^+(\mathbf{p})+\mu^-(\mathbf{k})[H^i]\rightarrow N^-(\mathbf{a})$; $P^+(\mathbf{p_0})[H^e]\rightarrow P^+(\mathbf{p})$.
6. (a) $P^-(\mathbf{p})[H^i]\rightarrow N^+(\mathbf{a})+\mu^+(-\mathbf{k})$; $N^+(\mathbf{a})+\mu^+(-\mathbf{k})[H^i]\rightarrow P^+(\mathbf{p})$; $P^+(\mathbf{p_0})[H^e]\rightarrow P^-(\mathbf{p})$.
   (b) $N^-(\mathbf{a})[H^i]\rightarrow P^+(\mathbf{p})+\mu^-(\mathbf{k})$; $P^-(\mathbf{p})+\mu^-(\mathbf{k})[H^i]\rightarrow N^-(\mathbf{a})$; $P^+(\mathbf{p_0})[H^e]\rightarrow P^-(\mathbf{p})$.

Note that

(*i*) All of the above processes in which an H^i transition follows an H^i transition are self-energy processes, so that the substitutions (17b) must be made in (17a).

(*ii*) The above list of processes is exhaustive, except that processes in which neither $P^+(\mathbf{p})$ nor $P^+(\mathbf{p_0})$ are involved in the H^i transitions can also occur. These, however, cancel since the contribution of such a process to the third term of (17a) just compensates the contribution to the first two (for which (17b) must be used). These processes correspond to irrelevant vacuum fluctuations.

(*iii*) 4 (*a*) cancels half the contribution of 1; 6 (*a*) cancels half of 2.

In the usual manner, the above processes are found to result in a total contribution:

$$G_{\mathbf{k}}{}^{+n}=\frac{1}{2\epsilon}\left\{\frac{1+A'}{(E_a+\epsilon-E_p)^2}+\frac{1-A'}{(E_a+\epsilon+E_p)^2}\right\}\times\left(1+\frac{\boldsymbol{\alpha}\cdot\mathbf{p}+\beta M}{E_p}\right)+\frac{1}{2\epsilon}\left(1+\frac{\boldsymbol{\alpha}\cdot\mathbf{p_0}+\beta M}{E_{p0}}\right)\times\left\{\frac{1+B}{(E_b+\epsilon-E_{p0})^2}+\frac{1-B'}{(E_b+\epsilon+E_{p0})^2}\right\}. \tag{39}$$

It is significant that the highest term in a power series expansion in k^{-1} is $+(1/k^3)$. Since the highest term of $G_{\mathbf{k}}{}^{+m}$ (see (38) and Section III) is $-(1/k^3)$, these two terms, which give rise separately to logarithmically divergent contributions, just cancel, so that $G^+=G^{+m}+G^{+n}$ converges as in the neutron case. One could then compute the correction to Rutherford scattering of protons and electrons, but this will not be done here.

The spin-dependent term, not only the first term of the power series expansion, is found from (39), by a brief calculation, to be zero exactly. Thus

$$D_\sigma{}^n=0 \quad \text{(charged mesons)}. \tag{40}$$

This result is physically clear, since all the processes in the above table are just contributions from the renormalization of the nucleon wave function, which is evidently a pure numerical factor independent of spin. Renormalization of the nucleon wave function might change the Dirac moment, but this would also only appear on reduction to two-component wave functions (see Section VI).

Neutral Mesons; Symmetrical Theory

Although neutral mesons contribute to neither neutron moment nor neutron-electron interaction, they contribute to proton processes. There is no meson contribution due to neutral mesons, and the nucleon contribution arises from the following two

sets of processes (again, canceling vacuum fluctuations are neglected):

(a) Every transition listed above under charged mesons, except that N must be changed to P, and μ^+, μ^- to μ^0. Since for neutral mesons the matrix element for emission or absorption of μ^0 by P is given by $-(2\pi/\epsilon L^3)^{\frac{1}{2}}g_0\alpha_1\alpha_2\alpha_3\beta$ (see (7)) as opposed to $-(2\pi/\epsilon L^3)^{\frac{1}{2}}g\alpha_1\alpha_2\alpha_3\beta$ for emission or absorption of charged mesons by neutrons or protons, this gives a contribution to G^+ of precisely $(g_0/g)^2$ times (39), or

$$G_{\mathbf{k}}^{0a}=(g_0/g)^2G_{\mathbf{k}}^{+n}=\tfrac{1}{2}G_{\mathbf{k}}^{+n};\quad D_\sigma^{0a}=0 \qquad (41)$$

since $g_0=g/\sqrt{2}$ for symmetrical theory. By (40), this gives rise to no spin-dependent term, i.e., to no contribution to the neutron moment.

(b) Every transition listed under (2) in the tabulation of Section III is possible, except that N must be changed to P and μ^+, μ^- to μ^0. Just as above, this gives precisely $G_{\mathbf{k}}^n$, apart from a factor $(g_0/g)^2$ or $\frac{1}{2}$. Thus,

$$G_{\mathbf{k}}^{0b}=(g_0/g)^2G_{\mathbf{k}}^{n}=\tfrac{1}{2}G_{\mathbf{k}}^{n};\quad D_\sigma^{0b}=\tfrac{1}{2}C_\sigma^n. \qquad (42)$$

Note that the highest term in the expansion of $G_{\mathbf{k}}^{0a}$ is $+(g_0/g)^2(1/k^3)$, while that of $G_{\mathbf{k}}^{0b}$ is $-(g_0/g)^2(1/k^3)$. The sum $G^0=G^{0a}+G^{0b}$ thus converges.

The final result for the magnetic moments in nuclear magnetons is thus:

$$\mu_N=-\pi g^2(C_\sigma^m+C_\sigma^n);\quad \mu_P-1=+\pi g^2C_\sigma^m \qquad \text{(pure charged)} \quad (43c)$$

and

$$\mu_N=-\pi g^2(C_\sigma^m+C_\sigma^n);\quad \mu_P-1=+\pi g^2(C_\sigma^m-\tfrac{1}{2}C_\sigma^n) \qquad \text{(symmetrical)} \quad (43s)$$

where C_σ^m and C_σ^n are given by (33). This agrees with results obtained recently by Case, as well as with the results of Luttinger.

For $(\mu/M)=0.154$, (43) becomes

$$\mu_N=-0.128g^2;\quad \mu_P-1=+0.0535g^2 \qquad \text{(pure charged)} \quad (44c)$$

$$\mu_N=-0.128g^2;\quad \mu_P-1=+0.0164g^2 \qquad \text{(symmetrical)}. \quad (44s)$$

VI. NON-RELATIVISTIC METHODS, THE CHARGE CLOUD, AND COMPARISON WITH EXPERIMENT

In this section, the previous results, especially those pertaining to the neutron-electron interaction, will be discussed in a more qualitative and pictorial manner, and the connection with "non-relativistic" methods and experimental results will be given.

The Non-Relativistic Approximation. Comparison with Present Method

In the usual "non-relativistic" method (more properly, non-relativistic nucleon method), it is assumed that the nucleon is so heavy that it can be well localized, that negative-energy processes, which involve energy changes $\sim 2M$, contribute negligibly, and that the nucleon recoil is negligibly small. In fact, M is usually set equal to infinity at the outset and the nucleon is taken as localized at a point. This procedure gives zero for calculations with pseudoscalar coupling, as is evident from (27) or (28), and a slightly modified procedure will be discussed below in connection with the charge cloud. First, however, we will consider a different method that is less graphic, but simpler and more direct.

We will assume that the nucleon mass M, though finite, is so large that all quantities can be expanded in a series in M^{-1}, and only the term of lowest order kept. The scattering element K_{pp_0}, as well as (29), (31), and (32), may still be used, though matrix elements and energy denominators will be replaced by the simpler "non-relativistic" expressions.

In general, processes involving negative-energy nucleons are thus excluded because of the large energy denominators, so only processes 1 (a α), 1 (a β), 1 (a γ), and 2 (a α) of Section III are involved. For pseudoscalar coupling, their contribution can easily be computed using the simpler expressions from the start, or, since we have already done the work, directly from the appropriate terms in the exact expression (22). In either case we easily obtain

$$G_{\mathbf{k}}^{m1}=\frac{2}{M^2}\frac{\mathbf{a}\cdot\mathbf{b}+i\boldsymbol{\sigma}\cdot\mathbf{a}\times\mathbf{b}}{\epsilon_a\epsilon_b(\epsilon_a+\epsilon_b)};\quad G_{\mathbf{k}}^{n1}=-\frac{1}{M^2}\frac{k^2}{\epsilon^3}. \qquad (45)$$

Note that G^{m1} and G^{n1} individually diverge quadratically, and the sum G^1 diverges logarithmically. However, since it is known that the exact expressions for G^1 converge, we can compute it approximately by integrating only up to a finite cut-off momentum. Since the integrand is large only in the neighborhood of $|\mathbf{k}|\sim\mu$, and the integral varies quite slowly with the cut-off momentum if it is taken several times as large as μ, this procedure will give a result close to the true value.

At this point, a phenomenon peculiar to pseudoscalar coupling must be mentioned. Matrix elements of H^i between positive-energy states are proportional to M^{-1}, while matrix elements joining positive- and negative-energy states are seen to be of order unity. Thus even though the energy denominators are large, the total contribution of the processes 1 (b) and 2 (b α) of Section III are seen to be of the same order in M as (45). In fact, these processes contribute

$$G_{\mathbf{k}}^{m2}=\frac{2}{M^2}\frac{1}{\epsilon_a+\epsilon_b};\quad G_{\mathbf{k}}^{n2}=-\frac{1}{M^2}\frac{1}{\epsilon} \qquad (46)$$

to $G_{\mathbf{k}}^m$ and $G_{\mathbf{k}}^n$ respectively. These terms too give

rise to a logarithmically divergent contribution that must be cut off.

If (45) and (46) are expanded as in (29), we find readily that

$$C_\Delta{}^{m1}=-\int_0^K\frac{dk}{2\pi^2}\left(\frac{k^2}{4\epsilon^3}\right)\left\{\frac{5}{3}+\frac{\mu^2}{6\epsilon^2}-\frac{5\mu^4}{6\epsilon^4}\right\}\quad C_\Delta{}^{n1}=0$$

$$C_\Delta{}^{m2}=-\int_0^K\frac{dk}{2\pi^2}\left(\frac{k^2}{4\epsilon^3}\right)\left\{\frac{1}{3}+\frac{\mu^2}{6\epsilon^2}\right\}\qquad C_\Delta{}^{n2}=0$$

$$C_\Delta{}^{m}=-\int_0^K\frac{dk}{2\pi^2}\left(\frac{k^2}{2\epsilon^3}\right)\left\{1+\frac{1}{6}\frac{\mu^2}{\epsilon^2}-\frac{5}{12}\frac{\mu^4}{\epsilon^4}\right\}$$

$$C_\Delta{}^{n}=0 \quad (47)$$

where K is the cut-off momentum and ϵ as usual is $(k^2+\mu^2)^{\frac{1}{2}}$. Note that the above expressions for $C_\Delta{}^m$ and $C_\Delta{}^n$ (as well as $C_\sigma{}^m$ and $C_\sigma{}^n$ to be discussed below) are easily obtained from (34) (and (33)) by keeping only the first term in M. If K is much greater than μ, (47) is given very closely by

$$2\pi^2C_\Delta{}^{m1}=-\frac{1}{4}\left\{\frac{5}{3}\log\frac{2K}{\mu}-\frac{3}{2}\right\};$$

$$2\pi^2C_\Delta{}^{m2}=-\frac{1}{4}\left\{\frac{1}{3}\log\frac{2K}{\mu}-\frac{1}{2}\right\};$$

$$2\pi^2C_\Delta{}^{m}=-\frac{1}{2}\left(\log\frac{2K}{\mu}-1\right);\quad C_\Delta{}^{n}=0. \quad (48)$$

K must be taken large enough to include the region in which the integrands are large, but not so large that the incorrect asymptotic behavior that causes the logarithmic divergence affects the integral appreciably. A value of K midway between μ and M, or about $M/2$, seems plausible. (We see incidentally from (48) that the C_Δ's are not very sensitive to changes of the meson mass.)

For $K=M/2$ and $\mu/M=0.154$, we obtain

$$2\pi^2C_\Delta{}^{m1}\approx-0.37;\quad 2\pi^2C_\Delta{}^{m2}\approx-0.025;$$
$$2\pi^2C_\Delta{}^{m}\approx-0.40;\quad C_\Delta{}^{n}=0. \quad (49)$$

Comparing (49) and (35), we see that errors of about 20 or 30 percent arise from this approximation. We note too that negative-energy processes have little effect even for the singular case of pseudoscalar coupling. In Fig. 1, the exact integrands of $C_\Delta{}^m$ and $C_\Delta{}^n$ are compared with the non-relativistic expressions, for $\mu/M=0.154$. It is seen that even for this mass ratio, which is not very small, the agreement is fair for low momenta.

The spin-orbit interaction cannot be used to compute the magnetic moments by the above non-relativistic approximation, essentially because the spin-orbit interaction is a higher order effect. At first sight, this seems false, since (45) contains a spin-dependent term that converges and is easily evaluated. Moreover, it gives a value of the neutron moment in better agreement with experiment than the exact method, because it gives a zero nucleon contribution. (The exact method gives a nucleon contribution that will be seen below to be much too high.)

However, this agreement is illusory, since the substitution (25) makes (45) give zero for both meson and nucleon contributions to μ_N (cf. the second form of (33m)). Moreover, this substitution, which has no effect on the C_Δ's, is to be insisted upon, since otherwise, when (45) is expanded, it is seen to contain a spurious term in $\mathbf{s}^2$, which violates charge conservation. A "non-relativistic" method for computing the moments by considering interaction with a magnetic field is possible, but will not be attempted here. It is interesting to note that many phenomena noted above have counterparts in the calculation of the Lamb effect and the radiative corrections to the electron moment.

The Neutron-Electron Interaction for Other Types of Mesons

Since pseudoscalar and pseudovector couplings are equivalent (using (28)) for positive-energy processes in non-relativistic approximation, and to this order, as may be verified from (20), no negative-energy processes (including the contact interaction) contribute, we obtain for pseudovector coupling,

$$U_0V_e=(8\pi^2e^2f^2/\mu^2)(C_\Delta{}^{m1}+C_\Delta{}^{n1}). \quad (50)$$

We have used (28), (32), and (47). However, we have seen that cutting off is here unjustified except for the special choice of contact term mentioned above. Note that the $C_\Delta{}^{m2}$ term for pseudoscalar coupling is small, so that (28) may be applied to (36) without very great error to get the pseudovector value.

The non-relativistic calculation may very easily be carried through for the case of vector mesons. Here too, two couplings occur, characterized by constants f_v and g_v, which, however, are not equivalent. Moreover, both couplings have matrix elements of order unity for positive-energy transitions, so that no negative-energy processes need be investigated.

For charged vector mesons we have:

$$H^{em}=(e/2L^3)\int d\tau V(\mathbf{r})\sum_{\mathbf{kk'jj'}}(\epsilon_k\epsilon_{k'})^{-\frac{1}{2}}(\mathbf{j}\cdot\mathbf{j'})$$
$$\times\{(q_{+\mathbf{j'k'}}{}^\dagger q_{+\mathbf{jk}}-q_{-\mathbf{j'k'}}{}^\dagger q_{-\mathbf{jk}})(\epsilon_k+\epsilon_{k'})$$
$$\times\exp(i(\mathbf{k}-\mathbf{k'})\cdot\mathbf{r})+q_{-\mathbf{j'k'}}q_{+\mathbf{jk}}(\epsilon_k-\epsilon_{k'})$$
$$\times\exp(i(\mathbf{k}+\mathbf{k'})\cdot\mathbf{r})-q_{+\mathbf{j'k'}}{}^\dagger q_{-\mathbf{jk}}{}^\dagger(\epsilon_k-\epsilon_{k'})$$
$$\times\exp(-i(\mathbf{k}+\mathbf{k'})\cdot\mathbf{r})\}, \quad (51)$$

where $\mathbf{j}$ is the polarization unit vector and can have three possible values for each $\mathbf{k}$: one along $\mathbf{k}$ (longitudinal mesons), and two others perpendicular to $\mathbf{k}$ and to each other (transverse mesons). In non-relativistic approximation, the matrix elements for emission and absorption of a meson of momentum $\mathbf{k}$ are, disregarding q, a, and τ factors as well as the u_p's,*

$$(2\pi/\epsilon L^3)^{\frac{1}{2}}\{\pm i(g_v/\mu_v)k\} \tag{52II}$$

for longitudinal mesons and

$$(2\pi/\epsilon L^3)^{\frac{1}{2}}\{\pm i(f_v/\mu_v)\boldsymbol{\sigma}\cdot\mathbf{j}\times\mathbf{k}\} \tag{52$\perp$}$$

for transverse, where the upper signs are for absorption.

Then from (51), (52), and (17a), we have immediately for the relevant processes of Section III the contributions:

$$\mathfrak{M}=\frac{g_v^2}{\mu_v^2}(G_{\text{II}}{}^m+G_{\text{II}}{}^n)+\frac{f_v^2}{\mu_v^2}(F_\perp{}^m+F_\perp{}^n); \tag{53}$$

$$G_{\text{II}}{}^m=\sum_{\mathbf{k}}\frac{2}{\epsilon_a\epsilon_b}\left\{\frac{\mathbf{a}\cdot\mathbf{b}}{\epsilon_a\epsilon_b}(\epsilon_a+\epsilon_b)-\frac{(\epsilon_a-\epsilon_b)(-\mathbf{a}\cdot\mathbf{b})}{\epsilon_a(\epsilon_a+\epsilon_b)}+\frac{(\epsilon_a-\epsilon_b)(-\mathbf{a}\cdot\mathbf{b})}{\epsilon_b(\epsilon_a+\epsilon_b)}\right\}=\sum_{\mathbf{k}}\frac{8\mathbf{a}\cdot\mathbf{b}}{\epsilon_a\epsilon_b(\epsilon_a+\epsilon_b)}$$

$$G_{\text{II}}{}^n=\sum_{\mathbf{k}}\frac{2}{\epsilon^2}\left\{-\frac{2\epsilon\mathbf{k}\cdot\mathbf{k}}{\epsilon^2}\right\}=\sum_{\mathbf{k}}-\frac{4k^2}{\epsilon^3}, \tag{54II}$$

and similarly

$$F_\perp{}^m=\sum_{\mathbf{k}}\frac{8}{\epsilon_a\epsilon_b(\epsilon_a+\epsilon_b)}\sum_{\mathbf{j}a\mathbf{j}b}(\boldsymbol{\sigma}\cdot\mathbf{j}_a\times\mathbf{a})(\mathbf{j}_a\cdot\mathbf{j}_b)(\boldsymbol{\sigma}\cdot\mathbf{j}_b\times\mathbf{b})$$

$$=\sum_{\mathbf{k}}\frac{8}{\epsilon_a\epsilon_b(\epsilon_a+\epsilon_b)}[2\mathbf{a}\cdot\mathbf{b}-i\boldsymbol{\sigma}\cdot\mathbf{a}\times\mathbf{b}]$$

$$F_\perp{}^n=\sum_{\mathbf{k}}\left(-\frac{4}{\epsilon^3}\right)\sum_{\mathbf{j}}(\boldsymbol{\sigma}\cdot\mathbf{j}\times\mathbf{k})(\mathbf{j}\cdot\mathbf{j})(\boldsymbol{\sigma}\cdot\mathbf{j}\times\mathbf{k})$$

$$=\sum_{\mathbf{k}}-\frac{4}{\epsilon^3}[2k^2]. \tag{54$\perp$}$$

Comparing (53) and (54) with (45) and (47), we see that

$$U_0V_e=(8\pi e^2/\mu_v{}^2)(C_\Delta{}^{m1}+C_\Delta{}^{n1})(g_v{}^2+2f_v{}^2). \tag{55}$$

Note that here, the legitimacy of cutting off has not been investigated. Assuming it possible, we have for an arbitrary mixture of pseudoscalar and vector mesons (neglecting $C_\Delta{}^{m2}$ and other small effects, as well as the change in the C_Δ's due to the difference between μ and μ_v):

$$U_0V_e=8\pi e^2(C_\Delta{}^{m1}+C_\Delta{}^{n1})\times\left[\frac{1}{\mu_v{}^2}(g_v{}^2+2f_v{}^2)+\frac{1}{\mu^2}\left(f-\frac{\mu g}{2M}\right)^2\right]. \tag{56}$$

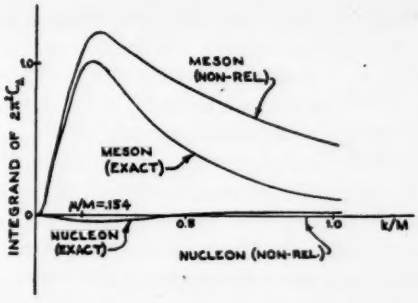

FIG. 1. Comparison of exact (Eq. (34)) and non-relativistic (Eq. (47)) integrands of $2\pi^2C_\Delta$. Note that minus the integrand is drawn. For $C_\Delta{}^n$, multiply abscissas by 2 and divide ordinates by 2.

In fact, if we adjust (56) to agree with the exact expression (36) for $f=f_v=g_v=0$ and $\mu/M=0.154$, we obtain

$$U_0=57.3\left[\left(f-\frac{\mu g}{2M}\right)^2+\left(\frac{\mu}{\mu_v}\right)^2(g_v{}^2+2f_v{}^2)\right]\text{kev}. \tag{57}$$

The Charge Cloud. Charge Renormalization

If the spin-independent parts of the scattering matrix element $K_{\mathbf{p}\mathbf{p}_0}$ can be interpreted as resulting from the interaction of a charge cloud $\rho(|\mathbf{r}-\mathbf{r}_0|)$ around a nucleon at $\mathbf{r}_0$, and an electric field $V(\mathbf{r})$, we would have

$$K_{\mathbf{p}\mathbf{p}_0}=\int d\tau_0(L^{-\frac{1}{2}}u_p{}^*\exp(-i\mathbf{p}\cdot\mathbf{r}_0))\times\left\{\int d\tau V(\mathbf{r})\rho(|\mathbf{r}-\mathbf{r}_0|)\right\}\times(L^{-\frac{1}{2}}u_{\mathbf{p}_0}\exp(i\mathbf{p}_0\cdot\mathbf{r}_0)). \tag{58}$$

Comparing this with (19), we see that we must have

$$\int\rho(|\mathbf{r}-\mathbf{r}_0|)\exp(i\boldsymbol{\Delta}\cdot\mathbf{r}_0)d\tau_0=(-e\pi/2L^3)\exp(i\boldsymbol{\Delta}\cdot\mathbf{r})\mathfrak{M}, \tag{58a}$$

where $\mathfrak{M}$ is a function of $\mathbf{p}_0$ and $\boldsymbol{\Delta}$ only. By Fourier's integral theorem:

$$\rho(\mathbf{r}-\mathbf{r}_0)=\int\exp(i\boldsymbol{\Delta}\cdot(\mathbf{r}-\mathbf{r}_0))\frac{d^3\boldsymbol{\Delta}}{(2\pi)^3}\left(-\frac{e\pi}{2L^3}\right)\mathfrak{M}$$

$$=\left(-\frac{e\pi}{2L^6}\right)\sum_\Delta\exp(i\boldsymbol{\Delta}\cdot(\mathbf{r}-\mathbf{r}_0))\mathfrak{M}(\boldsymbol{\Delta},\mathbf{p}_0), \tag{59}$$

so that ρ is essentially the Fourier transform of $\mathfrak{M}$.

* The u's for the intermediate states may be omitted, since they are effectively two-component wave functions and are summed over both spin indices. Thus $\sum_{p'\text{ spins}}(u_p{}^*\mathcal{O}_1u_{p'})\times(u_{p'}{}^*\mathcal{O}_2u_{p_0})=(u_p{}^*\mathcal{O}_1\mathcal{O}_2u_{p_0})$ for any operators $\mathcal{O}_1$ and $\mathcal{O}_2$ involving $\boldsymbol{\sigma}$ and unity. Of course, the $u_p{}^*$ and u_{p_0} must be inserted.

We therefore see immediately that a constant term in $\mathfrak{M}$ corresponds to a δ-function charge distribution; i.e., a point charge at the position of the nucleon. It follows, for instance, that the constant term in G^m (Eq. (29)) corresponds to an alteration of the nucleon charge by g^2 times a logarithmically divergent integral. Since G^n gives an equal and opposite alteration, the nucleon charge is entirely unchanged. The divergent point charges are thus not to be looked on in any sense as a renormalization of nucleon charge due to the meson field. This circumstance, guaranteed by charge conservation, is necessary if proton and electron charges are to be of the same magnitude. However, the fact that G^m, etc., give rise to a (divergent) point charge plus a convergent continuous distribution shows that it is sensible to separate meson and nucleon contributions. (It might have been objected that since G^m and G^n individually diverge, only their sum has any significance and a separation into $C_\Delta{}^m$ and $C_\Delta{}^n$ is inadmissible.)

Equation (59) can be rewritten, with $\mathbf{R}=\mathbf{r}-\mathbf{r}_0$, as

$$\rho(R)=\left(-\frac{e\pi}{2L^6}\right)\sum_\Delta\sum_{\mathbf{k}} M_{\mathbf{k}}\exp(i\boldsymbol{\Delta}\cdot\mathbf{R})$$

$$=\left(-\frac{e\pi}{2L^6}\right)\sum_{\mathbf{a}}\sum_{\mathbf{b}} M_{\mathbf{k}}\exp(i(\mathbf{b}-\mathbf{a})\cdot\mathbf{R}). \quad (60)$$

The usual non-relativistic method of obtaining the charge density is to evaluate the expectation value of the charge density operator $-ie(\Pi\Psi-\Pi^\dagger\Psi^\dagger)$ (see Eq. (3)) for an infinitely heavy nucleon at rest at the origin. Using perturbation theory, precisely the value (60) is obtained if the non-relativistic $\mathfrak{M}$ is used. The double-summation in (60) is there due to the neglect of nucleon recoil, and hence momentum conservation, so that $\mathbf{a}$ and $\mathbf{b}$ are independent. If this method is to be applied to pseudoscalar coupling, one need only remember that g/M is finite, but that for other purposes M may be taken infinite, and that a contribution from negative-energy processes is being omitted. (59) may also be looked on as a transformation back to coordinate representation, or as resulting from a summation of plane-wave matrix elements $K_{\mathbf{pp_0}}$ to give the matrix element for a localized neutron.

The charge density will now be evaluated in the non-relativistic approximation for a mixture of pseudoscalar and vector mesons (neglecting the small negative-energy contribution for pseudoscalar coupling). We have then from (60), (45), and (54):

$$\rho(R)=\left(-\frac{e\pi}{2L^6\mu^2}\right)\left[\left(f-\frac{\mu g}{2M}\right)^2+(g_v{}^2+2f_v{}^2)\right]$$

$$\times\sum_{\mathbf{k}}\sum_\Delta\left\{\frac{8\mathbf{a}\cdot\mathbf{b}}{\epsilon_a\epsilon_b(\epsilon_a+\epsilon_b)}-\frac{4k^2}{\epsilon^3}\right\}\exp(i\boldsymbol{\Delta}\cdot\mathbf{R}). \quad (61)$$

The second term in this summation—the nucleon contribution—is independent of $\boldsymbol{\Delta}$ and corresponds entirely to a δ-function charge. This is due to the fact that the nucleon charge is smeared out over approximately the neutron Compton wave-length (divided by 2π), which is here assumed zero (see Fig. 1). We will accordingly omit this term, but remember that it cancels the δ-functions arising from the meson portion and causes the total charge to be zero. The integrals in the meson contribution may with this understanding be computed in the sense of summability, which has the effect of neglecting such singularities. We then obtain, integrating first over the angles of $\mathbf{a}$ and $\mathbf{b}$:

$$\rho(R)=\frac{-e}{\pi^3\mu^2}\left[\left(f-\frac{\mu g}{2M}\right)^2+(g_v{}^2+2f_v{}^2)\right]$$

$$\times\int_0^\infty\int_0^\infty dadba^2b^2\left(\frac{\cos aR}{R}-\frac{\sin aR}{aR^2}\right)$$

$$\times\left(\frac{\cos bR}{R}-\frac{\sin bR}{bR^2}\right)\frac{1}{\epsilon_a\epsilon_b(\epsilon_a+\epsilon_b)}$$

$$=-\frac{2e}{\pi^3\mu^2}\left[\quad\right]$$

$$\times\int_0^\infty\int_0^\infty dadba^2b^2\left(\frac{\cos aR}{R}-\frac{\sin aR}{aR^2}\right)$$

$$\times\left(\frac{\cos bR}{R}-\frac{\sin bR}{bR^2}\right)\frac{1}{\epsilon_b(a^2-b^2)}$$

$$=\frac{e}{\pi^2\mu^2}\left[\quad\right]\frac{1}{R^3}\int_0^\infty\frac{b^2db}{(\mu^2+b^2)^{\frac{1}{2}}}$$

$$\times\left[\cos 2bR+\frac{1}{2}\left(bR-\frac{1}{bR}\right)\sin 2bR\right]$$

$$=\frac{e}{2\pi}\left[\quad\right]\frac{1}{R^3}\left\{\frac{5i}{4}H_0{}^{(1)}(2i\mu R)\right.$$

$$\left.-\frac{5}{4\mu R}H_1{}^{(1)}(2i\mu R)-\frac{\mu R}{2}H_1{}^{(1)}(2i\mu R)\right\}. \quad (62)$$

Though this converges at any finite R, it has a $1/R^5$ singularity, and should be cut off at a value of R that gives a value for the neutron-electron interaction near that given by (57). For the total meson charge outside the cut-off radius R_c, we obtain

$$\int_{>R_c}\rho(R)d\tau=-\frac{e}{2}\left[\quad\right]$$

$$\times\left\{\frac{-5H_1{}^{(1)}(2iR_c\mu)}{2R_c\mu}+iH_0{}^{(1)}(2iR_c\mu)\right\} \quad (63)$$

which diverges $\sim 1/R_c{}^2$ as $R_c\to 0$.

The volume integral of the electrostatic potential U_e due to a charge distributed with density (62) outside of R_c, and with a charge at the origin sufficient to make the total charge zero is

$$\int U_e d\tau = -(4\pi)^2 \int_{R_c}^{\infty} RdR \int_{R}^{\infty} r^2 \rho dr$$

$$-(4\pi)^2 \int_{0}^{R_c} RdR \int_{R_c}^{\infty} r^2 \rho dr$$

$$+\frac{(4\pi)^2}{3} \int_{R_c}^{\infty} \rho R^4 dR$$

$$= -(4\pi/6) \int_{R_c}^{\infty} \rho R^4 dR$$

$$= e\pi/6\mu^2 [\quad] \{ 5iH_0^{(1)}(2iR_c\mu)$$

$$+\tfrac{1}{2}(2R_c\mu)^2 iH_0^{(1)}(2iR_c\mu)$$

$$-7/2(2R_c\mu)H_1^{(1)}(2iR_c\mu)\}. \quad (64)$$

(The three terms in the first line are due respectively to charges inside R for $R>R_c$, to the bare nucleon for $R<R_c$, and to charges outside R for all R.) The volume integral of the potential of a neutron in the field of an electron is given by $U_0 V_e = -e\int U_e d\tau$. For agreement with (56) or (57) the expression in curly brackets in (64) must be about unity, so that $2R_c\mu$ must be slightly greater than 1. The total dissociated meson charge given by (63) is correspondingly about $\frac{1}{10}$ or $\frac{1}{5}$ of an electronic charge, using a value of about 0.2 for the factor in square brackets, as will be discussed in the next paragraph. The range of this interaction is about R_c, or a little more than $\sim 1/(2\mu)$, or about $\frac{1}{4}$ of the classical electron radius for $\mu = 282$ e.m. Figure 2 is an attempt to depict very roughly the meson charge cloud and neutron-electron potential as a function of the distance from the neutron. In it, the cut-off distributions have been smoothed out to simulate the result that would have been obtained from an exact calculation.

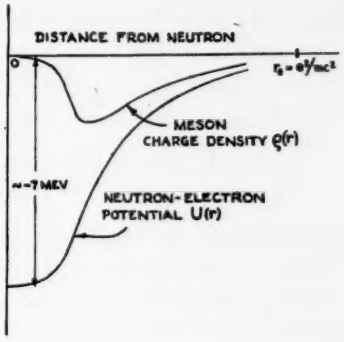

FIG. 2. Neutron-electron potential and meson charge cloud around neutron (very rough).

VII. COMPARISON WITH EXPERIMENT AND CONCLUSIONS

To compare the results (44), (36), and (57) with experiment, the coupling constants will be evaluated by comparison with the known nuclear forces. To avoid questions associated with the highly singular tensor force, the ^1S neutron-proton potential will be examined, since it does not involve the tensor force. For a mixture of pseudoscalar and vector mesons of mass μ, the theory gives a singlet potential

$$-\left[\left(f-\frac{\mu g}{2M}\right)^2 + 2f_v^2 - g_v^2\right] r^{-1} \exp(-\mu r)$$

for symmetric theory

and

$$-2\left[\left(f-\frac{\mu g}{2M}\right)^2 + 2f_v^2 - g_v^2\right] r^{-1} \exp(-\mu r)$$

for pure charged theory.

All non-static terms have been neglected in these expressions, so an unknown—perhaps quite large—error has been introduced. On the other hand, the experimental data can be fitted to a potential $-0.239 r^{-1} \exp(-\mu r)$ calculated for a singlet scattering length of $-2.375 \cdot 10^{-10}$ cm and $\mu = 282$ e.m. from Eq. (35), of Rosenfeld's book.[16]

We first assume $f = f_v = g_v = 0$. Then from the above equations, $(\mu g/2M)^2 = 0.239$ or $g^2 = 40.3$ for symmetrical, and similarly $g^2 = 20.1$ for pure charged theory. We then have from (36) and (44)

$$U_0 = -13.7 \text{ kev}; \quad \mu_N = -5.15; \quad \mu_P - 1 = +0.66 \quad (65s)$$

for symmetric theory, and

$$U_0 = -6.9 \text{ kev}; \quad \mu_N = -2.56; \quad \mu_P - 1 = 1.08 \quad (65c)$$

for pure charged theory, as compared to the experimental values

$$U_0 \sim -\text{several kev}; \quad \mu_N = -1.91; \quad \mu_P - 1 = 1.79. \quad (65e)$$

It should be remembered that pure charged theory gives unsatisfactory nuclear forces even apart from the tensor force difficulty, so that (65c) is not to be taken too seriously.

The most important conclusion to be drawn from (65) is that pseudoscalar-coupled pseudoscalar meson theory gives results that are convergent and correct in sign and order of magnitude. Quantitatively, however, the magnetic moments depart con-

[16] L. Rosenfeld, *Nuclear Forces I* (Interscience Publishers, Inc., New York, 1948), p. 88.

siderably from the experimental values. This is not due merely to the coupling constant, since for the ratio $-(\mu_P-1)/\mu_N$, which is independent of g^2, we have

$$-(\mu_P-1)/\mu_N=0.128 \text{ (sym.)};\ 0.418 \text{ (charged)};\ 0.936 \text{ (exp.)} \quad (66)$$

respectively for symmetrical theory, pure charged theory, and experiment. As mentioned before, quantitative disagreements due to higher order terms, other meson masses, etc., are to be expected, but the disagreement of $-(\mu_P-1)/\mu_N$ may indicate a more serious fault. The difficulty stems from the fact that if equations such as (43s) or (43c) are to be fitted to experiment, the nucleon contribution to the moments must be very small, while in fact, (35) shows it to be 40 percent greater than the meson contribution to the neutron moment. If the nucleon contribution is omitted altogether, we find for symmetrical theory $\mu_N=-2.16$, $\mu_P-1=2.16$, in good agreement with experiment even for the present coupling constant.

The large size of the nucleon contribution may also seem surprising in the light of simple qualitative considerations.[1] For instance, if a neutron of $S_z=+\frac{1}{2}$ is dissociated into a negative meson of $L=1$ and $L_z=+1$ and a proton of $S_z=-\frac{1}{2}$ for about $\frac{1}{10}$ or $\frac{1}{5}$ of the time (in accord with the total meson charge estimated in the last paragraph) we would expect a negative contribution of about $\frac{1}{10}$ to $\frac{1}{5}$ from the proton, and a further negative contribution from the meson about M/μ times as large (since the meson magneton is M/μ times the proton magneton). Instead, we find a nucleon contribution even larger than the meson contribution (and negative, so it does not arise from transitions involving mesons of $L=0$) for the neutron moment, and none at all for the proton moment.

To understand these results, we note that the nucleon contribution, at least to the spin-orbit interaction, does not seem to arise in the manner suggested above. In fact, the spin-orbit interaction in the ordinary Dirac case arises because the electrical matrix element

$$(q/L^3)\int d\tau V(\mathbf{r})\exp(i\boldsymbol{\Delta}\cdot\mathbf{r})(u_{\mathbf{p}}{}^*u_{\mathbf{p}0}),$$

becomes

$$\sim(q/L^3)\left\{\int d\tau V(\mathbf{r})\exp(i\boldsymbol{\Delta}\cdot\mathbf{r})\right\}\times\left(u_{\mathbf{p}}{}^{1*}\left[1+\frac{\mathbf{p}\cdot\mathbf{p}_0}{4M^2}+\frac{i\boldsymbol{\sigma}\cdot\mathbf{p}\times\mathbf{p}_0}{4M^2}\right]u_{\mathbf{p}_0}{}^1\right)$$

when reduction to 2-component wave functions $u_{\mathbf{p}}{}^1$ etc., is made. Here q is the charge of the particle. Thus, since the charge of the proton is reduced (by an infinite amount!) due to "dissociation," the expected decrease of the Dirac moment does appear on going to the 2-component functions. However, the meson charge results in a term in

$$\int d\tau V(\mathbf{r})\exp(i\boldsymbol{\Delta}\cdot\mathbf{r})(u_{\mathbf{p}}{}^*u_{\mathbf{p}0})$$

in the Hamiltonian that just compensates the reduction of proton charge. The case of the neutron is exactly similar. Charge conservation thus ensures that the spin-orbit interaction does not change on reduction to 2-component functions. The nucleon contribution is thus to be thought of as arising from sharing of the orbital motion by the nucleon, which also explains the zero result for the proton moment (orbital motion of the neutron gives no contribution). Though this too may be thought to be small, we have seen that high momentum ($\sim M$) contributions are important, and here relativistic mass increases makes the sharing large. It should also be remembered that higher radiative corrections, which, judging from the "dissociation time," are $\frac{1}{10}$ to $\frac{1}{5}$ or even larger, have been entirely neglected. For vector mesons, which possess an intrinsic angular momentum, the situation may be entirely different.

From (57), noting that for symmetric theory

$$\left[\left(f-\frac{\mu g}{2M}\right)^2+2f_v{}^2-g_v{}^2\right]=0.239$$

for a mixture of vector and pseudoscalar mesons, we see that unless g_v is very large, U_0 is still about -15 kev. Thus, if they converge, the other couplings do not give a substantially different neutron-electron interaction.

To summarize, the results of the above investigation seem sufficiently positive to warrant examination of other couplings and higher corrections. However, use of the newer methods seems advisable for more secure treatment of divergences.

ACKNOWLEDGMENTS

This research was concluded while one of the authors (M.S.) was an Atomic Energy Commission Predoctoral Fellow in the Physical Sciences of the National Research Council, under the direction of Professor I. I. Rabi. He would like also to express his gratitude to Professor H. A. Bethe for his very generous aid during the long period when detailed correspondence between the two authors was impracticable. His many valuable suggestions and his criticism of the entire manuscript have resulted in numerous important improvements.

APPENDIX

If u_p and u_{p0} are Dirac 4-component columns corresponding to positive energies E_p and E_{p0}, then for any Dirac operator $\mathfrak{D}$ an operator $\mathfrak{D}'$ of the form const$+(\mathbf{const}\cdot\boldsymbol{\sigma})$ can be found so $(u_p^*\mathfrak{D}u_{p0})=(u_p^*\mathfrak{D}'u_{p0})$. The operators and their replacements (indicated by $\rightarrow$) are as follows: (Of course, $1\rightarrow 1$ and $\boldsymbol{\sigma}\rightarrow\boldsymbol{\sigma}$.)

$$\beta\rightarrow\frac{E_pE_{p0}+M^2-\mathbf{p}\cdot\mathbf{p}_0-i\boldsymbol{\sigma}\cdot\mathbf{p}\times\mathbf{p}_0}{M(E_p+E_{p0})}$$

$$\boldsymbol{\alpha}\cdot\mathbf{c}\rightarrow\frac{\mathbf{c}\cdot\mathbf{s}+i\boldsymbol{\sigma}\cdot\mathbf{c}\times\boldsymbol{\Delta}}{E_{p0}+E_p}$$

$$\beta\boldsymbol{\alpha}\cdot\mathbf{c}\rightarrow\frac{\mathbf{c}\cdot\boldsymbol{\Delta}+i\boldsymbol{\sigma}\cdot\mathbf{c}\times\mathbf{s}}{2M}-\left(\frac{E_{p0}-E_p}{E_{p0}+E_p}\right)\frac{\mathbf{c}\cdot\mathbf{s}+i\boldsymbol{\sigma}\cdot\mathbf{c}\times\boldsymbol{\Delta}}{2M}$$

$$\beta\boldsymbol{\sigma}\cdot\mathbf{c}\rightarrow-\frac{E_pE_{p0}+M^2}{M(E_p+E_{p0})}-\frac{2i\mathbf{c}\cdot\mathbf{s}\times\boldsymbol{\Delta}+(\mathbf{s}^2-\boldsymbol{\Delta}^2)\boldsymbol{\sigma}\cdot\mathbf{c}+2(\mathbf{c}\cdot\boldsymbol{\Delta})(\boldsymbol{\sigma}\cdot\boldsymbol{\Delta})-2(\mathbf{c}\cdot\mathbf{s})(\boldsymbol{\sigma}\cdot\mathbf{s})}{4M(E_p+E_{p0})}$$

$$\alpha_1\alpha_2\alpha_3\rightarrow\frac{i\boldsymbol{\sigma}\cdot\mathbf{s}}{E_p+E_{p0}}$$

$$\alpha_1\alpha_2\alpha_3\beta\rightarrow-\frac{i\boldsymbol{\sigma}\cdot\boldsymbol{\Delta}}{2M}+\left(\frac{E_{p0}-E_p}{E_{p0}+E_p}\right)\frac{i\boldsymbol{\sigma}\cdot\mathbf{s}}{2M}$$

where $\mathbf{s}=\mathbf{p}_0+\mathbf{p}$, $\boldsymbol{\Delta}=\mathbf{p}_0-\mathbf{p}$, and $\mathbf{c}$ is an arbitrary ordinary vector.

Note on Meson Contribution to the Lamb Shift

An estimate of the shift of the $2s$ hydrogen level caused by the meson charge cloud around the proton is of some interest. As may be seen from the non-relativistic approximation or from (39) directly, the nucleon contributions are not very important, while the meson contribution is by (38) just the negative of that for the neutron case. Thus, in analogy to (30), we have for the proton

$$K_{pp0}\approx+\frac{\pi eg^2}{2L^3}\int d\tau V(\mathbf{r})\exp(i\boldsymbol{\Delta}\cdot\mathbf{r})\frac{\boldsymbol{\Delta}^2}{M^2}C_\Delta{}^m=-\frac{\pi eg^2}{2L^3}\int d\tau V(\mathbf{r})\boldsymbol{\nabla}^2\exp(i\boldsymbol{\Delta}\cdot\mathbf{r})\frac{C_\Delta{}^m}{M^2}.$$

By Green's theorem, this is, apart from a surface integral,

$$(-\pi eg^2/2L^3)\int d\tau\exp(i\boldsymbol{\Delta}\cdot\mathbf{r})\boldsymbol{\nabla}^2V(\mathbf{r})(C_\Delta{}^m/M^2).$$

Now for a proton localized at the origin, the product of the initial and final wave functions is $\delta(\mathbf{r})$ rather than $L^{-3}\exp(i\boldsymbol{\Delta}\cdot\mathbf{r})$. Also, $\boldsymbol{\nabla}^2V=-4\pi\rho(\mathbf{r})=+4\pi e\psi^*\psi$, where $\psi(\mathbf{r})$ is the electron wave function, so that the change in energy due to smearing of the proton charge is approximately

$$-(\pi eg^2C_\Delta{}^m/2M^2)\int d\tau\delta(\mathbf{r})\cdot 4\pi e\psi^*\psi=-(2\pi^2C_\Delta{}^me^2g^2/M^2)\,|\psi(0)|^2.$$

For an s electron, $|\psi(0)|^2=(\pi n^3a_0^3)^{-1}$ ($a_0=$ Bohr radius). Thus with $2\pi^2C_\Delta{}^m\approx-0.5$ and $g^2\approx 40$ we obtain $+0.08$ Mc for the shift of the $2s$ level, considerably less than the present experimental error.

Theory of Proposed Reactions Involving Polarized Protons

LINCOLN WOLFENSTEIN*
Department of Physics, University of Chicago, Chicago, Illinois
(Received January 17, 1949)

The use of fast polarized projectiles in nuclear reactions provides a possible tool for studying the spin-dependence of nuclear interactions. In the first section general properties of such reactions are discussed. For incident neutrons or protons and a value L_{max} for the maximum partial wave that need be considered in the incident beam, the results are summarized in theorems 3 and 4.

The following reactions involving polarized protons are shown to be possible: (a) production of polarized protons by the (n,p) reactions of N or He^3 using polarized thermal neutrons, (b) detection of polarization by means of the $Li^7(p,\alpha)\alpha$-reaction, and (c) production or detection by the resonance scattering of protons from helium. Considering these reactions alone and exploring the fundamental limitations on intensity, one finds that the intensity problem appears to be least critical if (c) is used for both production and detection. The polarization effect usually depends on at least one parameter which does not affect or affects much less critically the unpolarized result. The polarization effect caused by the spin-dependent Coulomb scattering is calculated and found to be less than 5 percent for atomic number Z less than 5, except for special cases. Protons retain their polarization while being slowed down.

I. INTRODUCTION

THE production of a beam of polarized elementary particles might provide a useful tool for the study of the spin-dependent interactions of these particles. During the past twenty years a number of methods have been suggested for accomplishing this. The most successful of these has been the polarization of thermal neutrons by scattering in iron in a magnetic field.[1] The use of these neutrons to study spin-dependent nuclear interactions is limited by their low velocity. Proposed methods for polarizing fast particles depend upon the presence of spin-orbit coupling in the scattering of the particles. Mott first proposed such a method for polarizing electrons in 1929,[2] but the experiments did not prove successful until recently.[3] Similar methods for polarizing fast neutrons have been discussed recently by Schwinger.[4,5] The experiments suggested by Schwinger have not as yet been attempted because of the difficulties associated with the double scattering of neutrons.

The present investigation concerns the possibilities of producing and utilizing polarized beams of protons. In the introduction the general properties of reactions involving polarized particles of spin $\frac{1}{2}$ are considered, while in succeeding sections specific reactions involving polarized protons are proposed and discussed. It will be assumed throughout that the target nuclei involved in the reactions are unpolarized.[6]

The spin function corresponding to a state of complete polarization is written

$$A_{\frac{1}{2}}s^{\frac{1}{2}}+A_{-\frac{1}{2}}s^{-\frac{1}{2}} \tag{1}$$

with $|A_{\frac{1}{2}}|^2+|A_{-\frac{1}{2}}|^2$ equal to unity. The expectation value of the components of the spin operator $\boldsymbol{\sigma}$ are:

$$\begin{aligned}\bar{\sigma}_x&=2Re(A_{\frac{1}{2}}{}^*A_{-\frac{1}{2}}),\\ \bar{\sigma}_y&=2Im(A_{\frac{1}{2}}{}^*A_{-\frac{1}{2}}),\\ \bar{\sigma}_z&=|A_{\frac{1}{2}}|^2-|A_{-\frac{1}{2}}|^2.\end{aligned} \tag{2}$$

A superposition of n states of the form (1) with arbitrary phase relations is expressed

$$\sum_{\lambda=1}^{n}\{A_{\frac{1}{2}\lambda}s^{\frac{1}{2}}+A_{-\frac{1}{2}\lambda}s^{-\frac{1}{2}}\}c_\lambda\epsilon_\lambda\Big/\left(\sum_{\lambda=1}^{n}c_\lambda{}^2\right)^{\frac{1}{2}}, \tag{3}$$

where c_λ is the weight with which a particular state is introduced, and ϵ_λ is an arbitrary phase factor[7] which enters into any meaningful result (such as an expectation value) only in the form $\epsilon_\lambda{}^*\epsilon_{\lambda'}$, which is defined to be equal to $\delta_{\lambda\lambda'}$. In this notation an unpolarized spin state may be represented

$$\{s^{\frac{1}{2}}\epsilon_1+s^{-\frac{1}{2}}\epsilon_2\}/2^{\frac{1}{2}}. \tag{4}$$

For the states given by Eq. (3) the expectation value of the spin operator $\boldsymbol{\sigma}$ is

$$\bar{\boldsymbol{\sigma}}=\sum_{\lambda=1}^{n}c_\lambda{}^2\bar{\boldsymbol{\sigma}}_\lambda\Big/\sum_{\lambda=1}^{n}c_\lambda{}^2, \tag{5}$$

where the components of $\bar{\boldsymbol{\sigma}}_\lambda$ are determined from

---

* Now at Carnegie Institute of Technology, Pittsburgh, Pennsylvania.

[1] F. Bloch, Phys. Rev. **50**, 259 (1936); **51**, 994 (1937). A summary of the latest work is given by D. J. Hughes, J. R. Wallace, and R. H. Holtzmann, Phys. Rev. **73**, 1277 (1948).

[2] N. F. Mott, Proc. Roy. Soc. **A124**, 425 (1929); **A135**, 429 (1932).

[3] C. G. Shull, C. T. Chase, and F. E. Myers, Phys. Rev. **63**, 29 (1943).

[4] Julian Schwinger, Phys. Rev. **69**, 681 (1946).

[5] Julian Schwinger, Phys. Rev. **73**, 407 (1948).

[6] Possibilities involving polarized target nuclei have been discussed by M. E. Rose, Phys. Rev. **75**, 213 (1949).

[7] A similar factor is used by G. Breit and B. T. Darling, Phys. Rev. **71**, 402 (1947). The ϵ_λ's may be thought of as basis unit vectors, and the summation over λ indicated in Eq. (6a) as a vector summation.

Eq. (2). If one makes the substitution in Eq. (3)

$$\sum_{\lambda=1}^{n} A_{\pm\frac{1}{2}\lambda} c_\lambda \epsilon_\lambda \Big/ \left(\sum_{\lambda=1}^{n} c_\lambda^2\right)^{\frac{1}{2}} = A_{\pm\frac{1}{2}} \nu_{\pm\frac{1}{2}}, \tag{6a}$$

where $\nu_{\frac{1}{2}}$ and $\nu_{-\frac{1}{2}}$ are unit vectors like ϵ_λ but are not mutually orthogonal, Eq. (5) yields a generalization of Eq. (2);

$$\begin{aligned} \bar{\sigma}_x &= 2Re(A_{\frac{1}{2}}{}^* \nu_{\frac{1}{2}}{}^* A_{-\frac{1}{2}} \nu_{-\frac{1}{2}}), \\ \bar{\sigma}_y &= 2Im(A_{\frac{1}{2}}{}^* \nu_{\frac{1}{2}}{}^* A_{-\frac{1}{2}} \nu_{-\frac{1}{2}}), \\ \bar{\sigma}_z &= |A_{\frac{1}{2}}|^2 - |A_{-\frac{1}{2}}|^2. \end{aligned} \tag{6b}$$

The most complete knowledge that may be found experimentally concerning a spin state is the mean value of an arbitrary operator for that state. Since any operator may be written in terms of σ_x, σ_y, σ_z, and the unity operator, a spin state is completely designated by the values of $\bar{\sigma}_x$, $\bar{\sigma}_y$, $\bar{\sigma}_z$; that is, a vector $\bar{\boldsymbol{\sigma}}$. For each vector $\bar{\boldsymbol{\sigma}}$, and thus for each spin state, there exists a representation in which the spin functions are quantized in the direction defined by $\bar{\boldsymbol{\sigma}}$, and $\nu_{\frac{1}{2}}$ and $\nu_{-\frac{1}{2}}$ are orthogonal. In this coordinate system it is seen directly that the percentage of polarization P is given by

$$P^2 = \bar{\boldsymbol{\sigma}} \cdot \bar{\boldsymbol{\sigma}} = (\bar{\sigma}_x)^2 + (\bar{\sigma}_y)^2 + (\bar{\sigma}_z)^2. \tag{7}$$

Since the right-hand side is a scalar, Eq. (7) holds in all coordinate systems.

Several general theorems concerning nuclear reactions involving polarized particles will now be demonstrated. (Theorems 1 and 1A not restricted to particles of spin $\frac{1}{2}$.)

Theorem 1.—If $L_{\max}$ is the maximum orbital angular momentum that need be considered in a nuclear reaction the maximum degree spherical harmonic that can enter into the angular distribution of the outgoing intensity is $2(L_{\max}+S)$, where S is the spin of the incident particle if it is polarized and S is zero if the particle is unpolarized. Furthermore, if $2(L_{\max}+S)$ is odd, the maximum degree is $2(L_{\max}+S-\frac{1}{2})$.

Theorem 1A.—The maximum degree is $2(L_{\max}+S+S')$ if the angular distribution of a specified state of polarization of an outgoing particle with spin S' is considered.

The following corollary follows immediately for particles of spin $\frac{1}{2}$:

Theorem 2.—The maximum degree spherical harmonic that can enter the angular distribution of the outgoing intensity is $2L_{\max}$ whether or not the incident particle is polarized. In particular, polarized particles can never be detected by a reaction in which only s-waves are involved.

These theorems may be proved most directly using a method given by Yang.[8] It will be convenient for later purposes, however, to follow the procedure of Eisner and Sachs.[9] (In both references Theorem 1 is proved for the case in which the incident particle is unpolarized.) A collision characterized by orbital angular momentum L of a projectile with spin S and a nucleus of spin I will be considered. The initial state may be written as a sum of products of functions of the spin and angle variables. If the nuclear spin is unpolarized the initial state in any coordinate system is written

$$\Psi_0 = \Sigma_{m_I m_S m_L} A_{m_S} B_{m_L} s^{m_S} b^{m_L} a^{m_I} \epsilon_{m_I} / (2I+1)^{\frac{1}{2}}, \tag{8}$$

where s^{m_S} represents the spin state of the projectile with a spin component m_S along the z axis, and a^{m_I} and b^{m_L} similarly represent nuclear spin and orbital angular momentum states. A_{m_S} and B_{m_L} are the coefficients with which the states s^{m_S} and b^{m_L} are introduced.[10] The products $s^{m_S} b^{m_L}$ may be expressed in terms of the eigenfunctions Θ_j of the total projectile angular momentum j,

$$s^{m_S} b^{m_L} = \Sigma_j (SLjm_S + m_L | SLm_S m_L) \Theta_j{}^{m_L+m_S},$$

using the usual transformation coefficients. The products $\Theta_j{}^{m_L+m_S} a^{m_I}$ may similarly be expressed in terms of the eigenfunctions ${}^i\chi_J{}^{m_L+m_S+m_I}$ of the total angular momentum J. (Since three angular momentum functions have been combined, the eigenfunctions for each J value are in general degenerate. Here a particular set of eigenfunctions has been selected according to the j values, and the members are distinguished by the left-hand superscript.) Equation (8) may now be written

$$\begin{aligned} \Psi_0 = \Sigma_{m_I m_S m_L j J} A_{m_S} B_{m_L} &(SLjm_S + m_L | SLm_S m_L) \\ &\times (IjJm_I + m_S + m_L | Ijm_I m_S + m_L) \\ &\times {}^i\chi_J{}^{m_L+m_S+m_I} \epsilon_{m_I} / (2I+1)^{\frac{1}{2}}. \end{aligned}$$

The effect of a nuclear reaction is to transform each state ${}^i\chi_J{}^M$ into $\Sigma_K (2I+1)^{\frac{1}{2}}\, {}^K\rho_J{}^i\, {}^K\Phi_J{}^M$, where ${}^K\rho_J{}^i$ is independent of M, and ${}^K\Phi_J{}^M$ is one of the states of the outgoing particles having the same transformation properties as $\chi_J{}^M$. The outgoing wave function then is

$$\begin{aligned} \Psi_f = \Sigma_{m_I m_S m_L j J K}\, {}^K\rho_J{}^i A_{m_S} B_{m_L} &\times (SLjm_S + m_L | SLm_S m_L) \\ &\times (IjJm_I + m_S + m_L | Ijm_I m_S + m_L) \\ &\times {}^K\Phi_J{}^{m_L+m_S+m_I} \epsilon_{m_I}. \end{aligned} \tag{9}$$

The argument of Eisner and Sachs[9] can be followed from here on. If the coefficient of Φ in Eq. (9) is written as α, the absolute square of the outgoing wave function has the form[11]

$$\begin{aligned} \Psi_f{}^\dagger \Psi_f = \Sigma_{m_I} \Sigma_{m_S m_L J K}\, &\alpha^*_{m_S m_L J K} ({}^K\Phi_J{}^{m_L+m_S+m_I})^\dagger \\ &\times \Sigma_{m_S' m_L' J' K'}\, \alpha_{m_S' m_L' J' K'} \\ &\times ({}^{K'}\Phi_{J'}{}^{m_L'+m_S'+m_I'}). \end{aligned} \tag{10}$$

[8] C. N. Yang, Phys. Rev. **74**, 764 (1948).

[9] E. Eisner and R. G. Sachs, Phys. Rev. **72**, 680 (1947); L. Wolfenstein and R. G. Sachs, **73**, 528 (1948).

[10] A_{m_S} may in general contain phase factors like ϵ_λ. Thus for an initial unpolarized state of spin $\frac{1}{2}$, $A_{\frac{1}{2}} = \epsilon_1/2^{\frac{1}{2}}$, $A_{-\frac{1}{2}} = \epsilon_2/2^{\frac{1}{2}}$.

[11] $\Psi^\dagger$ is the conjugate transpose of Ψ. $\Psi^\dagger\Psi$ implies a summation over all the spin variables involved in Ψ.

If the product of the Φ's in Eq. (10) is reduced to a sum of terms $\Psi_{\mathbf{J}}{}^{\mu}$ which transform under rotation like an eigenfunction of total angular momentum $\mathbf{J}$, the maximum value of μ that occurs is seen to be $2(L+S)$. Because this holds in all coordinate systems it follows that $\mathbf{J}$ must be less than $2(L+S)$, that is

$$\Psi_f{}^{\dagger}\Psi_f=\sum_{\mathbf{J}=0}^{\mathbf{J}=2(L+S)}\sum_{\mu=-\mathbf{J}}^{\mu=\mathbf{J}}C_{\mathbf{J}\mu}\Psi_{\mathbf{J}\mu}. \tag{11}$$

If $\Psi_f{}^{\dagger}\Psi_f$ is integrated over all the independent variables except the outgoing direction of one particle, it follows that the maximum degree spherical harmonic that can enter in the angular distribution of the intensity of this particle is $2(L+S)$. Furthermore, the parity of each term entering Eq. (9) is the same being determined by L, the intrinsic parties of the initial particles, and the conservation of parity. It follows that each product obtained in squaring Ψ_f has even parity, and consequently only even spherical harmonics enter the angular distribution. Theorem 1 is now proved for the case of a single L value. Theorem 1A may be proved in a similar manner.

The argument is easily extended to the case in which more than one orbital angular momentum is effective with L in the previous results interpreted as the maximum orbital angular momentum $L_{\max}$. Equation (10) takes the form

$$\Psi_f{}^{\dagger}\Psi_f=\sum_{mI}(Q^{\dagger}{}_{L_{\max}}+Q^{\dagger}{}_{L_{\max}-1}+\cdots)\times(Q_{L_{\max}}+Q_{L_{\max}-1}+\cdots).$$

The terms $Q_{L_{\max}}{}^{\dagger}Q_{L_{\max}}$ have been considered. By the previous argument the terms $Q_{L_{\max}}{}^{\dagger}Q_{L_{\max}-1}$ when reduced to the form (11) can contain no $\mathbf{J}$ value greater than $(L_{\max}+L_{\max}-1+2S)$. Furthermore, these terms must have odd parity. It follows that the maximum degree spherical harmonic which can arise from these terms is one less than that which can arise from the terms already considered.

For particles of spin $\frac{1}{2}$ the outgoing intensity is related to the initial direction of polarization by the following theorem:

Theorem 3.—(a) Polarization parallel to the axis of incidence (z axis) has no effect on the intensity.

(b) Assuming initial polarization along the y axis, the effect of the polarization on the angular distribution of the outgoing intensity is to produce a left-right asymmetry given by

$$\sum_{n=0}^{2L_{\max}-1}a_n\cos^n\theta\sin\theta\cos\phi,$$

where θ is the angle of scattering and ϕ is the azimuth angle measured from the x axis. If only one parity need be considered in the incident wave (that is, only odd or only even L), n is restricted to odd values.

To prove Theorem 3(a) an outgoing beam is considered with intensity I_0 in a given direction (x_0, y_0, z_0). Symmetry about the axis of incidence (z axis) must obtain because no other direction is defined; therefore, the intensity is I_0 at $(x_0, -y_0, z_0)$. Now consider the transformation

$$y'=-y,\quad x'=x,\quad z'=z.$$

The only effect of this on the incident wave is to reverse the direction of polarization (because the spin is an axial vector); for the outgoing wave it gives the intensity I_0 at $(x_0, -y_0, z_0)$. Thus the intensity is the same for the two directions of polarization.

The proof of 3(b) will be given in two steps, the first of which parallels the proof just completed. Let the intensity at (x_0, y_0, z_0) be I_0. In this case the transformation $y'=-y$ does not alter the incident state but gives the intensity I_0 at $(x_0, -y_0, z_0)$:

$$\begin{aligned}I(-y_0)&=I(y_0),\\ I(-\phi)&=I(\phi).\end{aligned} \tag{12}$$

Setting m_L equal to zero in Eq. (10), $\Psi_f{}^{\dagger}\Psi_f$ contains products of the form $(\Phi_J{}^{m_I+m_S})^{\dagger}(\Phi_J{}^{,m_I+m_S'})$. Analyzing Φ_J into products of the outgoing spin and orbital functions, carrying out the sums over the spin variables, and designating the remaining orbital functions $Y_l{}^M$, one is left with products of the form $(Y_l{}^{m_I+m_S+m})^*(Y_{l'}{}^{m_I+m_S'+m})$. Since $(Y_l{}^M)^*$ equals $\pm Y_l{}^{-M}$, these are of the form

$$Y_l{}^{-(m_I+m_S+m)}\,Y_{l'}{}^{,m_I+m_S'+m}.$$

Consequently, in Eq. (11) the maximum absolute value of μ is the maximum absolute value of $m_S'-m_S$, namely, 1. (For the unpolarized case, the maximum value of μ is zero.) For polarization parallel to the y axis, $A_{\frac{1}{2}}=1/2^{\frac{1}{2}}$, $A_{-\frac{1}{2}}=i/2^{\frac{1}{2}}$. For this case the sum of all the terms $(Y_l{}^{m_I+m_S+m})^{\dagger}Y_{l'}{}^{,m_I+m_S'+m}$ for which $m_S=m_S'$ gives the unpolarized result, considering Eq. (4). The remaining terms for which $m_S\neq m_S'$ represent the difference between the polarized and unpolarized cases and reduce into those terms of Eq. (11) for which μ equals ±1. Thus the angular distribution of the intensity difference between the unpolarized and polarized cases may be expanded in spherical harmonics $\Psi_{\mathbf{J}}{}^{1}$ and $\Psi_{\mathbf{J}}{}^{-1}$. To satisfy Eq. (12) the combinations proportional to $\cos\phi$ must be chosen; these are

$$\begin{aligned}&\mathbf{J}=1\ \sin\theta\cos\phi,\\ &\mathbf{J}=2\ \sin\theta\cos\theta\cos\phi,\\ &\mathbf{J}=3\ (5\sin\theta\cos^2\theta-\sin\theta)\cos\phi,\quad\text{etc.}\end{aligned}$$

The maximum value of $\mathbf{J}$ is $2L_{\max}$ (Theorem 2), and odd values of $\mathbf{J}$ are forbidden if only incident waves

of a single parity need be considered. Theorem 3(b) follows immediately.

The formalism employed here is clearly symmetrical in initial and final states. Theorems 1, 2, and 3 may therefore be easily transformed into theorems concerning the angular distribution of a specified state of polarization of an outgoing particle provided the incident particle is unpolarized. In particular, from Theorem 3 one obtains

Theorem 4.—For an incident unpolarized beam, the outgoing particle, if polarized, will be polarized perpendicular to the plane of the motion and the polarized intensity will have an angular distribution

$$\sum_{n=0}^{2L_{\max}-1} a_n \cos^n\theta \sin\theta.$$

The special case of elastic scattering will now be considered further. In the customary theory of scattering[12] extended to particles of spin $\frac{1}{2}$ the scattered wave may be written:

$$\Psi_f U(r) = f(\theta, \phi) u_0 U(r),$$

where $U(r)$ is essentially an outgoing spherical wave, u_0 is the initial spin state, and $f(\theta, \phi)$ is an operator operating on this state. An arbitrary operator f may be expanded

$$f(\theta, \phi) = g(\theta, \phi) + \boldsymbol{\sigma}\cdot\mathbf{h}(\theta, \phi). \tag{13}$$

The scattering cross section per unit solid angle is given by

$$\frac{dS}{d\omega} = u_0^\dagger |f(\theta, \phi)|^2 u_0$$
$$= |g|^2 + |\mathbf{h}|^2 + 2\bar{\boldsymbol{\sigma}}_0 \cdot Re(g^*\mathbf{h}), \tag{14}$$

where $\bar{\boldsymbol{\sigma}}_0$ describes the initial spin state. The polarization of the scattered wave is determined from

$$\boldsymbol{\sigma}_f \frac{dS}{d\omega} = u_0^\dagger f^\dagger(\theta, \phi) \boldsymbol{\sigma} f(\theta, \phi) u_0$$
$$= |g|^2 \bar{\boldsymbol{\sigma}}_0 + 2Re(g^*\mathbf{h}) + 2\bar{\boldsymbol{\sigma}}_0 \times Im(g^*\mathbf{h}) + 2\bar{\boldsymbol{\sigma}}_0 \cdot \mathbf{h}^*\mathbf{h} - |\mathbf{h}|^2 \bar{\boldsymbol{\sigma}}_0. \tag{15}$$

For an initially unpolarized beam

$$\bar{\boldsymbol{\sigma}}_f = 2Re(g^*\mathbf{h}) / \{|g|^2 + |\mathbf{h}|^2\}. \tag{16}$$

This expression, of course, is also equal to the percentage change in cross section introduced by polarizing the initial beam in the direction of $Re(g^*\mathbf{h})$, as obtained from Eq. (14). If the scattering is not dependent on the nuclear spin, it follows from Theorem 3 or 4 that $\mathbf{h}$ is normal to the plane of the motion and is proportional to $\sin\theta$. The last follows from the fact that $g(\theta, \phi)$ is as in usual scattering theory a polynomial in $\cos\theta$.

II. PRODUCTION OF POLARIZED PROTONS USING POLARIZED NEUTRONS

If polarized thermal neutrons[1] are used as projectiles in the (n, p) reactions of N^{14} or He^3 it is possible that the resultant protons may also be polarized. These possibilities are investigated following the formalism of Section I.[13]

For the (n, p) reaction with nitrogen, the spin I equals 1 so that J values of $\frac{3}{2}$ and $\frac{1}{2}$ are possible. Since both N^{14} and C^{14} have even parity, the final orbital angular momentum values l are limited to even numbers. Since C^{14} has zero nuclear spin, the values $J=\frac{3}{2}$ and $J=\frac{1}{2}$ must correspond to l equals 2 and 0, respectively.

Using Eqs. (9) and (6), the expectation value $\bar{\boldsymbol{\sigma}}$ of the proton spin may be calculated. The component of $\bar{\boldsymbol{\sigma}}$ normal to the plane defined by the outgoing particle direction and the original direction of polarization is zero, while the other components resolved perpendicularly and parallel to the outgoing direction are

$$\bar{\sigma}_\perp \equiv \bar{\sigma}_x \cos\theta - \bar{\sigma}_z \sin\theta = \tfrac{1}{3}(1+W)\sin\theta,$$
$$\bar{\sigma}_{11} \equiv \bar{\sigma}_x \sin\theta + \bar{\sigma}_z \cos\theta = -\tfrac{1}{3}(1-2W)\cos\theta, \tag{17}$$
$$W = \{|\rho_{3/2}|^2 + 2Re(\rho_{3/2}\rho_{\frac{1}{2}}^*)\} / \{|\rho_{3/2}|^2 + \tfrac{1}{2}|\rho_{\frac{1}{2}}|^2\}.$$

Here the z axis is the direction of the original neutron polarization, and the outgoing particle direction is given by the usual spherical coordinates θ and ϕ with ϕ equal to zero. The fact that no higher power of $\sin\theta$ or $\cos\theta$ than the first can enter Eq. (17) can be demonstrated on general grounds for this case.

The penetrability of the Gamow barrier for the outgoing protons is about 0.001 for outgoing d-waves ($J=\frac{3}{2}$) and 0.14 for outgoing s-waves ($J=\frac{1}{2}$). As a consequence it may be shown that the probability that the experimental cross section is primarily due to the $J=\frac{3}{2}$ resonance is only about one-sixth the probability that it is primarily due to the $J=\frac{1}{2}$ resonance. If the $J=\frac{3}{2}$ resonance has only a small effect, the outgoing proton will have a polarization of about 33 percent for θ equal to 90°.

For the (n, p) reaction with He^3, the spin I equals $\frac{1}{2}$ so that J values of 1 and 0 are possible. Since the product H^3 nucleus has spin $\frac{1}{2}$ the value $J=1$ may correspond to a final orbital angular momentum l of either 0 or 2, while the value $J=0$ corresponds to l equals 0. For the s-disintegration the proton energy is above the Coulomb barrier, while for the d-disintegration the barrier penetrability is only

[12] N. F. Mott and H. S. W. Massey, *Theory of Atomic Collisions* (Oxford University Press, New York, 1933).

[13] I wish to thank Dr. Frank C. Hoyt for showing me the work he had initiated on this problem.

about 0.02. It seems reasonable therefore to ignore the d-disintegration completely; one then obtains in the same manner as before

$$\bar{\sigma}_\perp = -\tfrac{2}{3}\sin\theta(1+R\cos\gamma)/(1+\tfrac{1}{3}R^2),$$
$$\bar{\sigma}_{11} = \tfrac{2}{3}\cos\theta(1+R\cos\gamma)/(1+\tfrac{1}{3}R^2), \quad (18)$$
$$Re^{i\gamma} = \rho_0/\rho_1.$$

If R is close to zero the proton polarization is about 67 percent, while if R is equal to infinity there can naturally be no polarization because only angular momentum $J=0$ is involved. The polarization is found to be at least 20 percent for a wide range of values of R and γ.

III. DETECTION OF POLARIZATION BY THE $Li^7(p, \alpha)\alpha$-REACTION

A possible reaction for the detection of polarized protons is[14]

$$Li^7+H^1 \rightarrow 2He^4.$$

For unpolarized protons the angular distribution of the reaction may be represented by[15]

$$(dS/d\omega)_0 \sim 1+A(E)\cos^2\theta+B(E)\cos^4\theta, \quad (19a)$$

where θ is the angle between the line of centers of the leaving particles and that of the incident particles, and E is the initial kinetic energy. This angular distribution has been successfully analyzed[16,17] on the assumption that the ground state of Li^7 has odd parity so that only odd orbital angular momenta are effective in the reaction. In particular, s-waves are not effective in the reaction, which makes it especially favorable for the detection of polarization. If p-waves alone are considered it follows from the general analysis that the only possible effect of polarizing the incident protons along the z axis is to add to the unpolarized angular distribution a term

$$(dS/d\omega)_p \sim C(E)\sin\theta\cos\theta\cos\varphi. \quad (19b)$$

If f-waves also are considered a still further term may be added;

$$D(E)\sin\theta\cos^3\theta\cos\phi.$$

An explicit expression for $C(E)$ will be worked out for the case of p-waves alone. Since $I=\frac{3}{2}$ (for Li^7), $L=1$, and $S=\frac{1}{2}$, and since the final state has even parity and no spin, there are three factors $\rho_J{}^j$: $\rho_0{}^{\frac{1}{2}}$, $\rho_2{}^{\frac{1}{2}}$, and $\rho_2{}^{\frac{3}{2}}$. The final intensity may be obtained by squaring Eq. (9) and interpreting $\Phi_J{}^M$ as the spherical harmonics $Y_J{}^M$. For initial protons unpolarized this yields

$$(dS/d\omega)_0 = \tfrac{1}{6}|\rho_0{}^{\frac{1}{2}}|^2+\tfrac{5}{6}|\rho_2{}^{\frac{1}{2}}|^2+\tfrac{5}{6}|\rho_2{}^{\frac{3}{2}}|^2$$
$$-\{\tfrac{5}{6}Re(\rho_2{}^{\frac{1}{2}}\rho_2{}^{\frac{3}{2}*})-(5^{\frac{1}{2}}/6)Re(\rho_0{}^{\frac{1}{2}}\rho_2{}^{\frac{3}{2}*})$$
$$+(5^{\frac{1}{2}}/6)Re(\rho_0{}^{\frac{1}{2}}\rho_2{}^{\frac{1}{2}*})\}(3\cos^2\theta-1). \quad (20)$$

For polarization along the y axis the difference $(dS/d\omega)_p$ between the polarized and unpolarized intensities is

$$(dS/d\omega)_p = \{(5^{\frac{1}{2}}/2)Im(\rho_0{}^{\frac{1}{2}}\rho_2{}^{\frac{3}{2}*})$$
$$-(5/2)Im(\rho_2{}^{\frac{1}{2}}\rho_2{}^{\frac{3}{2}*})\}\sin\theta\cos\theta\cos\phi. \quad (21)$$

From Eqs. (19a), (19b), (20), and (21),

$$\frac{C(E)}{A(E)} = \frac{5^{\frac{1}{2}}Im(\rho_2{}^{\frac{1}{2}}\rho_2{}^{\frac{3}{2}*})-Im(\rho_0{}^{\frac{1}{2}}\rho_2{}^{\frac{3}{2}*})}{5^{\frac{1}{2}}Re(\rho_2{}^{\frac{1}{2}}\rho_2{}^{\frac{3}{2}*})+Re(\rho_0{}^{\frac{1}{2}}\rho_2{}^{\frac{3}{2}*})-Re(\rho_0{}^{\frac{1}{2}}\rho_2{}^{\frac{1}{2}*})}. \quad (22)$$

The fractional change in the scattered intensity caused by polarization has a maximum for $\theta=45°$ and $\phi=0°$, given by

$$r = \frac{(dS/d\omega)_p}{(dS/d\omega)_0} = \frac{C/A}{1+2/A}. \quad (23)$$

Since A ranges between 1 and 2, for energies from

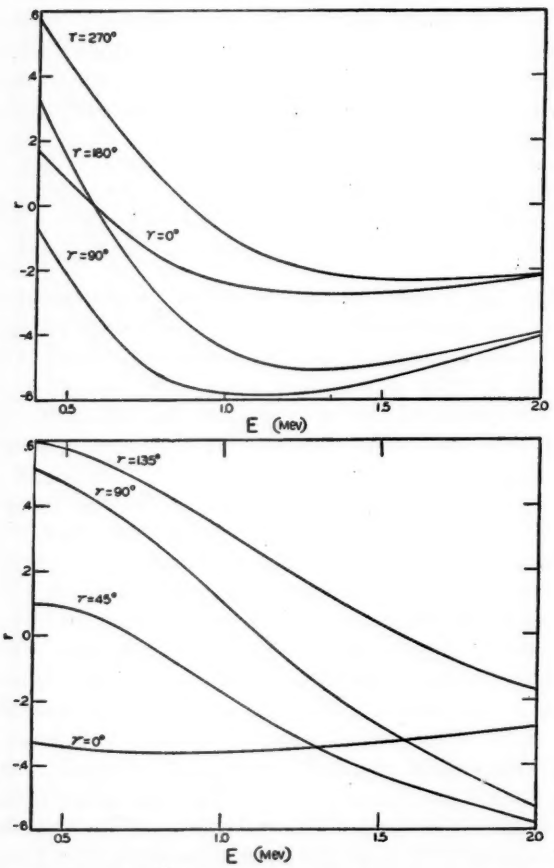

FIG. 1. Fractional change r in the scattered intensity as a result of the polarization of protons in the $Li^7(p,\alpha)\alpha$ reaction for $\theta=45°$ and $\phi=0°$ as a function of proton energy E and phase factor γ. Upper curve: one $J=0$ and one $J=2$ resonance assumed. Lower curve: two $J=2$ resonances assumed. (A change of 180° in γ changes the sign of r.)

[14] I am indebted to Dr. Robert G. Sachs for this suggestion and for discussions concerning it.

[15] Heydenburg, Hudson, Inglis, and Whitehead, Phys. Rev. **73**, 241 (1948).
[16] C. Critchfield and E. Teller, Phys. Rev. **60**, 10 (1941).
[17] David R. Inglis, Phys. Rev. **74**, 21 (1948).

0.5 to 2.0 Mev, an appreciable effect is expected unless (C/A) is in the neighborhood of zero. Equation (22) shows that (C/A) may vanish only if—

(1) $\rho_2^{\frac{1}{2}}=0$,
(2) $Im(\rho_0^{\frac{1}{2}}\rho_2^{\frac{1}{2}*})=5^{\frac{1}{2}}Im(\rho_2^{\frac{1}{2}}\rho_2^{\frac{1}{2}*})$.

Both of these conditions are very special and there is no reason to believe that they hold. Furthermore, even if the second condition were valid at one energy it would not be expected to hold over a sizeable energy interval. From the previous equations upper limits $r_{\max}$ may be set on the possible absolute values of r. If only $J=2$ is involved

$$r_{\max}=(3^{\frac{1}{2}}/2)(3+2A-A^2)^{\frac{1}{2}}/(A+2).$$

Using the experimental value of A,[15] this gives a maximum r of 0.36 at 1-Mev energy and of 0.6 at energies of 0.5 and 2.0 Mev. If both $J=0$ and $J=2$ are involved, for the values of A of interest,

$$r_{\max}=\tfrac{1}{4}(63+66A-A^2)^{\frac{1}{2}}/(A+2).$$

At 1 Mev this limit is 0.86, while at 0.5 and 2.0 Mev it is 0.95.

The use of the resonance formula to determine the value of r (Eq. 23) is not generally possible for two reasons: (1) it is not possible from the experimental data to determine all the constants in the resonance formula for the unpolarized angular distribution; (2) even if these constants are determined there remains completely undetermined a phase factor[18] which critically affects $(dS/d\omega)_p$ although not affecting $(dS/d\omega)_0$. However, it was thought of interest to calculate the polarization effect using the resonance formula for two cases:

(a) A very broad resonance with $J=0$ plus a narrower resonance with $J=2$ was assumed, using a set of constants suggested by Inglis[17] to fit the experimental data.

(b) Two resonances with $J=2$ were assumed, each having a width of 1 Mev and located at 0 and 2 Mev,[19] using one set of constants that fit the data roughly.

The results are given in Fig. 1 as a function of proton energy E and the undetermined phase factor γ.

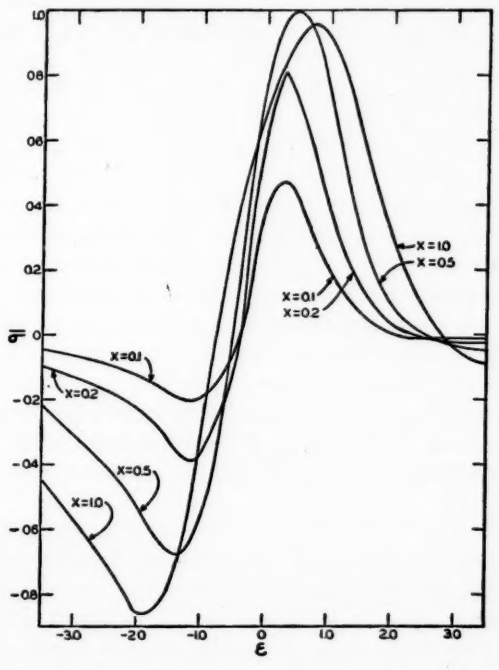

FIG. 2. Polarization $\bar{\sigma}$ of protons scattered from a doublet P resonance as a function of energy ϵ and splitting x. $\delta_0=45°$, $\eta=0$, $\theta=90°$.

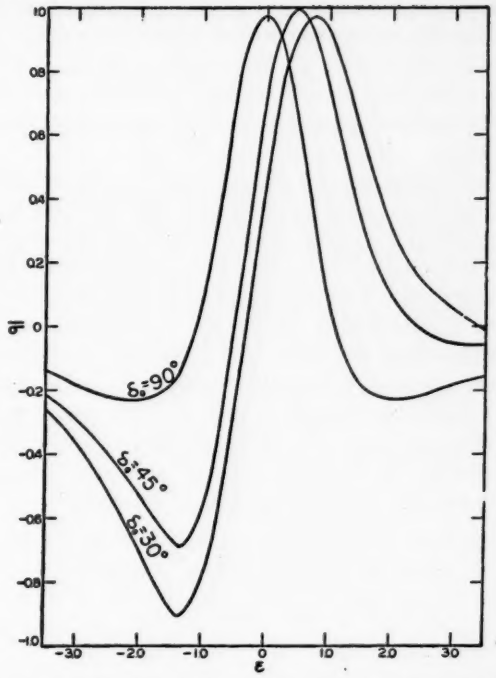

FIG. 3. Polarization $\bar{\sigma}$ of protons scattered from a doublet P resonance as a function of energy ϵ and s-phase shift δ_0. $x=0.5$, $\eta=0$, $\theta=90°$.

IV. POLARIZATION EFFECTS IN RESONANCE SCATTERING

The possibility of polarizing neutrons and also of detecting the polarization by means of the scattering from a resonance level that is split because of spin-orbit coupling was suggested by Schwinger.[4] In particular, he considered the scattering of neutrons with energy about 1 Mev from helium. Ex-

[18] This is the phase of the scattering from total spin 1 relative to that from total spin 2 (see the bottom of page 26 of reference 17). For purposes of calculation this phase factor was introduced by replacing $\sin\xi$ on page 14, of reference 16 by $\sin\xi e^{i\gamma}$. If two $J=2$ resonances are considered one obtains in a similar manner factors γ for the higher energy resonance and γ' for the lower energy. $(dS/d\omega)_0$ depends on $(\gamma-\gamma')$ but otherwise is independent of γ (or γ').

[19] This possibility has been suggested by R. Christy and S. Rubin, Phys. Rev. **71**, 275A (1947).

periments[20] indicate that a p-wave resonance exists around this energy and that there is a considerable splitting between the $^2P_{3/2}$ and $^2P_{\frac{1}{2}}$ levels. A similar split resonance level would be expected around 2 Mev in the case of the scattering of protons from helium.

The scattering of a proton from a nucleus without spin is first considered in general with only one assumption: that incident orbital angular momenta L greater than 1 need not be considered. (For convenience, the polarization of an initially unpolarized beam is discussed, although, of course, one can directly convert this into the effect of initial polarization on the outgoing intensity.) In terms of the s-wave phase shift δ_0 and the two p-wave phase shifts $\gamma_{3/2}$ and $\gamma_{\frac{1}{2}}$, which correspond to total angular momenta J of $\frac{3}{2}$ and $\frac{1}{2}$, respectively, the scattering cross section for an unpolarized beam is*

$$\begin{aligned} dS/d\omega=\lambda\!\!\!^{-2}\{|&-(\eta/2s^2)\exp[-i\eta\ln s^2]+\sin\delta_0 e^{i\delta_0}\\ &+\cos\theta[2\sin\gamma_{3/2}\exp[i(\gamma_{3/2}+\sigma_1)]\\ &+\sin\gamma_{\frac{1}{2}}\exp[i(\gamma_{\frac{1}{2}}+\sigma_1)]]|^2\\ &+\sin^2\theta\sin^2(\gamma_{3/2}-\gamma_{\frac{1}{2}})\}, \end{aligned} \tag{24}$$

and the expectation value $\bar{\sigma}$ of the spin after scattering is given by

$$\begin{aligned} \bar{\sigma}dS/d\omega=&-2\lambda\!\!\!^{-2}\sin\theta\sin(\gamma_{3/2}-\gamma_{\frac{1}{2}})\\ &\times\{\sin\delta_0\sin(\gamma_{3/2}+\gamma_{\frac{1}{2}}+\sigma_1-\delta_0)\\ &-(\eta/2s^2)\sin(\gamma_{3/2}+\gamma_{\frac{1}{2}}+\sigma_1+\eta\ln s^2)\\ &+3\cos\theta\sin\gamma_{3/2}\sin\gamma_{\frac{1}{2}}\}\mathbf{n}. \end{aligned} \tag{25}$$

Here

$$\begin{aligned} &\lambda\!\!\!^{-}=\hbar/Mv, \quad \eta=Ze^2/\hbar v, \quad \sigma_1=2\tan^{-1}\eta,\\ &s=\sin(\theta/2), \quad \mathbf{n}=(\mathbf{k}\times\mathbf{k}')/|\mathbf{k}\times\mathbf{k}'|, \end{aligned} \tag{26}$$

where v is the incident velocity, M is the reduced mass of the proton, and $\mathbf{k}$ and $\mathbf{k}'$ are incident and outgoing wave vectors, respectively. From Eq. (7) the percentage polarization is equal to the magnitude of $\bar{\sigma}\cdot\mathbf{n}$, which will be written $\bar{\sigma}$.

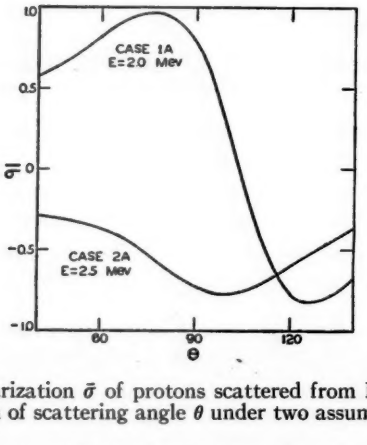

FIG. 4. Polarization $\bar{\sigma}$ of protons scattered from helium as a function of scattering angle θ under two assumptions.

[20] T. A. Hall and P. G. Koontz, Phys. Rev. **72**, 196 (1947); H. Staub and H. Tatel, Phys. Rev. **58**, 820 (1940).

* It is to be noted throughout that θ is in the center-of-mass system.

For a small value of the splitting as measured by $(\gamma_{3/2}-\gamma_{\frac{1}{2}})$ the polarization effect is directly proportional to the splitting. It is of interest to compare this with the effect of the splitting on the cross section. Introducing a mean phase shift $\bar{\gamma}$ into Eq. (24) by the substitution

$$\begin{aligned} &2\sin\gamma_{3/2}\exp[i(\gamma_{3/2}+\sigma_1)]+\sin\gamma_{\frac{1}{2}}\exp[i(\gamma_{\frac{1}{2}}+\sigma_1)]\\ &\quad=-3ie^{i\sigma_1}[(1-T)/2]+3T\sin\bar{\gamma}\exp[i(\bar{\gamma}+\sigma_1)],\\ &T=[1-8/9\sin^2(\gamma_{3/2}-\gamma_{\frac{1}{2}})]^{\frac{1}{2}}, \end{aligned} \tag{27}$$

$$\bar{\gamma}=\tfrac{1}{2}\tan^{-1}\left\{\frac{2\sin 2\gamma_{3/2}+\sin 2\gamma_{\frac{1}{2}}}{2\cos 2\gamma_{3/2}+\cos 2\gamma_{\frac{1}{2}}}\right\},$$

one finds that the effect of the splitting on the cross section is proportional to $\sin^2(\gamma_{3/2}-\gamma_{\frac{1}{2}})$ and thus to $(\gamma_{3/2}-\gamma_{\frac{1}{2}})^2$ for small values of the splitting. Consequently sizeable polarization effects may exist in some cases even though the splitting cannot be detected from the cross section alone.

If the p-wave scattering is assumed to be due to a split resonance with energies $E_{3/2}$ and $E_{\frac{1}{2}}$ and a single width Γ, the phase shifts at an energy E are expressed

$$\begin{aligned} &\gamma_{3/2}=\cot^{-1}(\epsilon+x),\\ &\gamma_{\frac{1}{2}}=\cot^{-1}(\epsilon-x),\\ &\epsilon=[(E_{3/2}+E_{\frac{1}{2}})/2-E](2/\Gamma),\\ &x=(E_{3/2}-E_{\frac{1}{2}})/\Gamma, \end{aligned} \tag{28}$$

where ϵ and x are dimensionless forms of the energy and the splitting.[20] Substituting Eq. (28) into Eqs. (24) and (25), the polarization $\bar{\sigma}$ is found as a function of ϵ and x, the s-phase shift δ_0, and the Coulomb factor η. The results for θ equal to 90° and η equal to zero are shown in Figs. 2 and 3. (The general features of the curves are the same for values of η up to 0.3.) It should be noted that a change in sign in x merely changes the sign of $\bar{\sigma}$ and a change in sign of δ_0 merely changes the sign of ϵ. One sees that for x greater than 0.2 a polarization of more than 80 percent is generally obtainable at one energy. For smaller values of x, the polarization is approximately proportional to x. A secondary polarization maximum with the polarization reversed in sign also exists, which becomes more important as x increases and as δ_0 decreases. The two maxima are separated by an energy of the order of the resonance width, assuming this is not less than the separation of the two resonances. In general, there exists an angular interval about 90° with a width of at least 30° over which the average polarization effect is similar in magnitude to that at 90°.

The particular case of the scattering of protons by helium will now be considered. The experimental angular distributions seem to show the presence of a p-wave resonance between 2.0 and 3.0 Mev.[21] An analysis made on the basis of the

[21] N. P. Heydenburg and N. F. Ramsey, Phys. Rev. **60**, 42 (1941); Freier, Lampi, Sleator, and Williams, Phys. Rev. **75**, 342 (1949).

earlier data and under the assumption that d-wave scattering is unimportant indicates that this p-wave resonance must be split. From this analysis the following conclusions about the polarization effect are drawn:

(a) The polarization for θ equal to 90° should reach a maximum value of about 80 percent at an energy between 2.0 and 2.5 Mev. (The earlier data goes only to 3.0 Mev and consequently does not allow the specification of a second polarization maximum.)

(b) The width of the polarization maximum may be as large as 1 Mev.

(c) The polarization $\bar{\sigma}$ as a function of scattering angle θ at an energy corresponding to a maximum of the polarization effect is given by one of the curves in Fig. 4. Cases 1A and 2A are distinguished by the assumed sign of δ_0: negative for 1A and positive for 2A.

These conclusions may be modified by consideration of the recent data.

V. POLARIZATION EFFECTS IN COULOMB SCATTERING

The earliest method suggested for the polarization of an elementary particle was to make use of the spin-orbit coupling in the Coulomb scattering of electrons.[2] Mott found that a polarization of the order of 30 percent should be possible at relativistic velocities and large atomic numbers. Recently Schwinger[5] has proposed a method for polarizing neutrons employing the interference between the spin-dependent Coulomb scattering and the nuclear scattering at small scattering angles where the two are of the same magnitude. For the case of protons, which will now be considered, however, the spin-independent Coulomb scattering greatly decreases this effect at small angles.

A classical treatment of this interaction between the proton spin and the Coulomb field is not significant at any energy as may be shown from an uncertainty principle argument.[22] In the quantum-mechanical approach, the proton is treated by the Dirac equation with an added Pauli term to describe the anomalous magnetic moment:

$$(E-eV+\beta mc^2)\Psi=-c\boldsymbol{\alpha}\cdot\mathbf{p}\Psi-(e\hbar/2Mc)(\mu_a/i)\beta\boldsymbol{\alpha}\cdot\mathbf{E}\Psi, \quad (29)$$

where V is the Coulomb potential, $\mathbf{E}=-\nabla V$, and μ_a is the anomalous moment in units of $e\hbar/2Mc$. The discussion of this equation will be restricted to the condition $v^2/c^2\ll 1$. An approximate solution for the scattered wave valid under the conditions, $\alpha^2\equiv(Z/137)^2\ll 1$ and $\eta<1$, is the following:

$$f(\theta)=-\lambda\!\!\!^{-}(\eta/2)\{\csc^2(\theta/2)-(v^2/c^2)(\mu_a+\tfrac{1}{2})i\boldsymbol{\sigma}\cdot\mathbf{n}\cot(\theta/2)\}\exp[-i\eta\ln\sin^2(\theta/2)], \quad (30)$$

where $\mathbf{n}$ is the unit normal to the plane of motion. This result is identical with the Born approximation except for the addition of the characteristic Coulomb phase factor, which multiplies not only the ordinary Coulomb scattering but the spin-dependent scattering as well.[23]

From Eqs. (13), (16), and (30), it follows that to this approximation the Coulomb scattering gives no polarization effect. The highest order polarization effect is obtained by adding to $f(\theta)$ of Eq. (30) the nuclear scattering

$$f_n(\theta)=\lambda\!\!\!^{-}[\sin\delta_0 e^{i\delta_0}+3\cos\theta\sin\delta_1 e^{i(\delta_1+\sigma_1)}+\cdots]. \quad (31)$$

From Eq. (16) one then obtains for the expectation value of the spin for scattering at an angle θ

$$\bar{\sigma}=\mathbf{n}(\mu_a+\tfrac{1}{2})\lambda\!\!\!^{-}\eta(v^2/c^2)\cot(\theta/2)\left\{\frac{\cos(\eta\ln s^2)Im(f_n)+\sin(\eta\ln s^2)Re(f_n)}{|f_n-(\lambda\!\!\!^{-}\eta/2s^2)e^{-i\eta\ln s^2}|^2+\frac{1}{4}(\mu_a+\frac{1}{2})^2(v^4/c^4)\lambda\!\!\!^{-2}\eta^2\cot^2(\theta/2)}\right\}, \quad (32)$$

where $\mathbf{n}$, η, s, and σ_1 are defined in Eq. (26). The region of validity of the equation is energy $E>0.025Z^2$ Mev, $E\ll 465$ Mev, and $(Z/137)^2\ll 1$; these conditions follow from $\eta<1$, $(v^2/c^2)\ll 1$ and $\alpha^2\ll 1$, respectively.

The polarization effect is seen to vanish for both $\theta=180°$ and $\theta=0°$. The order of magnitude at moderate angles may be obtained by setting the product of $\lambda\!\!\!^{-}$, the fractional expression in Eq. (32), and $\cot\theta/2$ equal to unity, giving

$$\bar{\sigma}\simeq(u_a+\tfrac{1}{2})\eta(v^2/c^2)=1.23\cdot 10^{-3}Z[E(\text{Mev})/2.5]^{\frac{1}{2}}.$$

Calculations of the maximum polarization effect considering only s-wave nuclear scattering are given in Table I. These results were calculated from Eq.

TABLE I. Maximum polarization effect caused by Coulomb scattering and nuclear s-wave scattering as a function of s-wave phase shift δ_0, atomic charge Z, and proton energy E. $\epsilon=E$ (Mev)/2.5 Mev. $\bar{\sigma}$ = maximum polarization. θ = angle of scattering for maximum effect.

	$Z=1\epsilon^{\frac{1}{2}}$		$Z=5\epsilon^{\frac{1}{2}}$		$Z=10\epsilon^{\frac{1}{2}}$	
δ_0	$\bar{\sigma}/\epsilon$	θ	$\bar{\sigma}/\epsilon$	θ	$\bar{\sigma}/\epsilon$	θ
90°	0.0032	31°	0.0068	66°	0.0076	90°
60°	0.0072	30°	0.026	64°	0.026	96°
30°	0.026	39°	0.090	90°	0.020	130°
15°	0.100	52°	0.032	138°	—	—
−30°	0.0016	54°	0.0032	68°	0.0038	80°
−60°	0.0024	39°	0.0062	62°	0.0084	76°

[22] This result is to be expected from the general argument given in reference 12, p. 45.

[23] For $\mu_a=0$ Eq. (30) is obtained by Mott (see reference 2) as the first terms in the expansion of the exact solution of Eq. (29) in powers of α^2. The extension of the spin-dependent part of the solution to include a non-zero anomalous moment follows from considering Mott's expansion as a perturbation-theory solution of the second-order equation corresponding to Eq. (29).

(32) neglecting the term in (v^4/c^4) in the denominator and thus are not accurate for large values of $\bar{\sigma}$ (greater than 0.2). In general the polarization effect varies only slowly with θ; the width of the maxima are of the order of 30°. The very large polarization effects occurring for certain positive phase shifts result from a large amount of cancellation in the denominator of Eq. (32) and therefore are associated with minima in the scattered intensity. For energies much greater than $0.025Z^2$ Mev ($\eta \ll 1$) it may be shown that for a given value of δ_0, the maximum polarization $\bar{\sigma}$ is proportional to $Z^{\frac{1}{3}}E^{\frac{1}{3}}$. This may be used to extrapolate some of the data of Table I.

In the special case of proton-proton scattering this effect is of a smaller order of magnitude because polarization effects can occur only for the triplet state, for which there is no s-wave scattering. A considerably larger polarization effect for this case is likely to be that due to the tensor force in the nuclear interaction. This too, however, is extremely small (less than 0.1 percent at 7 Mev) under any reasonable form of interaction. A discussion of polarization effects in $n-p$ and $p-p$ scattering will be given in a later paper.

VI. DEPOLARIZATION OF POLARIZED PROTONS

For experimental purposes it is important to know the extent to which polarized protons are depolarized by various types of scattering as they are slowed down. A beam of completely polarized protons is considered; the percentage depolarization $(1-P_f)$ after passing through a thickness dt containing N scattering centers per unit volume will be expressed

$$1-P_f=S_{\text{dep}}Ndt. \tag{33}$$

P_f is the average polarization of all particles scattered through an angle less than θ_0, plus all particles not scattered; that is, of all particles to be included experimentally in the direct beam. It follows from Eqs. (5) and (7) that

$$P_f^2=\frac{\left|\left(1-Ndt\int(dS/d\omega)d\omega\right)\bar{\sigma}_0+Ndt\int_{<\theta_0}\bar{\sigma}_f(dS/d\omega)d\omega\right|^2}{\left[1-Ndt\int_{>\theta_0}(dS/d\omega)d\omega\right]^2}.$$

Neglecting terms in $(dt)^2$ this gives

$$P_f=1-Ndt\int_{<\theta_0}(1-\bar{\sigma}_0\cdot\bar{\sigma}_f)(dS/d\omega)d\omega, \tag{34}$$

$$S_{\text{dep}}=\int_{<\theta_0}(1-\bar{\sigma}_0\cdot\bar{\sigma}_f)(dS/d\omega)d\omega.$$

Substituting from Eqs. (14) and (15)

$$S_{\text{dep}}=2\int_{<\theta_0}\{|\mathbf{h}|^2-|\bar{\sigma}_0\cdot\mathbf{h}|^2\}d\omega. \tag{35}$$

If $\mathbf{h}$ is a well defined vector, that is, independent of the spin of the scatterer, the integration over ϕ may be carried out using the fact that $\mathbf{h}$ must be perpendicular to the plane of the motion and independent of ϕ in magnitude. This gives

$$S_{\text{dep}}=(1+\cos^2\xi)2\pi\int_0^{\theta_0}|\mathbf{h}(\theta)|^2\sin\theta d\theta, \tag{36}$$

where ξ is the angle between the initial polarization and the axis of incidence. It is to be noted that the depolarization is proportional to the square of the spin-dependent interaction and is not affected by interference between the spin-dependent and spin-independent scattering. Since the depolarization is found to be small the total depolarization for a thickness t may be given by $S_{\text{dep}}Nt$. In this case some particles will be included in the calculation that are scattered through a total angle greater than θ_0 due to plural small angle scattering, thus somewhat overstimating the depolarization. It will prove satisfactory for present purposes, however, to obtain an upper limit on the depolarization.

Five causes of depolarization are considered.

(1) Elastic Coulomb scattering from the nucleus. Using Eqs. (30) and (36), replacing the lower limit of the integral in the latter by an angle $\theta_{\min}$, and assuming $\theta_{\min}\ll\theta_0\ll 1$ one finds

$$(S_{\text{dep}})_1=2\pi(1+\cos^2\xi)(\mu_a+\tfrac{1}{2})^2\times(Ze^2/Mc^2)^2\ln(\theta_0/\theta_{\min}). \tag{37}$$

The angle $\theta_{\min}$ is determined by the screening of the Coulomb field by the atomic electrons; for a screening radius r_0

$$\theta_{\min}=\lambda\!\!\!^{-}/r_0. \tag{38}$$

A classical calculation based on the precession of the spin in the magnetic field also gives Eq. (37) but $\lambda\!\!\!^{-}$ in Eq. (38) must be replaced by the classical minimum distance of approach. Letting θ_0 equal 5.7°, $\cos\xi=0$, and $r_0=5.3\cdot10^{-2}/Z^{\frac{1}{3}}$ one obtains at reasonable energies the order-of-magnitude result

$$(S_{\text{dep}})_1=6\cdot10^{-30}Z^2. \tag{39}$$

(2) Inelastic Coulomb scattering from atomic electrons. As might be expected, this gives a

smaller depolarization than the previous case for $Z=1$ and depends linearly rather than quadratically on Z. Therefore

$$(S_{\text{dep}})_2<6\cdot10^{-30}Z. \tag{40}$$

(3) Interaction of the proton magnetic moment with the magnetic moment of the atomic electrons. It is interesting to note that this interaction is of the same order of magnitude as the Coulomb interaction. The Coulomb interaction is proportional to

$$\mu_0(e\hbar/Mc)(e/r^2)(v/c),$$

while this interaction is proportional to

$$\mu_0(e\hbar/Mc)(e\hbar/mc)(1/r^3),$$

where m is the electron mass and μ_0 is the effective proton moment. The minimum value of r for a collision with an electron is $(\hbar/mv)$; substituting this in the above expressions shows them to be equal. A Born approximation calculation substituted into Eq. (35) gives the result that Eq. (40) also holds for $(S_{\text{dep}})_3$. Adding up all the electromagnetic effects

$$(S_{\text{dep}})_{\text{electromagn.}}<6\cdot10^{-30}(Z^2+2Z). \tag{41}$$

(4) Nuclear scattering involving spin-orbit coupling but no spin-spin coupling. An example is the scattering from helium considered in Section IV. For such a case

$$|\mathbf{h}|=K\lambda\sin\theta,$$

where K is of the order of unity and the proportionality to $\sin\theta$ follows from the statement at the end of Section I. Substituting this into Eq. (36)

$$(S_{\text{dep}})_4=(1+\cos^2\xi)(\pi/2)\lambda^2K^2\theta_0^4$$

which is at most of the order of $10^{-4}\lambda^2$.

(5) Nuclear scattering involving only spin-spin coupling. Let the nuclear spin be I and

$$f_+(\theta)=f(\theta) \text{ for total spin } S=I+\tfrac{1}{2},$$
$$f_-(\theta)=f(\theta) \text{ for total spin } S=I-\tfrac{1}{2}.$$

If $\mathbf{I}$ is a vector in the direction of the nuclear spin with magnitude $I(I+1)$, $f(\theta)$ for both total spins may be written in the form of Eq. (13) with

$$\begin{aligned} g(\theta)&=[(I+1)f_+(\theta)+If_-(\theta)]/(2I+1),\\ \mathbf{h}(\theta)&=\mathbf{I}[f_+(\theta)-f_-(\theta)]/(2I+1). \end{aligned} \tag{42}$$

Substituting from Eq. (42) in Eq. (35), averaging over-all directions of $\mathbf{I}$, and assuming $f_+(\theta)$ and $f_-(\theta)$ to be fairly constant about $\theta=0°$,

$$(S_{\text{dep}})_5=\frac{4\pi}{3}\frac{I(I+1)}{(2I+1)^2}|f_+(0)-f_-(0)|^2\theta_0^2. \tag{43}$$

Writing the scattered waves in terms of phase shifts as in Eq. (31) one obtains

$$(S_{\text{dep}})_5=\frac{4\pi}{3}\frac{I(I+1)}{(2I+1)^2}\theta_0^2\lambda^2\Big|\sum_L(2L+1)\times\sin(\delta_L^+-\delta_L^-)e^{i(\delta_L^++\delta_L^-)}e^{i\sigma_L}\Big|^2. \tag{44}$$

If the phase-shift differences involved are large this will be the largest of all the depolarization effects and $(S_{\text{dep}})_5$ will be of the order of magnitude of $0.01\lambda^2$.

As a typical example the depolarization of 7-Mev protons stopped in hydrogen is considered. For this case

$$\delta_L^{\pm}=\tfrac{1}{2}(1\pm(-1)^{L+1})\delta_L.$$

The depolarization $(1-P_f)$ of the completely stopped protons due to all causes is only about 10^{-5}.

VII. CONCLUSION

It has been attempted in this paper to emphasize the general features of nuclear reactions involving polarized protons. In conclusion, it is worth while to indicate the practicability of experiments using solely the reactions considered here. Because any experiment on polarization effects involves of necessity a double scattering, the problem of obtaining sufficient intensity is a critical one. The intensity will be maximized if the experiment is designed merely to detect the polarization effect, so that good resolution of angles and energies is not required. Such experiments are simplified by the fact that polarization may be detected by the qualitative feature of a left-right asymmetry in the second scattering.

If the initial intensity is I_0 the intensity after a scattering or a nuclear reaction is

$$s_1I_0=(Nt)_1\int(dS/d\omega)_1d\omega_1I_0,$$

where N is the number of scattering centers per unit volume, t is the thickness, and the limits of the integral are determined by the experimental geometry. The polarized intensity equals

$$r_1s_1I_0=(Nt)_1\left|\int(\bar{\sigma}_1dS/d\omega)_1d\omega_1\right|I_0.$$

Similarly after the second scattering (or nuclear reaction) the symmetrical intensity may be written $s_2s_1I_0$, while the additional scattering to the right or left resulting from the polarization effect may be written $r_2s_2r_1s_1I_0$. After time T the total number of events observed to one side is

$$s_2s_1I_0T(1+r_1r_2)\pm[s_2s_1I_0T(1+r_1r_2)]^{\frac{1}{2}},$$

and to the other side

$$s_2s_1I_0T(1-r_1r_2)\pm[s_2s_1I_0T(1-r_1r_2)]^{\frac{1}{2}}.$$

The difference is approximately

$$s_2 s_1 I_0 T(2r_1 r_2) \pm 2[s_2 s_1 I_0 T]^{\frac{1}{2}}.$$

Setting the arbitrary criterion that the statistical error should be less than one-tenth of the effect to be measured, the total number of incident particles required is

$$I_0 T > 100/(s_2 s_1 r_2^2 r_1^2). \quad (45)$$

The required values of I_0T have been estimated from Eq. (45) for several experiments on the assumption that the scattering thickness and the solid angle of the scattering are determined from the following considerations: (1) the incident energy in each scattering act must be well-defined relative to the width of the polarization maximum, (2) the final proton must be able to reach the counting apparatus, (3) within these limitations product sr^2 is to be maximized for each reaction. Order-of-magnitude results follow:

A. Polarized protons produced by $He^3(n,p)$ reaction and detected by $Li^7(p,\alpha)$ reaction. Assuming a 100 percent concentration of He^3,

$$I_0 T > 1.5 \cdot 10^{14}/C^2 P^2,$$

where P is the polarization of the protons after the first reaction (Eq. (18)), and C is defined by Eq. (19b). If C^2 has a value of 0.3 in the energy interval around 0.5 Mev and P is equal to 0.5, a flux of about $5 \cdot 10^{11}$ polarized thermal neutrons per second would be required for one hour.

B. Polarized protons produced by scattering from helium and detected by $Li^7(p,\alpha)$ reaction. Assuming that the solid angle for the helium scattering is chosen symmetrically about 90°,

$$I_0 T > 2 \cdot 10^{16}/(r_{90°})^2 C^2,$$

where $(r_{90°})$ is the polarization for 90° scattering from helium. If $(r_{90°})$ has a value of 0.7, and C has a value of 1 in the energy interval about 1.5 Mev, 2.0 microampere-hour of protons around 3.0 Mev is required.

C. Double scattering from helium. This is particularly hard to estimate because it has not been possible to determine the expected energy dependence of the polarization effect. If a resonance actually exists, it appears to be as broad as the proton energy loss caused by 90° scattering. It therefore seems possible that the initial scattering could be done at the high energy side of a polarization maximum and the second scattering at the low energy side of the same maximum. Another possibility is that suggested by Schwinger for the case of neutrons; that is, using one polarization maximum for the first scattering and a second maximum (see Figs. 2 and 3) for the second scattering. In either case one has very roughly

$$I_0 T > 2 \cdot 10^{13}/(r_{90°})_1^2 (r_{90°})_2^2.$$

This gives about 0.005 microampere-hour of 3.0- to 4.0-Mev protons required.

Thus neither of the last two possibilities can be ruled out solely on the basis of the fundamental limitations considered here. On this basis the double scattering experiment from helium appears the most practical. Both of the last two are made more difficult by the fact that the energy at which the polarization effect occurs for each of the two reactions must be determined experimentally. It must be emphasized that important practical limitations have not been considered here; in particular, limitations on the usable solid angle in each reaction imposed by the experimental geometry and the background count. Consequently it cannot be concluded whether any of the possibilities considered here is practical at this time.

I wish to express my thanks to Professor Edward Teller for the suggestion of this problem and for many helpful discussions concerning it. I also wish to express my appreciation of a DuPont fellowship in physics, which I held while carrying out this research.

The Analysis of Neutron-Proton Scattering with Tensor Forces

RICHARD S. CHRISTIAN
Radiation Laboratory, University of California, Berkeley, California
(Received February 17, 1949)

The expansion in energy of the cross section for central force scattering proposed by Chew and Goldberger is extended to tensor force scattering. The change due to the addition of tensor forces, in both the effective range and in the shape dependent coefficient, is shown to be small. Hence, as has been previously shown by Blatt and Jackson for central forces, scattering below 10 Mev is practically independent of the potential shape assumed and is completely characterized by the scattering length and effective range.

A PERTURBATION method for the analysis of nucleon-nucleon scattering by central forces has recently been proposed by Chew and Goldberger[1] among others.[2-4] It is the purpose of the present note to extend the work of Chew and Goldberger to include tensor force scattering. We will, therefore, follow their notation as closely as practicable and their paper should be consulted for a discussion of the general problem.

The second-order differential system which arises in the consideration of the $({}^3S_1+{}^3D_1)$ state with tensor forces, we write in the matrix form

$$(L(x)+F(x))\,U(x)=-\kappa^2 U(x), \tag{1}$$

where $L=(L_{ij})$ and $F=(F_{ij})$ for $i,j=1,2$. That is, explicitly, $L_{11}=d^2/dx^2$, $L_{22}=(d^2/dx^2)-(6/x^2)$, $L_{12}=L_{21}=0$ and $F_{11}=f(x)$, $F_{22}=f(x)-2g(x)$, and $F_{12}=F_{21}=2^{\frac{1}{2}}g(x)$, where $f(x)$ and $g(x)$ are self-adjoint short range operators. $U(x)$ is a two-component vector, with components $u(x)$ and $w(x)$. There are in general four such independent vector solutions of Eq. (1). The wronskian of any two vector functions is defined by

$$W_x(U_i,\,U_j)=u_i(x)u_j'(x)-u_i'(x)u_j(x)+w_i(x)w_j'(x)-w_i'(x)w_j(x). \tag{2}$$

It is a consequence of this definition and the self-adjoint nature of Eq. (1) that the wronskian of any two solutions of (1) is a constant. We adopt the convention that the subscripts 1 and 3 shall indicate solutions which are zero at the origin, the so-called regular solutions, and the subscripts 2 and 4 those which are irregular at the origin. For convenience we specify that the solutions are chosen such that

$$W_x(U_1,\,U_2)=W_x(U_3,\,U_4)=1, \tag{3}$$

and all other wronskian combinations vanish identically.

The asymptotic forms of U_1 and U_3 are defined as the two-component vectors X_2 and X_4, respectively, which are themselves solutions of the system

$$(L)X_i=-\kappa^2 X_i. \tag{4}$$

The vectors U_2 and U_4 are defined to be such as to have the asymptotic forms $-X_1$ and $-X_3$, respectively.

The solutions of Eqs. (1) and (3) contain only three independent constants, these being sufficient to characterize scattering completely. We may conveniently choose the regular solutions such that both components of U_i have the same phase shift, δ_i. The remaining constant will then express the asymptotic ratio between the two components of a solution. This completes the definition of a complete set of U vectors which are explicitly tabulated below in terms of their asymptotic forms, the X vectors:

$$U_2\rightarrow -X_1=(1/1+R\kappa^4)\begin{pmatrix}(\sin\kappa x/\kappa)\\ R\kappa^4(j_2(\kappa x)/\kappa^3)\end{pmatrix}, \tag{5a}$$

$$U_1\rightarrow X_2=\begin{pmatrix}\kappa\cot\delta_1(\sin\kappa x/\kappa)+(\cos\kappa x)\\ R[\kappa^5\cot\delta_1(j_2(\kappa x)/\kappa^3)+(\kappa^2 n_2(\kappa x))]\end{pmatrix}, \tag{5b}$$

$$U_4\rightarrow -X_3=(1/1+R\kappa^4)\begin{pmatrix}-R(\sin\kappa x/\kappa)\\ (j_2(\kappa x)/\kappa^3)\end{pmatrix}, \tag{5c}$$

$$U_3\rightarrow X_4=\begin{pmatrix}-R[\kappa^5\cot\delta_3(\sin\kappa x/\kappa)+\kappa^4(\cos\kappa x)]\\ \kappa^5\cot\delta_3(j_2(\kappa x)/\kappa^3)+(\kappa^2 n_2(\kappa x))\end{pmatrix}. \tag{5d}$$

In general, $\kappa\cot\delta_1$, $\kappa^5\cot\delta_3$, and the ratio R are functions of κ^2. In the limit of $\kappa^2\rightarrow 0$ the forms $\kappa\cot\delta_1$ and $\kappa^5\cot\delta_3$ are finite and are the reciprocals of the scattering lengths a_1 and a_3, respectively. The contribution to the total cross section from this state is given by

$$\sigma=(4\pi/k^2)(\sin^2\delta_1+\sin^2\delta_3). \tag{6}$$

The U vectors in the limit of $\kappa^2\rightarrow 0$, we call the V vectors. They obviously satisfy the relation

$$(L+F)\,V_i=0. \tag{7}$$

[1] G. F. Chew and M. L. Goldberger, Phys. Rev. **75**, 1637 (1949).
[2] J. M. Blatt and J. D. Jackson, Phys. Rev. in press.
[3] Julian Schwinger, *Hectographed Notes on Nuclear Physics* (Harvard University, Cambridge, 1947).
[4] R. E. Peierls and F. C. Barker, Phys. Rev. **75**, 312 (1949).

The limiting X vectors we call the Y vectors. They satisfy the relation

$$(L)\,Y_i=0. \tag{8}$$

From Eqs. (1) and (7) we derive

$$W_{x_0}(V_i,\,U_j)=W_{x_1}(V_i,\,U_j)+\kappa^2\int_{x_0}^{x_1}(V_iU_j)dx, \tag{9}$$

where scalar multiplication is implied by the juxtaposition of the two vectors as in the integrand above.

Similarly from Eqs. (4) and (8) we get

$$W_{x_0}(Y_i,\,X_j)=W_{x_1}(Y_i,\,X_j)+\kappa^2\int_{x_0}^{x_1}(Y_iX_j)dx. \tag{10}$$

To eliminate the singular terms occurring in this last equation in the limit $x_0\to 0$ it is convenient to define the new vectors $X_2^{(l)}$ and $X_4^{(l)}$ which are formed by subtracting from the second component of X_2 and X_4, R and 1 (one) times the first l terms in the expansion of $(\kappa^2 n_2(\kappa x))$ in powers of $(\kappa x)^2$, respectively. These satisfy the relations

$$(L)X_i^{(l)}=-\kappa^2X_i^{(l-1)}. \tag{11}$$

Hence from Eqs. (8) and (11) we get

$$W_0(Y_i,\,X_j^{(l)})=W_{x_1}(Y_i,\,X_j^{(l)})+\kappa^2\int_0^{x_1}(Y_iX_j^{(l-1)})dx. \tag{12}$$

From Eqs. (9) and (12) and the definitions of the asymptotic forms we can derive several relations analogous to the central force fundamental identity, Eq. (10) of Chew and Goldberger. We consider only the combination formed from the first two solutions

$$W_0(Y_2,\,X_2^{(3)})=\kappa^2\int_0^{\infty}(Y_2X_2^{(2)}-V_1U_1)dx. \tag{13}$$

Evaluating the left-hand side we find

$$W_0(Y_2,\,X_2^{(3)})=(\kappa\cot\delta_1-1/a_1)+R_0R_s\kappa^5\cot\delta_1. \tag{14}$$

The right-hand side of Eq. (13) can be expanded in powers of κ^2 by an iteration procedure based on the integral equation satisfied by U_1, which is shown in the appendix to be

$$\begin{aligned}U_1=W_x(V_2,\,U_1)V_1+W_x(V_4,\,U_1)V_3&\\ \times\kappa^2\Big[V_1\int_x^{x_1}(V_2U_1)dx+V_3\int_x^{x_1}(V_4U_1)dx&\\ +V_2\int_0^{x}(V_1V_1)dx+V_4\int_0^{x}(V_3V_1)dx\Big],&\end{aligned} \tag{15}$$

which by use of Eqs. (9) and (10) can be written in the form

$$\begin{aligned}U_1=V_1+\kappa^2\Big[-V_1\int_0^{x}(V_2U_1)dx&\\ -V_3\int_0^{x}(V_4U_1)dx+V_2\int_0^{x}(V_1V_1)dx&\\ +V_4\int_0^{x}(V_3V_1)dx+V_1\int_0^{\infty}(V_2U_1+X_1Y_2)dx&\\ +V_3\int_0^{\infty}(V_4U_1+X_3Y_2)dx\Big].&\end{aligned} \tag{16}$$

Similarly we find for the irregular solution $X_2^{(2)}$ of Eq. (11) the integral equation

$$\begin{aligned}X_2^{(2)}=Y_2^{(1)}+\kappa^2\Big[-Y_1\int_0^{x}(Y_2X_2^{(1)})dx&\\ -Y_3\int_0^{x}(Y_4X_2^{(1)})dx+Y_2^{(1)}\int_0^{x}(Y_1X_2)dx&\\ +Y_4^{(1)}\int_0^{x}(Y_3X_2)dx&\\ +Y_1\int_0^{\infty}(Y_2X_2^{(1)}-V_1U_1)dx&\\ +Y_3\int_0^{\infty}(Y_4X_2^{(1)}-V_3U_1)dx\Big].&\end{aligned} \tag{17}$$

Using these last two equations and Eqs. (13) and (14) we can write

$$\kappa\cot\delta_1=1/a_1+W_0\kappa^2+W_1\kappa^4+\cdots, \tag{18}$$

where

$$W_0=\int_0^{\infty}[(x/a_1+1)^2-V_1V_1]dx. \tag{19}$$

and

$$\begin{aligned}W_1=-R_0^2/a_1-2\int_0^{\infty}[(x/a_1+1)x-V_1V_2]dx\int_0^{x}(V_1V_2)dx&\\ +2\int_0^{\infty}[(x/a_1+1)^2-V_1V_1]dx\int_0^{x}(x/a_1+1)xdx&\\ -2\int_0^{\infty}[(x/a_1+1)R_0x-R_0x/5-V_4V_1]dx\int_0^{x}(V_1V_3)dx&\\ +2\int_0^{\infty}[(x/a_1+1)(-R_0x/5a_3)+R_0x/5a_3-V_1V_3]dx\int_0^{x}[R_0x(x/a_1+1)-R_0x/5]dx.&\end{aligned} \tag{20}$$

It can be noted here that the integral of V_1V_1 is larger than that of the corresponding central force function, hence W_0 will be reduced by the addition of tensor forces. The exact expression for W_1 is complicated by the presence of all four V solutions, however it can be approximated by neglecting terms proportional to R^2. The result is then identical with the central force case. (The neglected terms are smaller by a factor of the order of the fraction of $^3D_1$ admixture in the ground state of the deuteron.)

The preceding analysis was carried out by expanding about the zero-energy state, however it is clear that this may be generalized to an expansion about any energy, even to negative energies corresponding to a bound state. In particular since the deuteron bound state wave function is generally available from calculations of the binding energy quadrupole moment, etc., it is desirable to calculate the expansion coefficients using the bound state wave function, $V_1(\alpha)$. We will then be able to calculate an approximate third coefficient simply from the change in the second coefficient. The expansion about the bound state is

$$\kappa\cot\delta_1=-\alpha+W_0'(\kappa^2+\alpha^2)+W_1'(\kappa^2+\alpha^2)^2+\cdots, \quad (21)$$

where $-\alpha^2$ gives the binding energy on the bound level, and

$$W_0'=\int_0^\infty[e^{-2\alpha x}-V_1(\alpha)V_1(\alpha)]dx, \quad (22)$$

with an expansion for W_1' similar to the one for W_1.

We can further relate the scattering length to the binding energy of the bound level, that is, we expand the bound level wave functions in the zero-energy wave functions as in Eq. (15). The result is evidently

$$1/a_1=-\alpha+W_0\alpha^2-W_1\alpha^4+\cdots. \quad (23)$$

Combining this result with Eqs. (18) and (21) we get the approximate expression for W_1

$$W_1\cong(1/2\alpha^2)(W_0-W_0'). \quad (24)$$

(The coefficient W_0' has been given by Schwinger[3] using a variational procedure and is one-half the effective range in the current terminology.)

Calculations with these formulas have been made for the meson potentials by E. W. Hart and the present author[5] in connection with the analysis of the high energy scattering. The modifications in the effective range due to the addition of tensor forces is at most a few percent for effective ranges less than 2×10^{-13} cm and with tensor strengths sufficient to account for the quadrupole moment. For example, the results with a meson potential of range 1.35×10^{-13} cm can be approximately expressed by

$$2W_0=1.64(1-0.0090P_D)\times10^{-13}\text{ cm}, \quad (25)$$

where P_D is the percentage $^3D_1$ state in the deuteron. The modification of W_1 is also small.

In particular it is possible to characterize scattering below 10 Mev by means of only two parameters scattering length and effective range, even in the presence of tensor forces.

The author wishes to thank Professor Serber and Drs. Chew and Goldberger for helpful discussions and advice.

This work was performed under the auspices of the AEC.

APPENDIX

The coupled second order differential system, Eq. (1) in the text, can be replaced by a system of four first-order differential substitutions $y_{1i}=u_i$, $y_{2i}=u_i'$, $y_{3i}=w_i$, and $y_{4i}=w_i'$. We can therefore write Eq. (1) as the matrix equation[6]

$$Y'(x)=A(x)Y(x), \quad (1A)$$

where

$$A(x)=-\begin{pmatrix}0 & -1 & 0 & 0\\ F_{11}(x) & 0 & F_{12}(x) & 0\\ 0 & 0 & 0 & -1\\ F_{21}(x) & 0 & F_{22}(x)-(6/x^2) & 0\end{pmatrix} \quad (2A)$$

and $Y=(y_{ij})$. That is, each column represents an independent solution. It is readily verified by direct application of (1A) that $\det Y(x)$ is a constant and further that if C is a constant matrix, $Y(x)C$ is the most general solution of (1A).

$$Z'(x)=-Z(x)A(x), \quad (3A)$$

which is the so-called adjoint system. By use of (1A) and (3A) it can be shown that the product $Z(x)Y(x)$ is a constant matrix. We can therefore choose an adjoint solution, such that $Z(x)Y(x)=I$, i.e., $Z(X)=Y^{-1}(x)$.

A general adjoint solution of (3A) is given by

$$Z(x)=\begin{pmatrix}u_2(x) & -u_2(x) & w_2(x) & -w_2(x)\\ -u_1(x) & u_1(x) & -w_1(x) & w_1(x)\\ u_4(x) & -u_4(x) & w_4(x) & -w_4(x)\\ -u_3(x) & u_3(x) & -w_3(x) & w_3(x)\end{pmatrix}. \quad (4A)$$

It is further equal to $Y^{-1}(x)$ if the conditions of Eq. (3) are imposed upon the otherwise arbitrary solutions. The relation $Y(x)Z(x)=I$, yields the following identities

$$u_1(x)u_2'(x)-u_1'(x)u_2(x)+u_3(x)u_4'(x)-u_3'(x)u_4(x)=1, \quad (5A)$$

$$w_1(x)w_2'(x)-w_1'(x)w_2(x)+w_3(x)w_4'(x)-w_3'(x)w_4(x)=1, \quad (6A)$$

$$w_1(x)u_2(x)-w_2(x)u_1(x)+w_3(x)u_4(x)-w_4(x)u_3(x)=0. \quad (7A)$$

which are just the relations necessary for establishing the validity of the integral Eq. (14) of the text.

[5] R. Christian and E. W. Hart, Bull. Am. Phys. Soc. **24**, No. 2, F6 (1949).

[6] G. D. Birkhoff and R. E. Langer, Proc. Am. Acad., **58**, No. 2 (1923).

The Scattering of Deuterons by Helium at Deuteron Energies from 0.9 to 3.5 Mev

J. Morris Blair,* George Freier, E. E. Lampi, and William Sleator, Jr.†
University of Minnesota, Minneapolis, Minnesota
(Received February 21, 1949)

The differential cross sections for the elastic scattering of deuterons by helium have been measured for deuterons of 0.9 to 3.5 Mev over an angular range from 15° to 160° in the center-of-mass system. The probable error in the absolute values of the cross sections is 3 percent or less. For angles greater than 60° the cross sections are roughly independent of angle except at 3.5 Mev where they decrease with increasing angle up to 90° and increase beyond.

As a continuation of our program of studying the scattering of various combinations of light nuclei[1-3] we have investigated the scattering of deuterons in helium for deuterons in the energy range of 0.9 to 3.5 Mev.

EXPERIMENTAL PROCEDURE

The same scattering chamber, counters, etc., were used in this work as the experiments on proton-proton[1] and deuteron-deuteron scattering[2] previously reported, except that the helium gas was admitted to the scattering chamber through a charcoal trap cooled with liquid nitrogen instead of through the palladium tube used for hydrogen and deuterium. The general procedure for taking data was the same as that described in reference 1, with the addition of background runs taken under normal operating conditions but with a small brass shutter moved in front of the counter slit system to prevent the entrance of scattered charged particles. The background counting rate observed in this was due mainly to recoil nuclei from the neutrons in the counter, and under proper operating conditions was only a few percent of the counting rate for scattered particles.

The electrostatic analyzer which controlled the energy of the incident deuterons was calibrated by means of the $Li^7(p,n)Be^7$ reaction, the threshold of which was taken to be 1.883 Mev. The effective thickness of the Nylon entrance window was measured both before and after the data were taken and at both times was found to be about 55 kv for 1.9-Mev protons. The energies were corrected for the energy losses in the windows and in the scattering gas between the window and the center of the chamber.**

Data were taken at various scattering angles from 10° to 90° in the laboratory system. For deuterons of energy 0.90 and 1.42 Mev the scattered deuterons would not pass through the counter window at angles larger than 30° and 60° respectively and the recoil helium atoms would not enter the counter at any angle. With incident deuterons of higher energy the deuterons could be observed to higher angles, up to 90° at 3.5 Mev; while at small angles the recoil helium atoms could be observed also. In most instances, where both sets of particles entered the counter, the helium atoms produced pulses which were sufficiently larger than those due to the deuterons so that the helium atoms could be counted separately by using a high bias setting on one of the pulse size discriminators. In a few cases the helium atoms had only enough energy to barely enter the counter and produce pulses smaller or so nearly the same size as the deuteron pulses that it was not possible to count the two separately.

The importance of counting the helium nuclei was that it provided a means of obtaining the cross section for deuteron scattering in the backward direction where the deuterons were not energetic enough to enter the counter. In this problem one does not have symmetry about 90° in the center of mass coordinate system, which is present in the proton-proton and deuteron-deuteron cases, so it was of interest to determine the scattering cross section to as large an angle as possible. Since to each deuteron which was scattered in the backward direction there corresponded a recoil helium in the forward direction one could obtain data for the backward directions by observing these recoil helium atoms in the cases where they had energy enough to enter the proportional counter. The cross section for scattering at 120° in the center-of-mass coordinate system, for example, was obtained from counting deuterons at 90° in the laboratory and also counting helium atoms at 30° in the laboratory.

* Now at Argonne National Laboratory, Chicago, Illinois.
† Now at Washington University, St. Louis, Missouri.
[1] Blair, Freier, Lampi, Sleator, and Williams, Phys. Rev. 74, 553 (1948).
[2] Blair, Freier, Lampi, Sleator, and Williams, Phys. Rev. 74, 1594 (1948).
[3] Freier, Lampi, Sleator, and Williams, Phys. Rev. 75, 1345 (1949).
** In the papers on deuteron-deuteron scattering and on the *d-d* reactions referred to in references 2 and 4, an error was made in evaluating these corrections. The best values of the deuteron energies used in these two investigations are, in Mev, 0.87, 1.43, 1.96, 2.49, 3.02 and 3.52 instead of the values 0.96, 1.49, 2.01, 2.51, 3.02 and 3.50 Mev which are given in the tables of these papers.

For taking data at angles where the cross sections were relatively constant and the counting rates low, a proportional counter and analyzing slit system which were larger than those used for previous elastic scattering measurements were used. (This counter was the one used in the measurements on the distribution of the products of the deuteron-deuteron disintegrations.[4]) At points where data were taken with both counters the results agreed within the statistical fluctuations expected from the number of counts recorded.

Throughout the course of the experiment bias curves were taken at several different angles for each deuteron energy to determine the proper bias settings for counting the deuterons and recoil helium nuclei separately. During these surveys no evidence appeared for the presence of protons or neutrons from deuteron disintegration such as have been observed in deuteron helium experiments at higher energies.[5] This is in agreement with calculations which indicate that at the energies we used these disintegration products did not have enough energy to enter the proportional counter.

CORRECTIONS

In contrast to the previously reported observations on deuteron-deuteron scattering,[2] the observed data in this experiment required few corrections. The runs, mentioned above, which were taken with the shutter in front of the analyzer slits determined the small fraction of the counting rate which was caused by recoil atoms from neutrons produced by deuteron bombardments of defining apertures, chamber windows, etc.; and other counts not due to the scattered particles. The accumulation of contaminating gases in the scattering chamber was measured by closing the empty chamber and observing the increase in counting rate over a period of a few hours. It was found that the number of deuterons scattered from the gas which accumulated during this time increased linearly with time and had an angular distribution which agreed with the Coulomb scattering law. From this information one could make corrections to be observed data to eliminate the effect of such contamination. In most cases this correction amounted to less than one percent of the total counting rate.

In order to find out how completely the liquid nitrogen-cooled charcoal trap used in filling the chamber removed the one or two percent of other gases present in the tank helium, a sample of gas was taken from the chamber immediately after filling and analyzed on one of Dr. A. O. C. Nier's mass spectrometers. This test indicated that the helium as it entered the chamber contained about 0.08 percent air nuclei. A correction to be applied to the observed cross sections was calculated from this on the assumption of Coulomb scattering by the air. It amounted to about 1.4 percent at most, and was negligible above 40°.

The presence of about 0.3 percent HH^+ ions in the deuteron beam[2] called for a correction to the beam current measurement, and also a correction for the beam protons scattered into the counter at each angle. However, since these effects were both small and tended to cancel each other, they were ignored.

The corrections due to the finite size of the incident beam of deuterons and of the angular aperture of the proportional counter ("second order geometry" corrections) were computed for us by Mr. Donald Dodder, applying the method used previously.[1] In the present case the scattering cross section at small angles were sufficiently close to the corresponding Coulomb cross sections so that a reasonably accurate determination of the corrections could be made on the assumption of pure Coulomb scattering. This assumption yields corrections which are independent of energy and have the following magnitudes: 2.9 percent at 10° (laboratory system), 1.3 percent at 15°, 0.7 percent at 20°, 0.4 percent at 25° and 0.3 percent at 30°. At larger angles the Coulomb assumption is not adequate, but the corrections certainly decrease as the cross-section curves become straighter and flatter.

RESULTS

The cross sections per unit solid angle in the center-of-mass coordinate system for the scattering of deuterons by helium are given in Table I and Fig. 1. The values for scattering in the forward direction, ϕ_{cm} less than 110°, were obtained from observing the scattered deuterons, while those for backward directions were deduced from counts of

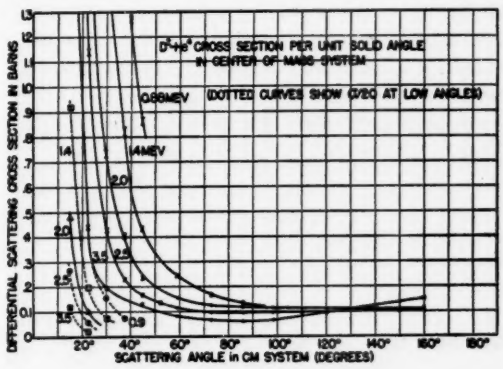
D+He⁴ CROSS SECTION PER UNIT SOLID ANGLE IN CENTER-OF-MASS SYSTEM
0.88MEV
(DOTTED CURVES SHOW 1/20 AT LOW ANGLES)
1.4MEV
2.0
DIFFERENTIAL SCATTERING CROSS SECTION IN BARNS
SCATTERING ANGLE in CM SYSTEM (DEGREES)

FIG. 1. Cross sections per unit solid angle in the center-of-mass coordinate system for the scattering of deuterons of various energies by helium. The dotted curves represent the same data on a scale reduced by a factor of twenty.

[4] Blair, Freier, Lampi, Sleator, and Williams, Phys. Rev. 74, 1599 (1948).

[5] Guggenheimer, Heitler, and Powell, Proc. Roy. Soc. 190, 196 (1947).

TABLE I. Cross sections in the center-of-mass coordinate system for the elastic scattering of deuterons by helium. Deuteron energies are given in the laboratory system, and cross sections are in barns (10^{-24} cm^2).

ϕ_{cm}/E_d	0.88 Mev	1.43 Mev	1.96 Mev	2.48 Mev	3.51 Mev
15° 11′	50.0 ±0.4	18.27 ±0.2	9.45 ±0.10	5.32 ±0.05	2.40 ±0.02
22° 39′	9.66 ±0.10	3.96 ±0.04	1.961±0.02	1.128±0.010	0.436 ±0.008
30° 5′	3.21 ±0.04	1.474±0.02	0.729±0.015	0.423±0.007	0.193 ±0.003
37° 27′	1.484±0.02	0.819±0.015	0.403±0.008	0.227±0.004	
44° 45′	0.856±0.016	0.432±0.008	0.234±0.006	0.167±0.003	0.128 ±0.005
51° 57′				0.135±0.004	
59° 2′		0.244±0.005	0.150±0.003	0.119±0.003	0.083 ±0.002
72° 50′		0.167±0.004	0.122±0.003	0.096±0.002	0.0654±0.0015
85° 59′		0.137±0.003	0.114±0.003	0.095±0.002	0.0585±0.0012
98° 22′			0.109±0.002	0.092±0.002	0.0638±0.0020
110°				0.090±0.002	
120°				0.095±0.0016	0.093 ±0.002
130°			0.102±0.003	0.101±0.002	
140°				0.103±0.002	0.123 ±0.002
150°			0.107±0.002	0.101±0.002	0.141 ±0.002
160°			0.112±0.002	0.107±0.002	0.151 ±0.003

the recoil helium atoms. At 2.5-Mev measurements of the 120° and 130° cross sections by both methods agreed within the probable errors, and at the other energies the two sets of data overlapped smoothly when converted to the center of mass system, indicating the absence of significant errors in geometry. The factors for conversion from laboratory to center-of-mass coordinates were obtained as outlined in reference 3. The probable errors given in the table are those expected from the number of counts recorded at each point. In addition there is a probable error of about 1.7 percent common to all points due to uncertainties in the factors involved in converting the original data into cross sections. The over-all probable error in most of the cross sections is about 3 percent.

The energies at the top of the columns apply to the deuterons in the laboratory system at the center of the chamber, and are accurate in absolute value to about ±20 kv.

Here, as in other charged particle scattering experiments, Coulomb scattering is predominant at the low angles: for example at 1.42 Mev and 30° 5′ the observed cross section differs from the Coulomb by about 14 percent. At higher energies nuclear scattering is relatively more important at the small angles, and completely dominates at the large. At 2.5 and 3.5 Mev the cross section increases with angle above 90°. This effect here, however, is quite small compared to the corresponding one in proton-deuteron scattering.[6] The rather sharp bend in the 3.5-Mev curve at about 25° and the crossing of the curves by each other is suggestive of proton-helium scattering and markedly different from the deuteron-deuteron results. However, the deuteron-helium cross sections are considerably more regular in both energy and angular dependence than are those for protons on helium where an energy resonance is apparent from qualitative examination of the curves.

ACKNOWLEDGMENTS

We are pleased to express our thanks to Professor J. H. Williams for help in designing the experiment, to Professor C. L. Critchfield for help in interpreting the results, and to Mr. Donald Dodder for help in calculations during the course of investigation.

This research was partially supported by the ONR Contract N5ori-147. It was also assisted by the University of Minnesota Technical Research Fund subscribed to by General Mills, Inc., Minneapolis Honeywell Regulator Company, Minneapolis Star Journal & Tribune Company, Minnesota Mining and Manufacturing Company, and Northern States Power Company.

[6] Sherr, Blair, Kratz, Bailey, and Taschek, Phys. Rev. **72**, 662 (1947).

Symmetrical Meson Theory of Nuclear Forces

TA-YOU WU AND H. M. FOLEY
Columbia University, New York, New York

(Received January 19, 1949)

The static and the first order non-static nucleon potential on the basis of the Møller-Rosenfeld-Schwinger mixture of a vector meson of mass κ_0 and a pseudoscalar meson of mass 315 m_e is assumed. One relation among the coupling constants is postulated to remove the inadmissable singularities in the tensor force term. The coupling constants are then determined by means of the binding energy of the deuteron and the total cross section for slow neutron scattering. The potentials so determined are used to calculate the "effective range" r_0 for the triplet and the singlet states (proton-proton scattering), the quadrupole moment Q of the deuteron, and the cross section σ and $\sigma(170°)/\sigma(90°)$ for proton-neutron scattering at 100 Mev. The value $\kappa_0=1.5\times315\ m_e$, while giving somewhat too low values for the r_0's, yields entirely too small a Q and too large a ratio $\sigma(170°)/\sigma(90°)$ whereas the value $\kappa_0=2\times315\ m_e$, while giving better values for Q and $\sigma(170°)/\sigma(90°)$ yields much too small values for the r_0's. It appears that this failure to account for both the high energy and the low energy scattering data is characteristic of any potential having the exchange properties of the symmetrical meson theory.

IT is well known that the various meson theories of nuclear forces in their present forms are met with several difficulties. Thus the neutral meson theory leads to an ordinary force instead of an exchange force; the charged meson theory, while leading to an exchange force, predicts quite different interactions for the proton-proton and proton-neutron systems, and all the neutral, the charged, and the symmetrical meson theories lead to divergence of the type $1/r^3$ in the tensor force part of the nucleon potential. Møller and Rosenfeld[1] point out that this difficulty of the divergence, in the case of the symmetrical theory, can be removed by assuming the nucleon to be coupled to a mixture of a vector and a pseudoscalar meson field, the coupling constants and the meson masses being the same for both fields. The resulting nucleon potential in the static approximation is then free, not only of the divergence, but also of the tensor force. On this theory the quadrupole moment of the deuteron will be accounted for by treating as a perturbation the tensor force which appears in the relativistic approximation. It has then been pointed out by Schwinger[2] that if the two mesons in the above mixture are assumed to have different masses, the vector meson being heavier to give the correct sign for the quadrupole moment of the deuteron, the resulting potential will retain the tensor force which is free of the divergences $1/r^3$ and $1/r^2$. Calculations on this idea have been carried out by Jauch and Hu[3] who found that on taking the lighter (pseudoscalar) meson to be 170 m_e, the quadrupole moment of the deuteron comes out to be consistently too low for various values of the mass of the vector meson.

On the empirical side, there is available at the present the following information concerning the proton-neutron and the proton-proton systems. (1) The binding energy of the deuteron is quite accurately known to be 2.18 Mev.[4] (2) The total cross section of the scattering of slow neutrons by protons is known to be 20.3×10^{-24} cm^2.[5] (3) The scattering of slow neutrons by parahydrogen leads to a value for the phase of ^3S $p-n$ scattering,[6] from which a characteristic quantity defined as the "effective range" r_0 can be determined to be 1.60×10^{-13} cm. (4) The analysis of Breit *et al.*[7] of the proton-proton scattering up to a few Mev leads to an "effective range" $r_0=2.7\times10^{-13}$ cm for the singlet states of proton-proton interaction. (5) The quadrupole moment of the deuteron is found to be 2.73×10^{-27} cm^2.[8] (6) The scattering of neutrons by protons at 90 Mev shows a total cross section $\sigma=0.076\times10^{-24}$ cm^2 and a differential cross section $\sigma(\vartheta)$ which is somewhat asymmetrical with respect to the direction $\vartheta=90°$, with $\sigma(\vartheta<90°)<\sigma(\vartheta>90°)$, and has a ratio $\sigma(170°)/\sigma(90°)\simeq3$.[9]

Various attempts have been made to obtain a nucleon potential to describe some of the above results and various assumed forms for the radial dependence of this interaction have been employed, namely, the rectangular well, the Gaussian, the exponential, and the Yukawa potential. While an empirical approach may prove necessary in the

[1] C. Møller and L. Rosenfeld, Kgl. Danske Vid. Selbs. Nat. Fys. Medd 17, No. 8 (1940); 23, No. 13 (1945).
[2] J. Schwinger, Phys. Rev. 61, 287 (1942).
[3] J. M. Jauch and N. Hu, Phys. Rev. 65, 289 (1944).
[4] M. L. Wiedenbeck and C. J. Marhoefer, Phys. Rev. 67, 54 (1945). Recently Bell and Elliott report the value $\sigma=2.237$ Mev (Phys. Rev. 74, 1552 (1948)). This new value will change the numerical results of this work a little, but will not appreciably affect the main features.
[5] Melkonien, Rainwater, and Havens, Phys. Rev. 75, 1295 (1949).
[6] Sutton, Hall, Anderson, Bridge, DeWire, Lavatelli, Long, Snyder and Williams, Phys. Rev. 72, 1147 (1947).
[7] Breit, Thaxston, and Eisenbud, Phys. Rev. 55, 1018 (1939); Hoisington, Share and Breit, Phys. Rev. 56, 884 (1939).
[8] Kellogg, Rabi, Ramsey, and Zacharias, Phys. Rev. 57, 677 (1940).
[9] Hadley, Kelly, Leith, Segrè, Wiegand, and York, Phys. Rev. 75, 351 (1949).

absence of a completely satisfactory theory, it is deemed worth while to examine more closely the possibilities of the meson theory. The calculations of Jauch and Hu[3] are in this direction, but it seems that they need some modifications in view of our present knowledge that the μ-meson (210 m_e) apparently does not play a role in nucleon interaction whereas the π-meson (285 m_e) probably does. The assumption was made by these authors that the mesonic charge g of the vector meson is zero. Also the solution of the coupled equations for the ground state of the deuteron seems to be not sufficiently accurate. The present work is an attempt to see whether it is possible to account satisfactorily for the observed data mentioned above on the basis of the symmetrical theory as suggested by Møller and Rosenfeld and by Schwinger as this still seems to be the most promising theory at present.*

We shall write the nucleon potential up to the first order non-static term for the vector meson (mass κ_0) and the pseudoscalar meson (mass μ_0) in the form[1]

$$\begin{aligned} V_v &= (\tau_1\cdot\tau_2/3)[3(g^2-(\kappa_0/M)fg)\kappa^2+2(\sigma_1\cdot\sigma_2) \\ &\quad\times(f^2-(\kappa_0/M)fg)\kappa^2-(f^2-(\kappa_0/M)fg) \\ &\quad\times S_{12}(3/r^2+3\kappa/r+\kappa^2)]e^{-\kappa r}/r, \\ V_{\text{p.s.}} &= (\tau_1\cdot\tau_2/3)[(\sigma_1\cdot\sigma_2) \\ &\quad\times(f'^2+(\mu_0/M)f'g')\mu^2+(f'^2+(\mu_0/M)f'g') \\ &\quad\times S_{12}(3/r^2+3\mu/r+\mu^2)]e^{-\mu r}/r, \end{aligned} \tag{1}$$

where M is the nucleon mass, g and f are the mesonic charge and moment, respectively, of the vector meson, etc., and

$$\kappa=\kappa_0 c/\hbar,\quad \mu=\mu_0 c/\hbar,\quad \kappa>\mu,$$
$$S_{12}=3(\sigma_1\cdot\mathbf{r})(\sigma_2\cdot\mathbf{r})/r^2-(\sigma_1\cdot\sigma_2).$$

To remove the $1/r^3$ and the $1/r^2$ divergences, we assume the following relation among the four coupling constants

$$f'^2+(\mu_0/M)f'g'=f^2-(\kappa_0/M)fg. \tag{2}$$

On denoting by

$$x=\mu r,\quad \xi=\kappa/\mu, \tag{3}$$

$$\begin{aligned} f(x) &= (3/x^2+3/x+1) \\ &\quad -(3/x^2+3\xi/x+\xi^2)e^{-(\xi-1)x}, \\ b &= (M/\hbar^2\mu)(1/\xi^2)(f^2-(\kappa_0/M)fg)\kappa^2, \\ {}^1a &= (M/\hbar^2\mu)[-(g^2-(\kappa_0/M)fg)\kappa^2 \\ &\quad +2(f^2-(\kappa_0/M)fg)\kappa^2], \\ {}^3a &= (M/\hbar^2\mu)[3(g^2-(\kappa_0/M)fg)\kappa^2 \\ &\quad +2(f^2-(\kappa_0/M)fg)\kappa^2]=8\xi^2 b-3\,{}^1a, \end{aligned} \tag{4}$$

one finds the potential $V=V_v+V_{\text{p.s.}}$ for the various states as follows:

$$\begin{aligned} {}^3V^{\text{even}} &= -{}^3a(e^{-\xi x}/x)-b(e^{-x}/x) \\ &\quad -bf(x)S_{12}(e^{-x}/x), \\ {}^3V^{\text{odd}} &= -\tfrac{1}{3}\,{}^3V^{\text{even}}, \\ {}^1V^{\text{even}} &= -{}^1a(e^{-\xi x}/x)-b(e^{-x}/x), \\ {}^1V^{\text{odd}} &= -3\,{}^1V^{\text{even}}, \end{aligned} \tag{5}$$

where ${}^3V^{\text{even}}$ denotes the potential for triplet even states, etc.

In the following we assume that the π-meson produced in the laboratory at Berkeley is the pseudoscalar meson. For the vector meson we assume various masses $\kappa_0>\mu_0$. For each pair of κ_0, μ_0, there are only two coupling constants f, g to be determined from two experimental data. For this purpose we take the binding energy of the deuteron and the total cross section of slow neutron scattering. The method of calculation is as follows.

I. Slow neutron scattering:

The Schrödinger equation for the ${}^1S$ wave is

$$d^2u/dx^2+(k^2+{}^1a(e^{-\xi x}/x)+b(e^{-x}/x))u=0, \tag{6}$$

where

$$k^2=ME/\hbar^2\mu^2, \tag{7}$$

E being the energy of the incident neutron in the center of mass system. The observed total cross section for slow neutrons is

$$\sigma=\tfrac{3}{4}\sigma_t+\tfrac{1}{4}\sigma_s=20.3\times10^{-24}\ \text{cm}^2.$$

The contribution of triplet state scattering σ_t to σ is known from the scattering of slow neutrons by parahydrogen, namely, $\sigma_t=2.5\times10^{-24}$ cm^2. Hence

$$\sigma_s=74\times10^{-24}\ \text{cm}^2. \tag{8}$$

As

$$\sigma_s\cong(4\pi/k_0^2)\sin^2\delta_0,\quad k_0^2=ME/\hbar^2,$$

one obtains, for $\mu_0=315m_e$,**

$$k/\sin\delta_0=0.051. \tag{9}$$

We shall seek a relation $F({}^1a, b)=0$ between ${}^1a$ and b for which the solution u of Eq. (6) gives the observed phase δ_0(9). We assume the trial wave function[10]

$$u=\cos\delta_0\sin kx+\sin\delta_0(1-e^{-x})(1+\beta e^{-x})\cos kx, \tag{10}$$

* In a recent note, W. H. Ramsey, Proc. Phys. Soc. London **61**, 297 (1948), believing the proton-proton scattering data (below 10 Mev) to indicate a shorter range for lower energies and a longer range for higher energies, comes to the conclusion that the Schwinger modification of the Møller-Rosenfeld theory is incompatible with these data. It has been shown, however, by Bethe (in recent lectures at Columbia University and in a forthcoming paper in the Physical Review) that within the accuracy of all the available data the proton-proton scattering can be satisfactorily described by the relation (28) with the integral there replaced by a constant "effective range," and that the scattering data for energies below $\simeq$10 Mev can determine only two parameters, namely, the "effective range" and the "effective depth" of the potential, but throws no light on the detailed shape of the potential. Hence the present proton-proton scattering data for energies below ~10 Mev alone cannot be sufficient criterion for testing the Møller-Rosenfeld-Schwinger theory.

** This work was begun in May 1948, when the mass of the π-meson was reported to be $315m_e$. Changing this to the present value, $285m_e$, would change the following results somewhat, but would not affect the conclusions at the end of this paper.

[10] Hulthén, K. fysiogr. Sällsk. Lund. Fövh. **14**, No. 21 (1944); **15**, No. 22 (1945).

where β is a variational parameter to be determined by the variational principle

$$\delta\int_0^\infty u[(d^2/dx^2)+k^2+{}^1a(e^{-\xi x}/x) +b(e^{-x}/x)]udx=0. \quad (11)$$

To obtain the required relation $F({}^1a, b)=0$, we make use of the following identity from the theory of scattering

$$\sin\delta_0=(1/k)\int_0^\infty \sin kx[{}^1a(e^{-\xi x}/x) +b(e^{-x}/x)]udx. \quad (12)$$

Equation (11) gives

$$[1-6{}^1a\ln((\xi+3)^2/(\xi+2)(\xi+4))-6b\ln(16/15)]\beta =-1+6{}^1a[\ln((\xi+2)^2/(\xi+1)(\xi+3)) +(k\cot\delta_0/(\xi+1)(\xi+2))] +6b[\ln(9/8)+(k\cot\delta_0/6)]. \quad (11')$$

Now, for energy of the order of 1 ev, one finds from (7) that k is of the order 10^{-4} so that (12) can be simplified into

$$\beta[{}^1a/(\xi+1)(\xi+2)+b/6] =1-{}^1a[1/\xi(\xi+1)+k\cot\delta_0/\xi^2] -b[\tfrac{1}{2}+k\cot\delta_0]. \quad (12')$$

Elimination of β between (11′) and (12′) gives the desired relation $F({}^1a, b)=0$ between ${}^1a$ and b.

II. Ground state of the deuteron:

The ground state wave function of the deuteron is $[u+(1/2\sqrt{2})S_{12}w]\chi_1{}^M$, where $\chi_1{}^M$ is the symmetric spin wave function and u and w are the ${}^3S$ and ${}^3D$ wave functions in the L, S representation. The equations for u and w are

$$\begin{aligned} &d^2u/dx^2+[-\alpha^2+{}^3a(e^{-\xi x}/x)+b(e^{-x}/x)]u \\ &\qquad =-2^{\frac{1}{2}}bf(x)(e^{-x}/x)w, \\ &d^2w/dx^2+[-\alpha^2-(6/x^2)+{}^3a(e^{-\xi x}/x)+b(e^{-x}/x) \\ &\qquad -2bf(x)(e^{-x}/x)]w=-2^{\frac{1}{2}}bf(x)(e^{-x}/x)u, \end{aligned} \quad (13)$$

where α^2 is related to the absolute value of the binding energy $\epsilon=2.18$ Mev by

$$\alpha^2=M\epsilon/h^2\mu^2=0.081.$$

We seek a relation $G({}^3a, b)=0$ between ${}^3a$ and b for which u and w satisfy the boundary conditions

$$u(0)=u(\infty)=w(0)=w(\infty)=0. \quad (14)$$

Two methods have been employed. One is to write

$$u=U(z)e^{-\alpha x}, \quad w=W(z)e^{-\alpha x}, \quad (15)$$

where

$$z=1-e^{-x}. \quad (16)$$

The differential equations for $U(z)$ and $W(z)$ are obtained by putting (15) and (16) into (13). We then assume

$$U(z)=\sum_{n=1} A_n z^n, \quad W(z)=\sum_{n=2} B_n z^n. \quad (17)$$

That the series for $W(z)$ must start with z^2 instead of z^3 is a consequence of the requirement that $u(x)$ and $w(x)$ satisfy the coupled Eqs. (13) at $x=0$. Instead of attempting an exact solution, we shall take m terms for each of the functions U and W in (17), and require these U and W to satisfy the coupled equations at m properly spaced points, say, $z=0, z_1, \cdots, z_{m-1}$. One then obtains $2m$ homogeneous equations in the $2m$ constants $A_1, \cdots, A_m$, $B_2, \cdots, B_{m+1}$, whose coefficients are numbers and ${}^3a$ and b. The condition that there be non-trivial solutions for the A's and B's is that the determinant of their coefficients in these $2m$ equations be zero. This determinantal equation gives the relation $G({}^3a, b)=0$ sought. In the actual calculation, instead of solving the determinantal equation for the relation $G({}^3a, b)=0$, it is more convenient to try pairs of values of ${}^3a, b$ in the determinant and obtain the relation $G({}^3a, b)=0$ by interpolation.

The two relations $F({}^1a, b)=0$, $G({}^3a, b)=0$ together with the third equation in (4), then determine ${}^1a$, ${}^3a$, b and hence the f and g.

The advantage of this method is that one can locate the approximate values of ${}^3a$ and b by starting with only a few points for which the order of the determinantal equation is low, and then improve the approximation by increasing the number of points at which the equations are satisfied and at the same time increasing the number of terms for $U(z)$ and $W(z)$ in (17). In the calculation, the points $z=0$, 0.4, 0.75, 0.95, 0.99326 corresponding to $x=0$,

TABLE I. Results.

	$\kappa_0=1.5\times315m_e$ $\mu_0=315m_e$	$\kappa_0=2\times315m_e$ $\mu_0=315m_e$	Observed values
$F({}^1a, b)=0$	${}^1a=2.357-1.455b$	${}^1a=3.243-2.00b$	
Equation (18)	${}^3a=22.365b-7.071$	${}^3a=38b-9.73$	
b (by (17))	0.430	0.326	
b (variational)	0.428	0.340	
${}^1a$ (variational)	1.733	2.563	
${}^3a$ (variational)	2.520	3.191	
$\beta(24)$	2.30	2.50	
$\gamma(24)$	2.25	2.45	
$y(24)$	0.071	0.114	
$f^2\kappa^2/\hbar c$	0.195	0.234	
$g^2\kappa^2/\hbar c$	0.064	0.079	
r_0 (singlet even states)	2.2×10^{-13} cm	1.2×10^{-13} cm	$(P-P)2.7\times10^{-13}$ cm
r_0 (triplet even states)	1.2×10^{-13} cm	1.1×10^{-13} cm	$(P-N)1.60\times10^{-13}$ cm
Quadrupole moment of deuteron	1.23×10^{-27} cm^2	1.94×10^{-27} cm^2	2.73×10^{-27} cm^2
$P-N$ scattering at 100 Mev			
Phases for singlet states			
δ_0 (exact)	0.810,8	0.931,6	
δ_1 (exact)	−0.373,5	−0.274,2	
δ_2 (exact)	0.045,8	0.036,1	
δ_3 (exact)	−0.050,8	−0.028,85	
δ_4 (Born)	0.009,56	0.005,46	
δ_5 (Born)	−0.010,8	−0.006,97	
$\sigma=(3/4)\sigma_t$ (Born) $+(1/4)\sigma_s$ (exact)	0.086×10^{-24} cm^2	0.070×10^{-24} cm^2	0.075×10^{-24} cm^2
$\sigma(170°)/\sigma(\pi/2)$	5.57	3.34	3.0
$\sigma(36°)/\sigma(\pi/2)$	1.34	1.15	1.8

0.51, 1.39, 3.0, 5.0 have been chosen. The last two points are chosen at much larger distances than in the work of Jauch and Hu to obtain better w wave functions at large distances where the contribution to the quadrupole moment is important. The correct asymptotic behavior of u and w at large x is guaranteed by the forms of u and w in (15).

The result so obtained is checked by the following variational calculation. The relation $F(^1a, b)=0$ obtained from (11′) and (12′) is almost a linear one over a large range of b (see Table I). Since the approximate values of b, ^1a, and ^3a are already known from the above calculation, it is possible to replace $F(^1a, b)=0$ in this immediate neighborhood by a linear relation. This, together with the third relation in (4), gives

$$^3a=c_1b-c_2, \tag{18}$$

where c_1 and c_2 are known numbers (see Table I). Equations (13) then become

$$\begin{aligned} &d^2u/dx^2-(\alpha^2+c_2(e^{-\xi x}/x))u \\ &\quad=-b[2^{\frac{1}{2}}f(x)w+u+c_1e^{-(\xi-1)x}u](e^{-x}/x), \\ &d^2w/dx^2-(\alpha^2+6/x^2+c_2(e^{-\xi x}/x))w \\ &\quad=-b[2^{\frac{1}{2}}f(x)u+w \\ &\qquad+c_1e^{-(\xi-1)x}w-2f(x)w](e^{-x}/x). \end{aligned} \tag{19}$$

The problem is then to obtain b as the lowest eigenvalue for the boundary conditions (14). On denoting by

$$\begin{aligned} P(x)&\equiv(1+c_1e^{-(\xi-1)x})(e^{-x}/x), \\ Q(x)&\equiv 2^{\frac{1}{2}}f(x)(e^{-x}/x), \\ R(x)&\equiv(1+c_1e^{-(\xi-1)x}-2f(x))(e^{-x}/x), \end{aligned} \tag{20}$$

it is seen that the problem is equivalent to the variational problem

$$\delta(I_1/I_2)=0$$

with

$$\begin{aligned} I_1=\int_0^\infty &[u'^2+w'^2+\alpha^2(u^2+w^2) \\ &+(c_2/x)e^{-\xi x}(u^2+w^2)+(6/x^2)w^2]dx \end{aligned} \tag{21}$$

and

$$I_2=\int_0^\infty [Pu^2+Qw^2+2Ruw]dx. \tag{22}$$

The eigenvalue b is then the minimum value of

$$b=I_1/I_2. \tag{23}$$

We employ in the calculation the trial wave functions

$$\begin{aligned} u(x)&=(1-e^{-\beta x})e^{-\alpha x}, \\ w(x)&=yw_0(x)=y(1-e^{-\gamma x})^2e^{-\alpha x} \end{aligned} \tag{24}$$

where y, β, γ are parameters to be determined by

$$\partial b/\partial y=0, \quad \partial b/\partial\beta=0, \quad \partial b/\partial\gamma=0. \tag{25}$$

The equation $\partial b/\partial y=0$ can be solved very simply and leads to the expression

$$b(2-2J_3)=J_1+J_2-[(J_2-J_1)^2+4J_1J_2J_3]^{\frac{1}{2}}, \tag{26}$$

where

$$\begin{aligned} J_1&=\left(\int_0^\infty [u'^2+\alpha^2u^2 \right. \\ &\qquad\left.+(c_2/x)e^{-\xi x}u^2]dx\right)\Big/\left(\int_0^\infty Pu^2dx\right), \\ J_2&=\left(\int_0^\infty [w'^2+\alpha^2w^2+(c_2/x)e^{-\xi x}w^2 \right. \\ &\qquad\left.+(6/x^2)w^2]dx\right)\Big/\left(\int_0^\infty Qw^2dx\right), \\ J_3&=\left(\left[\int_0^\infty Ruwdx\right]^2\right)\Big/\left(\int_0^\infty Pu^2dx\cdot\int_0^\infty Qw^2dx\right), \end{aligned}$$

and

$$\begin{aligned} y&=(b/(J_2-b)) \\ &\quad\cdot\left(\int_0^\infty Quw_0dx\right)\Big/\left(\int_0^\infty Rw_0^2dx\right). \end{aligned} \tag{27}$$

While all the integrals can be obtained in analytical forms, the minimizing of b with respect to β and γ is more conveniently carried out by trying various values of β and γ. The values of the eigenvalues b calculated by these two methods and the parameters in the wave functions (24) are given in Table I.

Having obtained the potential constants ^1a, ^3a, and b, and the wave functions for both the ground state of the deuteron and the scattering of slow neutron by proton, it is possible to test the potential so obtained by applying it to a study of the other problems mentioned at the beginning of this work. This is done below.

III. The "effective range" for the triplet and the singlet states:[11]

Consider first the singlet S states of the continuum and let u_1 and u_2 be the solutions of (6) for two energies k_1^2 and k_2^2 that go over asymptotically to the following functions

$$v_1=(\sin(k_1x+\delta_1))/\sin\delta_1, \quad v_2=(\sin(k_2x+\delta_2))/\sin\delta_2$$

where δ_1 and δ_2 are the phase shifts. It can readily be shown from (6) and the differential equations for v_1 and v_2 that

$$\begin{aligned} &k_2\cot\delta_2-k_1\cot\delta_1 \\ &\qquad=(k_2^2-k_1^2)\int_0^\infty (v_1v_2-u_1u_2)dx \end{aligned} \tag{28}$$

[11] The relation (28) and an analogous one for the triplet state are due to Bethe. For details see a forthcoming paper by H. A. Bethe in the Physical Review.

and that the integral $\int_0^\infty (v_1v_2-u_1u_2)dx$ is rather insensitive to the value of the energies for energies below a few Mev, and to a good approximation it can be regarded as a constant. This is used to define an "effective range" r_0 by

$$(1/2)r_0\equiv(1/\mu)\int_0^\infty (v_1v_2-u_1u_2)dx \cong(1/\mu)\int_0^\infty (v^2-u^2)dx, \quad (29)$$

where u and v are the functions for any energy below a few Mev. In order that any assumed nucleon potential $V(r)$ may reproduce the observed dependence of the phase δ on the energy k^2, it is necessary that the r_0 calculated from the solution u for the $V(r)$ be the same as the empirical value that is obtained from the empirical data, such as from the analysis of Breit *et al.*[7] in the case of the proton-proton scattering.

With the solution (10), we obtain

$$\mu r_0=18-8\beta-\beta^2+(4-3\beta)k\cot\delta_0, \quad (30)$$

where β is the parameter in (10). As the symmetrical meson theory is based on the hypothesis of charge independence of the nucleon interaction, we may compare the calculated r_0 with the value which is given by the analysis of Breit *et al.*, namely, $r_0=2.7\times10^{-13}$ cm. The result of our calculation is given in Table I.

For the triplet states in the case of a purely central force potential, the scattering at energies below a few Mev can again be described by means of a similarly defined "effective range" r_0.[11] In our present case with tensor forces, the situation is more complicated. It has been shown by Schwinger[12] that to a good approximation, the following relation holds

$$k\cot\delta=-\alpha+(\alpha^2+k^2)(1/\mu)\times\int_0^\infty [v_\alpha{}^2-(u^2+w^2)]dx, \quad (31)$$

where u and w are the solutions of (13) but normalized in such a way that u^2 goes asymptotically to $v_\alpha{}^2=e^{-2\alpha r}$. The empirical value of r_0 is given by the scattering of slow neutrons by parahydrogen and has the value 1.60×10^{-13} cm.[11] The result of our calculation is also given in Table I.

IV. Quadrupole moment of the deuteron:

The quadrupole moment of the deuteron is given by

$$Q=(\sqrt{2}/10\mu^2)\int_0^\infty x^2(u-(1/2\sqrt{2})w)wdx,$$

where u and w are the solutions of (13) normalized according to

$$\int_0^\infty (u^2+w^2)dx=1.$$

In our calculation, the variational wave functions (24) have been employed. The result is shown in Table I.

V. Proton-neutron scattering at high energies (100 Mev):

The theory of scattering including tensor forces has been given by Rarita and Schwinger[13] and by Ashkin and Wu.[14] It was found by Ashkin and Wu that at 100 Mev the error involved in the usual Born approximation is not very large for the triplet state, whereas it is quite large in the case of the singlet state scattering. This large error has its origin in the large interaction (on account of factor -3) for the singlet odd states in the symmetrical theory. On account of the large amount of numerical work that would be involved in an exact calculation of the triplet state scattering, and as the

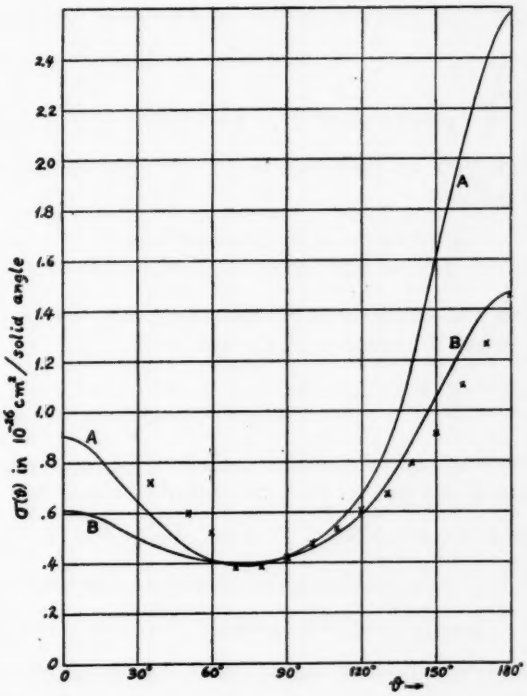

FIG. 1. Differential cross section for proton-neutron scattering at 100 Mev.

$$\sigma(\theta)=(3/4)\sigma_t\ (\text{Born})+(1/4)\sigma_s\ (\text{exact}).$$

A: $\mu_0=315\ m_e$, $\kappa_0=1.5\times315\ m_e$.
B: $\mu_0=315\ m_e$, $\kappa_0=2\times315\ m_e$.
X: experimental values in reference 9 for $p-n$ scattering at 90 Mev.

[12] Lecture notes at Harvard University, 1947.

[13] W. Rarita and J. Schwinger, Phys. Rev. **59**, 436 (1941).
[14] J. Ashkin and T-Y. Wu, Phys. Rev. **73**, 973 (1948).

Born approximation is not too bad here, we have calculated the triplet state scattering according to the Born approximation and the singlet state scattering from the exact phases obtained by numerical integration of the wave equation. The actual cross section is given by

$$\sigma=\tfrac{3}{4}\sigma_t+\tfrac{1}{4}\sigma_s.$$

It has been shown by Ashkin and Wu[14] that the triplet scattering cross section is, to the Born approximation,

$$\sigma_t(\vartheta)=(1/9)[F(\vartheta)+2F(\pi-\vartheta)]^2 +(8/9)[C^2(\vartheta)-2C(\vartheta)C(\pi-\vartheta)+4C^2(\pi-\vartheta)]. \quad (32)$$

The $F(\vartheta)$, $F(\pi-\vartheta)$, $C(\vartheta)$, $C(\pi-\vartheta)$ are the scattered amplitudes, due to the central force and the tensor force part, respectively, which in our present notations (3), (4) and (5) are

$$F(\vartheta)=(1/\mu)\int_0^\infty (\pi/2qx)^{\frac{1}{2}} \times J_{\frac{1}{2}}(kx)[{}^3a(e^{-\xi x}/x)+b(e^{-x}/x)]x^2dx, \quad (33)$$

$$C(\vartheta)=(1/\mu)\int_0^\infty (\pi/2qx)^{\frac{1}{2}} \times J_{5/2}(kx)b(e^{-x}/x)f(x)x^2dx,$$

where

$$q^2=2k\sin(\vartheta/2), \quad k^2=ME/\hbar^2\mu^2. \quad (34)$$

Integration of (33) leads to the rather simple expressions

$$\mu F(\vartheta)=({}^3a/(\xi^2+q^2))+b/(1+q^2), \quad \mu C(\vartheta)=b(\xi^2-1)q^2/(\xi^2+q^2)(1+q^2). \quad (35)$$

For the singlet state scattering, one starts the numerical integration of the equation

$$d^2u_l/dx^2+[k^2+{}^1a(e^{-\xi x}/x) +b(e^{-x}/x)-l(l+1)/x^2]u_l=0$$

at $x=0$ and continues to a sufficiently large x where $V(x)\ll l(l+1)/x^2$ so that the solution there will be

$$u_l\cong AJ_{l+\frac{1}{2}}(kx)+BJ_{-l-\frac{1}{2}}(kx)=C\sin(kx-l\pi/2+\delta_l).$$

If x_0 is a node in this region, then it can be seen that

$$\tan\delta_l=(-1)^{l+1}(J_{l+\frac{1}{2}}(kx_0)/J_{-l-\frac{1}{2}}(kx_0)). \quad (36)$$

For high values of $l(l\geq 4)$ where δ_l is small and Born's approximation is valid, the δ_l's are again calculated from the Born approximation.

The result of these calculations are given in Table I and Fig. 1.

DISCUSSION

From Table I it is seen that (*i*) with the meson masses $\mu_0=315\ m_e$ and $\kappa_0=1.5\times 315\ m_e$, the "effective range" r_0 for both the triplet and the singlet states are somewhat too small compared with the empirical values. The quadrupole moment of the deuteron is much too small. The value $y=0.07$ leads to a value of $\sim\frac{1}{2}$ percent for $\int_0^\infty w^2dx$ in $\int(u^2+w^2)dx$, compared with the value ~ 4 percent required to account for the magnetic moment of the deuteron. On the other hand, the ratio $\sigma(170°)/\sigma(\pi/2)$ of backward to transverse scattering at 100 Mev is too high compared with the observed value.*** This would indicate that the potential has too large a range to account for the scattering observed at 90 Mev.

With the meson masses $\mu_0=315\ m_e$ and $\kappa_0=2\times 315\ m_e$, the quadrupole moment becomes better, but still $\int_0^\infty w^2dx$ amounts to only about 1 percent of $\int_0^\infty (u^2+w^2)dx$. The total cross section and the ratio $\sigma(170°)/\sigma(\pi/2)$ for scattering at 100 Mev are in good agreement with the observed data. On the other hand, the "effective range" r_0 is now too small compared with the empirical values for both the triplet and the singlet states.

Considerations of these and some incomplete calculations for the ratio $\xi=1.75$, 3.0, together with the relations (3), (4) and (5) show that any potential on the basis of this form of the symmetrical theory, when adjusted to give the observed "effective range" r_0 for the low energy region (neutron scattering by parahydrogen and proton-proton scattering below a few Mev) will have too long a range to be compatible with the high energy scattering data, while a potential adjusted to account for the latter will have too short a "range" for the lower energy scatterings. It is also seen that the value of the ratio $\sigma(36°)/\sigma(\pi/2)$ is appreciably smaller than the experimental value.

It is true that one may be expecting too much from the meson theory in its present form, but the above calculations have been made with a number of approximations, such as the neglect of radiative corrections and the use of non-relativistic wave functions. Hence, before abandoning the theory for purely phenomenological approaches, it still seems worth while to see whether the conclusion above may be changed by including these effects. Estimates by Snyder and Marshak[15] show indeed that the relativistic effect is not entirely negligible even at 100 Mev. Such a study is being undertaken.

ACKNOWLEDGMENT

The writers wish to thank Professor H. A. Bethe for his interest and helpful discussions.

*** We compare the ratio $\sigma(170°)/\sigma(\pi/2)$ rather than $\sigma(180°)/\sigma(\pi/2)$ as the experimental value $\sigma(170°)$ may be more accurate than $\sigma(180°)$.

[15] H. Snyder and R. E. Marshak, Phys. Rev. 72, 1253 (1947).

Radioactive Isotopes of the Rare Earth Elements
II. Neodymium Isotopes

GEOFFREY WILKINSON AND HARRY G. HICKS
Radiation Laboratory and Department of Chemistry, University of California, Berkeley, California

(Received February 23, 1949)

The techniques of study of radioactive isotopes of the rare earth elements described previously have been applied to neodymium. Using the 60-inch Crocker Laboratory cyclotron, bombardments have been made of praseodymium with 19- and 9-Mev deuterons and 10-Mev protons. The characteristics of the neodymium isotopes are given below.

Isotope	Type of radiation	Half-life	Energy of radiation in Mev: Particles	Energy of radiation in Mev: γ-rays	Produced by
Nd^{140}	K	3.3±0.1 days		K x-rays ~1.2 (weak)	Pr-d-3n
Nd^{141}	K, β^+(2%), γ	145±3 min.	0.7(β^+)	K x-rays 1.05	Pr-d-2n Pr-p-n

THE isotope Nd^{141} has been reported[1] to have a 2.5-hour half-life, and to emit positrons of energy 0.78 Mev. The activity was produced by proton bombardment of praseodymium,[1] by $n,2n$[1–3] and γ,n[1,3] reactions on neodymium, and possibly by a d,H^3 reaction on neodymium.[1,2] Chemical separations were not made.

In the present work, chemical separations were made by ion exchange columns. The 2.5-hr. activity has been characterized in more detail and allocated to Nd^{141}, while a new isotope, Nd^{140}, has been observed by Pr-d-3n reaction. This isotope decays by orbital electron capture to form the positron emitter Pr^{140}. In bombardments, spectroscopically pure, column separated praseodymium oxide, Pr_6O_{11}, was used.[4] The techniques of bombardments, chemical separations, and measurements of radioactivity have been previously described.[5]

I. 145-MINUTE Nd^{141}

Measurements of the radiation characteristics of this isotope were made on unseparated praseodymium which had been bombarded with 10-Mev protons. The proof of the chemical identity by the standard ion-exchange resin column procedure used previously was almost impossible, since the neodymium fraction leaves the column only after about 2.5 days. A 4-cm×0.4-cm column was therefore used, with conditions of flow, eluting agent, etc., the same as before. Although the separation of neodymium and praseodymium is unsatisfactory from the chemical standpoint, these fractions leave the small column in about 12 hours, a time short enough to allow detection of the 145-minute activity. Such an experiment was made for a Pr+d bombardment. The ratio of the 145-minute activity to the 19.3-hr. Pr^{142} activity formed by d,p reaction was estimated, corrections for decay from a reference time being made for both activities. The ratio decreased rapidly in samples following the "break through" of active material showing that the 145-minute activity elutes before praseodymium. Further, spectroscopic analysis showed that the

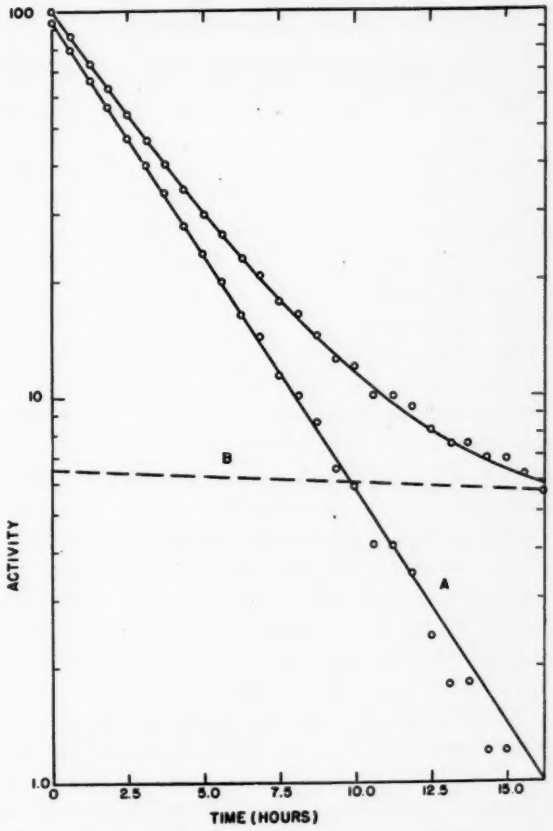

FIG. 1. Decay of 145-min. Nd^{141} positron from Pr+d bombardment followed on crude beta-ray spectrometer. A is the 145-min. activity and B the 3.3-day background.

[1] Kurbatov, MacDonald, Pool, and Quill, Phys. Rev. **61**, 106 (1942).
[2] M. L. Pool and L. L. Quill, Phys. Rev. **53**, 437 (1938).
[3] Law, Pool, Kurbatov, and Quill, Phys. Rev. **59**, 936 (1941).
[4] We are indebted to Mr. R. C. Lilly of this laboratory for preparation of this material.
[5] G. Wilkinson and H. G. Hicks, Phys. Rev. **75**, 1370 (1949).

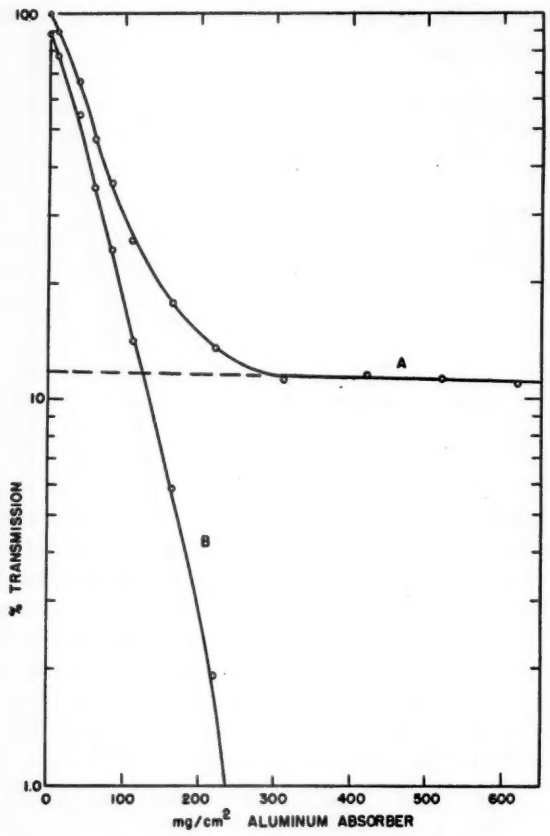

FIG. 2. Aluminum absorption of radiations of 145-min. Nd^{141} from $Pr+p$ bombardment. Electromagnetic radiation background (A), positron radiation range 245 mg/cm² (B).

19.3-hour activity followed the praseodymium, while in the first active sample where the 145-minute decay was observed, praseodymium was below the limits of detection. The chemical identity of the 145-minute activity as neodymium is, therefore, fairly certain.

The gross decay of the activity was followed through eight half-lives, the hard γ-radiation, through six half-lives, and the positron decay (Fig. 1), followed on a crude beta-ray spectrometer, also through six half-lives. The half-life is 145 ± 3 minutes.

The radiations consist of positrons, x-rays and γ-rays. No negative electrons were observed. The aluminum absorption curve of the 145-minute activity from $Pr+p$ bombardment, corrected for decay during the time of measurement, is shown in Fig. 2. The range of the electron, 245 ± 5 mg/cm² (0.7 Mev), agrees with the value of the positron energy measured on the crude beta-ray spectrometer. The lead absorption (Fig. 3) shows electromagnetic radiations of half-thicknesses 39 ± 2 mg/cm² (38 kev), ~4.5 g/cm² (0.5 Mev) and 11.5 g/cm² lead (1.2 Mev). The soft component agrees well with the K x-radiation of praseodymium, while the low abundant 0.5-Mev γ-ray is almost certainly annihilation radiation.

From the measurements, the following ratios were calculated; counting efficiencies of 0.5 percent for the K x-rays and 0.5-Mev γ-rays, and 1.2 percent for the 1.2-Mev γ-radiation were assumed, together with a fluorescence yield of 0.8 for the K x-radiation.

$$\beta^+ : K \text{ x-rays} : 0.5\text{-Mev } \gamma : 1.2\text{-Mev } \gamma = 0.02 : 1 : 0.02 : 0.02.$$

It is thus clear that the isotope decays by orbital electron capture with approximately 2 percent positron branching. The hard γ-radiation probably arises from an excited or metastable state of the daughter nucleus following electron capture.

From the measured K x-ray intensities, together with data on chemical yields and bombardment, the cross section for production of the 145-minute activity has been calculated. For 10-Mev protons a value of 3×10^{-2} barn was obtained. The deuteron cross sections are given in Table I below.

II. 3.3-DAY Nd^{140}

In the column separated neodymium fraction from $Pr+d$ bombardments a new long-lived ac-

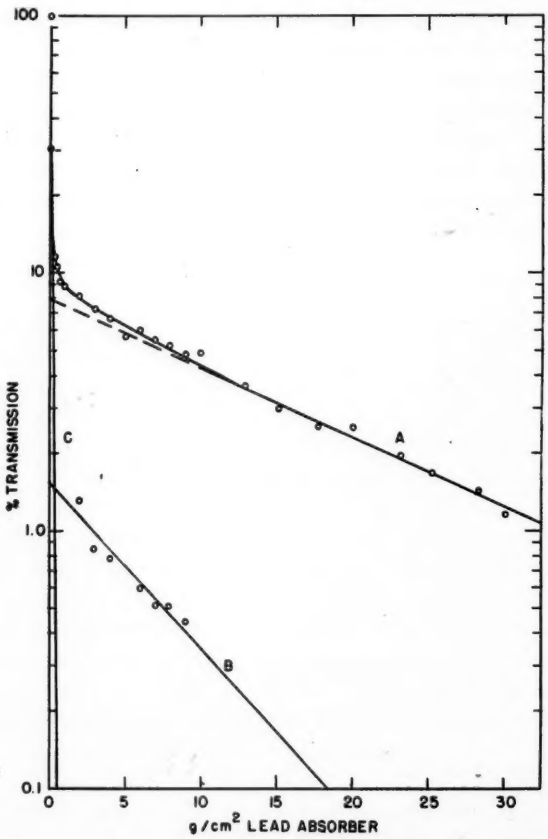

FIG. 3. Lead absorption of electromagnetic radiation of 145-min. Nd^{141} from $Pr+p$ bombardment. Hard γ-radiation (A), 0.5-Mev γ-ray (B) and K x-rays (C).

tivity was observed. The half-life, measured through seven periods, is 3.3±0.1 days. The aluminum absorption (Fig. 4) shows a hard electron, range 1150±50 mg/cm² (2.4 Mev) with K x-ray and γ-ray background. The lead absorption (Fig. 5) shows K x-radiation, 40 mg/cm² (38 kev) half-thickness, together with harder γ-radiation. If a small percentage of hard γ-radiation ~12 g/cm² lead (1.2 Mev) is assumed to be present, the bulk of the γ-radiation has a half-thickness of 4.6±0.1 g/cm² lead (0.51 Mev). The ratio of electrons to the various electromagnetic radiations obtained is:

Positrons: K x-rays: 0.51-Mev γ: ~1.2-Mev γ
= 0.2 : 1 : 0.2 : 0.01

Study of the electron radiations on the crude beta-ray spectrometer showed that positrons of energy 2.4 to 2.5 Mev, were present; no negative electrons were observed. The positron energy agrees well with that reported for the 3.5-minute Pr^{140}.[6]

The observed radiations of the 3.3-day activity are consistent with the isotope, Nd^{140}, decaying by

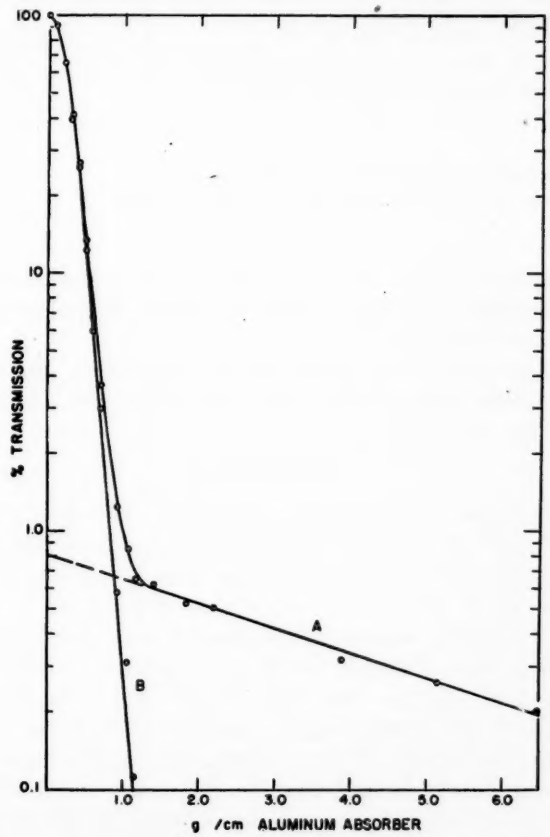

FIG. 4. Aluminum absorption of radiations of column separated 3.3-day Nd^{140} from Pr+d bombardment. Electromagnetic radiation background (A) positrons range 1150±50 mg/cm² (B).

[6] Huber, Lienhard, Scherrer, and Wäffler, Helv. Phys. Acta 18, 22 (1945); DeWire, Pool, and Kurbatov, Phys. Rev. 61, 544, 564 (1942); Weimer, Pool, and Kurbatov, Phys. Rev. 63, 67 (1943).

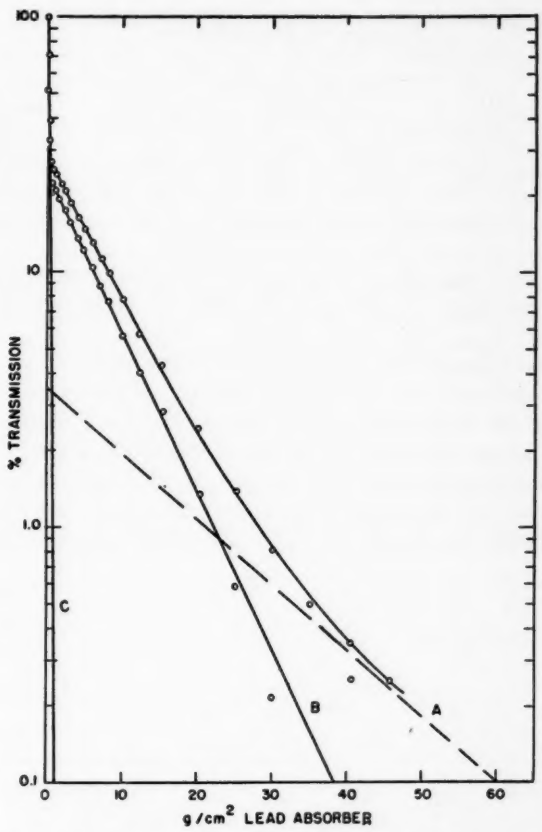

FIG. 5. Lead absorption of radiations of column separated 3.3-day Nd^{140} from Pr+d bombardment. Estimated hard γ-ray contribution (A), 0.51-Mev γ-ray (B) and K x-rays (C).

orbital electron capture, in equilibrium with its positron emitting Pr^{140} daughter. The observed 0.5-Mev γ-radiation is undoubtedly annihilation radiation; the harder γ-ray may be associated with either Pr^{140} or Nd^{140}. From the ratio of positrons to K x-radiation, it appears that the daughter Pr^{140} activity is not a pure positron emitter, but decays also by orbital electron capture, about two-thirds of the Pr^{140} disintegrations proceeding by this process.

A rapid chemical separation[7] of praseodymium and neodymium was attempted in order to show the chemical identity of the daughter of the 3.3-day activity. The mixed rare earth chlorides were fused with potassium hydroxide at 450°C for periods from 5 to 15 minutes. After extracting the melt with water, the mixed oxides were leached with 1N acetic acid. The neodymium oxide which dissolves preferentially was recovered as hydroxide for counting. The praseodymium remains largely in the residue insoluble in acetic acid. Although the chemical separation achieved is unsatisfactory, the activity of the neodymium fraction has been observed to grow, showing the formation of a daughter activity. The half-life of the daughter

[7] N. E. Ballou, private communication.

TABLE I. Cross sections in barns for deuteron reactions on praseodymium.

Half-life	Deuteron energy 19 Mev	9 Mev	Reaction	Isotope
19.3 hours	0.06	0.1	*d,p*	Pr^{142}
145 minutes	0.3	0.9	*d,2n*	Nd^{141}
3.3 days	0.08	—	*d,3n*	Nd^{140}

activity appears to be about 1.5 minutes, somewhat shorter than the value of 3.5 minutes reported[2] for Pr^{140}.

Additional evidence for the allocation of the 3.3-day activity to Nd^{140}, and its production by Pr-*d*-3*n* reaction has been obtained from yields in the deuteron bombardment of praseodymium. It was assumed that 0.6 of the measured *K* x-radiation of the 3.3-day activity represent one disintegration of Nd^{140}. In Table I are given the cross sections for production of the isotopes Pr^{142}, Nd^{141}, and Nd^{140}. The yields of the Pr^{142} were calculated from measured beta-particle activity. The absolute values of the yields may be in error in view of the uncertainties in counting efficiencies, etc., but the relative yields of the three reactions at the two bombarding energies should be more reliable.

ACKNOWLEDGMENTS

We would like to thank Professor J. G. Hamilton, Mr. T. Putnam, Mr. B. Rossi, and the crew of the 60-inch Crocker Laboratory cyclotron for their cooperation and assistance in bombardments; we are also indebted to Professors G. T. Seaborg, I. Perlman, and B. B. Cunningham for their continued interest and advice.

This work was done under the auspices of the AEC.

PHYSICAL REVIEW VOLUME 75, NUMBER 11 JUNE 1, 1949

Columbium 96

D. N. KUNDU AND M. L. POOL
Mendenhall Laboratory of Physics, Ohio State University, Columbus, Ohio

(Received February 16, 1949)

Cb^{96} has a half-life of 23.35 hours. It decays with the emission of negative beta-particles of maximum energy 0.67-Mev and 1.03-Mev gamma-rays. No x-rays are emitted. The assignment is made by using enriched isotopes of Zr.

INTRODUCTION

THE proton bombardment of zirconium was reported[1] to have produced Cb^{96} which has a half-life of 4 days. Later workers[2] reported its production by (*d*,2*n*) and (*d*,α) reactions from zirconium and molybdenum, respectively, and changed the value of the half-life to 3 days. Recently[3] by the bombardment of enriched Mo^{98} with deuterons, the half-life has been further changed to 2.8 days and the decay characteristics given as negative beta-rays of 1.8 Mev by absorption in aluminum and gamma-rays of 1 Mev by coincidence absorption in lead.

The data to be presented in this paper are in complete disagreement with the above and will be briefly described.

TABLE I. Percent isotopic constitution of bombarded target samples of Zr.

Sample	Mass numbers 90	91	92	94	96
Natural Zr	51.46	11.23	17.11	17.40	2.80
Zr enriched in 90	91.7	3.5	2.2	1.8	0.8
Zr enriched in 91	6.2	86.6	5.9	1.3	0.1
Zr enriched in 92	2.4	2.2	92.7	2.3	0.4
Zr enriched in 96	8.7	2.2	4.3	10.3	74.6

RESULTS

Isotopes of zirconium separately enriched* in Zr^{90}, Zr^{91}, Zr^{92} and Zr^{96} were bombarded with 5-Mev protons and 10-Mev deuterons. The isotopic composition of the samples are shown in Table I.

A rotating target arrangement[4] was employed by which two isotopes could be bombarded simultaneously under the same beam and thus any activity produced could be associated with one or the other or none of the rotated isotopes. The degree of enrichment is such that the difference in activity between two samples will be a factor between 14 and 870, depending upon the selection made, if the particular activity be produced from either of the rotated isotopes. Deuteron bombardments produce

[1] L. A. DuBridge, private communication quoted by G. T. Seaborg and I. Perlman, Rev. Mod. Phys. **20**, 585 (1948).
[2] L. Jacobson and R. Overstreet, Plutonium Project Report CC-2345 (December 1944).
[3] G. E. Boyd, private communication (October 1948), quoted by G. T. Seaborg and I. Perlman, Rev. Mod. Phys. **20**, 585 (1948).

* Kindly supplied by the Y-12 Plant, Carbide and Carbon Chemicals Corporation, through the Isotope Division, US-AEC, Oak Ridge, Tennessee.
[4] D. N. Kundu and M. L. Pool, Phys. Rev. **74**, 1574 (1948).

such a large amount of various activities especially the 17-hour Zr^{97} that in the following study the main emphasis will be laid on proton bombardments.

From the table, Zr^{90}, Zr^{92}, and Zr^{96} are selected for comparative study. In every case a 23.3-hour Cb activity is produced. On rotating Zr^{90} with Zr^{92}, this activity is produced in the ratio 2.6/4.3 which indicates that this half-life is not produced from either of these isotopes. This 23.3-hour activity must be associated with one of the remaining three isotopes which is present in small comparable amounts in each of Zr^{90} and Zr^{92} samples. Bombardment of the Zr^{96} with protons, however, brings out the 23.3-hour activity in amounts larger than any of the previous amounts by a factor of about 190 when Zr^{92} was taken for comparison and about 320 when Zr^{90} was compared. From the table the factors expected under ideal conditions would be 90 and 180 when Zr^{96} is compared with Zr^{90} and Zr^{92}, respectively. The uncertainties introduced in course of mounting the material for measurement and from other sources may amount to a small factor at most. The order of magnitudes, therefore, clearly indicates that the 23.3-hour activity is produced from

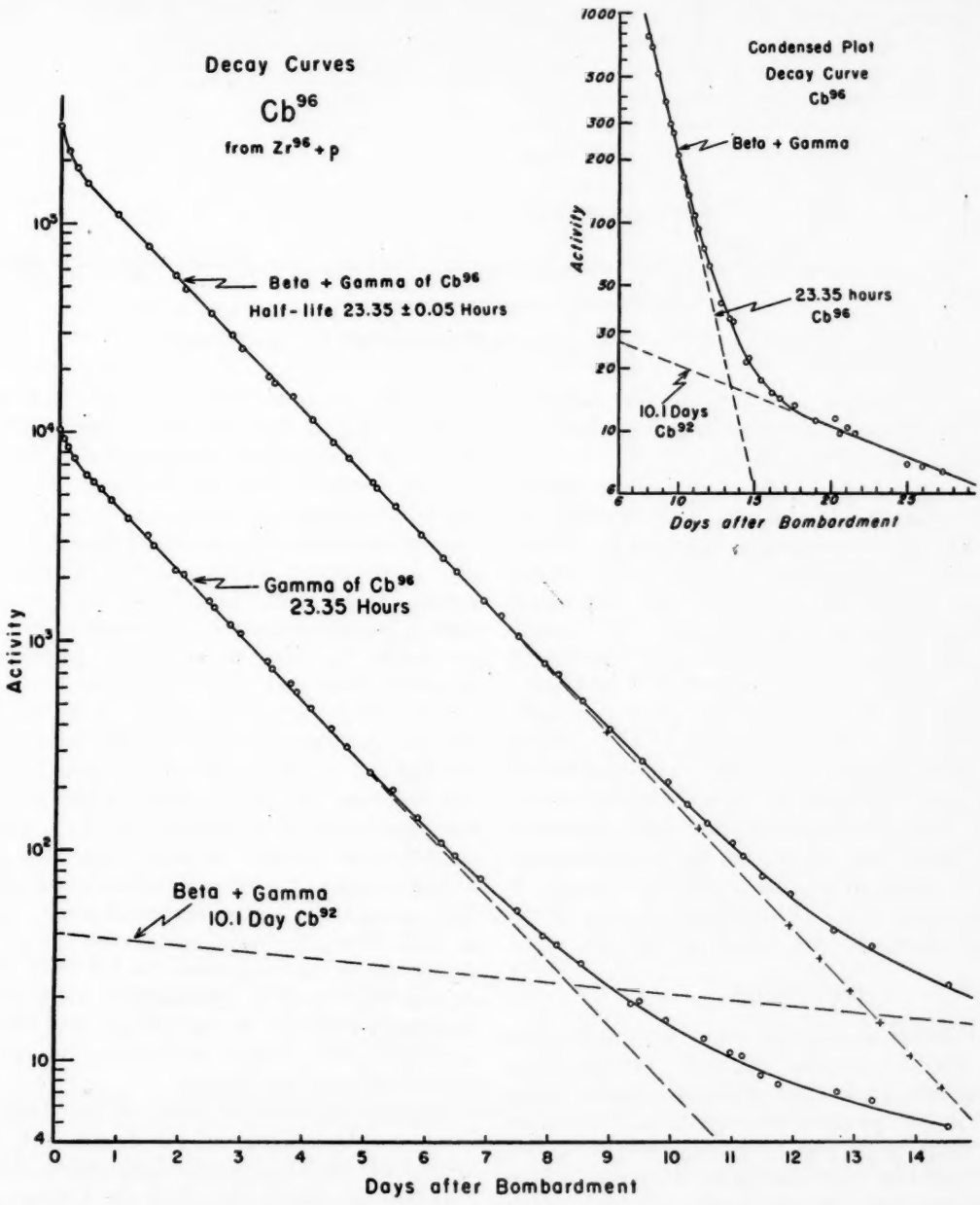

FIG. 1. Beta+gamma- and gamma-decay curves of $Zr^{96}O_2-p$, showing the 23.35-hour Cb^{96} activity. The inset shows a condensed plot in which the 10.1-day Cb^{92} activity is seen but no 2.8- or 4-day activity.

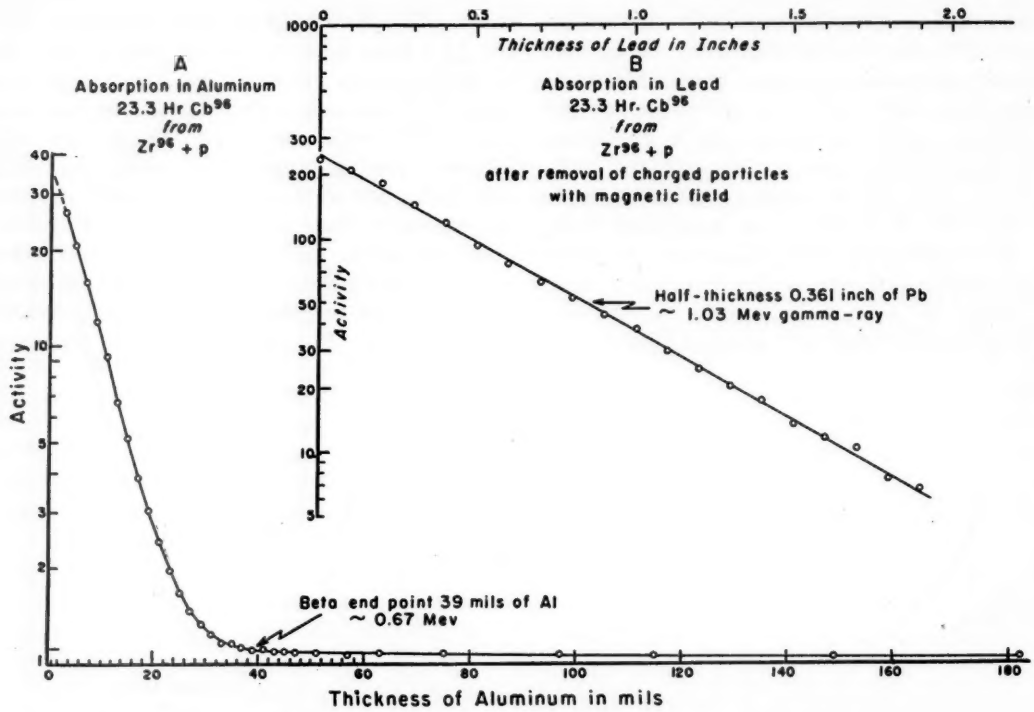

FIG. 2. Absorption curves of Cb^{96}: (A) absorption in aluminum; (B) absorption in lead.

Zr^{96} by (p,n) reaction, since both the isobaric chains 95 and 97 have already been well-established by the study of fission fragments.

The beta+gamma- and the gamma-decay curves of a sample of $Zr^{96}O_2$ bombarded with protons are shown in Fig. 1. From a total interval of fifteen half-lives the value is given as 23.35 ± 0.05 hours. No 4-day or 2.8-day half-life is observed. The curve passes immediately into the 10.1-day Cb^{92} period which has been produced from the small amount of Zr^{92} (4.3 percent) and, perhaps, of Zr^{91} (2.2 percent), present in the enriched Zr^{96} (74.6 percent).

The absorption curves are shown in Fig. 2. The energy of the beta-rays is 0.67 Mev. They are found to be negatively charged by separation in a magnetic field. The gamma-absorption was measured with lead foils after removing the beta-particles away with an electromagnet and the energy is found to be 1.03 Mev. The activity at zero thickness of lead shows that no x-rays are present.

DISCUSSION

Without entering into the question whether the 4-day or 2.8-day activity could be produced by bombarding with particles of energy higher than that used in the present investigation, it may be remarked that with the energies used here, the 10.1-day Cb^{92} has been produced in considerable strength from Zr^{92}. In the study of Mo^{98} with deuterons in this connection, it was found that this molybdenum isotope has such a large cross section for (d,p) reaction leading to the 2.8-day Mo^{99} activity, that it was difficult to chemically remove traces of Mo^{99} from Cb fractions. The 2.8-day activity decays into the 5.9-hour Tc^{99} daughter which disintegrates mainly with x-ray emission. Also by deuteron bombardment of Mo, the 3.75-day Cb^{95} is produced which again decays by emitting x-rays. With such sources of x-rays suspected, energy measurements by absorption in aluminum are liable to error as reported[5] previously. The apparent beta-end point is pushed towards the higher energy side, thus giving a higher value for the maxima beta-energy. In the decay curves on the Mo fraction from Mo+d bombardments where the Mo was enriched in Mo^{92} (92.07 percent) and contained only 1.65 percent of Mo^{98}, the 2.8-day activity was present in very large amounts. Absorption measurements with aluminum foils showed that though the actual beta-end point ought to be at 1.16 Mev, the tail end of the curve could be drawn so as to correspond to 1.8 Mev. When enriched Mo^{98} itself is bombarded, so much of x-ray is present both due to the 2.8-day and the 3.75-day activities, that energy measurements are spurious if not corrected for x-rays.

Acknowledgment is made of the help received from the Development Fund and the Graduate School of the Ohio State University. Thanks are also due the Ghosh Board of the Calcutta University for aid in traveling to this country.

[5] D. N. Kundu and M. L. Pool, Phys. Rev. **74**, 1775 (1948).

Radioactive Scandium and Vanadium

N. L. KRISBERG* AND M. L. POOL
The Ohio State University, Columbus, Ohio

(Received February 14, 1949)

An activity with a half-life of 33.0±0.5 minutes was produced by the reaction $Ti^{47}(p,n)$ with approximately 10 times the intensity which was produced by the reaction $Ti^{46}(p,\gamma)$ and is assigned to V^{47}. It was found that V^{47} decays by the emission of a γ-ray and a positive β-particle of 1.65 Mev. Assignment of the 3.43±0.03 day half-life to Sc^{47} was definitely confirmed by comparing the reactions $Ti^{49}(d,\alpha)$ and $Ti^{50}(d,\alpha)$. Sc^{47} decays to stable Ti^{47} by the emission of a γ-ray and a negative β-particle of 0.61 Mev. The $Ti^{50}(d,\alpha)$ reaction was found to give the 1.83-day half-life of Sc^{48}.

I. INTRODUCTION

IT is the purpose of this paper to report a series of experiments which give additional information about the radioactive isotopes of scandium and vanadium. All radioactivities shown in the following figures were produced by cyclotron bombardment. Electromagnetically enriched isotopes of Ti^{46}, Ti^{47}, Ti^{49}, and Ti^{50} were used to compare the intensity of a given activity produced in each enriched sample as an aid in isotopic assignment.** In order to obtain this comparison, two samples of material enriched in different isotopes were weighed and mounted on opposite faces of the cyclotron internal probe. During bombardment the probe was rotated so that each sample was subjected to the same time of bombardment and as nearly as possible to the same beam intensity. Whenever TiO_2 samples were bombarded and no subsequent chemistry performed, the activity produced from the oxygen served as a control for the resulting comparison since the amount of oxygen present was independent of the isotopic composition.

II. THE 33-MINUTE V^{47} ACTIVITY

A proton bombardment of titanium of standard isotopic composition and subsequent chemical

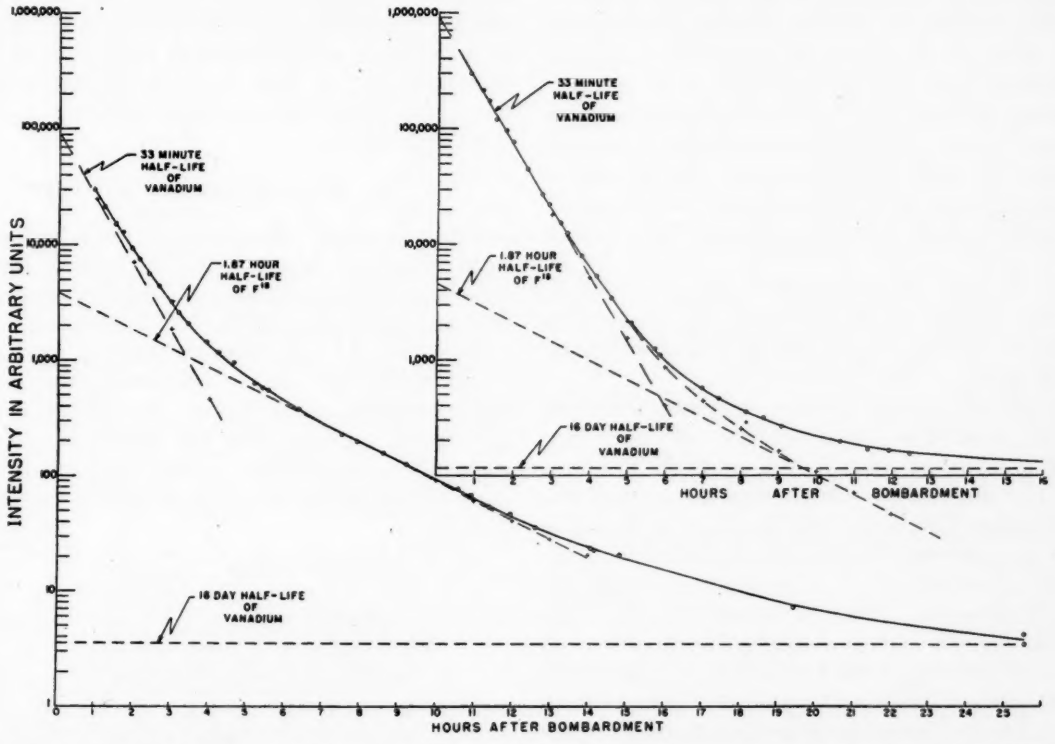

FIG. 1. Decay of the β-particle activity produced by proton bombardments of enriched $Ti^{46}O_2$ and $Ti^{47}O_2$ respectively. Note the 1:1 ratio of the F^{18} intensities and the 10:1 ratio of the 33-minute half-life intensities.

* Lt. Col. U. S. Air Forces, research done under auspices A.A.F. Institute of Technology, Wright Field, Dayton, Ohio.
** Supplied by the Y-12 plant, Carbide and Carbon Chemicals Corporation, through the Isotopes Division, U.S.A.E.C. Oak Ridge, Tennessee.

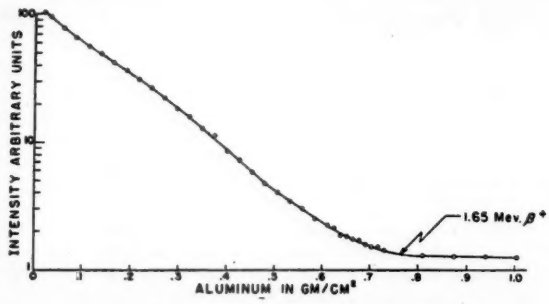

FIG. 2. Aluminum absorption taken while a Ti+p bombardment was decaying with a half-life of 33 minutes.

separation showed the vanadium fraction to decay with the previously reported half-lives of 33 minutes and 16 days.[1,2] From these earlier experiments it was not possible to definitely assign a mass number to the 33-minute half-life. This activity was not observed when either titanium or scandium was bombarded with α-particles. Nor was it observed when a large sample of vanadium was exposed to an intense flux of fast neutrons. This activity, however, was produced by a proton bombardment of enriched $Ti^{49}O_2$ and $Ti^{50}O_2$ with the same intensity in both samples. When the bombardment was performed using $Ti^{46}O_2$ and $Ti^{47}O_2$ it was found that the 33-minute period was ten times as intense in the Ti^{47} sample as it was in the Ti^{46}, as shown in Fig. 1. The 1.87-hour half-life of F^{18} produced by the reactions, $O^{17}(p,\gamma)F^{18}$ and $O^{18}(p,n)F^{18}$, appeared with approximately equal intensity in both compared samples of each set. The 33-minute activity was found to decay by the emission of a positive β-particle and an associated γ-ray. By means of aluminum absorption measurements the energy of the positive β-particle was found to be 1.65 Mev as shown in Fig. 2.

Figure 3 shows the region of the isotope chart in which the experiments described in this paper were performed. All results reported here are indicated by heavy line.

Since the 33-minute activity was not observed from an α-particle bombardment of titanium, possible assignment to V^{48}, V^{49}, and V^{50} is eliminated. The elimination of V^{48} and V^{50} as possible assignments is also confirmed by the fact that this activity was not observed from an α-particle bombardment of scandium or a fast neutron bombardment of vanadium. The elimination of V^{49} was confirmed by the fact that proton bombardments of titanium enriched with Ti^{49} and Ti^{50} respectively produced this activity with equal intensity in both samples. Since a proton bombardment of Ti^{47} produced the 33-minute half-life with ten times the intensity that a proton bombardment of Ti^{46} produced it, assignment is made to V^{47} as shown in Fig. 3.

III. THE 3.7-HOUR V^{50} ACTIVITY

A 3.7-hour half-life[1] emitting a positive β-particle has been assigned to V^{50}. The ionization chamber used for all measurements presented in this paper is filled with freon to a pressure of two atmospheres and has an aluminum window of 20 mg/cm². This chamber is efficient for the detection of γ-rays and any annihilation radiation should therefore be observed. X-rays produced by elements in the vanadium region have a half-thickness of approximately 3.65 mg/cm² of aluminum. In order to observe these possible x-rays a Geiger tube was used with a quartz window of 2.5 mg/cm². This Geiger tube had previously been successfully used for observing titanium x-rays from the 600-day activity of vanadium which is known to decay by K-electron capture. Measurements to observe the 3.7-hour half-life were made on activities resulting from deuteron and α-particle bombardments of titanium and fast neutron bombardments of vanadium. In addition attempts were made to observe this vanadium activity by bombarding $Ti^{49}O_2$ and $Ti^{50}O_2$ with protons. No activity with a 3.7-hour half-life was observed in the vanadium fractions of any of the above bombardments and it is concluded that the 3.7-hour half-life is not an activity of vanadium. In accordance with the above results no activity is shown for V^{50} in Fig. 3. It is suggested that the previously observed 3.7-hour half-life may have been due to Sc^{44}.

IV. THE 1.83-DAY Sc^{48} ACTIVITY

Figure 4 shows the decay of the scandium fractions obtained from deuteron bombardments of titanium enriched with Ti^{49} and Ti^{50} respectively. The left-hand side of Fig. 4 shows an activity with a half-life of 1.83 days which is produced by bombarding Ti^{50} with deuterons. By means of spectrographic observations the 1.83-day half-life was found to decay by the emission of negative β-particles. Aluminum absorption measurements showed the energy of this β-particle to be 0.57 Mev.

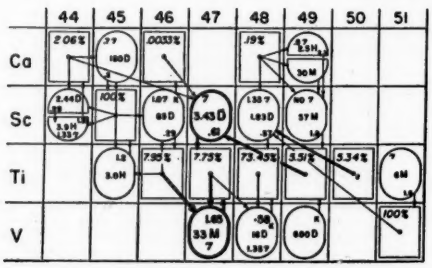

FIG. 3. Isotope chart of the region in which the experiments of this paper were performed. Results discussed in the text are indicated by heavy line.

[1] H. Walke, Phys. Rev. 52, 777 (1937).
[2] J. J. O'Connor, M. L. Pool, and J. D. Kurbatov, Phys. Rev. 62, 413 (1942).

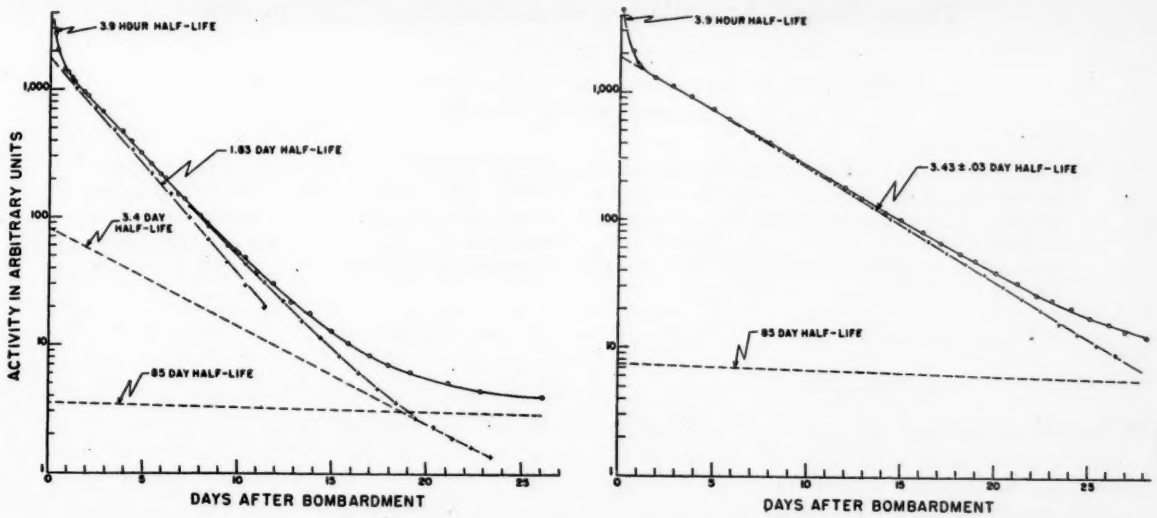

FIG. 4. Decay of the β-activity produced in the scandium fractions of deuteron bombardments of TiO_2 enriched with $Ti^{49}O_2$ and $Ti^{50}O_2$ respectively. The comparison is used to confirm the half-lives assigned to Sc^{47} and Sc^{48}.

These observations are in agreement with the characteristics of Sc^{48} previously observed[3,4] and the 1.83-day half-life is therefore produced by the reaction $Ti^{50}(d,\alpha)Sc^{48}$.

V. THE 3.43-DAY Sc^{47} ACTIVITY

As shown in Fig. 4, an activity with a half-life of 3.4 days was observed in the scandium fractions of deuteron bombardments of titanium enriched with Ti^{49} and Ti^{50} respectively. This activity was observed to be over twenty times as intense when enriched Ti^{49} was bombarded as it was when Ti^{50} was used. Observations over seven half-lives, as shown on the right side of Fig. 4, determined the half-life to be 3.43 ± 0.03 days. The activity was found to decay by the emission of a negative β-particle and an associated γ-ray. By means of aluminum absorption measurements the energy of the negative β-particle was found to be 0.61 Mev as shown in Fig. 5.

This activity has been assigned to Sc^{47} by means of α-particle and deuteron bombardment of calcium.[4,5] The above data serves to confirm the earlier assignment of this activity by the reaction $Ti^{49}(d,\alpha)Sc^{47}$.

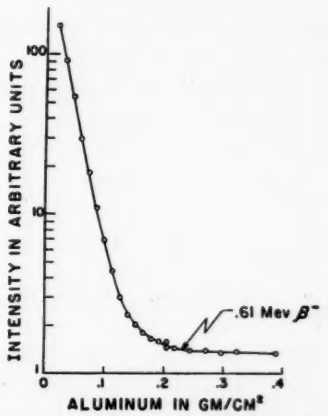

FIG. 5. Aluminum absorption taken while the activity shown on the right side of Fig. 4 was decaying with a half-life of 3.43 days.

When isotopic concentrations for the enriched samples used in these experiments are known the above data can be used to compute the relative reaction cross sections for all activities referred to in this paper.

VI. ACKNOWLEDGMENTS

Chemical separations for the above work were done by H. L. Finston and Rolla M. Dyer. The authors are grateful for the support received from the Ohio State University Development Fund and the Graduate School.

[3] H. Walke, Phys. Rev. **57**, 163 (1940).
[4] C. T. Hibdon and M. L. Pool, Phys. Rev. **67**, 313 (1945).
[5] C. T. Hibdon, M. L. Pool, and J. D. Kurbatov, Phys. Rev. **63**, 462 (1943).

Three-Photon Annihilation of an Electron-Positron Pair

A. ORE* AND J. L. POWELL*
Institute for Nuclear Studies, University of Chicago, Chicago, Illinois
(Received January 12, 1949)

Annihilation of an electron-positron pair accompanied by the emission of three photons is discussed for the case of small relative velocity of the two particles. The energy spectrum of the photons is derived and the cross section for the process is calculated. The ratio of this cross section to that of ordinary two-photon annihilation is found to be 1:370. When the result is applied to the ^3S ground state of the positronium atom, for which two-photon annihilation is forbidden, one finds a lifetime 1.4×10^{-7} sec.

INTRODUCTION

TWO-PHOTON annihilation[1,2] of an electron and a positron is forbidden for states of the electron-positron pair for which the wave function is symmetric in the space and spin coordinates of the two particles. However, annihilation resulting in the simultaneous creation of *three* photons can occur.

In particular, if the electron-positron pair forms a positronium atom in the ground (S) state, two-quantum or three-quantum annihilation is allowed according as the state is a singlet or triplet. Because of the multiple character of the three-quantum process, the triplet state will have a longer lifetime than the singlet.

The lifetime of the singlet state is [1,2]

$$^1\tau=2(\hbar c/e^2)^4(\hbar^2/me^2c)=1.25\times10^{-10}\text{ sec.} \quad (1)$$

This value is obtained from the cross section for two-quantum annihilation of an electron and a positron in free relative motion, as given by Dirac.[3] The Coulomb binding in the positronium atom has a negligible effect upon the decay probability (see below).

In this paper, we present a calculation, by the method of time-dependent perturbation theory, of the cross section for three-photon annihilation in the limit of small velocities, and of the energy spectrum of the photons. We also obtain the lifetime of the positronium atom in the triplet state.

CALCULATIONS

The annihilation of an electron-positron pair by emission of three photons takes place via two intermediate states, I and II. The probability per unit time for the process is given, in natural units ($\hbar=c=1$), by

$$P=2\pi|H_{FA}|^2\rho_F; \qquad H_{FA}=\sum_{I,II}\frac{H_{FII}H_{II\ I}H_{IA}}{(E_A-E_I)(E_A-E_{II})}, \quad (2)$$

where A refers to the initial state consisting of the electron-positron pair, F to the final state composed of three light quanta, and ρ_F is the density of final states per unit energy interval. The matrix elements H_{IA}, etc., are associated with the emission of the quanta in the various transitions and have the general form

$$H_{IA}=e(2\pi/kL^3)^{\frac{1}{2}}(u_I,\ \boldsymbol{\alpha}\cdot\mathbf{a}u_A),$$

where e is the electronic charge, $\mathbf{k}$ and $\mathbf{a}$ are the momentum and polarization vectors of the quantum, $\boldsymbol{\alpha}$ is the Dirac matrix, u_A and u_I are the Dirac amplitudes of the electron wave functions in the states I and A, and L^3 is the normalization volume. The total momentum is conserved in each transition.[4]

The various transitions which can lead from A to F by the emission of three quanta are illustrated in Fig. 1, in which the symbols $\pm$, k refer to the presence of a pair and a quantum, respectively.

The transitions through the intermediate states denoted by b are those which do not involve the formation of a virtual pair. To these transitions one can apply arguments similar to those used by Pirenne[5] in the two-quantum problem and show, firstly, that only an initially symmetric state will give a non-vanishing contribution to H_{FA}, and secondly, that the Coulomb binding may be neglected, its effect being to change the matrix elements by a fractional amount of the order 1/137. In the present problem, we shall assume that the binding can also be neglected for the remaining transitions. Therefore, in the calculation of the decay probability, we use simple plane wave functions. With this approximation, the lifetime of the bound state

* Post-Doctoral Fellow.
[1] J. Pirenne, Thesis, University of Paris (1944), Chapter III. (See also Archives des Sciences physiques et naturelles **28**, 273 (1946) and **29**, 121 (1947).)
[2] J. A. Wheeler, Ann. New York Acad. Sci. **48**, 219 (1946).
[3] P. A. M. Dirac, Proc. Camb. Phil. Soc. **26**, 361 (1930).
[4] W. Heitler, *The Quantum Theory of Radiation* (Oxford University Press, London, 1944), second edition, p. 96.
[5] See reference 1, pp. 124, 129.

is obtained by introducing a normalization which corresponds to the correct particle density at coincidence for the positronium atom.

For non-relativistic velocities, the cross section for three-photon annihilation obeys the $1/v$ law. That is, the rate at which annihilation takes place is determined by the density of electrons at the position of the positron. As a consequence, one can obtain the cross section for small velocities from the limiting case of zero velocities. The assumption of zero velocities leads to considerable mathematical simplification, and we shall here carry out the calculation for this case only, although the following discussion of matrix elements and of methods of calculation applies to the general case of arbitrary relative velocity of the electron and positron.

The transitions through the intermediate states denoted by *a* and *c* in Fig. 1 involve the formation of a virtual pair. In the states *c*, in which two pairs are present simultaneously, one must exclude those intermediate states which would violate the Pauli exclusion principle. However, if one calculates the total contribution of such states, one finds that it is zero, so that the requirements of the Pauli principle are automatically fulfilled. This may be verified by consideration of the energy denominators and signs of the matrix elements involved.

With regard to the signs of the matrix elements, it should be mentioned that in transitions involving the annihilation of the members of the virtual pair by those of the original, a change in sign is necessary, corresponding to an exchange of two negative-energy electrons in the final state. These effects of the exclusion principle are brought in automatically if the problem is treated in terms of the Jordan-Wigner operators,[6] but the essential facts are contained in the above discussion.

Among the transitions through the states *a* and *c* are some which are of a character which leads to divergence, namely, those in which a virtual pair is first created and subsequently annihilates itself. The reason for the divergence is that the condition of conservation of momentum only requires that the sum of the momenta of the members of the virtual pair shall be equal to that of the annihilation quantum, but places no restriction upon the momenta individually. Hence, in the sum over intermediate states one must include an integration over the momentum space for one of the members of the virtual pair. For each of these groups of transitions, this integral is divergent. However, if one considers the *total* contribution of all such transitions, the result is a detailed cancellation of these divergent terms.

Taking the above remarks into account, one finds

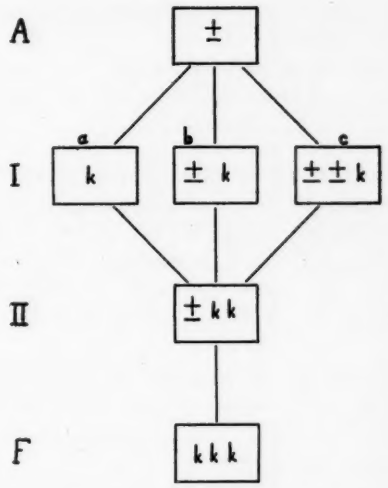

FIG. 1. Diagram illustrating the transitions which result in three-photon annihilation of an electron-positron pair.

that the final expression for H_{FA} is the same as the expression which one obtains if one considers the problem of the transition of an electron, by emission of three quanta, from a given state of positive energy to a given state of negative energy, all negative energy states being initially unoccupied, namely,

$$H_{FA}=e^3((2\pi)^3/k_1k_2k_3L^3)^{\frac{1}{2}}$$
$$\times\sum_k\sum_{I,II}\frac{(u_F,\ \boldsymbol{\alpha}\cdot\mathbf{a}_3u_{II})(u_{II},\ \boldsymbol{\alpha}\cdot\mathbf{a}_2u_I)(u_I,\ \boldsymbol{\alpha}\cdot\mathbf{a}_1u_A)}{(E_1-k_1-E')(k_3-E_2-E'')}$$

where E_1 and E_2 are the initial energies of the electron and positron, respectively, $\mathbf{k}_1$, $\mathbf{k}_2$, $\mathbf{k}_3$ are the momenta of the quanta and E' and E'' are the energies of the electron in the first and second intermediate states, respectively. $\sum_k$ denotes summation over all terms obtained from the above by permutation of $\mathbf{k}_1$, $\mathbf{k}_2$, and $\mathbf{k}_3$. Taking $E_1=E_2=m$, the conservation of momentum and energy is expressed by

$$\mathbf{k}_1+\mathbf{k}_2+\mathbf{k}_3=0;\quad k_1+k_2+k_3=2m. \tag{3}$$

In order to pass from the case of free particles to that of the positronium atom, the normalization factor $L^{-\frac{3}{2}}$ must be replaced by $(\kappa^3/\pi)^{\frac{1}{2}}$, where $1/\kappa$ is equal to two times the Bohr radius. The sum over intermediate states, which must include both positive and negative energies, and both spin directions of the electron, may be carried out by the method of Casimir.[7] The result of these transformations is

$$H_{FA}=-(2\pi e^3/m^2L^3)(\kappa^3/k_1k_2k_3)^{\frac{1}{2}}(\mathbf{t}_1+\mathbf{t}_2+\mathbf{t}_3)\cdot\mathbf{u}$$

where $\mathbf{t}_1$ is the following function of the polarization

[6] See G. Wentzel, *Quantentheorie d. Wellenfelder* (Franz Deuticke, Vienna, 1943), p. 183.

[7] See reference 4, p. 149.

vectors:

$$\mathbf{t}_1=\mathbf{a}_1(\mathbf{a}_2\cdot\mathbf{a}_3)-\mathbf{a}_2(\mathbf{a}_3\cdot\mathbf{a}_1)-\mathbf{a}_3(\mathbf{a}_1\cdot\mathbf{a}_2)$$
$$+\mathbf{a}_1(\mathbf{a}_2'\cdot\mathbf{a}_3')-\mathbf{a}_2'(\mathbf{a}_3'\cdot\mathbf{a}_1)-\mathbf{a}_3'(\mathbf{a}_1\cdot\mathbf{a}_2')$$
$$\mathbf{a}_1'=\mathbf{a}_1\times(\mathbf{k}_1/|\mathbf{k}_1|)$$

and $\mathbf{t}_2$ and $\mathbf{t}_3$ are obtained by cyclic permutation of the subscripts. $\mathbf{u}$ is a complex unit vector which characterizes the initial triplet state of the positronium atom.[8] Three independent triplet states are represented by three mutually orthogonal unit vectors $\mathbf{u}_1$, $\mathbf{u}_2$, $\mathbf{u}_3$. For an initial singlet state H_{FA} vanishes.

Finally, taking the average of $|H_{FA}|^2$ over the three independent triplet states, and summing the result over the directions of polarization of the three quanta, one finds

$$\sum_{\text{polarizations}}\langle|H_{FA}|^2\rangle_{Av}=(32\pi^2e^6/3L^3)(\kappa^3/k_1k_2k_3)$$
$$\times\{[1-\cos(\mathbf{k}_2\mathbf{k}_3)]^2+[1-\cos(\mathbf{k}_3\mathbf{k}_1)]^2$$
$$+[1-\cos(\mathbf{k}_1\mathbf{k}_2)]^2\}\quad(4)$$

where $(\mathbf{k}_2\mathbf{k}_3)$, etc. are the angles between the vectors indicated.

The density of final states is calculated in the usual way, by making use of the momentum conservation law. One obtains

$$\rho_F=(2\pi)^{-5}L^6k_1k_2k_3dk_2dk_1d\Omega_1\quad(5)$$

representing the number of final states per unit energy in which k_1 is in the interval (k_1, k_1+dk_1) and its direction within the element of solid angle $d\Omega_1$, the magnitude of k_2 being at the same time in the interval (k_2, k_2+dk_2).

Combining the Eqs. (2), (4) and (5) and making use of (3), one finds, after integration over k_1 and k_2

$$1/{}^3\tau=(16e^6\kappa^3/9\pi m^3)\int_0^m F(k_1)dk_1$$
$$=(16/9\pi)(\pi^2-9)(e^6\kappa^3/m^2)$$

where

$$F(k_1)=\int_{m-k_1}^m\left\{\frac{m^2(m-k_1)^2}{k_2^2k_3^2}+\frac{m^2(m-k_2)^2}{k_3^2k_1^2}\right.$$
$$\left.+\frac{m^2(m-k_3)^2}{k_1^2k_2^2}\right\}\frac{dk_2}{m}=2\left\{\frac{k_1(m-k_1)}{(2m-k_1)^2}\right.$$
$$-\frac{2m(m-k_1)^2}{(2m-k_1)^3}\ln\frac{m-k_1}{m}+\frac{2m-k_1}{k_1}$$
$$\left.+\frac{2m(m-k_1)}{k_1^2}\ln\frac{m-k_1}{m}\right\}.$$

A factor $\frac{1}{6}$ has also been included in the above formula, since the 6 permutations of the three quanta all correspond to the same final state.

Restoring $\hbar$ and c, and using the relation (1), our result may be conveniently written in the form

$${}^1\tau/{}^3\tau=(4/9\pi)(\pi^2-9)(e^2/\hbar c)\approx(1/8)(e^2/\hbar c)$$
$${}^3\tau=1.4\times10^{-7}\text{ sec.}$$

This may also be expressed in terms of the cross section for annihilation of *free* particles with small relative velocity. We have

$$\sigma_{3k}/\sigma_{2k}=3({}^1\tau/{}^3\tau)\approx1/370$$

where σ_{2k} and σ_{3k} are respectively the cross sections for two- and three-photon annihilation of a free electron and positron with arbitrary spins. The statistical factor 3 enters because only singlet states contribute to σ_{2k}, and only triplets to σ_{3k}.

The function $F(k_1)$, which is proportional to the total probability that one of the photons has energy in the interval (k_1, k_1+dk_1), represents the energy spectrum of the quanta. A graph of this function is shown in Fig. 2 (solid curve). The dashed curve represents the function

$$\int_{m-k_1}^m\rho_Fdk_2\sim k_1^2(6m^2-6mk_1+k_1^2),$$

i.e., the spectrum which one would obtain from a statistical estimate based upon a consideration of the available volume in momentum space.

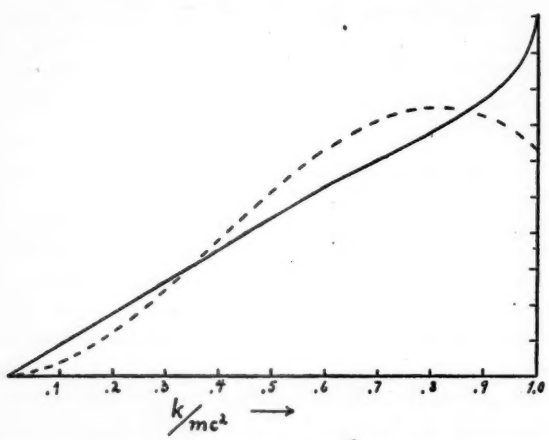

FIG. 2. Energy spectrum of photons resulting from three-photon annihilation of an electron and a positron. The abscissa is the photon energy in units mc^2 and the ordinate is proportional to the number of photons per unit energy interval. (Dashed curve: statistical estimate.)

[8] See reference 1, p. 108.

DISCUSSION

In the ground state of the positronium atom, the fine-structure separation between the triplet and singlet states is approximately 8×10^{-4} ev.[1] The

former, relatively long-lived state lies above the short-lived singlet state. However, radiative transitions from triplet to singlet state are forbidden. Provided that transitions resulting from thermal collisions between the positronium atom and, say, gas molecules have a small probability of occurrence, the long-lived triplet state should manifest itself.

For S states in general, the lifetime with respect to annihilation increases as the cube of the principle quantum number. For the other excited states (P, D, etc.) this lifetime will be long, since the absolute value of the wave function goes to zero as the electron and positron approach coincidence.

The existence of excited states of the positronium atom can have a decisive effect upon the time required for such an atom to undergo annihilation, even though annihilation in an excited state is itself unlikely. The lifetimes of the excited states with respect to spontaneous radiative transitions are twice the natural lifetimes of the corresponding excited states of the hydrogen atom. They are, therefore, of the order 10^{-7} to 10^{-9} sec., except in the case of the $2S$ state, which is metastable in this respect.[9] Hence, if a free positronium atom has been formed in an excited state, the observed lifetime may be essentially the time required for spontaneous de-excitation.

However, if formed in a gas of normal temperature and pressure, the positronium atom will undergo thermal collisions at a rate of the order 10^{12} sec.$^{-1}$. The time for de-excitation may in this case be negligible as compared to the lifetime of the lowest states against annihilation.

Excitation from the ground state, due to thermal collisions, is not to be expected, since the energy of even the first excited state lies about 5 ev. above that of the ground state.

The study of the three-photon annihilation process is of importance quite apart from the relation of this process to the lifetime of positronium. In particular, a comparison of the theoretical predictions with experimental results is of interest since it seems to offer a means of checking the theoretical foundations of the calculation.

The simplest way of testing the results seems to be by observing the relative frequency of the two- and three-photon annihilation radiation from a target irradiated by slow positrons.

Also, three-photon annihilation might be of importance in a detailed study of the mechanism of cosmic ray showers. The present calculation is not applicable in this case, since it has been performed for small relative velocities. However, one will expect that the multiple process becomes relatively more important at high energy.

The energy spectrum (Fig. 2) shows that photons of any energy not exceeding the rest energy of the electron have an appreciable probability of occurrence, except photons of very low energy. The Coulomb force, whether in the positronium atom or in a target bombarded with positrons, will be expected to affect the annihilation process appreciably only when a photon of small momentum is involved. The energy spectrum indicates that such processes are rare. Therefore, the neglect of the Coulomb force should not be a serious limitation to the applicability of the results.

The spectrum is seen to deviate considerably from that estimated statistically. It may be mentioned that Tiomno and Wheeler[10] have obtained a somewhat similar result in the case of electrons resulting from the decay of a μ-meson, under certain assumptions as to the mass of the neutral meson and the ineractions of the particles involved.

The authors are indebted to Professor E. Teller and Dr. C. N. Yang for valuable discussions.

Note added in proof.—The statement that certain transitions are forbidden for the positronium atom is true only in a limited sense. Conversion between triplet and singlet ground states can take place by magnetic dipole radiation. However, the lifetime of the triplet state with respect to this kind of decay is several months, which at normal temperatures is an order of magnitude longer than the corresponding thermally induced transition. Also, $2S$–$1S$ transitions can take place via P states by the emission of two photons. As in the case of the hydrogen atom,** the lifetime is again long (1–0.1 sec.).

Consequently, these effects are not important. However, this may not be true of the effect of direct annihilation of the positron with an electron of an atom or molecule with which the positronium atom collides.

[9] See reference 4, p. 118.

[10] J. Tiomno and J. A. Wheeler, Rev. Mod. Phys. **21**, 144 (1949).

** G. Breit and E. Teller, Astrophys. J. **91**, 215 (1940).

Measurements of Ambipolar Diffusion in Helium*

MANFRED A. BIONDI AND SANBORN C. BROWN
Research Laboratory of Electronics, Massachusetts Institute of Technology, Cambridge, Massachusetts
(Received February 10, 1949)

Microwave techniques are applied to the study of the diffusion of electrons and positive ions in helium. For the electron and ion densities realized experimentally, the diffusion takes place ambipolarly; that is, the flow of charged particles of both signs is equalized by the space charge field which they set up. At 1 mm Hg pressure and 0.039-ev average energy, the measured value of the ambipolar diffusion coefficient, D_a, is 540 cm²/sec. The measured variation of D_a with gas density, energy of the particles, and diffusion container size and shape agrees closely with theory.

AMBIPOLAR diffusion is the simultaneous diffusion of electrons and positive ions in the presence of their own space charge fields. Although the theory of ambipolar diffusion has been investigated extensively, experimental measurements in the past have been difficult to interpret because of the presence of undesired secondary processes. The recent advancement of microwave technique has led to an experiment capable of giving quantitative results which may be compared with theory.

THEORY

The motion of positive ions and electrons in a gas under the action of concentration gradients and an electric field may be expressed as:

$$\Gamma_- = n_-\bar{v}_- = -D_-\nabla n_- - \mu_- E n_-, \quad (1)$$

$$\Gamma_+ = n_+\bar{v}_+ = -D_+\nabla n_+ + \mu_+ E n_+, \quad (2)$$

where Γ represents particle current density; n is particle density; $\bar{v}$ is the average drift velocity; D, the diffusion coefficient; μ, the mobility; and E, the electric field. The subscripts refer to the positive ions and the electrons. If the only field present is that due to the space charge of the particles and if the particle densities are sufficiently large, then $(n_+ - n_-) \ll n_-$, and the currents Γ_+ and Γ_- will be equal. Equations (1) and (2) simplify to

$$\Gamma = -D_a\nabla n, \quad (3)$$

where Γ and n refer to either positive ions or electrons. The ambipolar diffusion coefficient, D_a, is defined by:

$$D_a = (D_+\mu_- + D_-\mu_+)/(\mu_+ + \mu_-). \quad (4)$$

The particle continuity equation may be written

$$P = (\partial n/\partial t) + \nabla\cdot\Gamma, \quad (5)$$

where $P = \nu n$ is the rate of production of positive ions or electrons, and ν is the production rate per electron.

When Eq. (3) is substituted into Eq. (5), we obtain

$$D_a\nabla^2 n + \nu n = \partial n/\partial t. \quad (6)$$

Assuming an exponential decrease of n with a mean decay time, τ, one has

$$\nabla^2 n + ((\nu/D_a) + (1/D_a\tau))n = 0. \quad (7)$$

The boundary condition which is applied to Eq. (7) is that n goes to zero at the walls. This condition leads to a series of characteristic values and characteristic functions for Eq. (7).

$$\nabla^2 n_m + n_m/\Lambda_m^2 = 0, \quad (8)$$

where the Λ_m's are lengths which describe the size of the container with regard to diffusion loss and are called the characteristic diffusion lengths. The boundary condition is satisfactory as long as the mean free paths of the particles are small compared to the dimensions of the container.

The solution of the diffusion Eq. (7) is in general a sum of the characteristic functions of Eq. (8). To measure the diffusion, however, it is necessary to have a single function, corresponding to the lowest characteristic value, as the solution of Eq. (7). In the experiment, two intervals are used, one during which the gas is broken down and a steady state is set up ($\nu \neq 0$, $\tau = \infty$), followed by a second in which there is no applied field and therefore no production

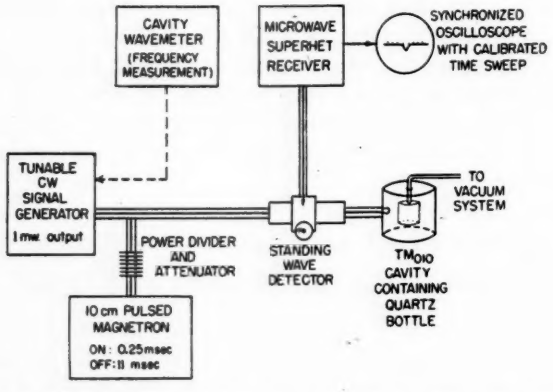

FIG. 1. Block diagram of the apparatus. The oscilloscope sweep is synchronized to start as the magnetron is turned off.

* This work has been supported in part by the Signal Corps, the Air Materiel Command, and the ONR.

of ions or electrons ($\nu=0$, $\tau<\infty$), and the electron density decays. Measurements of n as a function of time are made during the second period. By making the ionization rate per electron, ν, constant throughout the diffusion container, the lowest mode density distribution is generated during the first period, and maintained during the second period when ν is zero. No data are taken until two milliseconds after the ionization ceases. This allows the electrons to come to thermal equilibrium with the gas and also insures that no higher modes are present during the measurements. Under these conditions, Eqs. (7) and (8) lead to

$$D_a=\Lambda_1^2/\tau_1, \tag{9}$$

where Λ_1 represents the lowest characteristic diffusion length. Thus the ambipolar diffusion coefficient may be determined by measuring the rate of decay of charge density in a container of known dimensions.

From kinetic theory,[1] the definition of the diffusion coefficient of a particle in terms of its mean free path, l, and velocity, v, is

$$D=(lv/3)_{Av}, \tag{10}$$

where the average is over the distribution in velocity of the particles

Equations (4), (9), and (10) suggest the proper experimental variations to study. The effect of container size and shape, of gas density, and of the electron and ion energy upon measured values of D_a will be compared with theoretical predictions.

EXPERIMENTAL METHOD

The experimental method consists of measuring the mean decay time of charge density in a container of known dimensions by observing the change of the resonant wave-length of a microwave cavity enclosing the container. Provided that $\sigma_i \ll \epsilon_0(2\pi c/\lambda_0)$ and $\sigma_r \ll \sigma_i$, the change in resonant wave-length of a cavity due to a complex conductivity within the cavity is given by[2]

$$\Delta\lambda/\lambda=(\lambda_0-\lambda)/\lambda$$

$$=-\left(\lambda_0\int_V \sigma_i E^2 dv\right)\Big/\left(4\pi c\epsilon_0\int_V E^2 dv\right). \tag{11}$$

λ represents the resonant wave-length of the cavity with electrons inside; λ_0 is the resonant wave-length of the cavity in the absence of electrons; σ_i and σ_r are the imaginary and real parts of the conductivity due to the electrons; E is the electric field in the cavity; c is the velocity of light, and ϵ_0 is the permittivity of free space. The relation between σ_i and electron density is given by

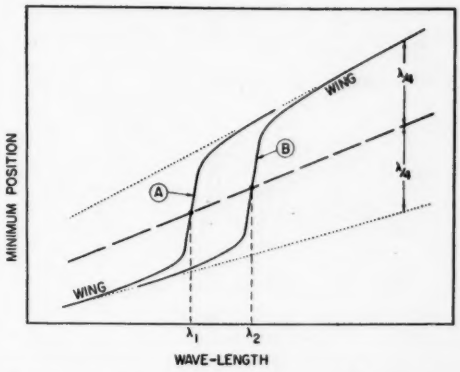

FIG. 2. Position in the coaxial line of a particular minimum of the standing wave pattern as a function of wave-length.

$$\sigma_i=-ne^2\lambda/2\pi mc, \tag{12}$$

where n is the electron density, and e and m are the charge and mass of the electron, respectively. For ambipolar diffusion, where the electron and the positive ion densities are nearly equal, the contribution to σ_i, and hence to $\Delta\lambda$, of the positive ions is negligible because of their large mass. Substituting Eq. (12) into Eq. (11) and integrating, one finds that

$$\Delta\lambda=C\lambda^2\bar{n}. \tag{13}$$

C is a geometrical coefficient which takes into account the distribution of electron density and electric field in the cavity; $\bar{n}$ is the average electron density within the quartz bottle. Thus the electron density within the cavity is related to the change of resonant wave-length of the cavity.

The experimental arrangement is shown in Fig. 1. Helium of a high degree of purity is introduced in the quartz bottle in the cavity. The vacuum system used in the experiment is thoroughly outgassed before each run. The quartz bottle in which the diffusion measurements are made is baked at 500°C, and a charcoal trap in the system is baked at 200°C for several days. For each run, a one liter flask of Air Reduction Sales Company spectroscopically pure[3] helium is used. When the system is isolated from the pumps by a mercury cut-off, a vacuum of between 10^{-7} mm and 10^{-6} mm is maintained for at least five hours (the maximum duration of a run). The helium in the quartz bottle is ionized by a 250-microsecond pulse from the 10-cm wave-length magnetron. A stationary charge distribution is reached during the pulse, and densities of the order of 10^{10} to 10^{11} electrons or ions/cc are produced. By placing the quartz bottle in the near-uniform field region of the

[1] J. Jeans, *The Dynamical Theory of Gases* (The Cambridge University Press, New York, 1921), p. 201.
[2] J. C. Slater, Rev. Mod. Phys. 18, 481 (1946).
[3] Mass spectrographic analysis indicates none of the following impurities present within the resolution of the instrument (1 part in 10^4): H_2, N_2, O_2, CO_2, A, and Ne. However, the manufacturer believes that the contamination may be of the order of 1 part in 10^5.

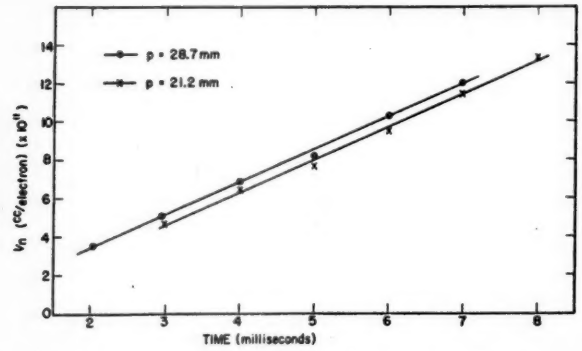

FIG. 3. Electron-positive ion recombination in helium at 0.039 ev average energy.

cavity, a density distribution is generated corresponding closely to the lowest mode of Eq. (8). The magnetron is then turned off for 11 milliseconds. The free electrons and ions lose energy by collision with gas atoms and come to equilibrium with the gas in less than 50 microseconds. Thus their energies during the measuring interval are thermal.

A small continuous signal is fed from the signal generator to the cavity. The field produced in the cavity by this signal does not appreciably alter the energy distribution of the electrons and ions. A standing wave pattern is set up in the coaxial line connecting the generator and the cavity. At the fixed frequency of the signal, the cavity impedance changes with time because of the decreasing electron density within the cavity. As a result, the minima of the standing wave pattern move along the coaxial line. At the time at which the resonant frequency of the cavity with residual electrons is equal to the signal frequency, the minima occur at so-called resonant minimum positions in the line. A probe inserted in the line at one of these points will receive a minimum signal at the time of resonance and a dip will occur on the oscilloscope trace. The method of determining the location of these resonant minimum positions will be discussed shortly.

By measuring the time at which resonance occurs (as indicated by the dip on the oscilloscope trace) for a number of different signal generator frequencies, the change of resonant wave-length of the cavity as a function of time is determined. Equation (13) then permits the determination of electron density as a function of time from which D_a may be found.

The positions of the minima of the standing wave pattern as a function of the resonant wave-length of the cavity and electrons are determined in the following manner: For the coupling between coaxial line and cavity used in this experiment, the position of a particular minimum of the standing wave pattern as a function of wave-length is given by the solid curves of Fig. 2. (For a discussion of this subject see reference 2.) Curve A represents the minimum position when the cavity contains an electron density, n_1, giving a resonant wave-length, λ_1. Curve B represents the minimum position when a smaller density, n_2, is present, giving a resonant wave-length, λ_2. The wings of the curve approach the dotted lines when λ is very different from the resonant wave-length. As indicated in the figure, the position of the minimum at resonance falls on the dashed curve which is called the resonant minimum curve.

One determines the resonant minimum curve by placing a shorting post at the center of the cavity, causing the resonant wave-length to be very greatly changed. As a result, the point at which the minimum curve crosses the dashed line is moved completely off the graph. The wings of the curve now coincide with the dotted lines over the wave-length range in which we are interested. The position of the minimum is measured as a function of wave-length using a slotted section and probe. By adding (or subtracting) a distance equal to $\lambda/4$ to the ordinate of this curve, the resonant minimum curve for a particular minimum is determined.

CORRECTION FOR RECOMBINATION

The experimental measurement of the ambipolar diffusion coefficient is complicated by the presence of electron-positive ion recombination. Loss of particles to recombination may be expressed by

$$\partial n_+/\partial t = \partial n_-/\partial t = -\alpha n_+ n_- = -\alpha n^2, \qquad (14)$$

where α is the recombination coefficient. Studies of this recombination in neon and argon (where ambipolar diffusion loss is secondary to recombination loss over the range of experimental variables used) indicate that α is independent of pressure and energy at low energies.

At pressures above 20 mm in helium, the diffusion loss, which decreases with increasing pressure, be-

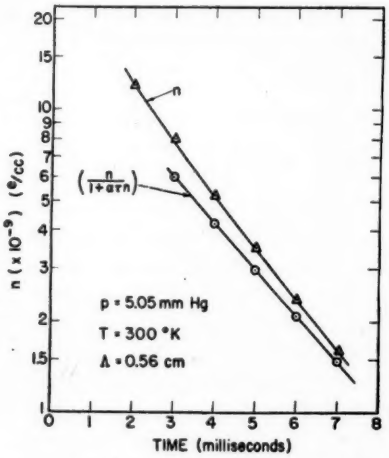

FIG. 4. Loss of electrons in helium by recombination and ambipolar diffusion.

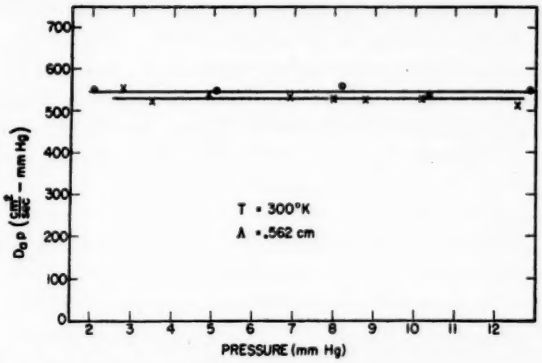

FIG. 5. Variation with pressure of the ambipolar diffusion coefficient for helium.

comes less important than the recombination loss, and Eq. (14) represents the principal loss of particles. The solution of Eq. (14) is

$$1/n = 1/n_0 + \alpha t, \tag{15}$$

where n_0 represents the electron density at time $t=0$.

The recombination coefficient may be determined by measuring the slope of a reciprocal density *versus* time plot. The density is found by measuring $\Delta\lambda/\lambda^2$ as a function of time and substituting in Eq. (13). Experimental data are shown in Fig. 3. The value of α for helium is 1.7×10^{-8} (cc/ion-sec.).

At low pressures and low electron densities where diffusion loss outweighs recombination, the rate of decay of electron density is given approximately by:

$$\partial n/\partial t = -(n/\tau) - \alpha n^2, \tag{16}$$

where τ is the mean decay time due to diffusion. The solution of this equation is

$$n/(1+\alpha\tau n) = [n_0/(1+\alpha\tau n_0)]\exp(-t/\tau), \tag{17}$$

where n_0 represents the density at $t=0$. Equation (17) permits the correction of the data to find τ and hence D_a. Figure 4 is a typical experimental curve. The upper curve shows the original data while the lower curve results when the recombination loss is subtracted. The time $t=0$ was taken 3 milliseconds after the ionization ceased.

EXPERIMENTAL RESULTS

Data of the type shown in Fig. 4 are taken as a function of pressure, temperature, and the size and shape of the container to complete the study of ambipolar diffusion. According to Eq. (10), at constant energy, the diffusion coefficient is proportional to the mean free path; that is, $D_a p$ should be constant. Since the ions and electrons are in equilibrium with the gas, we control their energy by keeping the gas temperature constant. Figure 5 represents measurements on two different flasks of Air Reduction

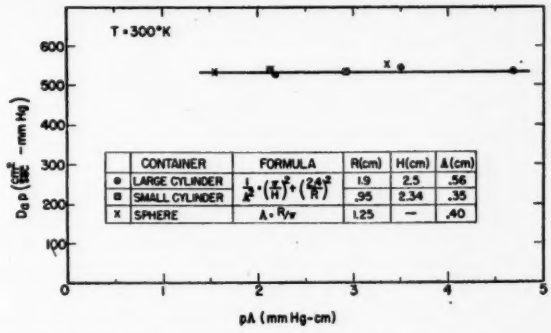

FIG. 6. Effect of the variation of the diffusion container size and shape upon the measured values of D_a.

Sales Company spectroscopically pure helium. Experimentally, $D_a p$ is found to be independent of pressure within an error of less than 5 percent. The absolute magnitude of $D_a p$ differs for the two samples by 3 percent.

The measured value of D_a should not depend on the size or the shape of the container in which the diffusion is taking place. Measurements of D_a were made in three containers whose dimensions are given in Fig. 6. Since different samples of helium give slightly different values of D_a (due to the presence of very small amounts of impurity), one cylinder was used as a reference, and measurements were made using one sample of helium for the large and the small cylinder and another sample for the large cylinder and the sphere. The results are plotted in Fig. 6. At constant energy, the value of $D_a p$ is found to be independent of $p\Lambda$ within 3 percent, and since $D_a p$ has been shown to be independent of pressure, we conclude that the measured value of D_a does not depend on our choice of Λ.

Finally, the energy dependence of the ambipolar diffusion coefficient has been studied. Under the conditions of the experiment, the electrons and ions are in equilibrium with the gas and possess a Maxwellian energy distribution so that

$$D_+/\mu_+ = D_-/\mu_- = kT/e, \tag{18}$$

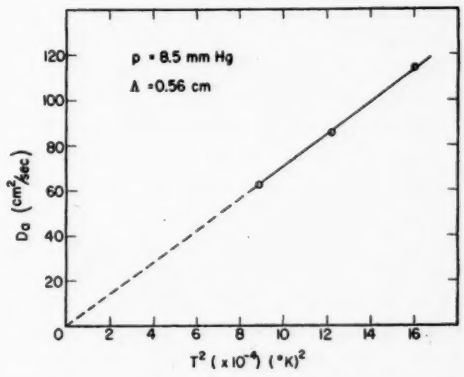

FIG. 7. Variation of the ambipolar diffusion coefficient with energy.

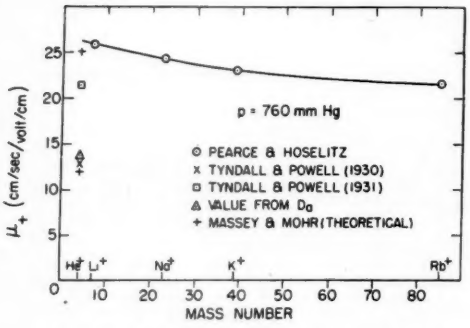

FIG. 8. Mobility of various positive ions in helium.

where T is the gas temperature. Under these conditions, Eq. (4) becomes

$$D_a=(2D_+\mu_-)/(\mu_-+\mu_+)\approx 2D_+, \qquad (19)$$

because μ_+ is very much smaller than μ_-. Positive ions in helium interact with the helium atoms according to an inverse fifth power law of force because of the induced dipole of the atom. Jeans[4] has shown that the diffusion coefficient for particles obeying this law of force is given by

$$D_+ \propto \bar{u}_+/n_g,$$

where $\bar{u}_+$ is the average energy of the ion and n_g is the gas density. This means that the collision cross section for positive ions in helium varies as the reciprocal of the positive ion velocity. Experimental measurements of the collision cross section of positive ions in noble gases agree with the theoretical prediction.[5]

At constant pressure, the gas density varies inversely with the gas temperature so that under these conditions

$$D_a \propto T^2.$$

Experimental data are shown in Fig. 7. The energy range is small because of experimental limitations; however, the extrapolated curve passes through the origin in agreement with theoretical predictions.

DISCUSSION

The measured value of $D_a p$ at 0.039-ev average energy is 540 (cm²/sec.)/(mm Hg). There is good agreement between experiment and theory with regard to the dependence of D_a on pressure, energy, and the size and shape of the diffusion container.

In the early part of the experimental work larger values of D_a were found, but the measured values of D_a became smaller as vacuum technique improved. We attribute this effect to the reduction of the amount of impurity with which the gas samples were contaminated by the vacuum system. If the impurities exhibit electron attachment, they cause an additional loss of electrons which will lead to a spurious, high value of D_a. With present vacuum and gas preparation techniques, the impurity in the gas samples is not believed to be greater than 1 part in 10^5. If this impurity has an attachment probability of 10^{-3} attachments/collision, the effect on the measured value of D_a is only a few percent. Thus, the experiment has been done with what may be considered as a pure sample of helium.

The results of this experiment may help to resolve the discrepancy between the theoretical value of positive ion mobility in helium calculated by Massey and Mohr[6] and the experimentally determined value of Tyndall and Powell.[7] Equations (18) and (19) permit the conversion of the measured value of D_a to positive ion mobility. When our value of D_a is extrapolated to 760-mm pressure, a value of $\mu_+=13.7$ (cm/sec.) per (volt/cm) is obtained. This value is represented by the triangular symbol in Fig. 8. Massey and Mohr calculate the mobility quantum mechanically, including the effect of charge transfer between the positive ion and atom on close approach, to be 12 (cm/sec.) per (volt/cm). Tyndall and Powell's measured value is 21.4 (cm/sec.) per (volt/cm). The quantum mechanical calculation of Massey and Mohr, omitting the effect of charge transfer, leads to a value of 25 (cm/sec.) per (volt/cm). Later work by Pearce[8] and Hoselitz[9] measured the mobility of various ions in helium. The results of their measurements are shown in Fig. 8. The theoretical value of Massey and Mohr, for the case in which charge transfer is neglected, lies quite close to the extrapolated mobility *versus* mass curve, as it should, since other ions cannot exhibit the charge transfer effect in helium. The theoretical value, including the charge transfer effect, lies close to both the value determined in the present experiment on D_a, and to the value of mobility which Tyndall and Powell measured in an earlier experiment published in 1930.[10]

The explanation of the difference between the values obtained in the two experiments of Tyndall and Powell is not clear. Their first experiment, in which the mobility was measured as 13 (cm/sec.) per (volt/cm) involved the generation of ions by α particles. The second, in which the value 21.4 (cm/sec.) per (volt/cm) was obtained, generated ions by a point or wire-to-plane glow discharge. Brown[11] has shown that it is possible to generate appreciable amounts of He^{++} in the inhomogeneous fields of this type of discharge.

[4] J. Jeans, *The Dynamical Theory of Gases* (The Cambridge University Press, New York, 1921), p. 247.
[5] C. Ramsauer and O. Beeck, Ann. d. Physik **87**, 1 (1928).
[6] Massey and Mohr, Proc. Roy. Soc. **A144**, 188 (1934).
[7] Tyndall and Powell, Proc. Roy. Soc. **A134**, 125 (1931).
[8] Pearce, Proc. Roy. Soc. **A155**, 490 (1936).
[9] Hoselitz, Proc. Roy. Soc. **A177**, 200 (1941).
[10] Tyndall and Powell, Proc. Roy. Soc. **A129**, 162 (1930).
[11] S. C. Brown, Phys. Rev. **62**, 244 (1942).

If the effect of charge transfer is neglected, the theoretical mobility of He^{++} should be nearly equal to that of He^{+}, since in doubling the charge, the mean free path between ion and atom is reduced to about half the value for the singly charged ion. On the other hand, the effect of total charge transfer between He^{++} and He should be nearly absent. Therefore, it is suggested that Tyndall and Powell may actually have measured the mobility of He^{++} in their second experiment, inasmuch as their criterion was to select the fastest ion as the one which was to be measured.

PHYSICAL REVIEW VOLUME 75, NUMBER 11 JUNE 1, 1949

The Optical Constants of Germanium in the Infra-Red and Visible

W. H. Brattain and H. B. Briggs
Bell Telephone Laboratories, Murray Hill, New Jersey
(Received February 14, 1949)

Thin films of germanium have been evaporated on glass, quartz, and calcium fluoride slides. The thickness of these films ranged from 4×10^{-6} to 1×10^{-4} cm. Transmission of infra-red light through the films exhibited the usual interference phenomena, showing alternate maxima and minima as the wave-length was varied. From these maxima and minima the index of refraction of the films was determined. This index was 4.3 for λ greater than 6×10^{-4} cm wave-length. It increased to 5.2 at 8.0×10^{-5} cm and then fell off rapidly to 2.3 at 4.0×10^{-5} cm. To determine the values of the index and extinction coefficients in the visible region where the absorption is large, a wedge of germanium was made. Transmission was then determined as a function of film thickness for several wave-lengths. The values of the optical constants in this region were then obtained by comparing these results with the theoretical transmission equations. The extinction coefficient increased from 0.4 at $\lambda=1\times10^{-4}$ cm to 2.8 at $\lambda=4\times10^{-5}$ cm. The density of the films was determined by an interferometric method and was found to be the same as bulk germanium. The real and imaginary parts of the dielectric constant for germanium are calculated and compared with the known results for silicon. The absorption bands for both elements are shown to be consistent with the electron band structure deduced from their semiconducting properties.

I. EXPERIMENTAL RESULTS

A TYPICAL result for a germanium film on calcium fluoride is shown in Fig. 1. Here the transmission through the film is plotted as a function of the reciprocal of the wave-length λ in cm. The data were obtained with an infra-red spectrometer.[1] It is seen that seven orders of reinforcement were obtained before the absorption at shorter wave-lengths became too large. Another set of results on a thinner germanium film on glass is shown in Fig. 2. These results were obtained with a quartz spectrometer. Here both the transmission through the film at normal incidence, and the reflection from the film at 45° incidence are plotted against the wave-length λ in cm. Three orders of reinforcement are obtained and it is seen that the transmission maxima and minima correspond respectively to the reflection minima and maxima as they should. The well-known simple relations which govern the position of the maxima and minima are: The condition for transmission maxima

$$2nt=m\lambda, \tag{1}$$

where n is the index of refraction, t the thickness, m the order, and λ the wave-length; and the condition for transmission minimum

$$2nt=\tfrac{1}{2}(2m+1)/\lambda. \tag{2}$$

[1] We are indebted to P. P. Debye of these laboratories for use of the spectrometer to make these measurements.

It is therefore obvious that if one knows the thickness of the film and the order number m, one can calculate the index n for every value of λ for which either a maxima or minima occurs. Since the order number must be an integer, choice of the wrong order number makes a large difference in n. It is therefore easy to assign the correct order numbers if data are available on films of several thicknesses.

If the films are uniform in thickness and the density of the films is known, one can determine the thickness by weighing the films. The slides on which films of germanium were deposited were weighed before and after deposition of the film, and the area of the film was determined in each case. The uniformity in thickness of a film was determined by choosing a particular wave-length and measuring the transmission through different parts of the film. Since λ is fixed, n should be the same for all parts of the film, and therefore, if the thickness varies, the order m in Eq. (1) must vary. The percentage variation in the thickness of the film can be determined from the change in order:

$$\Delta t/t=\Delta m/m, \tag{3}$$

where t is the thickness and m the order for a particular spot on the film, and Δt is the change in thickness for a given change Δm in order as the position on the film is changed. By making such measurements on a single film for two different wave-lengths, the interpretation could be made

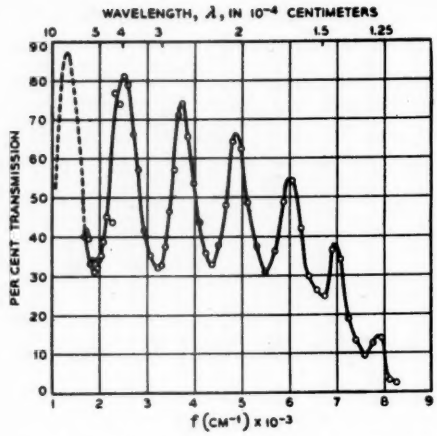

FIG. 1. Percent transmission *vs.* the reciprocal of the wave-length for a germanium film, 9.0×10^{-5} cm thick on a fluorite slide.

unambiguous. As might be expected for films evaporated from finite sources, considerable variation in thickness was found over the area of the films, of the order of 20 percent on some of the first films. It was found possible, however, by using four properly spaced sources, to make films with less than 5 percent variation in one direction across the film, and less than 10 percent in a direction normal to that. Then, with the spectrometer slit parallel to the direction of least variation, accurate measurements could be taken over an area of the film that was quite uniform in thickness, and moreover, the actual thickness of this area could be determined if the weight, density, and percentage variation in thickness along the film were known. Thus, the index could be determined for this film for various wave-lengths, and then using wave-lengths in this same region, one could in turn determine the correct effective thickness for all the other less uniform films.

The density of a typical film was measured in the following manner. A film of germanium was evaporated on a glass slide[2] so arranged that a small section in the center of the slide was left bare. The area of the glass covered with germanium was measured carefully. The slide was weighed both before and after evaporation to determine the weight of the germanium. An additional film of germanium was then evaporated over the whole surface of the slide just to make the reflection from all parts of the surface uniform. Another blank glass slide was then placed on top of the first slide while both slides were immersed in water. The combination was then examined in sodium light. The shift in the fringes could be observed between the region where the first germanium film was on the glass and where only the second germanium film was on the glass, thus enabling one to determine the thickness of the first germanium film, and from its area and weight, the density. The area covered by the first film was 9.7 cm.[3] The fringe shift was 4.25 fringes of sodium light ($\lambda=5.9\times10^{-5}$ cm) in water (the medium between the two glass slides) giving a thickness of 9.4×10^{-5} cm. The weight of the film was 4.83×10^{-3} gram. This gives 5.3 for the density of the film, agreeing with the bulk density of germanium. All films were therefore assumed to have the bulk density.

In order to determine both the index n and the extinction coefficient k for these films in the region of wave-length 3.5×10^{-5} to 7×10^{-5} cm, where the absorption is so large that interference maxima and minima are not easily seen, a germanium wedge was evaporated on a glass slide using a two-source arrangement to assure that the thickness was uniform to at least 5 percent across the wedge. The variation in thickness with distance along the wedge was determined by getting the change in order with distance for several wave-lengths in the range 8.0×10^{-5} to 2.0×10^{-4} cm. The relation between thickness and distance that was found is shown in Fig. 3. The transmission *vs.* thickness was then determined for each of four wave-lengths 3.65×10^{-5}, 4.36×10^{-5}, 5.02×10^{-5}, and 6.8×10^{-5} cm. These results are shown in Fig. 4. The solid curves represent the experimental results; at least 20 points were taken for each curve. The circles are from theoretical calculations and will be discussed later. The results for the shorter wave-lengths approximate the simple case where the transmission is just an exponential function of the thickness, and the logarithm of the transmission *vs.* the thickness should give a curve which is a straight line with a slope which determines the value of the extinction coefficient k. Deviations from such a linear relation are, however, apparent for the 3 longer wave-

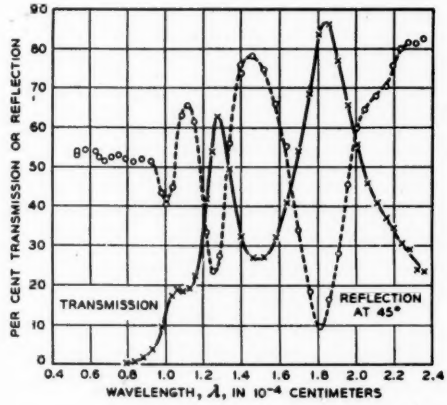

FIG. 2. Reflection and transmission *vs.* wave-length for a germanium film, 3.9×10^{-5} cm thick on glass.

[2] The four-source method was used here to give a film of uniform thickness.

[3] This method was suggested by W. Shockley of these Laboratories.

lengths, and for the case of $\lambda = 6.8 \times 10^{-5}$ cm these deviations are very pronounced. As will be seen in the next section, the index n and the extinction coefficient k can be determined from these curves.

Before closing this section, a few more of the experimental details should be mentioned. The germanium was evaporated from tantalum boats. Care was taken to load the boats uniformly. In each case more germanium was put in the boats than was used in depositing the film. The germanium was of the high purity type used for making point contact rectifiers.[4] The slides were heat treated to approximately 400°C before depositing the germanium, and each germanium film was heat treated to approximately the same temperature after deposition. Both of these operations were performed in vacuum. The pressure during deposition was less than 10^{-5} mm of Hg. The weight of the germanium films was of the order of milligrams. The weighing was done on a balance good to 0.05 milligram. Slides were generally heat treated in vacuum and then weighed before deposition to eliminate weight

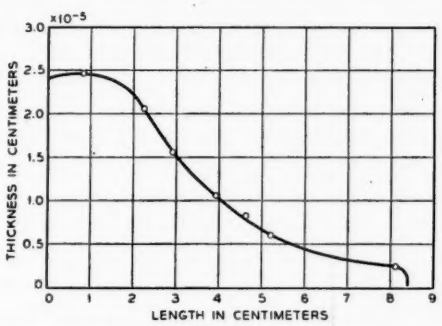

FIG. 3. Thickness contour of germanium wedge on glass.

loss due to removal of adsorbed films. As another check on the variation of index with density of film, one slide was made in which the germanium was deposited when the slide was at a temperature of 150°C. Transmission measurements were then made on the film. After this it was put back in vacuum and heat treated to 400°C and taken out and measured again. The results of this test are shown in Fig. 5. They correspond to a shift in index of about 3 percent probably due to an increase in density on heat treatment. This result indicates that there was no large density change due to heat treatment.

II. THEORY

Starting from Drude's equation for transmission of light in various media, Barnes and Czerny[5] have

[4] H. C. Torrey and C. A. Whitmer, *Crystal Rectifiers* (McGraw-Hlil Book Company, Inc., New York, 1948).

[5] R. B. Barnes and M. Czerny, Phys. Rev. **38**, 338 (1931). See also T. C. Fry, J. Opt. Soc. Am. **22**, 307 (1932); and A. W. Crook, J. Opt. Soc. Am. **38**, 954 (1948).

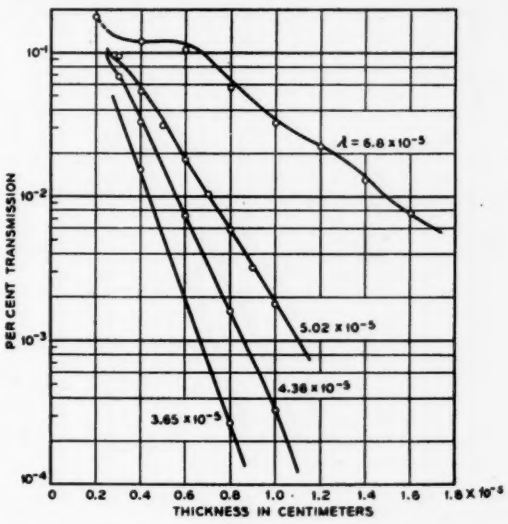

FIG. 4. Transmission *vs.* thickness for several wave-lengths obtained for germanium wedge.

worked out the equations for reflection at normal incidence from a film of index n, extinction coefficient k, and thickness t immersed in a medium of index n_1. Our case is more complicated. We have first air, then the film, and then the glass, quartz, or fluorite as the case may be, and then air again. It was decided that the approximation would be sufficiently good if the last interface between the slide and the air were neglected. The problem then involves air of index $n_1 = 1$, the film, of index n, extinction coefficient k, and thickness t; and the slide of index n_2. Working out the correct boundary conditions for this case, one gets the two equations for reflection and transmission at normal incidence.

$$\frac{E_R}{E_I} = \frac{(1-a)(1+b)\epsilon^{-ip} + (1+a)(1-b)\epsilon^{+ip}}{(1+a)(1+b)\epsilon^{-ip} + (1-a)(1-b)\epsilon^{+ip}} \qquad (4)$$

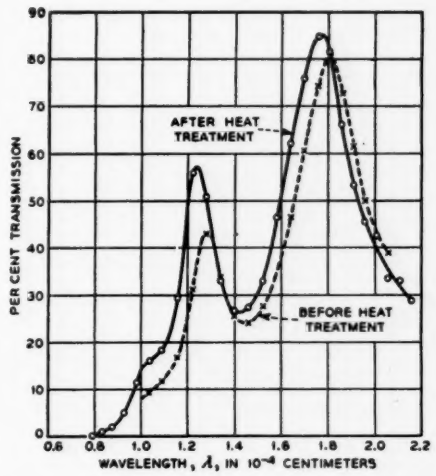

FIG. 5. Dependence of transmission on heat treatment of a germanium film, 3.7×10^{-5} cm thick on glass.

and

$$\frac{E_T}{E_I}=\frac{4\epsilon^{ip_2}}{(1+a)(1+b)\epsilon^{-ip}+(1-a)(1-b)\epsilon^{+ip}}, \quad (5)$$

where

$$a=(n-ik)/n_1, \quad b=n_2/(n-ik),$$
$$p=(2\pi t/\lambda)(n-ik), \quad p_2=(2\pi t/\lambda)n_2;$$

t is the thickness, λ the wave-length in a medium of index 1, and E_I, E_T, and E_R are the incident, transmitted, and reflected amplitudes, respectively. Multiplying by the complex conjugate in each case, one obtains (R) the fraction of the power reflected, and (T) the fraction transmitted as follows.

$$R=\left|\frac{E_R}{E_I}\right|^2=\frac{r_1^2[(\epsilon^x-(\rho_1/r_1)\epsilon^{-x})^2+4(\rho_1/r_1)\sin^2(y+\frac{1}{2}(\varphi_1-\theta_1))]}{r^2[(\epsilon^x-(\rho/r)\epsilon^{-x})^2+4(\rho/r)\sin^2(y+\frac{1}{2}(\varphi-\theta))]}, \quad (6)$$

$$T=\frac{n_2}{n_1}\left|\frac{E_T}{E_I}\right|^2=\frac{16n_1n_2(n^2+k^2)}{r^2[(\epsilon^x-(\rho/r)\epsilon^{-x})^2+4(\rho/r)\sin^2(y+\frac{1}{2}(\varphi-\theta))]}, \quad (7)$$

where

$$r^2=[(n_1+n)^2+k^2][(n_2+n)^2+k^2],$$
$$\rho^2=[(n_1-n)^2+k^2][(n_2-n)^2+k^2],$$
$$r_1^2=[(n_1-n)^2+k^2][(n_2+n)^2+k^2],$$
$$\rho_1^2=[(n_1+n)^2+k^2][(n_2-n)^2+k^2],$$
$$\tan\varphi=[-k(2n+n_1+n_2)]/[(n_1+n)(n_2+n)-k^2],$$
$$\tan\theta=[-k(2n-n_1-n_2)]/[(n_1-n)(n_2-n)-k^2],$$
$$\tan\varphi_1=[-k(2n-n_1+n_2)]/[(n-n_1)(n+n_2)-k^2],$$
$$\tan\theta_1=[-k(2n+n_1-n_2)]/[(n+n_1)(n-n_2)-k^2],$$
$$x=(2\pi kt/\lambda) \quad \text{and} \quad y=(2\pi nt/\lambda).$$

In Eq. (7) the nominal result has been multiplied by n_2, and divided by n_1, to compensate for the fact that the ratio of the transmitted power to incident power is not equal to the square of the absolute magnitude of the ratio of the amplitudes, when the amplitudes are measured in media of different index of refraction.

When k is small or zero, Eqs. (6) and (7) become much simpler. The phase angles become zero, and from Eq. (7) one can verify at a glance that T will be a maximum when $\sin^2 y$ is zero and a minimum when $\sin^2 y=1$, giving Eqs. (1) and (2), respectively. Also when k is large so that the ϵ^{-x} and the $\sin^2 y$ terms in the denominator of (7) can be neglected in comparison with ϵ^x, one gets the well-known transmission formula,

$$T=A\exp(4\pi kt/\lambda), \quad (8)$$

where

$$A=[16n_1n_2(n^2+k^2)]/r^2.$$

For all cases in between these two limits, it is necessary to use the complete equation. It is fairly obvious that when this is necessary, it is easier to keep the wave-length fixed and vary the film thickness t, and look for one n and one k that will fit the data, than it is to work with a fixed thickness t and vary the wave-length which means finding a different value of n and k for each wave-length. This is the reason that the wedge described in Section I was made. The circles shown in Fig. 4 are calculated from Eq. (7) using the values for n and k that were found to give the best fit in each case. For example, consider the results for $\lambda=6.8\times10^{-5}$ in Fig. 4. After several trials the values $k=1.3$ and $n=5.15$ were found to be approximately right. Substituting these values into Eq. (7) one gets the specific equation for this case,

$$T=0.375/[(\epsilon^x-4\epsilon^{-x})^2+1.6\sin^2(y+0.135)], \quad (9)$$

where $x=1.2\times10^5 t$ and $y=4.76\times10^5 t$. The fit that can be obtained is quite sensitive to the values of n and k used. A ten percent change in either n or k would make the fit very poor. It should also be mentioned that it would be quite impossible to fit these data if account had not been taken of the fact that the index of the slide was different from that of the air.

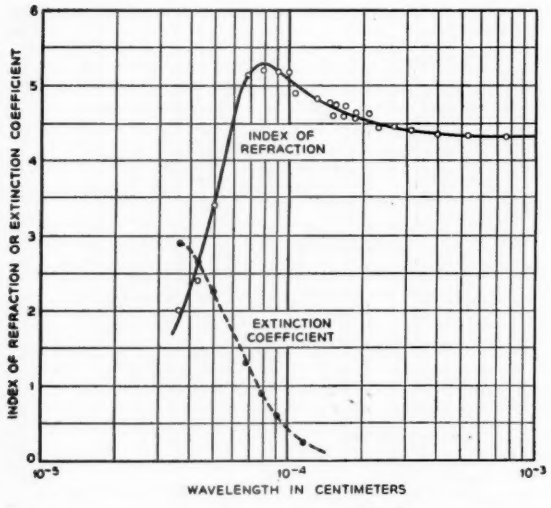

FIG. 6. Index of refraction and extinction coefficient *vs.* wave-length, for germanium, experimental points with smooth curves drawn through them.

III. SUMMARY AND CONCLUSIONS

Using the experimental data from all the germanium films that were measured and Eqs. (1) and (2), or when necessary Eq. (7), values of n and k were determined as a function of wave-length λ. These results are shown in Fig. 6. The open

circles are the separate determinations of n and likewise the solid points are the values of k. The solid lines are simply smooth curves drawn through the experimental points. The only other data on the optical constants n and k for germanium were taken by O'Bryan.[6] His values of n range from 2.85 at $\lambda=4.046\times10^{-5}$ to 3.42 at $\lambda=5.78\times10^{-5}$, and the respective values of k are 1.67 and 1.35. The values of n are the same order as ours in the range we covered, but they do not vary as rapidly with wave-length, and his values of k are considerably smaller than ours. We do not know how to explain these differences. His method involved measurements of reflection at other than normal incidence, whereas our results in this region involve the actual transmission through the germanium film at normal incidence.

Having values for n and k at all wave-lengths such as shown in Fig. 6, it should be possible to calculate from Eq. (7) the actual shapes of the transmission *vs.* wave-length curves for any of the germanium films we measured. This was done for one film which was found to be quite uniform in thickness. In this case, the transmission through the germanium film and its glass backing was compared with the transmission through a blank glass slide to eliminate, as nearly as possible, the effect of the glass air interface that has been neglected in Eq. (7). The results are shown in Fig. 7. The experimental points are shown with a smooth curve through them, and for comparison, the points calculated from Eq. (7) are shown as circles. The agreement is good and it can be said that the values of the optical constants n and k obtained for these films explain the intensity relations as well as the position of the maxima and minima.

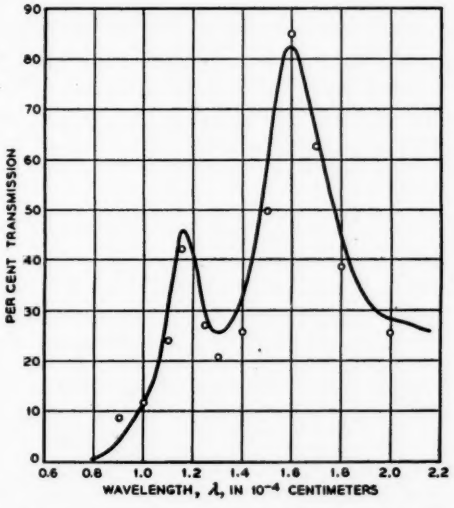

FIG. 7. Comparison of calculated (circles) and experimental results (smooth curve) for transmission through a germanium film, 3.4×10^{-5} cm thick on glass.

[6] H. M. O'Bryan, J. Opt. Soc. Am. 26, 122 (1936).

TABLE I. Reflecting power of germanium.

Wave-length	R calculated	R for thick film	R for bulk surface
10^{-3}	0.39		
5×10^{-4}	0.39		
2×10^{-4}	0.42		0.40
1.5×10^{-4}	0.43		0.41
1.0×10^{-4}	0.47	0.46	0.42
9×10^{-5}	0.48	0.48	0.46
8×10^{-5}	0.48	0.51	0.48
7×10^{-5}	0.48	0.53	0.52
6×10^{-5}	0.46	0.54	0.56
5×10^{-5}	0.45		0.48
4.5×10^{-5}	0.47		0.54
4.0×10^{-5}	0.52		

As another check on the values we have obtained for n and k, the reflection coefficient for a thick germanium film was calculated for these values. These results were compared with experimentally determined values of reflection coefficient obtained for near normal incidence on a polished sample of bulk germanium and a thick germanium film. It is difficult to obtain good data on reflection coefficients. The experimental data were taken by comparing the reflection from germanium with that from an evaporated aluminum film. No correction was made for reflection loss at the aluminum surface. The data are given in Table I. The agreement is not perfect but does indicate that the reflection from bulk germanium is approximately the same as that from the germanium film, and that these results are of the same order as calculated.

All these results indicate that the values of n and k obtained are characteristic of these germanium films, and there is no reason to think that they are not also characteristic of bulk germanium.

The results that have been obtained are a typical example of how the optical constants n and k vary in the region of a well defined absorption band. The absorption band in this case is due to the excitation of electrons from the filled band in germanium to the empty conduction band by absorption of the incident radiation.

From the values of n and k one can calculate the real and imaginary parts of the dielectric constant n^2-k^2 and $2nk$, respectively. The real part n^2-k^2 is shown in Fig. 8, and the imaginary part $2nk$ is shown in Fig. 9. It is interesting to compare these results for germanium with another similar case. The optical constants for silicon have been measured by several observers,[7] and the real and imaginary parts of its dielectric constant are also shown in Figs. 8 and 9, respectively. It is seen that the curves are quite similar in shape. The main differences are in magnitude and in the wave-length at which the absorption occurs. Silicon and ger-

[7] E. O. Hulburt, Astrophys. J. 42, 222 (1915); G. Pfestorf, Ann. d. Physik 81, 906 (1926).

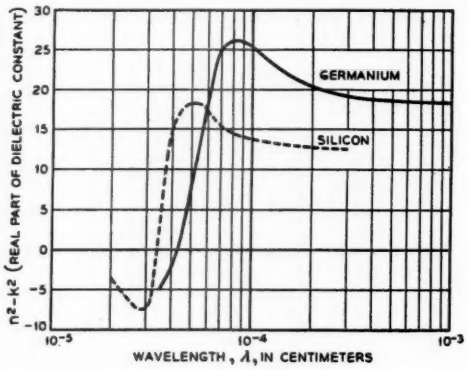

FIG. 8. The real part of the dielectric constant for silicon and germanium *vs.* wave-length.

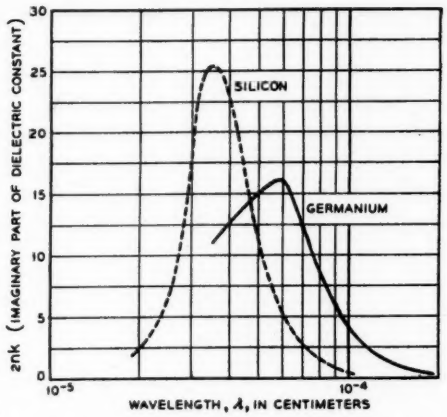

FIG. 9. The imaginary part of the dielectric constant for silicon and germanium *vs.* wave-length.

manium both have the diamond lattice structure, the atoms in each case being held together by covalent bonds (filled band). The absorption occurs when a quantum of light has sufficient energy to remove an electron from one of these bonds. This minimum energy can be estimated from the wave-length at which absorption sets in. From Fig. 9 these wave-lengths are approximately $\lambda = 1.0 \times 10^{-4}$ cm for silicon, and $\lambda = 1.6 \times 10^{-4}$ cm for germanium, corresponding to energies of 1.2 and 0.77 equivalent electron volts, respectively. These values are to be compared with the values determined from the intrinsic electrical conductivity of silicon and germanium (thermal excitation of electrons from the covalent bonds to the conduction band), namely 1.1 and 0.76 electron volts.[4] The asymptotic value of the dielectric constant at long wave-lengths, 12.5 for silicon and 18.5 for germanium, are important in the theory of the impurity conductivity in these semiconductors.[4]

Mention should be made of the fact that the real and imaginary parts of the dielectric constant are not independent. If either part is known for all wave-lengths, the other part is also determined for all wave-lengths.[8] While the data here are not quite that inclusive, the relation is such that an approximate check can be made for internal consistency of the data in Figs. 8 and 9. It was found that the data for silicon were quite consistent, but for germanium there was evidence of a considerable inconsistency. The indications were that, for λ less than 10^{-4} cm, either the experimental values of k are too small or the rate of change of n with wave-length is too large, and that the discrepancy could not be resolved without extending the wave-length range to smaller wave-lengths and taking more data. Since there is little likelihood that we will be able to do this in the near future, it was thought best to published the data we now have. There is little question about the essential correctness of the results for λ greater than 1×10^{-4} cm, and it is not impossible that a peculiar behavior in the absorption in germanium at still shorter wave-lengths would explain the present inconsistency.

The authors wish to thank F. S. Goucher for his interest and help in connection with the experimental work, and R. H. Dietzold of these Laboratories who helped in resolving the mathematical difficulties involved in the theory.

[8] H. W. Bode, *Network Analysis and Feedback Amplifier Design* (D. Van Nostrand Company, Inc., 1945), Chapter XIV.

Continuous X-Ray Spectrum from 8A to 14A*

S. T. STEPHENSON AND F. D. MASON
Washington State College, Pullman, Washington
(Received November 1, 1948)

The continuous x-ray spectrum has been studied at voltages from 1.1 kv to 2 kv and at wave-lengths from 8A to 14A using a vacuum single crystal Geiger counter spectrometer. The measurements were corrected for window absorption and counter efficiency but were not corrected for absorption in the target or for the reflecting power of the crystal. The total intensity in the continuous spectrum, as measured and partially corrected, is found to be proportional to the atomic number of the target, a result similar to results obtained for shorter wave-lengths, but the total intensity is not proportional to the square of the voltage applied to the tube. The shapes of the curves approach the shape to be expected from a thin target.

INTRODUCTION

AMONG the earlier experimental investigations of the energy distribution in the continuous x-ray spectra of various elements were those made by Ulrey,[1] whose curves have been reprinted many times in textbooks on x-rays, and those of Behnken,[2] Dauvillier,[3] Wagner,[4] Wagner and Kulenkampff,[5] Kulenkampff,[6] and Kirkpatrick.[7] The curves given by Ulrey were presented without correction although the data were sufficiently complete to allow Pike[8] to compute some pertinent corrections at a later date. Kirkpatrick's work covered the region from 0.4A to 1A and included corrections for: superposition of higher orders, incomplete absorption by the ionization chamber, absorption by the tube wall and ion chamber window, and variation of the reflecting power of the crystal. Kulenkampff carried out a thorough study in the range 1A to 2.8A making correction for absorption in the target in addition to the corrections made by Kirkpatrick. A survey of all the literature cited indicates that the total energy in the continuous spectrum is approximately proportional to the atomic number of the target and to the square of the voltage applied to the x-ray tube. There seems to be little general agreement as to the specific nature of the shape of the curve or the position of the maximum. Kulenkampff found empirically that the expression

$$I_\lambda = \frac{CZ}{\lambda^2}\left(\frac{1}{\lambda_0}-\frac{1}{\lambda}\right)+\frac{BZ^2}{\lambda^2} \qquad (1)$$

represented his experimental data fairly well, where I_λ is the intensity at any wave-length λ, Z is atomic number, λ_0 is the minimum wave-length present, and C and B are constants, with B so small that the last term is much smaller than the first. Differentiating the equation for I_λ in order to find the wave-length of maximum intensity we find

$$\lambda_{max} = \frac{3\lambda_0}{2(1+BZ\lambda_0/C)} \qquad (2)$$

in agreement again with Kulenkampff's data. If B is small, $\lambda_{max}=3\lambda_0/2$ which is the empirical formula proposed by Dauvillier. Kirkpatrick, however, found $\lambda_{max}=k+k'\lambda_0$ where k and k' are two different constants.

The most successful of the earlier theoretical attempts to arrive at an expression for the intensity as a function of the wave-length was made by Kramers[9] using an application of the ideas underlying Bohr's correspondence principle. Kramers obtained

$$I_\lambda = \frac{CZ}{\lambda^2}(1/\lambda_0-1/\lambda) \qquad (3)$$

for the intensity from a thick target where C could be determined from fundamental constants and the tube current. This expression leads directly to $\lambda_{max}=3\lambda_0/2$. The total intensity should be proportional to the atomic number of the target and the square of the applied voltage, according to Kramers. An application of quantum mechanics to the problem was made by Sommerfeld.[10] The results of the quantum-mechanical calculations have been made available by Kirkpatrick and Wiedmann[11] in a form more suitable for comparison with experiment. They show that the total intensity should be roughly proportional to the atomic number of the target and the square of the applied voltage.

It should be emphasized that most of the experimental work has been carried out at voltages of

* This work was carried out under contract with the U. S. Navy, ONR.

[1] C. T. Ulrey, Phys. Rev. **11**, 401 (1918).
[2] H. Behnken, Zeits. f. Physik **3**, 48 (1920).
[3] A. Dauvillier, Ann. de physique **13**, 49 (1920).
[4] E. Wagner, Physik. Zeits. **21**, 621 (1920).
[5] E. Wagner and H. Kulenkampff, Ann. d. Physik **68**, 369 (1922).
[6] H. Kulenkampff, Ann. d. Physik. **69**, 548 (1922).
[7] P. Kirkpatrick, Phys. Rev. **22**, 37 (1923).
[8] Eugene W. Pike, J. App. Phys. **12**, 206 (1941).
[9] H. A. Kramers, Phil. Mag. **46**, 836 (1923).
[10] A. Sommerfeld, Ann. d. Physik **11**, 257 (1931).
[11] P. Kirkpatrick and L. Wiedmann, Phys. Rev. **67**, 321 (1945).

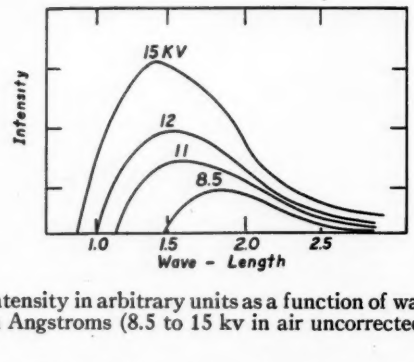

FIG. 1. Intensity in arbitrary units as a function of wave-length in Angstroms (8.5 to 15 kv in air uncorrected).

20 kv to 70 kv and at wave-lengths extending out to 1A as an upper limit. The lowest voltages, 7–12 kv, and longest wave-lengths were used by Kulenkampff but the upper wave-length limit was only 2.8A. The present paper is based upon data taken with a vacuum x-ray spectrometer at voltages from 1.1 kv to 2 kv and at wave-lengths extending out as far as 14A. The reason for the present study was to see whether the intensity in the continuous x-ray spectrum depends upon atomic number, voltage, and wave-length, in the same fashion as outlined earlier in this introduction when the wave-length is extended by a factor of five and the voltage is reduced by a factor of five. The vacuum x-ray spectrometer described in this paper was designed for x-ray spectroscopy of the solid state, and it is important to know the nature of the continuous radiation at the long wave-lengths used in such a study. This is especially true for absorption measurements where one wishes to choose the target which will give the strongest radiation in the region being studied. The experiments and theories already outlined, if extrapolated to long wave-lengths, predict the use of targets with large atomic number for obtaining maximum intensity. One cannot be sure of this extrapolation, especially when one considers the observation of Munier, Bearden, and Shaw[12] that, at the isolated wave-length of 10A, the radiation from an Al target was 30 percent stronger than the radiation from a W target. Further doubt is cast on the extrapolation because some of Kulenkampff's curves for different atomic numbers actually cross over one another in the region 2.5A to 2.8A, and the question arises as to whether this behavior is real or is entirely caused by characteristic absorption in the target.

EXPERIMENTAL

A vacuum x-ray spectrometer[13] was constructed for the purpose of making either single or double crystal measurements in the region out to 15A. The double crystal arrangement is of the Ross[14] type with the x-ray tube target and the axis of crystal B stationary. Crystal A, on a table halfway between, is moveable on ways perpendicular to a line joining the target to the axis of crystal B. A Geiger counter rotates around the axis of crystal B. This arrangement is laid out on a steel base plate $23\frac{1}{2}$ inches in diameter and $\frac{7}{8}$ inch thick. A large Pyrex bell jar with inner diameter 18″ fits over the spectrometer assembly and rests on the base plate compressing a lightly greased Koroseal gasket.

For the experiments herein described, crystal A was replaced by a slit system on the line joining the target and the axis of crystal B. Thus the vacuum spectrometer becomes a single crystal spectrometer of the simple Bragg type working under an evacuated bell jar. Two slits of 0.4-mm width were used with a distance between slits of 8 cm. The first slit was 6 cm from the target and the second slit was 6 cm from the axis of crystal B. The mica crystal was mounted so that the reflecting planes were the cleavage planes with a grating space of 9.9A. The slit for the Geiger counter was 6 cm from the crystal and was 1 mm wide. The crystal and Geiger counter can be turned independently from outside the spectrometer or they can be locked together in such a manner that the counter sweeps through twice the angle of the crystal.

The Geiger counter presents peculiar difficulties in a vacuum spectrometer because the window must be very thin and yet must be capable of withstanding an excess pressure from outside when there is air in the spectrometer and an excess pressure from inside when the spectrometer is evacuated. The metal counter described below has been found to be satisfactory. The window of 0.008-mm Al foil was sandwiched between two brass pieces which had been drilled with a series of $\frac{1}{32}$-inch holes forming a grid 2 mm$\times$10 mm. The window was sealed with Picein wax and squeezed tightly in its sandwich by six screws. A window so supported has withstood over one hundred evacuations of the spectrometer without rupture. The Geiger tube was evacuated and torched mildly. The counter was designed to permit flashing of the central wire although this procedure seemed to make but little difference in the final performance. The counter was filled with 9 cm (Hg pressure) of argon and 1 cm of absolute alcohol vapor, and then sealed off. The threshold was 765 volts and a reasonably good plateau extended to 900 volts. The counter was operated at 840 volts using a commercial Cyclotron Specialties Company preamplifier, scaler, and mechanical counter. Automatic recording could be used when the intensity was sufficiently great by feeding the scaler output through a frequency meter to a pen and ink recorder. During automatic registration the crystal and the Geiger counter were locked together in

[12] Munier, Bearden, and Shaw, Phys. Rev. **58**, 537 (1940).
[13] S. T. Stephenson and F. D. Mason, Phys. Rev. **72**, 744 (1947).
[14] P. A. Ross, Rev. Sci. Inst. **3**, 253 (1932).

angular ratio of 1 to 2 and were driven slowly by a synchronous motor through a worm gear. Actually, because of low intensities, all the data collected in this study in the range 1.1 kv to 2.0 kv were taken by counting at least one thousand counts for each point and running each curve several times.

The water-cooled post which supports the x-ray tube target fits into the steel base plate through a ground cone and can be removed readily. Target blocks of Cu and Al were machined and threaded to match threads cut on the top of the target post. The target of W was prepared by sinking a W button into a copper block which was threaded to fit the target post. All target blocks were of identical geometry so that there would not be any variations in the electric field between different targets and the filament to cause variation in the focal spot and spurious intensity changes. As an added precaution the target faces were viewed edge on so that the entire 3-mm×8-mm focal spot, which lay in a vertical plane, would always see the crystal through the slits. The filament was of W partly enclosed in a hemi-cylindrical shield of Ni suspended from a ground glass seal at the top of the x-ray tube. The x-ray tube envelope was a bell jar within the main bell jar and consisted of a four-inch diameter Pyrex cylinder resting around the target post on the base plate. A hole 6 mm in diameter in the Pyrex cylinder opposite the focal spot permitted passage of the x-rays into the rest of the spectrometer. This hole could be covered with a foil for vacuum testing but, for the runs described herein, the hole was left uncovered. The x-rays emerged at right angles to the direction of the electrons striking the target.

The main bell jar and the x-ray tube were pumped by two separate pumping systems. An oil diffusion pump of 250 liters per second capacity was fastened directly beneath the bell jar and was backed by a Hypervac fore pump. The x-ray tube was pumped through a cold trap by another oil diffusion pump of similar capacity backed by a Duoseal pump #1405.

In the course of normal operation the x-ray target became fouled with a blackish deposit which appeared in a matter of minutes after the high voltage was turned on. Most of the runs made to determine the general shape of the continuous spectrum and its dependence upon the voltage across the tube were taken with well-coated targets. A target was considered to be well-coated after further running showed no change in the intensity of the x-rays produced. However, it was obviously impossible to obtain the dependence of the continuous spectrum upon atomic number with coated targets. Many schemes were tried in order to eliminate the coating for a period long enough to obtain readings on Al, Cu, and W targets at a few wave-lengths in this region. At first the oil in the diffusion pumps was suspected as the source of the deposit, but the introduction of a cooling trap in dry ice and acetone did not reduce the coating. A separate mercury pumping system for the x-ray tube failed to eliminate the deposit. The scheme described below reduced the deposit to such an extent that it was barely perceptible at the end of the first hour of running, which was sufficient time to make readings at several wave-lengths. Hillier[15] has suggested that deposits of this kind come: (*a*) from organic material diffusing out to the surface of the target being bombarded by the electrons; and (*b*) from vapors of the organic material present in the vacuum chamber, i.e., greases, pump oils, greasy surfaces of metal parts, etc. Accordingly, the target blocks were pre-heated for an hour in a quartz furnace at about 600°C and at a pressure of less than 0.1 micron before introduction into the spectrometer. This treatment removed organic impurities from the target. The target post was turned through 180°, thus placing the back side of the target opposite the filament, and the tube was run at regular voltage for about 20 minutes. A small deposit immediately formed on the back of the target but did not grow in magnitude. This treatment temporarily cleaned up the organic vapors from the vacuum chamber. The x-ray target was then turned back into proper position and remained free of coating for about an hour.

Power was supplied by an army radar power supply, Model RA 38, capable of furnishing up to 500 milliamperes current at voltages ranging from 300 volts to 15,000 volts. The output of the four rectifying tubes was smoothed by condensers and by an inductance so that the ripple was about one-half percent. All electrical power was supplied through a commercial voltage regulator capable of holding fluctuations to about one percent. Measurement of the potential applied to the x-ray tube was made to one percent using a meter in series with a high resistance. Currents from 5 to 80 milliamperes were used depending upon intensity requirements.

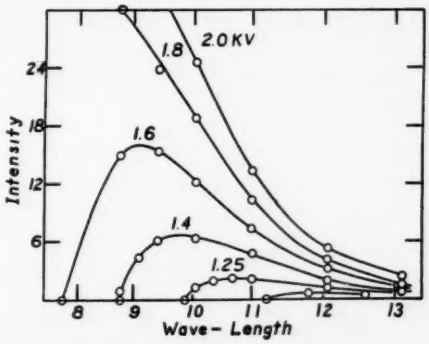

FIG. 2. Intensity in arbitrary units as a function of wave-length in Angstroms (1.11 to 2 kv in vacuum uncorrected).

[15] J. Hillier, J. App. Phys. 19, 226 (1948).

TABLE I. Intensities observed for clean targets at 1.6 kv and 40 ma.

Element	Atomic number	Intensity in counts/sec. at 9.1A	12A
Al	13	7.5	1.5
Cu	29	14.0	
W	74	30.0	8.0

RESULTS

The spectrometer assembly was tested by replacing the x-ray tube with a commercial, tungsten target tube and by running some curves in air at voltages ranging from 8.5 kv to 15 kv. These curves are reproduced without correction in Fig. 1 and are similar to curves shown by Kulenkampff for this region. The point of maximum intensity is close to $1.5\lambda_0$ and the areas under the curves are proportional to V^2. These curves constitute a test of the proper functioning of the spectrometer parts but contribute no new information.

Following this test the vacuum spectrometer was used for many runs on the continuous spectra from well-coated targets at voltages from 1.11 kv to 2.0 kv. The K edge of the Al window in the Geiger counter appears at 7.94A and at voltages above 1.55 kv and renders a determination of the shape of curves above 1.6 kv practically impossible. Fortunately the M series lines for tungsten are not excited at voltages below 1.9 kv and the L series lines for copper are at too long a wave-length to disturb the measurements. A typical set of curves is shown in Fig. 2. These curves are uncorrected except for counter and x-ray background and cover the range 8A to 13A. Occasionally points were taken to 14A. All experimental points are not shown but those presented are typical. The tube current was kept constant in all cases. A similar set of curves partially corrected as described below is shown in Fig. 3. It was not considered that correction factors were known accurately enough to correct beyond 13A. Corrections were applied as follows: (1) The amount of absorption in the Al window of the counter and in the dead gas space between the window and the counting region was calculated using absorption coefficients taken from Appendix IX of Compton and Allison.[16] (2) The efficiency of the counter was calculated from the percent of radiation absorbed by the known amounts of argon and alcohol vapor in the counter. Since all measurements were made with wave-lengths too long to excite the characteristic argon radiations, this calculation of the efficiency should be accurate. (3) A multiplying factor involving the frequency was used since a quantum causes a count independent of the energy of that quantum. An order correction was not necessary since the runs were cut off before any second-order radiation entered the counter. The curves were not corrected for any variations in the reflection coefficient of mica because no data were available on the reflection coefficient of mica in this region. The curves were not corrected for absorption in the target itself.

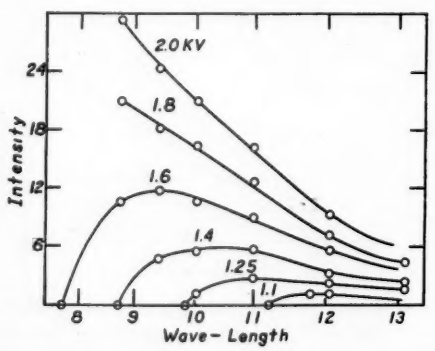

FIG. 3. Same as Fig. 2 but partially corrected.

In order to obtain accurate data on uncoated targets of W, Cu, and Al, the target blocks were vacuum fired as described above and the spectrometer was set at either 9.1A or 12A and readings taken at 1.6 kv and 40 ma (except that 12A for Cu was not done). The readings were made as soon as possible after turning up the high voltage and were continued for several minutes to note any trend caused by a coating. The intensity for the target of W gradually decreased while Al and Cu gradually increased. These curves were extrapolated to zero time to obtain a value characteristic of the pure metal. This extrapolation was quite accurate, since the coating caused a very slow change with time. The extrapolated values are presented in Table I. The coating did not become even faintly visible to the eye until after an hour had elapsed. Enough points were obtained with clean targets at wave-lengths other than 9.1A and 12A to indicate that the general shape of the curves for the pure metals was the same as is shown in Figs. 2 and 3 for a coated target.

DISCUSSION

A comparison of the curves of Fig. 1 with those of Fig. 2 reveals a very definite shift in the shapes of the curves if due cognizance is taken of the position of the point of zero wave-length. Whereas the high voltage curves of Fig. 1 and those of other investigators[1–7] reach a maximum at approximately $1.5\ \lambda_0$, the low voltage curves in the region 1.1 kv to 2 kv reach a maximum at approximately $1.05\ \lambda_0$ to $1.2\ \lambda_0$ (see Table II) and are evidently approaching the shape often assumed to be representative of a thin target in which the intensity rises immediately to a maximum at λ_0 and falls off thereafter as

[16] A. H. Compton and S. K. Allison, *X-Rays in Theory and Experiment* (D. Van Nostrand Company, New York, 1935).

TABLE II. The ratio of the wave-length of maximum intensity to the cut-off wave-length, λ_{max}/λ_0.

Kilovolts	Uncorrected Fig. 2	Partially corrected Fig. 3
1.11	1.05	1.05
1.25	1.1	1.1
1.4	1.1	1.2
1.6	1.15	1.2

$1/\lambda^2$. This general behavior might be expected if one considers the continuous spectrum from a thick target to be made up of a summation of the contributions of a number of thin targets. The contribution from each succeeding layer will decrease because of absorption of the electrons as they go in, and of the x-rays as they come out. At the low voltages used here the electrons do not penetrate far, and at these long wave-lengths the x-rays are strongly absorbed; thus the thick target spectrum is the sum of relatively few thin target contributions, each largely attenuated by electron and x-ray absorption. Consequently, at the lower voltages the thick target spectrum should approach the thin target spectrum[17] and this is observed.

The formula (2) given by Kulenkampff predicts that λ_{max} should shift toward λ_0 as λ_0 is increased; but in order to achieve the shift observed here, the constant B would have to be made so large that Eq. (1) would predict large quantities of radiation right at λ_0 which is contrary to experimental fact. Consequently, Kulenkampff's formulas do not adequately express the continuous spectrum in the region 8A to 14A as measured and partially corrected in the present work. One can determine empirically that the curves of Fig. 3 fit an expression of the type

$$I_\lambda = \frac{CZ}{\lambda^5}(1/\lambda_0 - 1/\lambda)$$

from 8A to 12A but not out to 14A.

The curves of Fig. 1 and of Figs. 2 and 3 cover approximately similar voltage ranges of almost two to one. Inspection of the curves reveals the fact that the dependence of the total integrated intensity upon voltage is decidedly different in the two wave-length regions. The region 8.5 kv to 15 kv yields curves whose integrated intensities are proportional to V^2. However, in the region covered by 1.1 kv to 2.0 kv the integrated intensity is proportional to a higher power of V. Part, at least, of the excessive drop in total intensity with decreasing voltage can be attributed to increasing absorption in the target itself with increasing wave-length. Fundamentally, one is here concerned with the question of what one means by total integrated intensity. In previous investigations the integration has been carried out

[17] Jesse W. M. DuMond, Phys. Rev. 72, 276 (1947).

TABLE III. The ratios of intensities at several wave-lengths and of the second and third powers of the voltage using 2 kv as standard.

Kilovolts	Intensity ratios 11A	12A	13.1A	Voltage ratios V^2	V^3	$(V-0.5)^2$
2.0	1.0	1.0	1.0	1.0	1.0	1.0
1.8	1.3	1.3	1.5	1.23	1.4	1.3
1.6	1.8	1.6	1.7	1.57	1.9	1.9
1.4	2.8	2.8	3.0	2.04	2.9	2.8
1.25	6.0	4.0	4.0	2.56	4.1	4.0
1.11		7.0		3.25	5.9	6.1

to two or three times the cut-off wave-length. It is not possible to follow this procedure for the wave-lengths used in the present experiment. Actually one should obtain the equation of the curves and integrate from cut-off to very long wave-lengths in order to obtain a true integrated intensity, but it is not possible to obtain a simple equation that fits all the present data. In any event, if one studies the intensities obtained at one particular crystal setting well beyond the maximum (at 11 or 12 or 13A, see Table III) as a function of voltage, one should obtain a picture independent of all factors involving target absorption or crystal reflectivity since these factors would be the same at the different voltages for the one wave-length. Reference to Table III for three isochromats shows that the intensity at a given crystal setting varies as the square of the voltage from 2 kv to 1.6 kv and about as the cube to 1.25 kv. It is probable, therefore, that the total integrated intensity at the voltages used in this work is dependent upon a higher power of the voltage than the square. Whether this is a true effect or an apparent effect caused by the increasing importance of electrons reflected from the target face before losing all of their energy cannot be decided. Presumably x-rays produced by these electrons subsequent to reflection, as they impinge on other parts of the apparatus, would not enter the slit system nor contribute appreciably to measured x-ray intensities. If one assumes that there is an effective loss of 0.5 kv energy by the electrons, one finds fairly good agreement between the intensity at one wave-length and $(V-0.5)^2$. (See Table III.) Such an assumption would allow one to retain the dependence upon the square of the voltage.

The total intensity of radiation from a target has been regarded as proportional to the atomic number for high voltages and short wave-lengths. The data illustrated by Table I indicate that at 9.1A and at 12A the measured intensity is proportional to the atomic number within experimental error. The largest source of error comes from difficulty in positioning the targets in exactly similar fashion. If one assumes that all ordinates are proportional to atomic number, the total intensity of

radiation will likewise be proportional to the atomic number.

CONCLUSION

The present work indicates that the total intensity in the continuous radiation of x-rays at 1.1 kv to 2.0 kv, as measured and partially corrected, is proportional to the atomic number and to some power of the voltage higher than the second. The shape of the curve resembles that to be expected from a thin target.

PHYSICAL REVIEW VOLUME 75, NUMBER 11 JUNE 1, 1949

The Mass of Cosmic-Ray Mesotrons*

J. GORDON RETALLACK** AND ROBERT B. BRODE
Department of Physics, University of California, Berkeley, California

(Received February 14, 1949)

By cloud-chamber observations of the curvature of mesotrons in a magnetic field of 4750 gauss and the subsequent range of these same particles in a second cloud chamber containing fifteen lead plates each 0.67 cm in thickness, the mass of 43 cosmic-ray particles has been determined. 37 of these particles appear to give a set of observations that are consistent with a unique mass of 215±4 times the mass of an electron. Of the 6 remaining observations 4 indicate a mass much too large (474, 538, 588, and 717) to be reasonably considered as statistical fluctuations in the observations of normal mesotrons. The remaining 2 observations (114 and 120) also appear to be inconsistent with the normal mass of the mesotron and the observed probable errors in individual measurements in this experiment.

A NUMBER of experimental studies of the mass of cosmic-ray mesotrons have been made. Some of the earlier data have been discussed by Wheeler and Ladenburg,[1] and by Hughes.[2] More recent studies have been reported by Fretter,[3] Lattes, Muirhead, Occhialini, and Powell,[4] LePrince-Ringuet and M. Lheritier,[5] and by Alichanian, Alichanow, and Weissenberg.[6] Since the work on which this report is based was completed, the detection and identification of mesotrons produced artificially by the 184-inch cyclotron has been accomplished by Lattes and Gardner.[7] The purpose of the work reported here was to add to the data on the mass of the mesotron and to try to improve the accuracy of the measurement.

THE EXPERIMENTAL APPARATUS

The experimental arrangement is illustrated in Fig. 1. The upper cloud chamber, CH_1, was placed in a magnetic field of 4750 gauss. The chamber was 12 inches in diameter and 3 inches deep. B represents a baffle system which consisted of two perforated brass sheets and a drilled plate 0.25 inch thick, which were separated by 0.25-inch spacers. Velvet was fastened to the front of the first perforated sheet to provide a black background for photography. The baffle was intended to smooth out irregularities in the expansion caused by uneven motion of the rubber diaphragm, R. An asymmetrical arrangement of two expansion ports, E, resulted in a detectable distortion of the tracks. This distortion was reduced but not eliminated by installing a symmetrical arrangement of three expansion ports (see the discussion of errors). The upper cloud chamber was filled with air and a 3:1 mixture of ethyl alcohol and water to a total pressure of 1.13 atmospheres in the expanded position. The chamber was not saturated with liquid but the amount of vapor was adjusted to keep the expansion ratio in the range of 14 percent to 16 percent. A clearing field of 100 volts between the metal back plate and an aquadag ring on the front glass was reduced to zero as soon as possible after the passage of the tripping particle through the Geiger counters, C. Illumination was provided by two GE FT 422 flash lamps each of which was excited by the discharge of a condenser of 160-μf capacity charged to 2000 volts. The illuminated region was 1 inch deep and the full height of the cloud chamber. The tracks were photographed on Ansco Ultra-Speed 35-mm film in a single frame camera using a Summar lens of focal length 5 cm at an aperture of f:9.

To reduce the effects of temperature variations a copper heat shield was built around the upper

* Assisted by the Joint Program of the ONR and the AEC.
** Now at Indiana University, Bloomington, Indiana.
[1] J. A. Wheeler and R. Ladenburg, Phys. Rev. 60, 754 (1941).
[2] Donald J. Hughes, Phys. Rev. 69, 371 (1946).
[3] William B. Fretter, Phys. Rev. 70, 625 (1946).
[4] Lattes, Muirhead, Occhialini, and Powell, Nature 159, 694 (1947).
[5] L. LePrince-Ringuet and M. Lheritier, J. de Phys. et Rad. 7, 65 (1946).
[6] Alichanian, Alichanow, and Weissenberg, J. Phys. U.S.S.R. 11, 97 (1947).
[7] C. M. G. Lattes and E. Gardner, Science 107, 270 (1948).

cloud chamber and the conical hole in the core of the magnet through which the chamber was photographed. Copper tubing soldered to the heat shield carried water which was temperature controlled to $\pm 0.25°C$. A sheet of transite between the heat shield and the back pole face of the magnet and asbestos lining in the conical hole in the front core insulated the heat shield and the cloud chamber from the magnet. Windows, *W*, in the heat shield permitted illumination of the chamber and helped to form the light beam.

The original intention had been to use helium in the upper cloud chamber because of the small scattering to be expected. To obtain an estimate of the error in the curvature measurements because of the turbulence in the gas in the chamber, 48 no-field tracks in helium were studied. The coordinates of the track were measured in a traveling microscope and the radius of curvature of the best fitting circle was calculated by the method of least squares. The average curvature of these 48 tracks was 0.053 ± 0.055 meter^{-1}. Since most of these particles would have much higher energy than the particles which were of interest in this experiment, it is seen that most of this spurious curvature is due to turbulence and very little of it is due to scattering. The residual, or no current, field was found to be less than one gauss, which is too small to explain any of the observed effect. For a particle of energy such that the radius of curvature of its trajectory in a magnetic field of 4750 gauss would be 1.5 meters—such a mesotron would stop near the middle of the lower cloud chamber—the probable error in radius of curvature resulting from turbulence would be 8 percent, while the probable error resulting from scattering would be 0.7 percent.

With air in the upper cloud chamber, 60 no-field tracks were measured in the same way. The average curvature was 0.03 ± 0.04 meter^{-1}, giving a 6.25 percent probable error caused by turbulence for a track of 1.5 meters radius in a field of 4750 gauss. The scattering probable error in air for the same particle would be 2 percent. It is seen that by using air in the chamber instead of helium the decrease in the error caused by turbulence more than offsets the increase in the scattering error. The

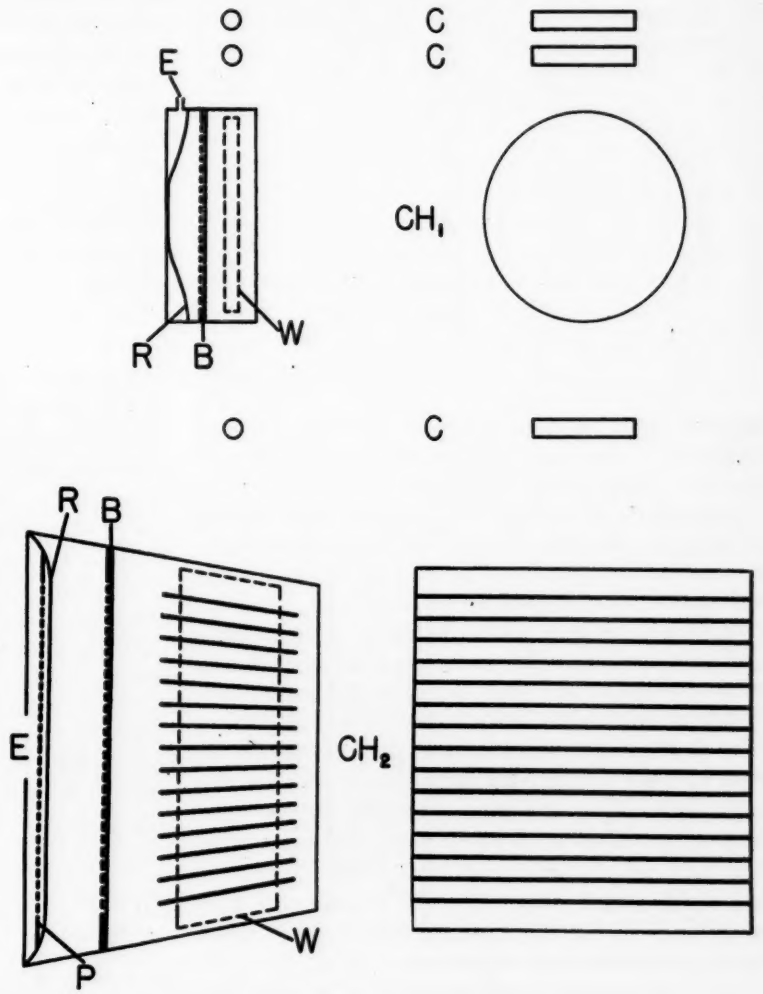

FIG. 1. Schematic arrangement of cloud chambers. CH_1 and CH_2, upper and lower cloud chambers. *E* exhaust port. *R* rubber diaphragm. *B* baffle plate. *W* window for illumination. *C* Geiger counter for control. The magnet in which cloud chamber CH_1 is placed is not shown, nor the heat shields for constant temperature control.

TABLE I. Mesotron mass measurements.

Track no.	Sign	C Curvature in unit field $\times 10^6$ (cm^{-1} $gauss^{-1}$)	R Range in lead (cm)	m Mass in electron mass units	Δm Probable error in mass
4505	−	1.189	9.72	231	37
5051	+	1.804	6.13	189	22
5441	+	1.621	7.11	160	22
5706	−	2.208	2.93	202	24
5881	−	1.983	4.22	185	20
5986	−	1.563	7.83	161	21
5992	−	1.088	10.19	257	49
6062	+	0.988	4.98	538	84
6189	−	2.358	2.83	198	23
6459	+	1.334	7.13	252	37
6496	−	1.516	7.05	198	29
6576	−	2.015	4.33	180	27
6602	−	0.831	9.14	474	88
6659	+	1.128	10.36	235	44
6923	+	1.176	10.87	189	39
7049	+	1.816	4.41	211	20
7273	+	1.655	5.11	223	32
7275	−	0.816	7.06	588	110
7350	−	1.019	9.23	320	59
7371	−	1.457	6.28	225	31
7374	−	1.189	10.47	194	36
7433	+	1.316	7.38	255	41
7457	−	3.023	3.10	114	16
7614	+	1.631	4.26	269	34
7645	−	1.706	5.02	210	26
7647	+	1.402	7.27	216	36
7821	+	2.091	3.68	189	20
7847	−	1.252	6.97	282	45
7884	−	1.229	9.48	212	36
7900	−	1.651	5.85	194	28
7910	−	1.381	8.60	185	25
7919	−	2.060	2.96	225	27
7938	+	1.322	8.42	207	35
8093	+	1.402	8.44	182	27
8103	−	1.012	2.92	717	121
8145	−	1.485	5.84	240	34
8217	−	1.812	3.74	235	28
8275	−	1.258	4.98	360	50
8674	−	2.369	2.83	186	26
8818	+	1.968	2.99	240	28
9183	−	1.737	7.74	120	16

direction of the average spurious curvature is such as to make a positive particle appear heavier and a negative particle appear lighter.

The lower cloud chamber, CH_2, in Fig. 1, in which the range in lead for the particles was measured, was a truncated pyramid 20 inches square at the middle of the illuminated region and 17 inches deep. It contained 15 lead plates 0.270 inch thick and about 1 inch apart. The walls were 0.5 inch dural, the front window 0.5 inch heat-treated glass, and the side windows for illumination, 0.5 inch lucite.

The walls of the chamber and the lead plates all pointed at the camera 50 inches away so that the camera saw all of the space between plates. The chamber was filled with air at first, and later with equal parts of air and argon, and a 3:1 mixture of ethyl alcohol and water to total pressure of 1.35 atmospheres in the expanded position. The vapor content was kept just under saturation. The vertical clearing field between plates was 20 volts and was reduced to zero as soon as possible after the passage of the tripping particle through the Geiger counters. A region 6 inches deep and the full height of the chamber was illuminated by four GE FT 422 flash lamps, each excited by the discharge of a condenser of 256-μf capacity charged to 2000 volts. This chamber contained a baffle system similar to that in the upper cloud chamber and a drilled plate, P, to prevent the rubber diaphragm stopping the exhaust port and interfering with the flow of air from the back of the chamber on expansion.

The lower cloud chamber was photographed by a stereoscopic camera using two Apos lenses of focal length 105 mm at an aperture of f:8. Eastman Super XX air reconnaissance film, split to 1.75 inches from 7-inch rolls, was used. This camera also photographed a meter in series with the magnet to give a record of the magnetic field associated with each picture.

The cloud chambers were expanded upon passage of a charged particle through the triple coincidence Geiger counters, C. These counters defined a solid angle which filled the illuminated region of the upper cloud chamber and which was considerably more shallow than the illuminated region of the lower cloud chamber. At first 12 inches, and later 16 inches of lead were placed above the apparatus to select penetrating particle and to increase the number of particles stopping in the lower chamber.[8] This additional lead is enough to slow down the mesostrons at the peak of the energy spectrum so that they will stop near the middle of the lower chamber if they have mass 200 times the mass of an electron.

OBSERVATIONS

The pictures from the upper cloud chamber projected full size, and the corresponding pictures from the lower chamber placed in a stereoscopic viewer, were examined together. Tracks of mesotrons of mass 200 m_e that would be expected to stop in the lower chamber would have radii of curvature of 0.75 to 2.0 meter in the upper chamber. For each track that had a radius in or near this region, the pictures from the lower chamber were examined carefully for evidence that a particle had stopped. Also, whenever the pictures from the lower chamber indicated that a particle may have stopped in one of the lead plates, the picture from the upper chamber was examined carefully and measured. The distance of the track in the upper chamber from the middle of the chamber was measured in the projection for

[8] L. S. Germain, Phys. Rev. **75**, 1458 (A) (1949), reports measurements that indicate that the differential range spectrum of mesotrons increases only to a lead thickness of 9 inches and then decreases with further lead absorber; this indicates that the lead used in this experiment was more than desirable and increases the number of stopping particles by less than 10 percent.

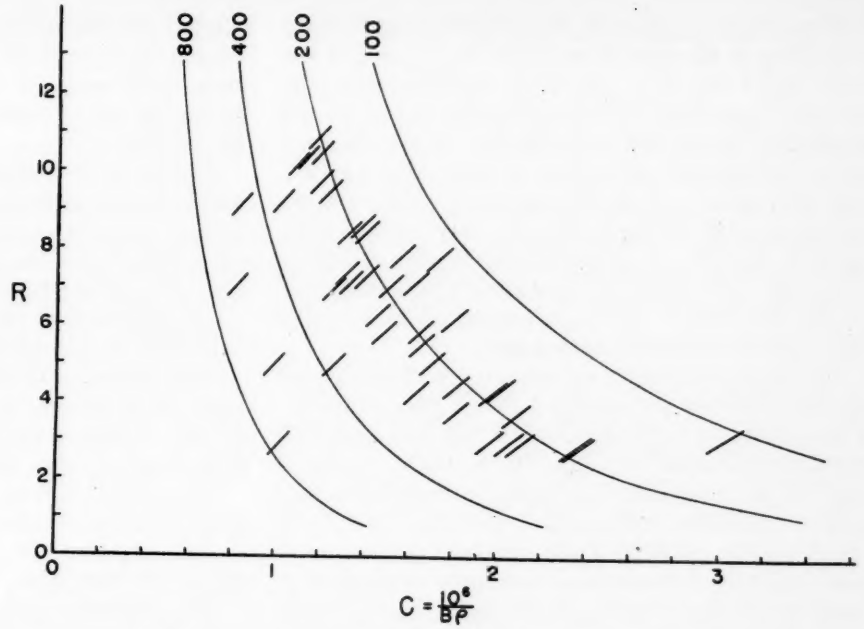

FIG. 2. Mesotron mass measurement. Each observation is plotted as a function of range, R, in centimeters of lead *vs.* curvature, C, in a unit magnetic field. The length of the lines representing individual observations is a measure of the probable error assigned to the measurement.

each of these particles. About 150 sets of pictures were examined carefully and measured. In about $\frac{2}{3}$ of these the particle had scattered out of the illuminated region before it had stopped, or it was not sufficiently clear that the particle had really stopped. The increase in ionization in the last two or three spaces traversed by the particle before it stops was helpful in distinguishing between particles that stop and those that are scattered out of the illumination. In five cases the presence of a lightly ionized track, indicating a decay electron, was strong evidence that a mesotron had stopped.[9] In one case, another track coming in from the side and of about the same age as the counter-controlled track could not be separated from the counter-controlled track and the data could not be used. This same case was the only one in which the data would be discarded because the measurement in the upper chamber was not acceptable, both ends of the track were separated into positive and negative columns by the clearing field, leaving a section in the middle which was too short to be accurately measured. A track ending in the first or second plate cannot be definitely identified as due to a penetrating particle. It is possible for an electron of 100 Mev to emerge from the bottom of the first plate unaccompanied by secondaries and then to stop in the second plate. For this reason, particles which stopped in one of the first two plates were not used unless, as happened in two cases, evidence for a decay electron indicated that the stopping particle actually was a mesotron.

For each particle that was of interest, the coordinates of the track in the picture from the upper cloud chamber were measured with a traveling microscope. These coordinates were plotted with considerable magnification in the direction perpendicular to the length of the track, and compared with the plots of circles to the same scale on celluloid to see how well the points fitted a circle. The radius of curvature of the best fitting circle was calculated for each track by the method of least squares. A correction to the curvature and the probable error in the measurement was assigned on the basis of the study of the 60 no-field tracks. The magnification of the camera system was measured by photographing a piece of millimeter cross section paper through a piece of 0.5-inch plate glass with the same geometry as was used in the experiment and measuring the film in the traveling microscope.

For each particle that was of interest one of the pair of pictures from the lower cloud chamber was examined in the traveling microscope. The projected angle on the film between the track and the normal to the plate was measured. The range in lead was taken to be the lead equivalent of the material between the chambers divided by the cosine of the angle in the top space of the lower cloud chamber, plus the sum over all the plates through which the particle passed of the thickness of the plate divided by the cosine of the angle in the space above the plate, plus half the thickness of the plate in which the particle stopped, divided by the cosine of the angle in the last space. The lead equivalent of the material between the chambers, the chamber walls, and the Geiger counter, as calculated from the equation for energy loss given by Rossi and Greissen[10] was 0.44 inch. This estimate of the range

[9] J. G. Retallack, Phys. Rev. **73**, 921 (1948).

[10] B. Rossi and K. Greissen, Rev. Mod. Phys. **13**, 240 (1941).

does not take account of the backward or forward scattering of the mesotron in the lead plates of the lower cloud chamber. All of the particles enter the chamber very nearly in the vertical plane. If the scattering backwards or forwards, as can be seen with the stereoscopic views, is large, the particle will soon go out of the illumination. A very large scattering after entering the last plate, so that the particle travels a considerable distance before stopping, will lead to an appreciable underestimate of the true range and to a computed mass value that is heavier than its true value.

The magnetic field was measured with a flip coil of 130 turns cm² area and a ballistic galvanometer. The circuit was calibrated with a magnetic standard from the University of California Radiation Laboratory which was checked against a mutual inductance and a carefully calibrated ammeter. A careful check on the reading of the magnet current meter was maintained throughout the measurement. The field was uniform to 12-cm diameter, down 1 percent at 17-cm diameter, and down 2 percent at 20-cm diameter. The effective field was taken to be that uniform field that would have produced the same displacement at the center of the track and was calculated by graphical integration as a function of the track length and the distance of the track from the middle of the upper cloud chamber. In the vicinity of the operating point the magnetic induction varied linearly with current. The variation in the current was about 3 percent. The value of the induction associated with each picture was estimated from the photographic record of the magnet current.

The mass of each particle was then calculated with the aid of the curve relating range to momentum given by Wheeler and Ladenburg. These mass values are given in Table I, with the corresponding value of range (R), radius of curvature (ρ), and magnetic field (B). The curvature in unit field $\times 10^6$ (C) is calculated from the radius of curvature and the magnetic field.

ERRORS

The largest errors in this experiment are due to the turbulence in the upper cloud chamber, distortion of the track by the front glass and camera system, and errors in the measurement of the track. The probable error in the curvature due to these causes is taken to be 0.04 meter^{-1}, as derived from the measurements on the 60 no-field tracks. For the average field used in this experiment of 4750 gauss, this error in curvature corresponds to a probable error in C, the curvature in unit field $\times 10^6$ of $\Delta C_T = 0.084$ cm^{-1} gauss^{-1}.

The probable error due to scattering[11] was calculated on the assumption of a mass of 200 m_e. This error depends on the length of track, the magnetic field, and the velocity of the particles. For scattering in nitrogen the probable error in C is $\Delta C_s = 0.02C$.

The error in magnification due to the plane in which the particle passes through the illuminated region introduces an error proportional to the curvature. From the depth of the illumination this error ΔC_m is estimated to be $0.01C$.

The probable error in measurement of the magnetic field is estimated as $\Delta C_B = 0.01C$.

The total error in the curvature, C, is compounded from these errors as $\Delta C = ((0.084)^2 + (0.025)^2 C^2)^{\frac{1}{2}}$. In the observations reported in Table I, C varies from 1 to 3 so that ΔC varies from 0.09 to 0.10.

The probable error in range is estimated as one-fourth the plate thickness divided by the cosine of the angle of the track with the vertical as it enters the last plate, i.e., $\Delta R = 0.17$ cm/cosθ.

The probable error in the calculated mass arises from the errors in range, ΔR, and in curvature ΔC. In the plot of the observed data in Fig. 2. the curves of constant mass have been derived from the curves of Wheeler and Ladenburg.[1] The diagonal lines have their centers at the observed values of range and curvature. The length of the lines are such that the projections on the R and C coordinates are the extent of the probable errors $\pm\Delta R$ and $\pm\Delta C$.

DISCUSSION

The results of the observations on 43 particles are shown in Fig. 2. The value of the mass corresponding to the curve that best fits this data can be determined by the least squares adjustment.[12] It can be seen, however, that the probable errors assigned to these observations are nearly constant in the range curvature coordinate system, and the measure of linear distance orthogonal to the curves of constant mass is closely proportional to the log of the mass. Taking all of the 43 observations and weighting each inversely as the square of $(\Delta m/m)$, the value of m corresponding to the mean of log$m$ is found to be 217 in units of the electron's mass.

The ratio of the probable error based on external consistency to the probable error based on internal consistency[13] is 1.81. For 43 observations the probable deviation from unity of this ratio is 0.11. The chance for a deviation from unity 7.5 times the probable deviation is extremely small indicating that these observations are not consistent with the assumption of a unique mass.

If the four highest and the two lowest mass values are omitted, the remaining 37 values form a consistent set of observations. The ratio of the probable error based on external consistency to the probable

[11] H. A. Bethe, Phys. Rev. **70**, 821 (1946).

[12] Robert B. Brode, Phys. Rev. **75**, 904 (1949).

[13] R. T. Birge, Phys. Rev. **50**, 207 (1932).

error based on internal consistency differs from unity by 0.10. For 37 particles the calculated deviation from unity of this ratio is 0.12. The mean value of the mass of the mesotron in electron mass units deduced from this consistent set of 37 observations is 215 ± 4.

The existence of six observations that are not consistent with the other observations may indicate that the probable errors assigned to the individual observations are too small, or that the mass of the mesotron as observed at sea level is not unique. The existence of a small percentage of the π-mesotrons[14] in the normal, or μ mesotron spectrum would not be resolved in a series of observations with probable errors as large as indicated here.

The existence of mesotrons with lighter and heavier masses has been suggested by the observations of Hughes,[2] LePrince-Ringuet,[5] and Alichanian, Alichanow, and Weissenberg.[6] Adequate evidence for the existence of these particle will require the accumulation of more data. The chance of mistaking a normal mesotron for such a particle can be appreciably reduced by using thinner absorbing plates to reduce the error in range and by careful design and control of the cloud chamber to reduce turbulence.

[14] Lattes, Occhialini, and Powell, Nature **160**, 453, 486 (1947).

ACKNOWLEDGMENTS

One of us (J.G.R.) takes this opportunity to acknowledge the assistance of a Westinghouse Fellowship in Physics. We are indebted to Professor R. T. Birge for his interest in the statistical interpretation of the data, and to Mr. R. R. Brown, who built most of the control circuits.

PHYSICAL REVIEW VOLUME 75, NUMBER 11 JUNE 1, 1949

The Properties of Cosmic Radiation in the Lower Atmosphere*

MARTIN A. POMERANTZ
Bartol Research Foundation of the Franklin Institute, Swarthmore, Pennsylvania
(Received January 21, 1949)

Experiments performed previously with apparatus carried to very high altitudes by free balloons have been conducted in the lower portion of the atmosphere. Two different instruments were operated in a B-29 airplane, and at Mt. Evans, Colorado. Absorption curves in lead, up to a thickness of 18 cm, were obtained at 14,260 feet, 25,000 feet, and 30,000 feet. Intensity *vs.* altitude curves for the lower regions of the atmosphere may now be combined with those for very high altitudes without an arbitrary normalization. A direct comparison has been made between the present measurements and those of others regarding the relative change of intensity between sea level and Mt. Evans, and the absorption in lead at Mt. Evans. Factors for the conversion of all of the data to absolute intensities have been determined utilizing a γ-ray howitzer method for measuring the effective length of a G-M counter. Satisfactory agreement is noted between values of the absolute intensity previously measured by others at sea level and at Mt. Evans, and those reported herewith. The absolute intensity of cosmic-ray particles near the "top of the atmosphere" at geomagnetic latitude 52°N is given as 10.1 ± 0.20 particles/min./cm²/unit solid angle. Consideration is given to the considerable error which may be introduced in the comparison of measurements of the "total" intensity at very high altitudes obtained with different G-M counters.

I. INTRODUCTION

THE results of a series of investigations of the cosmic radiation in the upper regions of the atmosphere have been described recently.[1] Owing to a combination of the smaller intensity present at lower altitudes, and the relative briefness of the time interval during which free-balloon flights remain in regions of high atmospheric pressure (a consequence of the exponential variation of pressure as a function of altitude, and accentuated by the particular ballooning techniques employed here), data obtained at altitudes corresponding to pressures exceeding approximately 200 mm of Hg were not in general regarded as statistically significant.

The purpose of the present series of experiments was threefold:

(1) To obtain data at lower altitudes with the same apparatus utilized in the free-balloon ascents, thereby providing complete intensity *vs.* altitude curves, as well as cosmic-ray absorption curves for lead from sea level to the "top of the atmosphere;"

(2) To permit comparison of certain of the numerous measurements at various low altitudes (4350 meters—sea level) previously reported by others with those which would be yielded by the aforementioned apparatus. Comparison at more than one point furnishes a less arbitrary normalization than has usually been assumed.[2]

(3) To provide experimental evidence regarding the validity of comparison of data obtained with different geometrical arrangements, and specifically, to furnish at several altitudes a direct and precise standardization between two particular counter trains of different dimensions utilized in the balloon flight program.

* Assisted by the Joint Program of the ONR and AEC. Field trips were sponsored by the National Geographic Society.

[1] M. A. Pomerantz, Phys. Rev. **75**, 69 (1949).

[2] This matter has been discussed in reference 1.

TABLE I. Data pertaining to the influence of latitude variations upon the present measurements. It should be emphasized that the maximum percentages listed refer to the extreme termini and should not be construed as representing the expected fluctuations of the composite data listed in Table II.

Altitude—feet	Thickness of interposed absorber—cm of Pb	Maximum departure from intensity at average latitude (− South) (+ North)
25,000	0.0	±1%
	9.0	±1%
	18.0	±1.2%
30,000	0.0	−3%+5%
	9.0	−4%+8%
	18.0	−3%+5%

The above ends were realized by operating the two instruments concerned in a B-29 aircraft during a series of flights sponsored recently by the U. S. Air Force and the National Geographic Society. Opportunity for taking the same sets to Mt. Evans, Colorado, during the summer of 1948 was also afforded by the N.G.S. The first apparatus, designated as *A*, has already been described in reference 1. The second, *B*, also embodied a quadruple coincidence counter train with provision for interposing up to 18 cm of absorber. Each tray of *B* consisted of 3 G-M counters, identical with those of *A*, connected in parallel and overlapped to present an uninterrupted horizontal plane. Complete dimensions of both *A* and *B* are given later (Section III).

The instruments were shock-mounted in the rear pressurized cabin of the B-29. The solid absorber overhead amounted to 0.5 g/cm² of Al. Both day and night missions were flown at isobaric levels of 282 and 226 mm of Hg, corresponding to approximately 25,000 feet and 30,000 feet, respectively.

The average geomagnetic latitude weighted with respect to the time actually spent in the various regions was 43.6° N for flights at both 25,000 feet and 30,000 feet. Cyclical and mixed alternation of absorber thicknesses was provided for, so that any small influence of the latitude effect was smoothed out, as was shown by the agreement of different runs within their statistical uncertainties. Measurements obtained simultaneously by Swann, Morris, and Seymour[3] concerning the knee of the latitude effect provide pertinent information regarding the maximum departures of the intensity from that at the average latitude. The values listed in Table I are only approximate, and represent conservative upper limits.

At the summit of Mt. Evans (geomagnetic latitude 49° N, altitude 14,260 feet, average atmospheric pressure 453 mm of Hg) the equipment was installed in the building of the Inter-University High Altitude Laboratory, under a light wooden roof.

In Swarthmore (geomagnetic latitude 52° N, altitude 296 feet, average atmospheric pressure 756 mm of Hg) the data were obtained in a thin wooden shelter on the roof of the laboratory.

[3] Swann, Morris, and Seymour, Phys. Rev. **75**, 1317 (1949).

TABLE II. Summary of data obtained at several altitudes with two different instruments.

Altitude—feet	Atmospheric pressure—mm of Hg	Thickness of interposed absorber—g/cm² of Pb	Total number of quadruple coincidences	Total time—minutes	Counting rate—counts per minute
		Apparatus A			
		0.0	14346	15648	0.917±0.007
		11.8	3759	4865	0.773±0.012
		23.6	5792	7593	0.763±0.010
		35.4	4598	6403	0.720±0.010
296	756	47.2	4591	6426	0.714±0.010
		59.0	2896	4044	0.716±0.013
		70.8	3734	5416	0.689±0.011
		85.0	2074	3087	0.672±0.014
10,700	515	0.0	874	365	2.39±0.08
		70.8	711	514	1.38±0.05
		0.0	3560	1090	3.27±0.054
		11.8	6470	2763	2.34±0.029
		23.6	5893	2759	2.14±0.027
14,260	453	35.4	2521	1324	1.90±0.037
		47.2	4608	2499	1.84±0.027
		59.0	2463	1413	1.74±0.035
		70.8	3820	2222	1.72±0.028
		85.0	2690	1645	1.64±0.032
		12.9C	3757	1455	2.58±0.042
		0.0	1832	182	10.07±0.23
		11.8	1565	241	6.49±0.16
		23.6	1342	243	5.52±0.15
25,000	282	35.4	1501	308	4.87±0.12
		51.9	427	100	4.27±0.20
		70.8	1863	465	4.01±0.09
		85.0	1555	393	3.96±0.10
		0.0	1010	70	14.43±0.45
		11.8	1683	168	10.02±0.24
		23.6	297	40	7.43±0.43
30,000	226	35.4	1018	153	6.65±0.20
		70.8	1524	274	5.56±0.14
		85.0	677	131	5.16±0.20
		Apparatus B			
		0.0	10569	6969	1.51±0.015
		20.8	6022	4290	1.40±0.018
		41.0	6000	4465	1.34±0.017
		61.5	6214	4733	1.32±0.017
296	756	81.2	8646	6939	1.24±0.013
		109.4	5964	4994	1.19±0.015
		137.0	5529	4582	1.21±0.016
		157.0	7566	6592	1.15±0.013
		205.0	11801	10603	1.11±0.010
		0.0	7479	1392	5.37±0.062
		20.8	5336	1318	4.05±0.056
		41.0	5201	1410	3.09±0.051
		61.5	8089	2550	3.17±0.035
14,260	453	81.2	6252	2106	2.97±0.037
		109.4	4255	1532	2.78±0.043
		137.0	3479	1253	2.78±0.047
		157.0	3911	1468	2.66±0.042
		205.0	3368	1400	2.41±0.041
		32.1C	3961	1071	3.70±0.059
		26.9 C+32.0 Pb	3689	1106	3.34±0.055
		0.0	2612	142	18.39±0.36
		61.5	4100	512	8.01±0.12
25,000	282	109.4	2460	359	6.85±0.14
		157.0	2442	424	5.76±0.16
		205.0	2377	459	5.18±0.11
		0.0	1964	75	26.19±0.60
		61.5	1198	104	11.52±0.33
30,000	226	109.4	2238	230	9.73±0.20
		157.0	2408	293	8.42±0.17
		205.0	2411	335	7.20±0.14

II. RESULTS

Table II contains a complete summary of the various measurements. The uncertainties indicated are statistical standard deviations. In all instances, data obtained under similar conditions were consistent from day to day, or from flight to flight. Frequent checks indicated the constancy of the sensitivity of the equipment.

A. Variation of Intensity with Absorber Thickness

Figure 1 shows the lead absorption curves for cosmic-ray particles at the several altitudes, plotted on the basis of the data in Table II, and incorporating the results from both instruments. Points are also included for the determination of the relative stopping powers of carbon and lead (Section C below).

The data obtained with Apparatus B were reduced to the same scale as that of Apparatus A on the basis of the single factor 1.90 calculated in Section III, *B* on the basis of geometrical considerations. Following the practice adopted in reference 1, absorber thicknesses when expressed in g/cm² represent the average path determined from calculations of E. E. Witmer and the author.[4] The harmony between the points obtained with the two instruments as exemplified by the curves in Fig. 1 verify the correctness of the factor 1.90 referred to above.

The results of Hall[5] have also been reduced to a common scale and are plotted in Fig. 1. The normalization was made at 1.5 cm of Pb, and a slight departure at zero interposed absorber thickness is probably attributable to the differences in the thicknesses of counter walls. From the agreement with the present measurements it is evident that the integral and differential distributions-in-range labelled "Hall" in reference 1 (Figs. 3 and 4) may be compared directly with the corresponding curves based upon the results of the free-balloon

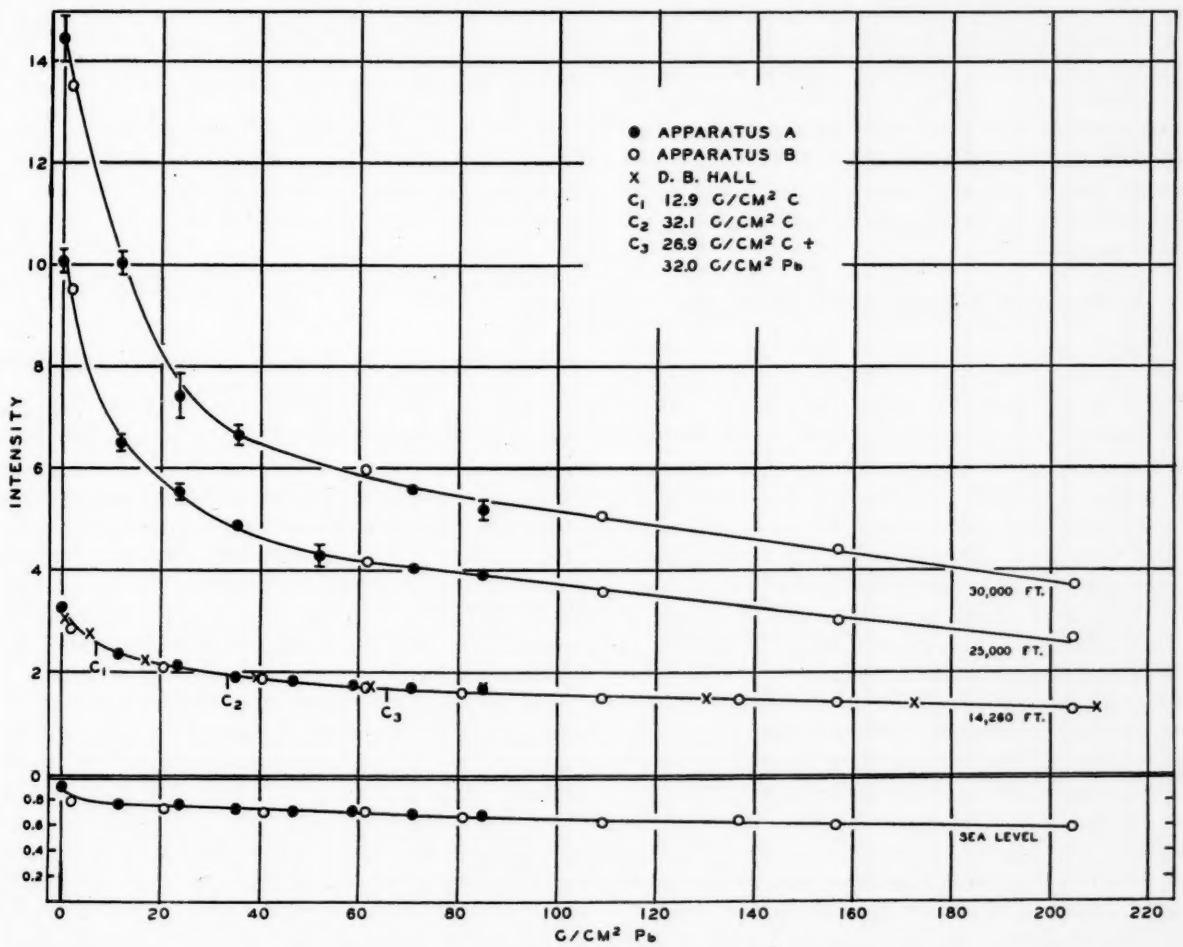

FIG. 1. Cosmic-ray absorption curves at several altitudes. The values of intensity correspond to counts per minute for Apparatus A, and counts per minute/1.90 for Apparatus B.

[4] E. E. Witmer and M. A. Pomerantz, J. Frank. Inst. **246**, 293 (1948).
[5] D. B. Hall, Phys. Rev. **66**, 321 (1944).

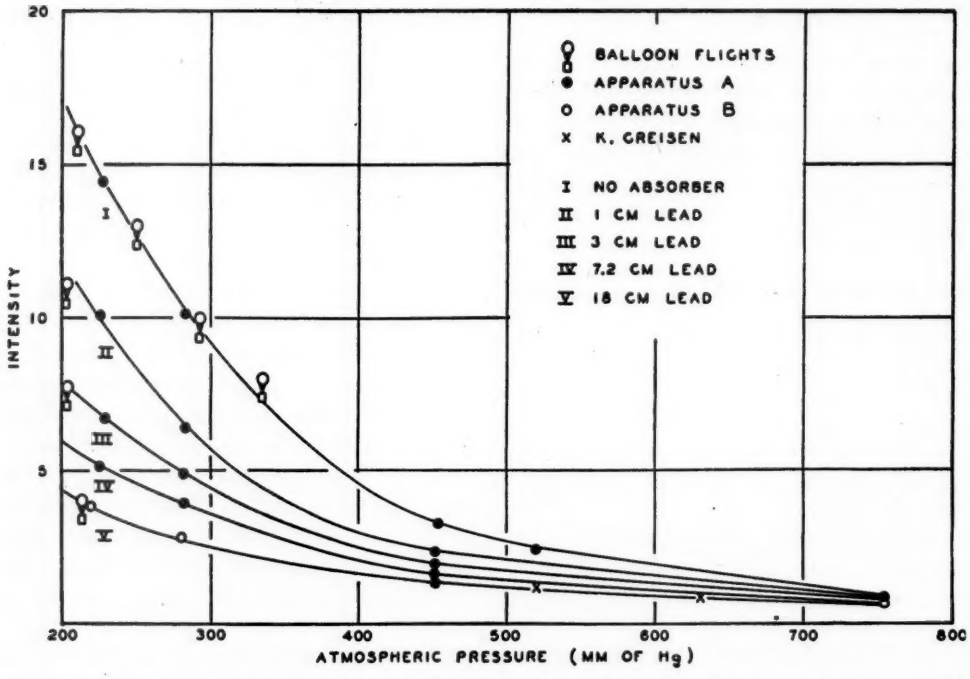

FIG. 2. Intensity *vs.* altitude curves obtained with different thicknesses of interposed absorber. The *V* large circles represent the balloon-flight data.

flights. Furthermore, the conclusion regarding the increase in the absorption coefficient between 4 and 6 cm of Pb from 0.003 cm²/g at Mt. Evans to 0.008–0.006 cm²/g at 200 mm–50 mm has received additional validation.

B. Variation of Intensity with Altitude

Figure 2 contains *intensity vs. altitude* curves for several different thicknesses of interposed absorber obtained from the B-29 flights and the Mt. Evans data. Similar curves could, of course, be plotted for any thickness up to 18 cm of Pb. In each instance, the points obtained in the free-balloon flights (Fig. 1, reference 1) are plotted in the figure. Since all the data were obtained with the same experimental arrangements, no normalization is required. The data have been plotted without regard to latitude changes which have a negligible influence upon the present considerations.

Experiments at very high altitudes are still in progress for interposed absorber thicknesses exceeding 7.5 cm. The balloon-flight data at the lower altitudes agree with the airplane data well within the rather large statistical uncertainties of the former.

A direct comparison may be made between the present results and those previously obtained by other investigators on Mt. Evans. Values of the ratio of the intensity of the penetrating component near sea level to that on Mt. Evans are summarized in Table III. Here again, the agreement is satisfactory.

On the basis of the present results, the analysis of the relative intensities of the non-electronic and electronic components undertaken in reference 1 for very high altitudes may be extended through the region in which only a rough interpolation was indicated previously. The results are presented in Fig. 3.

C. Relative Stopping Powers of Carbon and Lead

Values at Mt. Evans of the relative stopping powers of carbon and lead (S_C/S_{Pb}) are obtained by locating on the curve of Fig. 1 (14,260′) points with ordinates corresponding to the counting rates with a fixed amount of carbon (or carbon plus lead). The abscissa then indicates the amount of lead which produces equal absorption. The data are given in Table IV. The value with 12.9 g/cm² is comparable with those stated in reference 1 for higher altitudes.

The increase with the interposition of 32.1 g/cm² indicates that the lead becomes less effective per unit superficial mass compared with carbon as the minimum range required for penetration is increased. Differential comparison reveals that the net relative absorption is already approaching that expected for mesotrons alone, for cosmic rays having a residual range of somewhat less than 1 cm of Pb after passing through the absorber, and an initial range of 3 cm.

This is consistent with the observations of Hall[5] regarding the relative intensities of electrons and mesotrons at this location.

TABLE III. Ratio $N(0, t, h)/N(0, t, 4350)$ of the intensity of the penetrating component in the vertical direction near sea level to the intensity at Mt. Evans.

Reference	Location	Altitude, h—meters	Average atmospheric pressure—mm of Hg	Absorber thickness, t—g/cm² of Pb	$N(0, t, h)/N(0, t, 4350\text{ m})$
Rossi, Hillberry, and Hoag[a]	Chicago	180	743	145	0.444±0.004
Greisen[b]	Ithaca	259	740	167	0.437±0.007
Author	Swarthmore	90	756	157	0.433±0.009

[a] Rossi, Hillberry, and Hoag, Phys. Rev. **57**, 461 (1940).
[b] K. Greisen, Phys. Rev. **61**, 212 (1942).

D. Effects of Showers and Scattering

The arguments upon which the negligibility of the effects introduced by side showers and scattering are based, have been discussed in reference 1, Section IV. Additional evidence bearing upon the latter is of some interest; to this end, the counting rates corresponding to various positions of a given absorber within the coincidence counter train were observed at each of the altitudes. Comparisons were also made between rates with the absorber slightly wider than the counter (1 cm) and those with greater width (4.5 cm). In all instances the observed rate was independent of the geometrical arrangement, within the statistical uncertainties of the data.

III. REDUCTION OF DATA TO ABSOLUTE INTENSITIES

A. Determination of Effective Dimensions of the Counter Train

In order to compute the absolute intensities from the observed counting rates it is necessary to ascertain the effective dimensions of the G-M counters. It has been demonstrated by Street and Woodward,[6] and, for certain self-quenching counters by Greisen and Nereson,[7] that the effective diameter of a counter coincides very closely with the inside diameter of the cathode. However, owing to end effects, the active length of a tube without guard rings is somewhat less than either the length of the cylinder or the length of the fine anode wire. The customary procedure for determining the end-correction involves inclusion of the counter under test as a member of a coincidence train, and recording of the coincidence rate as this counter is displaced along its own axis perpendicular to the plane defined by the central wires of the other counters. Although unquestionably reliable, this method has the disadvantage of requiring inordinately long runs in some instances, particularly in the case of counters of small diameter such as have been utilized in the present experiments. This would preclude rapid determinations of the effects of operating voltage, filling mixture, or even changes from counter to counter.

TABLE IV. Experimental values of S_C/S_{Pb} at Mt. Evans.

Carbon thickness—g/cm²	Equivalent lead thickness—g/cm²	Range—g/cm² Initial	Residual	S_C/S_{Pb}
12.9	7.0	12.9 C	c.w.[a]	0.54
32.1	33.5	32.1 C	c.w.	1.04
19.2	26.5	32.1 C	12.9 C +c.w.	1.38
26.9	33.5	26.9 C +32.0 Pb	32.0 Pb +c.w.	1.25

[a] c.w. = counter walls = 1.8 g/cm² Cu + 2.6 g/cm² glass (mean thickness required for penetration).

An alternative method was therefore attempted, and, despite factors which were of course not unanticipated, this simple scheme provides satisfactory results. The arrangement is shown in Fig. 4. A γ-ray howitzer irradiates the counter through a narrow slit, and the counting rate is observed to

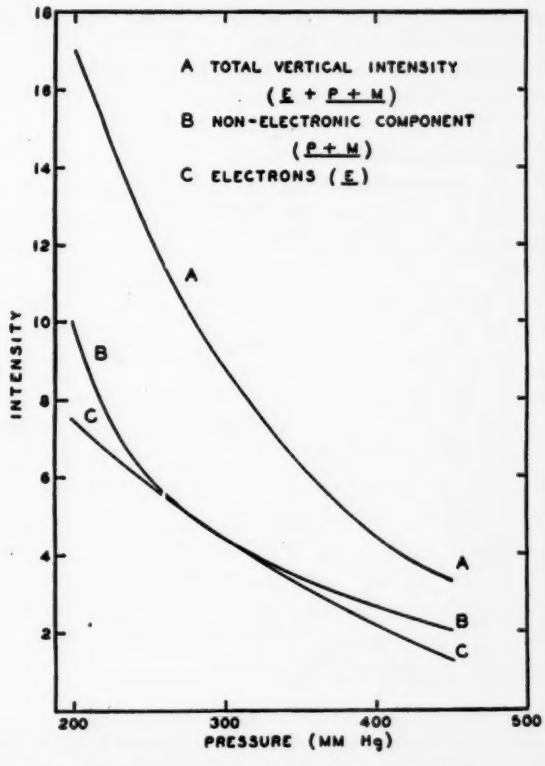

FIG 3. Variation with altitude of total vertical intensity $(E+P+M)$, heavy component intensity $(P+M)$, and electron intensity (E) for the lower portion of the atmosphere. The assumptions upon which the determination of these points are based have been discussed in reference 1, Section V. The above curves replace the broken lines (representing rough estimates) in Fig. 5 of that reference.

[6] J. C. Street and R. H. Woodward, Phys. Rev. **46**, 1029 (1934).
[7] K. Greisen and N. Nereson, Phys. Rev. **62**, 316 (1942).

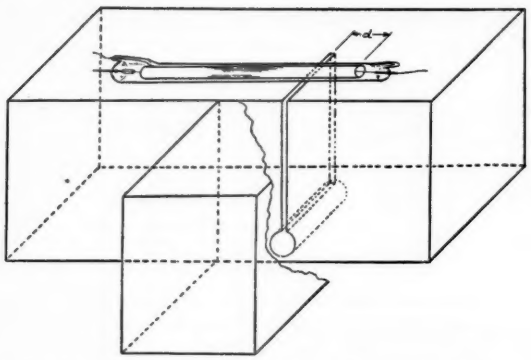

FIG. 4. Arrangement used in the determination of the effective length of a G-M counter. The radium source is inserted in the hole at the base of the slit in the pile composed of lead blocks. The length of the counter cathode is 20 cm.

depend upon the distance between the slit and the end of the counter.

Under these conditions, discharges of the G-M counter are produced by Compton electrons scattered out of the cylinder. The angular distribution of the Compton electrons is such that, for the energies present in the beam, the intensity falls to half value within roughly 15°. The preponderance in the forward direction renders this method feasible, as may be seen from the results plotted in Fig. 5. To a sufficient degree of approximation, the theoretical curve is easily calculated from an integration over the counter for each value of the abscissa x, utilizing the aforementioned distribution.[8]

Measurements were made with various geometrical arrangements, all of which gave equivalent conclusions. The final results do not depend critically upon the vertical distance of the counter above the lead, or upon the thickness of the shield.[9]

The background rate applicable to each value of x has been subtracted from the observed rate to obtain the relative counting rates of Fig. 5. This correction was obtained by plotting counting-rate as a function of x with the counter oriented parallel to the position indicated in Fig. 4, but off the slit.

Finally, it is necessary to ascertain the effect of any intrinsic inefficiency of the G-M counters introduced either by the dead-time or by the probability of the passage of a charged particle without the occurrence of at least one ionizing event. The combined contribution of both is negligible in these experiments.

[8] This may be deduced either from theory, or from various experimental results, e.g., D. Skobelzyn, Nature **X**, 411 (1929).

[9] Presumably the optimum set of conditions may be predicted by maximizing the function which represents the ratio of collimated beam intensity (signal $=I_S$) to background intensity (noise $=I_N$) as follows:

$$f(S)=I_S/I_N=(A/S^2)/(I_0e^{-\mu S}),$$

where μ = absorption coefficient in Pb for γ-ray energies present in beam, and S = depth of slit. For $f'(S)=0$, $S=2/\mu$.

A standard test of each of the counters used here consists of exposure to a graduated set of calibrated radium sources of identical form under conditions such that the individual counting rates exceed those of a single counter at any point in the atmosphere. The criterion for acceptance is that the recorded rates are proportional to the intensities. Additional tests have revealed that the dead-time of these counters is less than 10^{-4} sec.

B. Calculations

The quantity $N(O, h, t)$ represents the number of particles passing through a vertical cosmic-ray coincidence train in unit time. Here, the zenith angle of the principal axis of the train is zero, h is the altitude of the station of observation, and t the thickness of interposed absorber. If $I(\theta)$ is the number of particles arriving from a given direction θ, and passing through a unit area of the bottom tray within unit solid angle per second,

$$dN=I(\theta)d\omega dA_1\cos\theta, \tag{1}$$

where dA_1 is an element of area in the lower counter.

For a dependence of cosmic-ray intensity upon zenith angle given by

$$I(\theta)=I(O)\cos^p\theta, \tag{2}$$

this immediately leads to an integral of the form:

$$N(O, h, t)=\int\int\frac{I(O, h, t)\cos^{p+2}\theta dA_1dA_2}{\lambda^2}, \tag{3}$$

where λ is the distance between the element of area dA_2 in the upper tray and dA_1.

The final result of the integration for a $\cos^2\theta$ distribution ($p=2$), including terms taking into account the extension of the solid angle beyond the ends of the rectangular area (due to the cylindrical shape of the counters[6]), is:

$$N(O, h, t)=I(O, h, t)\frac{w^2}{4}\left\{3\frac{l}{L}\tan^{-1}\frac{l}{L}+\frac{l^2}{L^2+l^2}+\frac{\pi w}{2L}\left[1-\left(\frac{L^2}{L^2+l^2}\right)^2\right]\right\}, \tag{4}$$

where l is the active length of the counter, w the tray width (counter diameter), L the perpendicular distance between the axes of the extreme counters.

The small correction to the width because of the cylindrical form of the counters amounts only to 0.6 percent of the factor thus calculated.

Inasmuch as the value of p at higher altitudes is somewhat smaller than 2, the normalization of measurements at very high altitudes with respect to other determinations of $I(O, h, t)$ low in the atmosphere is not justified, in some instances.

As a matter of fact, recent experiments[10] have indicated that the nature of the distribution at the "top of the atmosphere" is isotropic. In this case by integration of Eq. (3) with $p=0$, and the addition of the end-correction term we arrive at the final relationship:

$$N(O,h,t)=I(O,h,t)w^2\left\{\frac{l}{L}\tan^{-1}\frac{l}{L}+\frac{\pi w}{4L}\left[1-\frac{L^2}{L^2+l^2}\right]\right\}. \quad (5)$$

As an intermediate possibility, we may consider $p=1$ ($\cos\theta$ distribution). In this case we obtain in a similar manner:

$$N(O,h,t)=I(O,h,t)\frac{2w^2}{3}\left\{\frac{2(L^2+l^2)^{\frac{1}{2}}}{L}-1-\frac{L}{(L^2+l^2)^{\frac{1}{2}}}+\frac{\pi w}{4L}\left[1-\left(\frac{L^2}{L^2+l^2}\right)^{\frac{1}{2}}\right]\right\}. \quad (6)$$

The dimensions of both instruments, together with the final values of the ratio $\varphi=N(O,h,t)/I(O,h,t)$ applicable to $\cos^2\theta$, $\cos\theta$, and isotropic distributions are listed in Table V. The resulting values of $I(O,h,t)$ on the basis of the present experiments, as well as several reported by other investigators for low altitudes, are given in Table VI. According to Sands,[11] there does not appear to be a significant departure from $p=2$ for the total intensity at 30,000 feet.

The factors (φ_A) listed in Table V may be divided into any of the various counting rates at very high altitudes reported in reference 1 to obtain $I(O,h,t)$. The stated value of the absolute intensity near the "top of the atmosphere" has been based upon all available data from the free-balloon flights at altitudes exceeding 90,000 feet. This embraces 9 flights with vertical telescopes, and includes data not contained in reference 1. Recent measurements in inclined directions have not been incorporated in this average.

Experiments now in progress will provide a complete determination of the zenith angle distribution law throughout the atmosphere for several values of t. Tentatively, one may assume that the $\cos\theta$ distribution is roughly applicable in the tropopause. This is in accord with the results of experiments performed during the National Geographic Society stratosphere flights.[12]

For various reasons it is not possible to compare the value of the absolute intensity near the "top of the atmosphere" directly with that recently published by Gangnes, Jenkins, and Van Allen.[13] However, their data obtained with coincidence telescopes in rockets do not appear to be inconsistent with the commencement of the constant intensity plateau at the altitudes attained in free-balloon ascents. Although the absolute intensities reported by the former are somewhat lower, the latitude effect alone may be sufficient to account for this, as has already been demonstrated.[14] Furthermore, an appreciable number of events which were rejected as involving multiples in the rocket experiments undoubtedly represent part of the genuine primary beam.

It should be mentioned that (in accordance with the warning in reference 1) the change with altitude in the value of φ affects the comparison (Fig. 6, reference 1) between our results, for 6 cm of interposed Pb, and those obtained by Schein and Allen

TABLE V. Geometrical factors for reduction of counting rates to absolute intensities.

Instrument	Effective length, l cm	Effective width, w cm	Separation, L cm	$\varphi=\frac{N(O,h,t)}{I(O,h,t)}$ $p=2$	$p=1$	$p=0$
A	19.4	0.9	11.5	1.23	1.29	1.45
B	19.4	2.3	26.6	2.33	2.50	2.52
φ_B/φ_A				1.90	1.94	1.74

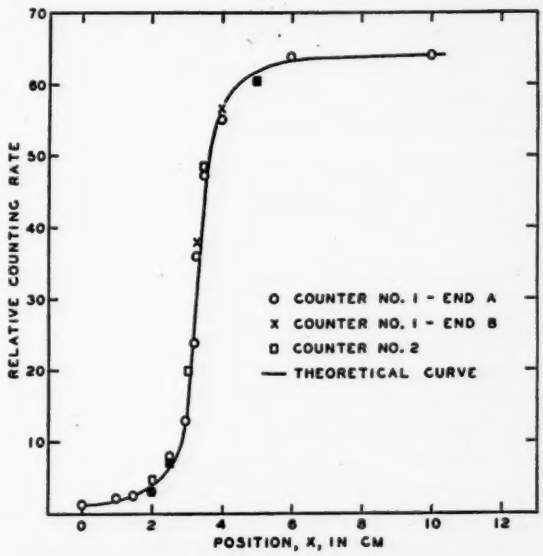

FIG. 5. Relative counting rate (after subtraction of background) as a function of the distance, x, between the slit and an arbitrary index on the counter. The theoretical curve (solid line) is calculated on the basis of an effective length, l, equal to 19.4 cm.

[10] M. A. Pomerantz, Phys. Rev. **75**, 1335 (1949).
[11] M. Sands, Phys. Rev. **73**, 1338 (1948).
[12] Swann, Locher, and Danforth, Nat. Geog. Soc. Cont. Tech. Papers, Stratosphere Series No. 2 (1936).
[13] Gangnes, Jenkins, and Van Allen, Phys. Rev. **75**, 57 (1949).
[14] Biehl, Montgomery, Neher, Pickering, and Roesch, Rev. Mod. Phys. **10**, 360 (1948).

TABLE VI. Absolute intensities in the vertical direction, $I(O, h, t)$—the number of particles per cm² per unit solid angle per minute.

$$\left(I(O, h, t)=\sum_{1}^{n}\int_{\epsilon(t)}^{\infty} i_n(O, h, \epsilon)d\epsilon,\right.$$

where the index n identifies the type of particle.)

Reference	Altitude, h—meters	Atmospheric pressure —mm of Hg	Absorber t—g/cm²	$I(O, h, t)$
Street and Woodward*	0	760	0.55[a]	0.80±0.028
Street and Woodward*	0	760	3.4[b]	0.74±0.026
Greisen**	259	740	1.7[c]	0.741±0.014
Greisen**	259	740	9.9[d]	0.623±0.004
Greisen**	259	740	167.0[e]	0.493±0.004
Greisen**	4350	453	1.7[c]	3.17±0.074
Greisen**	4350	453	9.9[d]	2.00±0.020
Greisen**	4350	453	167.0[e]	1.13±0.016
Author	90	756	4.4[f]	0.745±0.006
	90	756	157.0[g]	0.494±0.006
	4350	453	4.4[f]	2.66±0.044
	4350	453	157.0[g]	1.14±0.018
	25,000	282	4.4[f]	8.2±0.19
	25,000	282	157.0[g]	2.47±0.068
	30,000	226	4.4[f]	11.7±0.37
	30,000	226	157.0[g]	3.61±0.07
Reference 1	90,000	13	<89.0[g]	10.1±0.20***

* See reference 6.
** See reference b of Table III.
[a] Quoted minimum thickness between sensitive volumes of extreme counters, 0.32 g/cm² glass+0.23 g/cm² Cu.
[b] Quoted minimum thickness between sensitive volumes of extreme counters, 2.3 g/cm² glass+1.1 g/cm² Cu.
[c] Brass, minimum thickness between sensitive volumes of extreme counters.
[d] Minimum thickness between sensitive volumes at extreme counters, 8.2 g/cm² brass+1.4 g/cm² wood.
[e] Quoted value, includes counter walls, lead, and wood above and between counters.
[f] Mean thickness between sensitive volumes of extreme counters, 1.8 g/cm² Cu+2.6 g/cm² glass.
[g] Mean thickness of interposed absorber, not including counter walls (see note f).
*** This value represents an average of all available data obtained at altitudes exceeding 90,000 feet with vertical coincidence-counter trains. It is based upon the results of 9 flights having different amounts of interposed material. The indicated uncertainty is the statistical standard deviation.

with 18 cm of Pb. However, in the extreme case, the relative intensity of the latter would only be increased by about 15 percent near the "top of the atmosphere." This does not affect the general conclusions based on the difference which appreciably exceeds this amount.

IV. DISCUSSION

Although the above results are in good agreement with those of other investigators when an appreciable quantity of absorber is interposed in the counter train, the situation is quite different when only the counter walls determine the minimum range which must be penetrated for the registering of an event. The large absorption in small thicknesses of material is already strikingly evident in the data obtained by Greisen at the comparatively low altitude of 4350 meters (Table VI). Here the measured intensity increased by 58 percent when the interposed absorber was reduced by 8.2 g/cm². The absorption coefficient for small thicknesses becomes even greater at higher altitudes. A rather large difference between the relative total intensities computed from our data and those reported by Sands[11] on the basis of similar measurements, is doubtless attributable to this effect.

In the past, various methods for computing the effective thickness of the counter walls have been adopted, and the stated values are frequently not strictly comparable. It is desirable that the basis for the computation be explicitly stated, and it is therefore proposed that, following the custom which seems to have become somewhat prevalent, the minimum amount of material between the sensitive volumes be stated. The argument for omitting the upper wall has been based upon the hypothesis that as many soft particles are produced as are absorbed therein.

This minimum thickness may be multiplied by a constant which takes into account the fact that the mean thickness traversed is greater because of the cylindrical shape, and because of the distribution of cosmic-ray intensity with zenith angle.[4] On this basis, the absorber in Sands'[15] apparatus amounted to 3.8 g/cm² as compared with 4.4 g/cm² similarly calculated for our counters, the walls of which contained some material of lower atomic number. This is apparently sufficient to introduce a difference in the relative intensities varying from 15 percent on Mt. Evans to 32 percent at 30,000 feet.

This clearly demonstrates the error which may be introduced into attempts to compare measurements by different investigators of the so-called "total" intensity at high altitudes. Indeed, the disagreement has been quite marked.[16]

V. ACKNOWLEDGMENTS

It is a pleasure to thank D. W. Seymour for making most of the observations during the B-29 flights, and P. Morris for general cooperation in this phase of the program; F. Green and D. Watson for their invaluable assistance; the Inter-University High Altitude Laboratory Association for the use of their facilities at Mt. Evans; the U. S. Air Force for providing the airplane; and the National Geographic Society for their kindness in supporting the field trips which made it possible to perform these experiments.

[15] M. Sands (private communication).
[16] See, e.g., B. Rossi, Rev. Mod. Phys. **20**, 537 (1948).

On the Origin of Cosmic Rays

R. D. RICHTMYER
The Institute for Advanced Study, Princeton, New Jersey
AND
EDWARD TELLER
Institute for Nuclear Studies, The University of Chicago, Chicago, Illinois
(Received January 27, 1949)

The presence of heavy particles in cosmic rays makes it plausible that cosmic radiation is generated by the acceleration of charged particles in extended electromagnetic fields. The energy density of cosmic rays (3×10^{-10} Mc^2/cm^3) would lead to very great total amounts of energy if one assumes that cosmic radiation extends throughout intergalactic or throughout interstellar space. This would require very efficient methods of cosmic-ray production. It is therefore of interest to investigate the possibility that cosmic rays are generated in the vicinity of the sun and are confined to the solar system by extended magnetic fields. The strength of these fields is estimated to be 10^{-5} gauss. According to this picture, cosmic rays circulate in the neighborhood of the planetary system for thousands of years, during which time the radiation becomes isotropic. The electron component of the radiation is eliminated by collisions with solar light quanta.

DISCUSSIONS of the origin of cosmic rays have led so far to quite inconclusive results. The following note presents some considerations which may prove helpful in the search for an adequate explanation. Theories presented so far can be divided into three classes: First, the theories which explain cosmic radiation by acceleration of particles in extended electromagnetic fields; second, theories which postulate that great energies are acquired by a cosmic-ray particle in an elementary act; and third, the theories which assume that cosmic rays have been generated at the time of the origin of the universe. We shall show that of these alternatives the first one seems to be most promising, and in addition, we shall give arguments in favor of a more specific hypothesis: The origin of the cosmic rays may lie in the solar system itself.

It seems at present practically impossible definitely to disprove the theory that cosmic rays were generated at the time of the origin of the universe. Physical conditions at that time have certainly been very different from those prevailing at present. Such an explanation would probably be accepted only if good reasons were given that, under present conditions, cosmic rays cannot be produced.

The possibility that cosmic rays are produced in elementary acts has been practically disproved by the discovery[1] that among the cosmic rays there are found heavily charged nuclei. One might imagine elementary acts in which very energetic protons are produced, but it seems highly improbable that all the neutrons and protons of, for instance, a neon nucleus, should be produced or accelerated in an elementary act to an energy of two billion volts per nucleon without giving to the nucleus more than sufficient internal energy to break it up into its constituent particles.

It has been pointed out frequently[2] that electromagnetic fields on the stars, near stars, or in interstellar space may have sufficient strength and extension to accelerate individual particles to the energies observed in cosmic-ray experiments. In fact, it might seem that this process could occur so frequently and easily in the universe that there might arise some embarrassment as to what choice to make among these possibilities. There is, however, another requirement which a theory of cosmic rays must fulfill. It must explain the total energy present in cosmic radiation. This requirement indeed is quite restrictive. The cosmic rays impinging upon the earth indicate an energy density of approximately 3×10^{-10} Mc^2/cm^3, where M is the mass of the proton.[3] If we assume that cosmic rays are evenly distributed throughout all space, including intergalactic space, then the total energy in cosmic rays would be greater than any other energy known to us with the exception of the rest energy of matter.[4] Indeed, the energy represented by the cosmic rays would be approximately 10^{-4} of this rest energy. In order to account for the cosmic rays, one would then have to assume the presence of electromagnetic fields containing as much or more energy than the cosmic rays themselves. This is by no means impossible, but it is clear that such fields could not be due to any mechanism in which other known energies are transformed into electromagnetic fields, since these other energies are quantitatively insufficient for the purpose. The assumption that galaxies carry great charges, or

[1] Freier, Lofgren, Ney, Oppenheimer, Bradt, and Peters, Phys. Rev. **74**, 213 (1948); Freier, Lofgren, Ney, and Oppenheimer, Phys. Rev. **74**, 1818 (1948); H. L. Bradt and B. Peters, Phys. Rev. **74**, 1828 (1948).

[2] See for instance, W. F. Swann, Phys. Rev. **43**, 217 (1933); H. Alfvén, Zeits. f. Physik, **105**, 319 (1937).

[3] Estimated from review article by B. Rossi, Rev. Mod. Phys. **20**, 537 (1948).

[4] F. Hoyle (M. N. R. A. S. **106**, 384 (1946)) proposes that cosmic rays are produced by stars in which densities of 10^{14} g/cm^3 occur. At such a density energies comparable to the rest energy may be released. It seems remarkable, however, that this process gives rise to no other observable energies that are as great or greater than the energies contained in cosmic rays.

that electrically charged particles are accelerated by some fields due to a new type of coupling between gravitation and electricity, would hardly give an acceptable explanation. Even if one made such an assumption, the effective charge of the galaxies would have long since been neutralized.

It has been proposed[5] that the cosmic rays which are observed on the earth are confined by weak magnetic fields to the interior of galaxies. If this idea is accepted one finds that cosmic rays will be absorbed in a time short compared to the age of the universe. The main component which we observe in cosmic rays consists of protons. If the cosmic rays circulate within the galaxy then they will, from time to time, collide with other protons. These collisions lead to meson production accompanied by considerable decrease of the energy of the protons. Since the cross section of a meson production is approximately 0.02 barn, and since there is approximately one proton per cm^3 in the galaxy, the cosmic rays will have a mean free path for meson-producing collisions of about 5×10^{25} cm, or 5×10^7 light years. This distance is of course great compared to the dimensions of the galaxy, but the cosmic rays will stay inside the galactic system, being guided by magnetic fields. The mesons produced by the cosmic rays decay into electrons and into neutral particles. There is no effective way to return the energy of these particles to the protons. Since protons constitute the main component of cosmic rays, the energy given to mesons must be considered as lost to the cosmic radiation. In order to establish an unchanging level, the energy of these cosmic rays must be renewed every 50 million years. Estimates on stellar radiation intensity inside the galaxy show[6] that approximately 10^{-4} of the energy produced in stars would suffice to compensate the energy lost by cosmic rays in meson production. It is difficult to find a mechanism by which so great a fraction of the star light is converted into energy of protons carrying more than 10^9 ev.

One may assume that the galactic magnetic field does not constrain the cosmic-ray particles to move strictly inside the galaxy, but allows the cosmic-ray orbits to extend over a volume which is a few times greater than the volume of the galaxy. In this case each cosmic-ray particle would lose energy more slowly, but a greater number of particles would be present at any given time, and the energy that has to be fed into cosmic radiation remains the same.

We have considered so far only the observed cosmic-ray spectrum which extends from 2.5×10^9 ev toward higher energies. Cosmic rays below this lower limit may have escaped observation. In this case a great additional amount of energy may be present in the low regions of the cosmic-ray spectrum, and the energy needed for maintaining cosmic radiation would be increased.

The energy of cosmic rays may be derived from the kinetic energy of interstellar matter or of the stars. Assuming an average density of one hydrogen atom per cm^3, with an average velocity of 3×10^6 cm/sec., one finds that approximately 10 percent of the kinetic energy is used up by keeping the cosmic rays going for 2×10^9 years. Added low energy cosmic radiation would raise this estimate. It would seem difficult to explain such an efficient conversion of kinetic energy into high energy radiation.[7]

The difficulties mentioned above can be avoided if one assumes that cosmic rays originate in the neighborhood of the sun[8] and are kept for a protracted period within or near the solar system by an appropriate magnetic field. If one may apply Liouville's theorem and the ergodic hypothesis one would expect that an isotropic distribution of cosmic rays will be established within the region in which the radiation circulates. Deviations from an isotropic distribution would be expected (a) near the fringes of the region to which the cosmic rays are confined, or (b) if the cosmic radiation diffuses away rapidly from the neighborhood of the sun, or (c) if there exists an integral of the orbital motion of the cosmic-ray particles.

Because of (a), we have to assume that the earth lies well within the interior of the region accessible to cosmic radiation.

The point raised under (b) will be valid for most shapes of the magnetic field. We have to assume an appropriate shape of the magnetic field to prevent rapid loss of the cosmic radiation from the planetary system. A field of an appropriate shape would be, for instance, one caused by currents in the ecliptic circulating around the sun and extending throughout the planetary system. Even if such an appropriate magnetic field were established, cosmic rays could still diffuse out due to deflections by perturbing fields. This, however, need not give rise to any difficulty as long as such perturbing fields are confined to the part of the field which is closer to the sun. As long as a time-independent exterior field of appropriate shape exists, cosmic rays can

[5] H. Alfvén, Zeits. f. Physik **107**, 579 (1937).
[6] T. Dunham, Proc. Am. Phil. Soc. **81**, 277 (1939).

[7] E. Fermi (Phys. Rev. **75**, 1169 (1949)) has recently proposed a most ingenious mechanism which may furnish the required energy to the cosmic radiation. According to this proposal, cosmic radiation constitutes an essential component in the energy distribution within the galaxy, and the mechanism regulating the intensity of cosmic rays is based upon the balancing of the various forms of energy. Difficulties connected with the presence in cosmic radiation of nuclei carrying more than one charge give rise to some doubt whether or not Fermi's proposal is the correct explanation of cosmic rays. We are indebted to Professor Fermi for discussions of his paper and of the present note.

[8] The solar origin of cosmic rays has been proposed by M. A. Dauvillier, J. de phys. et rad. **5**, 640 (1934); and by D. H. Menzel and W. W. Salisbury, Nucleonics **2**, 67 (1948).

be confined for long periods of time. Such an effective confinement of the cosmic rays is necessary, not only to explain the isotropy, but also in order to explain the intensity of the radiation.

An integral of motion, as mentioned in (c), will exist if the magnetic field in which the cosmic rays circulate has strict axial symmetry. In this case an axially symmetrical vector-potential $\mathbf{A}$ may be introduced, and the vector $\mathbf{r}\times(m\mathbf{v}+(e/c)\mathbf{A})$, has a constant component along the axis of symmetry. This component, which is known as the Störmer integral, is the appropriate generalization of the angular momentum. It seems likely that axial symmetry is not fulfilled so rigorously as to insure the constancy of this integral for a protracted time. Thus we find no conclusive argument against an isotropic distribution of cosmic rays.

The intensity of the magnetic field which keeps the cosmic rays within or near to the planetary system can be estimated as follows: The most energetic singly charged particles observed in the cosmic rays have an energy of 10^{14} ev. (The Auger showers may be caused by heavier nuclei.) If we want to confine these particles to a region of the dimensions 3×10^{17} cm we need a field of 10^{-6} gauss. This distance is equal to a third of a light-year. Thus fields weaker than 10^{-6} gauss could hardly confine all cosmic rays to the neighborhood of the sun. On the other hand, a field of more than 10^{-4} gauss would have been discovered in the investigations of geomagnetism. Thus we are forced to introduce a field approximately equal to 10^{-5} gauss.

If we assume that all cosmic rays produced near the sun will eventually impinge upon the earth, one finds that less than 10^{-17} of the solar radiation will suffice to maintain the cosmic radiation. It is clear that other planets will serve as sinks of the cosmic rays. Meson-producing collisions could consume some of the energy of the cosmic rays. Collision of cosmic rays with the sun may be prevented or greatly reduced by the solar magnetic field. In any case it will be unnecessary to convert a considerable fraction of the solar energy into cosmic rays. Thus it will be less difficult to find an appropriate mechanism for producing cosmic rays.

The lifetime of a cosmic ray will vary according to the extension of its orbit. If the orbit is comparable to the distance from the sun to the earth, the cosmic ray is likely to collide with the earth in a time somewhat longer than a thousand years. In orbits of greater extension, cosmic rays may circulate for a longer time. In no case can we expect them to live much longer than about 5×10^{7} years, which is the lifetime of fast protons circulating in the galaxy.

According to the calculations of Feenberg and Primakoff,[9] electrons of cosmic-ray energies circulating near the earth's orbit will lose their energy in less than 100 years due to Compton collisions with solar light quanta. We should, therefore, not expect a strong electron component in cosmic rays. Protons and heavier nuclei will be unaffected by sunlight. Indeed, the upper limit of the proton energies is probably given by the escape from the solar system rather than by the results of Compton collisions.

The assumption that cosmic rays are essentially confined to our planetary system leads to a few conclusions which can be checked by cosmic-ray experiments. Among these are:

(1) No protons greatly in excess of 10^{14} ev and no particles greatly in excess of 10^{16} ev are to be expected. Such particles cannot be confined to the neighborhood of the planetary system.

(2) It is likely that particles of lower energy than 2.5×10^{9} ev will be found. To confine cosmic rays to the planetary system, but not to allow them to approach the sun closer than the earth's orbit, would indeed require rather artificial assumptions about the shape of the magnetic lines of force. It should be noted that the sun's dipole gives rise to a field of less than 10^{-5} gauss near the earth.

(3) The cosmic-ray intensity should not depend on the angle included by the cosmic ray and the velocity vector of the solar system with respect to the galaxy. Thus there should be no Compton-Getting effect.[10]

(4) There is no striking reason for different laws of acceleration of protons and heavier nuclei. These particles may be found in cosmic rays with approximately the same abundance ratio as they are found elsewhere in the planetary system. The spectra of the protons and of the heavy nuclei may be similar.

Summarizing the above discussion, we suggest that the energy of cosmic rays is derived from the most plentiful energy source in our neighborhood, the sun. We introduce a magnetic field of about 10^{-5} gauss which extends throughout and beyond the planetary system. This field serves to convert the cosmic rays into isotropic radiation. The long circulation periods in this field (10^{3}–10^{8} years) also explain why the cosmic-ray intensity does not show long-period fluctuations connected, for instance, with the sun-spot cycle. Finally, the magnetic field helps to keep the cosmic-ray intensity at a high level. In the following paper, H. Alfvén presents a plausible explanation of this magnetic field. He also describes a possible mechanism for the acceleration of charged particles near the sun.

If our ideas are correct, the expression "cosmic rays" is a misnomer. We wonder to what extent this name has hindered discussion of the solar origin of this radiation.

We are indebted to Professor Fermi for discussions and criticism. The value of these is the greater because of the necessarily speculative character of the views presented here.

[9] E. Feenberg and H. Primakoff, Phys. Rev. **73**, 449 (1948).

[10] A. H. Compton and J. A. Getting, Phys. Rev. **47**, 817 (1935). The effect is small and is hard to establish. Evidence in favor of the effect (and therefore in contradiction to our views) was given by J. Barnóthy and M. Forró, Nature **193**, 1064 (1937).

On the Solar Origin of Cosmic Radiation

HANNES ALFVÉN
Kungl. Tekniska Hogskolan, Stockholm, Sweden
(Received January 27, 1949)

The idea proposed by Teller and Richtmyer that the cosmic radiation is a local solar phenomenon is developed.

It is shown that motion of interstellar matter is likely to amplify a primary interstellar magnetic field up to the value of the order 10^{-5} gauss postulated by Richtmyer and Teller.

According to an earlier suggestion, magnetic storm variations of cosmic radiation are due to electric fields set up within the solar system by the storm-producing beams. It is shown that the long-time effect of the same mechanism may account for the generation of cosmic radiation. It is of special interest that there seems to be some hope to derive theoretically the observational energy spectrum.

I.

AT the recent Nuclear Physics Conference in Birmingham, Teller[1] proposed that cosmic radiation should be a local solar phenomenon, the cosmic-radiation particles being trapped by magnetic fields and confined to move in a region around the sun, which is small compared to stellar distances. Strong arguments in favor of this view have been given in the preceding paper by Richtmyer and Teller.[2] This picture requires magnetic fields around the sun, for example just outside the planetary system, which are much stronger than is usually supposed. At first sight there seems to be little reason to assume other fields than the solar dipole field, which is not at all sufficient to keep cosmic radiation trapped and to make it isotropic. We know, however, very little about the magnetic fields in our neighborhood and a closer examination of the problem is necessary.

II. TRAPPING MAGNETIC FIELDS

For the following discussion it is important to consider a process by which a magnetic field may be amplified. Suppose that in an electrically conducting medium with the mass density $=\rho$ there is an externally given magnetic field H_0. If parts of the medium are put into motion with velocity v, the magnetic field is distorted, so that an induced field H' is superimposed on the initial field. In the case of an infinite electrical conductivity the average value of H' increases until the magnetic energy equals the kinetic energy:

$$\frac{H'^2}{8\pi}=\frac{1}{2}\rho v^2. \tag{1}$$

When this limit is reached an equipartition of energy is accomplished and magnetic field energy converted back into kinetic energy. The state characterizing a magneto-hydrodynamic wave is reached.

III.

We shall apply these results to interstellar space around the solar system. Hence we put $\rho=10^{-24}$ g/cm which is the usually accepted value of interstellar density. This gives

$$H'=v(4\pi\rho)^{\frac{1}{2}}=3.5\cdot 10^{-12}\,v. \tag{2}$$

A magnetic storm is usually supposed to be produced by a corpuscular beam sent out radially from the sun with a velocity of the order $2\cdot 10^8$ cm sec.$^{-1}$. When it passes through the solar magnetic field, the beam will distort the magnetic lines of force and will cause an induced field which may grow up to the order of $H'=3.5\cdot 10^{-12}\cdot 2\cdot 10^8=7\cdot 10^{-4}$ gauss. It should also be observed that as the beam consists of ionized gas which has a high conductivity, the magnetic field in the region close to the sun where the beam emanates may in part be "frozen" into the matter of the stream. In this way magnetic field is "transported" outwards.

Both these effects produce magnetic fields in the outskirts of the solar dipole field which are much stronger than the dipole field itself. Considerations of the decay of these fields and the total energy necessary to produce fields of such an extension and strength as to trap cosmic radiation makes it rather dubious, however, if this effect is sufficient.

IV.

For an assumed galactic magnetic field the value 10^{-10} gauss is usually given. The only foundation for this value is that it constitutes the minimum field required to trap cosmic radiation within the galaxy. No other data confirm a value of this order of magnitude. If we start from a low value of the galactic magnetic field and investigate how this value would be transformed by motion of interstellar matter, we find that the final result is given by (1), i.e., the motion increases the magnetic field until equipartition between kinetic and magnetic

[1] E. Teller, Report on the Nuclear Physics Conference in Birmingham, Sept. 14–18, 1948.
[2] R. D. Richtmyer and E. Teller, Phys. Rev. **75**, 1729 (1949).

energy is established. Because of the very large dimensions the decay of the field is slow. Putting $v=3\cdot10^6$ cm sec.$^{-1}$ for the average (relative) velocity of interstellar matter, we find

$$H'\approx10^{-5}\text{ gauss.} \tag{3}$$

This field is likely to be irregular, produced as it is by motion of the interstellar matter. In a field of this order singly charged particles of momentum $p=10^{10}$ gauss cm $(=3\cdot10^{12}$ ev) have a radius of curvature of 10^{15} cm, and for 30-fold charged particles of 10^{16} ev the value is 10^{17} cm. Thus cosmic radiation would be confined to a region around the solar system which is small compared to stellar distances.

The value 10^{-5} gauss seems at first glance to be very high. In fact it is even somewhat larger than the solar dipole field near the earth's orbit. There is at present, however, no argument against this assumption and, as shown by Richtmyer and Teller, a field of this order greatly simplifies the understanding of cosmic radiation. A field of 10^{-6} gauss would give essentially the same result.

V. MAGNETIC STORM VARIATIONS

Before attempting to trace the origin of cosmic radiation we shall discuss the mechanism producing magnetic storm variations. It is well known that these variations cannot be produced by the storm variations of the terrestrial magnetic field. Instead we must suppose that the electric field associated with the storm-producing beam is responsible for them.[3]

Because of its motion in a magnetic field H a storm-producing beam *when seen from a fixed coordinate system* must be associated with an electric field

$$\mathbf{E}=-\frac{1}{c}\mathbf{v}\times\mathbf{H}. \tag{4}$$

When the earth is situated within the stream this electric field causes a discharge which hits the earth in the auroral zones, the current system of the discharge producing the magnetic storm field. The voltage difference V_b between the borders of the stream is $V_b=E\cdot d$, where d is the breadth of the beam. With $d=5\cdot10^{12}$ cm and $v=2\cdot10^8$ cm/sec. we obtain (expressing V_b in volts, and H in gauss),

$$V_b=10^{13}H\text{ (volt)}. \tag{5}$$

During magnetic storms variations of as much as 10 percent in cosmic radiation intensity are sometimes observed. As the main part of cosmic radiation has an energy of about $3\cdot10^{10}$ ev, V_b must be of the order $3\cdot10^9$ volt. This requires $H=3\cdot10^{-4}$ gauss. This is much more than the solar dipole field, which near the earth's orbit is of the order $2\cdot10^{-6}$ gauss. As pointed out above, the magnetic field in a beam coming from a region near the sun, where the field is much higher, could very well have a stronger magnetic field which is "frozen" into the beam. In fact, if the beam emanates in a region near the solar surface where $H=10$ gauss and moves radially outwards so that its breadth is proportional to the solar distance, this field should for geometrical reasons decrease only to 1/200 of its original value, or to $5\cdot10^{-2}$ gauss. Thus the value $3\cdot10^{-4}$ gauss is not unreasonably high. It should also be compared with the value from (2).

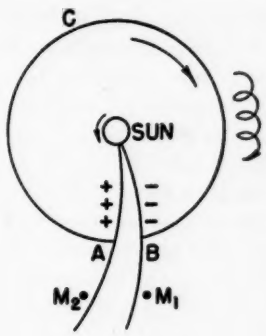

FIG. 1.

It is important to note that in general the field is non-potential. Although the conditions in a meridian plane probably are more important we shall confine the discussion to the equatorial plane (Fig. 1) where the conditions are simpler. The charge accumulated on the sides of the stream tends to produce a current for example along the line ACB. The inductance of this loop is so big, however, that its time-constant τ is very long, possibly of the order of years. When the time during which the beam has been on is short compared to τ there is no appreciable electric field outside the beam, because the field from the charges on the sides of the beam is neutralized by an induced field.

When before a storm the earth has the position M_1 in relation to the beam, positive cosmic-ray particles arriving from the left will be accelerated when traversing the beam. After the storm, positives from the right reaching the earth in position M_2 have in the same way been retarded. This explains the observed increase in cosmic radiation before a storm and the decrease after it. The difference between the two effects may—at least in part—be explained by the geometry of the beam and the particle paths.

VI. GENERATION OF COSMIC RADIATION

The idea that cosmic radiation is produced by induced electric fields has been proposed among others, by Swann,[4] who assumed that the accelera-

[3] H. Alfvén, Nature **158**, 618 (1946).

[4] W. F. G. Swann, Phys. Rev. **43**, 217 (1933); J. Franklin Inst. **215**, 273 (1933).

tion takes place in the electric field generated by the growth of a sunspot magnetic field. A serious objection against this model is that the conductivity of the corona outside a sunspot is so high that the generator is short-circuited. In other words, the electric field must accelerate all particles in the region in question, but the available energy does not suffice to give them cosmic-ray energies. It should also be observed that this model is not reconcilable with a solar origin of the whole cosmic radiation, because fields much stronger and more extensive than sunspot fields must be assumed in order to account for the highest cosmic-ray energies. In the case of the double star generator which has also been proposed to produce cosmic radiation, the acceleration takes place in the space between the stars where the density is much smaller than in the corona, but even in this case the conductivity may be high enough to short-circuit the generator.

The only way to avoid this diffculty seems to be to assume some mechanism which accelerates only particles which already have a high energy. We shall here consider a process of this kind, which takes place in the solar magnetic field. The acceleration is essentially a consequence of the process which we have assumed to be responsible for the magnetic storm variations.[5]

Suppose that no storm-producing beam has been on for a time much longer than the time constant τ of the "electric circuit." Consider the region where the solar dipole field is stronger than the galactic fields. In the solar equatorial plane a positive particle of cosmic-radiation energy may go clockwise either in a circular or a trochoidal path around the sun, the particle energy remaining unchanged.

If suddenly a beam with the voltage difference V_b between its sides is turned on, the particle loses an energy eV_b for every time it passes the beam. No change in energy takes place outside the beam on the way ACB. When the beam has been on for a time which is long compared to τ a potential field is restored so that the particle gains the same energy $eV_a=eV_b$ during the path ACB as it looses when passing the beam. If then the beam suddenly is switched off the particle still gains the energy eV_a when going the distance ACB but does not lose any energy. Hence the net gain per turn is eV_a, which in the above example equals $3\cdot10^9$ ev. This acceleration goes on for a time of the order τ.

This phenomenon can also be regarded in another way. The beam transports magnetic flux outwards at the rate $H\cdot v\cdot d$. This field must leak back towards the sun, causing an increase of the solar field. The betatron action of this accelerates the particles. In fact when equilibrium is reached the path ACB is cut by the magnetic flux Hvd leaking back, and the voltage V_a induced by this is

$$V_a=\frac{1}{c}vHd$$

which again makes $V_a=V_b$.

The above example with $V_a=3\cdot10^9$ volt certainly represents an extreme case. In fact, storms changing cosmic-radiation intensity by as much as 10 percent are very rare. Usually the storm effect is less than 1 percent, so the normal value of V_a is probably of the order of 10^8 volts. The total flux F of the solar magnetic field outside the sun is $F=\pi R_0^2H_p=3.8\cdot10^{23}$ gauss cm^2, $R_0=7\cdot10^{10}$ cm being the solar radius and $H_p=25$ gauss the polar magnetic field. In the case of $V=3\cdot10^9$ volts the outward transport of flux occurs at the rate $Hvd=3\cdot10^{-4}\cdot2\cdot10^8\cdot5\cdot10^{12}=3\cdot10^{17}$ gauss cm^2 sec.$^{-1}$ which shows that it cannot possibly go on as long as 10^6 sec. unless a rapid leaking back occurs. A value of $V_a=10^8$ volt and a time constant of the order of a year ($3\cdot10^7$ sec.) would probably be more like a normal state.

The maximum energy which a particle can gain is given by the maximum value of Hr in the solar field. For an orbit close to solar equator we have $H=10$ gauss and $r=7\cdot10^{10}$ cm which gives $p=Hr=7\cdot10^{11}$ gauss cm and $V=300p=2\cdot10^{14}$ ev. A heavy nucleus with the charge 30 e could reach $6\cdot10^{15}$ ev which is of the order of the most energetic particles assumed to cause the extensive showers.

VII.

The kinetic energy W_b transported outwards per second by a storm-producing beam is

$$W_b=\tfrac{1}{2}\rho v^3S \qquad (6)$$

where S is the cross section of the beam. Supposing it to be circular, we have $S=\pi d^2/4$. The value of the beam density ρ is uncertain, but $\rho=10^{-22}$ (near the earth's orbit) is probably a very conservative estimate. With $v=2\cdot10^8$ and $d=5\cdot10^{12}$ this gives $W_b=0.8\cdot10^{28}$ erg sec.$^{-1}$. Comparing this value with Richtmyer-Teller's figures, it is easily seen that the energy which must be converted into cosmic radiation is only a very small fraction of the beam energy.

VIII.

For the acceleration of cosmic-radiation particles two different possibilities should be considered. The first one is that cosmic-radiation particles coming from the outer regions and accidentally passing near the sun are accelerated by the varying field.

[5] E. Fermi, Phys. Rev. **75**, 1169 (1949), has proposed that cosmic rays are produced in extensive electric fields associated with magneto-hydrodynamic waves in interstellar space. It seems at present difficult to judge whether this mechanism or that one discussed in this paper is to be preferred.

The change in energy during one passage is of the order of V_a.

Consider particles of momentum $p=Hr$. The space U to which they are confined is of the order

$$U=(10r)^3=10^3p^3H^{-3}. \tag{7}$$

The number of times N they will reach a solar distance of R during the time T before they are absorbed is

$$N=\pi R^2cTU^{-1}=\pi\cdot 10^{-3}cR^2TH^3p^{-3}. \tag{8}$$

With $T=3\cdot 10^{14}$ sec., $H=10^{-5}$ gauss, $p=10^{11}$ gauss cm, we find $N=3\cdot 10^{-26}R^2$. Even if the acceleration is active at a solar distance of $R=10^{14}$ cm, a particle will not have a chance of being accelerated more than 30 times, each time by the order of 10^8 ev. This is obviously insufficient, so this mechanism does not work, at least not for the high energy range of cosmic radiation.

IX. THE ENERGY SPECTRUM

The other possibility is that the main acceleration occurs for particles in trapped orbits. Consider a particle at the solar distance R. In the dipole field it may go in a circular path around the sun if its energy is $V'=H\cdot R=aR^{-2}$, where $a=4.2\cdot 10^{33}$ gauss cm^3 is the solar dipole moment. The time for a revolution is $T'=2\pi R/c$. The circular orbit is unstable but if the energy is say $V=0.1V'$ it will go in a stable trochoidal path at the same average solar distance. The time T for one revolution around the sun is at the same time increased to the order of $T=10T'$. If the acceleration per turn $\Delta V_t=V_a-V_b$ remains approximately constant during a time τ, the change in energy during this time is

$$\Delta V=(\tau/T)\Delta V_t=c\tau\Delta V_t/20\pi R \tag{9}$$

so that its relative change in energy becomes

$$\frac{\Delta V}{V}=\frac{c\tau}{2\pi a}\Delta V_t\cdot R. \tag{10}$$

Putting $\tau=10^6$ sec., $\Delta V_t=3\cdot 10^5$ gauss cm ($=10^8$ volt) we find $\Delta V/V=0.3\cdot 10^{-12}R$ so that as soon as R is larger than a few solar radii, the relative increase in momentum is very rapid.

As the absorption during the short time $\tau=10^6$ sec. which we have considered is small, particles will change their energy up and down with the same probability. The result is that in the neighborhood of the sun, the particle spectrum will be constant, i.e. the number of particles with energies between V and $V+\Delta V$ will be independent of V up to the vicinity of the maximum energy which the solar field can keep.

The solar dipole field is certainly disturbed very much for example by the storm-producing stream. Hence particles will frequently change from one periodic orbit to another. They will also pass over from periodic orbits in the dipole field into orbits to the surrounding space, in which case they are emitted from the sun. If we change the solar distance R and at the same time change the particle energy V proportionally to R^{-2}, the particle orbits have the same geometrical form. This similarity indicates that the rate of emission f should be a simple power function of the solar distance or of the energy. Hence let us suppose that the emitted spectrum is $f(V)=f_0V^{n_1}$ where f_0 and n_1 are constants. It is possible to determine n_1 only after a detailed analysis of the scattering process.

The emitted cosmic rays fill a volume proportional to V^3. If the intensity of cosmic radiation is given by the equilibrium between emission and absorption, the energy spectrum would be

$$N=N_0V^{n_1-3}.$$

On the other hand, if the main loss is not due to absorption, but to diffusion outwards towards infinity, the loss is proportional to the surface of the volume filled by cosmic radiation, i.e. to V^2 and we would have

$$N=N_0V^{n_1-2}.$$

In order to obtain agreement with the observational curve

$$N=N_0V^{-2.8},$$

we should have $n_1\approx 0$ in the first case, or $n_1\approx -1$ in the second case.

The S Matrix in Quantum Electrodynamics

F. J. DYSON
Institute for Advanced Study, Princeton, New Jersey
(Received February 24, 1949)

The covariant quantum electrodynamics of Tomonaga, Schwinger, and Feynman is used as the basis for a general treatment of scattering problems involving electrons, positrons, and photons. Scattering processes, including the creation and annihilation of particles, are completely described by the S matrix of Heisenberg. It is shown that the elements of this matrix can be calculated, by a consistent use of perturbation theory, to any desired order in the fine-structure constant. Detailed rules are given for carrying out such calculations, and it is shown that divergences arising from higher order radiative corrections can be removed from the S matrix by a consistent use of the ideas of mass and charge renormalization.

Not considered in this paper are the problems of extending the treatment to include bound-state phenomena, and of proving the convergence of the theory as the order of perturbation itself tends to infinity.

I. INTRODUCTION

IN a previous paper[1] (to be referred to in what follows as I) the radiation theory of Tomonaga[2] and Schwinger[3] was applied in detail to the problem of the radiative corrections to the motion of a single electron in a given external field. It was shown that the rules of calculation for corrections of this kind were identical with those which had been derived by Feynman[4] from his own radiation theory. For the one-electron problem the radiative corrections were fully described by an operator H_T (Eq. (20) of I) which appeared as the "effective potential" acting upon the electron, after the interactions of the electron with its own self-field had been eliminated by a contact transformation. The difference between the Schwinger and Feynman theories lay only in the choice of a particular representation in which the matrix elements of H_T were calculated (Section V of I).

The present paper deals with the relation between the Schwinger and Feynman theories when the restriction to one-electron problems is removed. In these more general circumstances the two theories appear as complementary rather than identical. The Feynman method is essentially a set of rules for the calculation of the elements of the Heisenberg S matrix corresponding to any physical process, and can be applied with directness to all kinds of scattering problems.[5] The Schwinger method evaluates radiative corrections by exhibiting them as extra terms appearing in the Schrödinger equation of a system of particles and is suited especially to bound-state problems. In spite of the difference of principle, the two methods in practice involve the calculation of closely related expressions; moreover, the theory underlying them is in all cases the same. The systematic technique of Feynman, the exposition of which occupied the second half of I and occupies the major part of the present paper, is therefore now available for the evaluation not only of the S matrix but also of most of the operators occurring in the Schwinger theory.

The prominent part which the S matrix plays in this paper is due to its practical usefulness as the connecting link between the Feynman technique of calculation and the Hamiltonian formulation of quantum electrodynamics. This practical usefulness remains, whether or not one follows Heisenberg in believing that the S matrix may eventually replace the Hamiltonian altogether. It is still an unanswered question, whether the finiteness of the S matrix automatically implies the finiteness of all observable quantities, such as bound-state energy levels, optical transition probabilities, etc., occurring in electrodynamics. An affirmative answer to the question is in no way essential to the arguments of this paper. Even if a finite S matrix does not of itself imply finiteness of other observable quantities, it is probable that all such quantities will be finite; to verify this, it will be necessary to repeat the analysis of the present paper, keeping all the time closer to the original Schwinger theory than

[1] F. J. Dyson, Phys. Rev. **75**, 486 (1949).

[2] Sin-Itiro Tomonaga, Prog. Theor. Phys. **1**, 27 (1946); Koba, Tati, and Tomonaga, Prog. Theor. Phys. **2**, 101 (1947) and **2**, 198 (1947); S. Kanesawa and S. Tomonaga, Prog. Theor. Phys. **3**, 1 (1948) and **3**, 101 (1948); Sin-Itiro Tomonaga, Phys. Rev. **74**, 224 (1948); Ito, Koba, and Tomonaga, Prog. Theor. Phys. **3**, 276 (1948); Z. Koba and S. Tomonaga, Prog. Theor. Phys. **3**, 290 (1948).

[3] Julian Schwinger, Phys. Rev. **73**, 416 (1948); **74**, 1439 (1948); **75**, 651 (1949).

[4] Richard P. Feynman, Phys. Rev. **74**, 1430 (1948).

[5] The idea of using standard electrodynamics as a starting point for an explicit calculation of the S matrix has been previously developed by E. C. G. Stueckelberg, Helv. Phys. Acta, **14**, 51 (1941); **17**, 3 (1944); **18**, 195 (1945); **19**, 242 (1946); Nature, **153**, 143 (1944); Phys. Soc. Cambridge Conference Report, 199 (1947); E. C. G. Stueckelberg and D. Rivier, Phys. Rev. **74**, 218 (1948). Stueckelberg anticipated several features of the Feynman theory, in particular the use of the function D_F (in Stueckelberg's notation D^c) to represent retarded (i.e., causally transmitted) electromagnetic interactions. For a review of the earlier part of this work, see Gregor Wentzel, Rev. Mod. Phys. **19**, 1 (1947). The use of mass renormalization in scattering problems is due to H. W. Lewis, Phys. Rev. **73**, 173 (1948).

has here been possible. There is no reason for attributing a more fundamental significance to the S matrix than to other observable quantities, nor was it Heisenberg's intention to do so. In the last section of this paper, tentative suggestions are made for a synthesis of the Hamiltonian and Heisenberg philosophies.

II. THE FEYNMAN THEORY AS AN S MATRIX THEORY

The S matrix was originally defined by Heisenberg in terms of the stationary solutions of a scattering problem. A typical stationary solution is represented by a time-independent wave function Ψ' which has a part representing ingoing waves which are asymptotically of the form Ψ_1', and a part representing outgoing waves which are asymptotically of the form Ψ_2'. The S matrix is the transformation operator S with the property that

$$\Psi_2' = S\Psi_1' \tag{1}$$

for every stationary state Ψ'.

In Section III of I an operator $U(\infty)$ was defined and stated to be identical with the S matrix. Since $U(\infty)$ was defined in terms of time-dependent wave functions, a little care is needed in making the identification. In fact, the equation

$$\Psi_2 = U(\infty)\Psi_1 \tag{2}$$

held, where Ψ_1 and Ψ_2 were the asymptotic forms of the ingoing and outgoing parts of a wave function Ψ in the Ψ-representation of I (the "interaction representation" of Schwinger[3]). Now the time-independent wave function Ψ' corresponds to a time-dependent wave function

$$\exp[(-i/\hbar)Et]\Psi'$$

in the Schrödinger representation, where E is the total energy of the state; and this corresponds to a wave function in the interaction representation

$$\Psi = \exp[(+i/\hbar)t(H_0 - E)]\Psi', \tag{3}$$

where H_0 is the total free particle Hamiltonian. However, the asymptotic parts of the wave function Ψ', both ingoing and outgoing, represent freely traveling particles of total energy E, and are therefore eigenfunctions of H_0 with eigenvalue E. This implies, in virtue of (3), that the asymptotic parts Ψ_1 and Ψ_2 of Ψ are actually time-independent and equal, respectively, to Ψ_1' and Ψ_2'. Thus (1) and (2) are identical, and $U(\infty)$ is indeed the S matrix. Incidentally, $U(\infty)$ is also the "invariant collision operator" defined by Schwinger.[3]

There is a series expansion of $U(\infty)$ analogous to (32) of I, namely,

$$U(\infty) = \sum_{n=0}^{\infty} \left(\frac{-i}{\hbar c}\right)^n \frac{1}{n!} \int_{-\infty}^{\infty} dx_1 \cdots \int_{-\infty}^{\infty} dx_n \times P(H_1(x_1), \cdots, H_1(x_n)). \tag{4}$$

Here the P notation is as defined in Section V of I, and

$$H_1(x) = H^I(x) + H^e(x) \tag{5}$$

is the sum of the interaction energies of the electron field with the photon field and with the external potentials. The Feynman radiation theory provides a set of rules for the calculation of matrix elements of (4), between states composed of any number of ingoing and outgoing free particles. Also, quantities contained in (4) are the only ones with which the Feynman rules can deal directly. The Feynman theory is thus correctly characterized as an S matrix theory.

One particular way to analyze $U(\infty)$ is to use (5) to expand (4) in a series of terms of ascending order in H^e. Substitution from (5) into (4) gives

$$U(\infty) = \sum_{m=0}^{\infty} \sum_{n=0}^{\infty} \left(\frac{-i}{\hbar c}\right)^{m+n} \frac{1}{m!n!} \int_{-\infty}^{\infty} dx_1 \cdots \times \int_{-\infty}^{\infty} dx_{m+n} P(H^e(x_1), \cdots, H^e(x_m), \times H^I(x_{m+1}), \cdots, H^I(x_{m+n})). \tag{6}$$

In this double series, the term of zero order in H^e is $S(\infty)$, given by (32) of I. The term of first order is

$$U_1 = (-i/\hbar c) \int_{-\infty}^{\infty} H_F(x)dx, \tag{7}$$

where H_F is given by (31) of I. Clearly, $S(\infty)$ is the S matrix representing scattering of electrons and photons by each other in the absence of an external potential; U_1 is the S matrix representing the additional scattering produced by an external potential, when the external potential is treated in the first Born approximation; higher terms of the series (6) would correspond to treating the external potential in the second or higher Born approximation. The operator H_F played a prominent part in I, where it was in no way connected with a Born approximation; however, it was there introduced in a somewhat unnatural manner, and its physical meaning is made clearer by its appearance in (7). In fact, H_F may be defined by the statement that

$$(-i/\hbar)(\delta t)(\delta\omega)H_F(x)$$

is the contribution to the S matrix that would be produced by an external potential of strength H^e, acting for a small duration δt and over a small volume $\delta\omega$ in the neighborhood of the space-time point x.

The remainder of this section will be occupied with a statement of the Feynman rules for evaluating $U(\infty)$. Proofs will not be given, because the rules are only trivial generalizations of the rules

which were given in I for the evaluation of matrix elements of H_F corresponding to one-electron transitions.

In evaluating $U(\infty)$ we shall not make any distinction between the external and radiative parts of the electromagnetic field; this is physically reasonable since it is to some extent a matter of convention how much of the field in a given situation is to be regarded as "external." The interaction energy occurring in (4) is then

$$H_1(x) = -ieA_\mu(x)\bar{\psi}(x)\gamma_\mu\psi(x) - \delta mc^2\bar{\psi}(x)\psi(x), \quad (8)$$

where A_μ is the total electromagnetic field, and the term in δm is included in order to allow for the fact that the interaction representation is defined in terms of the total mass of an electron including its "electromagnetic mass" δm (see Section IV of I). The first step in the evaluation of $U(\infty)$ is to substitute from (8) into (4), writing out in full the suffixes of the operators $\bar{\psi}_\alpha$, ψ_β which are concealed in the matrix product notation of (8). After such a substitution, (4) becomes

$$U(\infty) = \sum_{n=0}^{\infty} J_n, \quad (9)$$

where J_n is an n-fold integral with an integrand which is a polynomial in $\bar{\psi}_\alpha$, ψ_β and A_μ operators.

The most general matrix element of J_n is obtained by allowing some of the $\bar{\psi}_\alpha$, ψ_β and A_μ operators to annihilate particles in the initial state, some to create particles in the final state, while others are associated in pairs to perform a successive creation and annihilation of intermediate particles. The operators which are not associated in pairs, and which are available for the real creation and annihilation of particles, are called "free"; a particular type of matrix element of J_n is specified by enumerating which of the operators in the integrand are to be free and which are to be associated in pairs. As described more fully in Section VII of I, each type of matrix element of J_n is uniquely represented by a "graph" G consisting of n points (bearing the labels $x_1, \cdots, x_n$) and various lines terminating at these points.

The relation between a type of matrix element of J_n and its graph G is as follows. For every associated pair of operators $(\bar{\psi}(x), \psi(y))$, there is a directed line (electron line) joining x to y in G. For every associated pair of operators $(A(x), A(y))$, there is an undirected line (photon line) joining x and y in G. For every free operator $\bar{\psi}(x)$, there is a directed line in G leading from x to the edge of the diagram. For every free operator $\psi(x)$, there is a directed line in G leading to x from the edge of the diagram. For every free operator $A(x)$, there is an undirected line in G leading from x to the edge of the diagram. Finally, for a particular type of matrix element of J_n it is specified that at each point x_i either the part of $H_1(x_i)$ containing $A_\mu(x_i)$ or the part containing δm is operating; correspondingly, at each vertex x_i of G there are either two electron lines (one ingoing and one outgoing) and one photon line, or else two electron lines only. Lines joining one point to itself are always forbidden.

In every graph G, the electron lines form a finite number m of open polygonal arcs with ends at the edge of the diagram, and perhaps in addition a number l of closed polygonal loops. The corresponding type of matrix element of J_n has m free operators $\bar{\psi}$ and m free operators ψ; the two end segments of any one open arc correspond to two free operators, one $\bar{\psi}$ and one ψ, which will be called a "free pair." The matrix elements of J_n are now to be calculated by means of an operator $J(G)$, which is defined for each graph G of n vertices, and which is obtained from J_n by making the following five alterations.

First, at each point x_i, $H_1(x_i)$ is to be replaced by either the first or the second term on the right of (8), as indicated by the presence or absence of a photon line at the vertex x_i of G. Second, for every electron line joining a vertex x to a vertex y in G, two operators $\bar{\psi}_\alpha(x)$ and $\psi_\beta(y)$ in J_n, regardless of their positions, are to be replaced by the function

$$\tfrac{1}{2}S_{F\beta\alpha}(x-y), \quad (10)$$

as defined by (44) and (45) of I. Third, for every photon line joining two vertices x and y of G, two operators $A_\mu(x)$ and $A_\nu(y)$ in J_n, regardless of their positions, are to be replaced by the function

$$\tfrac{1}{2}\hbar c\delta_{\mu\nu}D_F(x-y), \quad (11)$$

defined by (42) of I. Fourth, all free operators in J_n are to be left unaltered, but the ordering by the P notation is to be dropped, and the order of the free $\bar{\psi}$ and ψ operators is to be arranged so that the two members of each free pair stand consecutively and in the order $\bar{\psi}\psi$; the order of the free pairs among themselves, and of all free A_μ operators, is left arbitrary. Fifth, the whole expression J_n is to be multiplied by

$$(-1)^{n-l-m}. \quad (12)$$

The Feynman rules for the evaluation of $U(\infty)$ are essentially contained in the above definition of the operators $J(G)$. To each value of n correspond only a finite number of graphs G, and all possible matrix elements of $U(\infty)$ are obtained by substituting into (9) for each J_n the sum of all the corresponding $J(G)$. It is necessary only to specify how the matrix element of a given $J(G)$ corresponding to a given scattering process may be written down.

The matrix element of $J(G)$ for a given process may be obtained, broadly speaking, by replacing

each free operator in $J(G)$ by the wave function of the particle which it is supposed to create or annihilate. More specifically, each free $\bar{\psi}$ operator may either create an electron in the final state or annihilate a positron in the initial state, and the reverse processes are performed by a free ψ operator. Therefore, for a transition from a state involving A electrons and B positrons to a state involving C electrons and D positrons, only operators $J(G)$ containing $(A+D)=(B+C)$ free pairs contribute matrix elements. For each such $J(G)$, the $(A+D)$ free ψ operators are to be replaced in all possible combinations by the A initial electron wave functions and the D final positron wave functions, and the $(B+C)$ free $\bar{\psi}$ operators are to be similarly replaced by the initial positron and final electron wave functions, and the results of all such replacements added together, taking account of the antisymmetry of the total wave functions of the system in the individual particle wave functions. In the case of the free A_μ operators, the situation is rather different, since each such operator may either create a photon in the final state, or annihilate a photon in the initial state, or represent merely the external potential. Therefore, for a transition from a state with A photons to a state with B photons, any $J(G)$ with not less than $(A+B)$ free A_μ operators may give a matrix element. If the number of free A_μ operators in $J(G)$ is $(A+B+C)$, these operators are to be replaced in all possible combinations by the $(A+B)$ suitably normalized potentials corresponding to the initial and final photon states, and by the external potential taken C times, and the results of all such replacements added together, taking account now of the symmetry of the total wave functions in the individual photon states.

In practice cases are seldom likely to arise of scattering problems in which more than two similar particles are involved. The replacement of the free operators in $J(G)$ by wave functions can usually be carried out by inspection, and the enumeration of matrix-elements of $U(\infty)$ is practically complete as soon as the operators $J(G)$ have been written down.

The above rules for the calculation of $U(\infty)$ describe the state of affairs before any attempt has been made to identify and remove the various divergent parts of the expressions. In particular, contributions are included from all graphs G, even those which yield nothing but self-energy effects. For this reason, the rules here formulated are superficially different from those given for the one-electron problem in Section IX of I, which described the state of affairs after many divergencies had been removed. Needless to say, the rules are not complete until instructions have been supplied for the removal of all infinite quantities from the theory; in Sections V–VII of this paper it will be shown how the formal structure of the S matrix makes such a complete removal of infinities appear attainable.

Another essential limitation is introduced into the S matrix theory by the use of the expansion (4). All quantities discussed in this paper are expansions of this kind, in which it is assumed that not only the radiation interaction but also the external potential is small enough to be treated as a perturbation. It is well known that an expansion in powers of the external potential does not give a satisfactory approximation, either in problems involving bound states or in scattering problems at low energies. In particular, whenever a scattering problem allows the possibility of one of the incident particles being captured into a bound state, the capture process will not be represented in $U(\infty)$, since the initial and final states for processes described by $U(\infty)$ are always free-particle states. It is the expansion in powers of the external potential which breaks down when such a capture process is possible. Therefore it must be emphasized that the perturbation theory of this paper is applicable only to a restricted class of problems, and that in other situations the Schwinger theory will have to be used in its original form.

III. THE S MATRIX IN MOMENTUM SPACE

Both for practical applications to specific problems, and for general theoretical discussion, it is convenient to express the S matrix $U(\infty)$ in terms of momentum variables. For this purpose, it is enough to consider an expression which will be denoted by M, and which is a typical example of the units out of which all matrix elements of $U(\infty)$ are built up. A particular integer n and a particular graph G of n vertices being supposed fixed, the operator $J(G)$ is constructed as in the previous section, and M is defined as the number obtained by substituting for each of the free operators in $J(G)$ one particular free-particle wave function. More specifically, for each free operator $\psi(x)$ in $J(G)$ there is substituted

$$\psi(k)e^{ik_\mu x_\mu}, \tag{13}$$

where k_μ is some constant 4 vector representing the momentum and energy of an electron, or minus the momentum and energy of a positron, and where $\psi(k)$ is a constant spinor. For each free operator $\bar{\psi}(x)$ there is substituted

$$\bar{\psi}(k')e^{-ik_\mu' x_\mu}, \tag{14}$$

where $\bar{\psi}(k')$ is again a constant spinor. For each free operator $A_\mu(x)$ there is substituted

$$A_\mu(k'')e^{ik_\mu'' x_\mu}, \tag{15}$$

where $A_\mu(k'')$ is a constant 4 vector which may

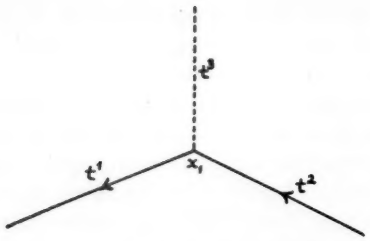

FIG. 1.

represent the polarization vector of a quantum whose momentum-energy 4-vector is either plus or minus k_μ''; alternatively, $A_\mu(k'')$ may represent the Fourier component of the external potential with a particular wave number and frequency specified by the 4 vector k''. There is no loss of generality in splitting up the external potential into Fourier components of the form (15). When the substitutions (13), (14), (15) are made in $J(G)$, the expression M which is obtained is still an n-fold integral over the whole of space-time, and in addition depends parametrically upon E constant 4 vectors in momentum-space, where E is the number of free operators in $J(G)$.

The graph G will contain E external lines, i.e., lines with one end at a vertex and the other end at the edge of the diagram. To each of these external lines corresponds one constant 4 vector, which may be denoted by $k_\mu{}^i$, $i=1, \cdots, E$, and one constant spinor or polarization vector appearing in M, either $\psi(k^i)$ or $\bar{\psi}(k^i)$ or $A_\mu(k^i)$.

Suppose that G contains F internal lines, i.e., lines with both ends at vertices. To each of these lines corresponds a D_F or an S_F function in M, as specified by (11) or (10). These functions have been expressed by Feynman as 4-dimensional Fourier integrals of very simple form, namely

$$D_F(x)=\frac{1}{4\pi^3}\int e^{-ip_\mu x_\mu}\delta_+(p^2)dp, \tag{16}$$

$$S_F(x)=\frac{1}{4\pi^3}\int e^{-ip_\mu x_\mu}[+ip_\mu\gamma_\mu-\kappa_0] \times\delta_+(p^2+\kappa_0^2)dp, \tag{17}$$

where κ_0 is the electron reciprocal Compton wavelength,

$$p^2=p_\mu p_\mu=p_1{}^2+p_2{}^2+p_3{}^2-p_0{}^2, \tag{18}$$

and the δ_+ function is defined by

$$\delta_+(a)=\tfrac{1}{2}\delta(a)+\frac{1}{2\pi ia}=\frac{1}{2\pi}\int_0^\infty e^{-iaz}dz. \tag{19}$$

Substituting from (16) and (17) into M will introduce an F-fold integral over momentum space. Corresponding to each internal line of G, there will appear in M a 4 vector variable of integration, which may be denoted by $p_\mu{}^i$, $i=1, \cdots, F$. However, after this substitution is made, the space-time variables $x_1, \cdots, x_n$ occur in M only in the exponential factors, and the integration over these variables can be performed. The result of the integration over x_j is to give

$$(2\pi)^4\delta(q_j), \tag{20}$$

where the δ represents a simple 4-dimensional Dirac δ-function, and q_j is a 4 vector formed by taking an algebraic sum of the k^i and p^i 4 vectors corresponding to those lines of G which meet at x_j. The factor (20) in the integrand of M expresses the conservation of energy and momentum in the interaction occurring at the point x_j.

The transformation of M into terms of momentum variables is now complete. To summarize the results, M now appears as an F-fold integral over the variable 4 vectors $p_\mu{}^i$ in momentum space. In the integrand there appear, besides numerical factors;

(i) a constant spinor or polarization-vector, $\psi(k^i)$ or $\bar{\psi}(k^i)$ or $A_\mu(k^i)$, corresponding to each external line of G;

(ii) a factor

$$D_F(p^i)=\delta_+((p^i)^2) \tag{21}$$

corresponding to each internal photon line of G;

(iii) a factor

$$S_F(p^i)=[+ip_\mu{}^i\gamma_\mu-\kappa_0]\delta_+((p^i)^2+\kappa_0^2) \tag{22}$$

corresponding to each internal electron line of G;

(iv) a factor

$$\delta(q_j) \tag{23}$$

corresponding to each vertex of G;

(v) a γ_μ operator, surviving from Eq. (8), corresponding to each vertex of G at which there is a photon line.

The important feature of the above analysis is that all the constituents of M are now localized and associated with individual lines and vertices in the graph G. It therefore becomes possible in an unambiguous manner to speak of "adding" or "subtracting" certain groups of factors in M, when G is modified by the addition or subtraction of certain lines and vertices. As an example of this method of analysis, we shall briefly discuss the treatment in the S matrix formalism of the "Lamb shift" and associated phenomena.

Suppose that a graph G, of any degree of complication, has a vertex x_1 at which two electron lines and a photon line meet. These three lines may be either internal or external, and the momentum 4 vectors associated with them in M may be either p^i or k^i; these 4 vectors are denoted by t^1, t^2, t^3 as indicated in Fig. 1. The factors in the integrand of

M arising from the vertex x_1 are

$$-ie\gamma_\mu(2\pi)^4\delta(t^1-t^2-t^3), \tag{24}$$

the two spinor indices of the γ_μ being available for matrix multiplication on both sides with the factors in M arising from the two electron lines at x_1.

Now suppose that G' is a graph identical with G, except that in the neighborhood of x_1 it is modified by the addition of two new vertices and three new lines, as indicated in Fig. 2. With the three new lines, which are all internal, are associated three 4 vector variables p^1, p^2, p^3, which occur as variables of integration in the expression M' formed from G' as M is from G. It can be proved, in view of Eqs. (21), (22), (23), that M' may be obtained from M simply by replacing the factor (24) in M by the expression

$$\begin{aligned}&-\frac{ie^3}{\hbar c}(2\pi)^3\int\int\int dp^1dp^2dp^3\\&\quad\delta(t^1-p^2+p^3)\delta(p^2-p^1-t^3)\delta(p^1-p^3-t^2)\\&\quad\gamma_\lambda(+ip_\rho{}^2\gamma_\rho-\kappa_0)\gamma_\mu(+ip_\sigma{}^1\gamma_\sigma-\kappa_0)\gamma_\lambda\\&\quad\delta_+((p^2)^2+\kappa_0{}^2)\delta_+((p^1)^2+\kappa_0{}^2)\delta_+((p^3)^2).\end{aligned} \tag{25}$$

(The factorial coefficients appearing in (4) are just compensated by the fact that the two new vertices of G' may be labelled x_i, x_j in $(n+1)(n+2)$ ways, where n is the number of vertices in G.) In (25), two of the 4-dimensional δ-functions can be eliminated at once by integration over p^1 and p^2, and the third then reduces to the δ-function occurring in (24). Therefore M' can be obtained from M by replacing the operator γ_μ in (24) by an operator

$$\begin{aligned}L_\mu&=L_\mu(t^1,t^2)\\&=2\alpha\int dp[\gamma_\lambda(+i(p_\rho+t_\rho{}^1)\gamma_\rho-\kappa_0)\gamma_\mu\\&\qquad\times(+i(p_\sigma+t_\sigma{}^2)\gamma_\sigma-\kappa_0)\gamma_\lambda]\\&\qquad\times\delta_+((p+t^1)^2+\kappa_0{}^2)\\&\qquad\times\delta_+((p+t^2)^2+\kappa_0{}^2)\delta_+(p^2).\end{aligned} \tag{26}$$

Here α is the fine-structure constant, $(e^2/4\pi\hbar c)$ in Heaviside units. The operator L_μ can without great difficulty be calculated explicitly as a function of the 4 vectors t^1 and t^2, by methods developed by Feynman.

In the special case when Fig. 1 represents the graph G in its entirety, M is a matrix element for the scattering of a single electron by an external potential. Figure 2 then represents G' in its entirety, and M' is a second-order radiative correction to the scattering of the electron. In this case then the operator L_μ gives rise to what may be called "Lamb shift and associated phenomena." However, the above analysis applies equally to an expression M which may occur anywhere among the matrix elements of $U(\infty)$, and may represent any physical process whatever involving electrons, positrons and photons. There will always appear in $U(\infty)$, together with M, terms M' representing second-order radiative corrections to the same process; one term M' arises from each vertex of G at which a photon line ends; and M' is always to be obtained from M by substituting for an operator γ_μ the same operator L_μ. Furthermore, some higher radiative corrections to M will be obtained by substituting L_μ for γ_μ independently at two or more of the vertices of G.

By a "vertex part" of any graph will be meant a connected part of the graph, consisting of vertices and internal lines only, which touches precisely two electron lines and one photon line belonging to the remainder of the graph. The central triangle of Fig. 2 is an example of such a part. In other words, a vertex part of a graph is a part which can be substituted for the single vertex of Fig. 1 and give a physically meaningful result. Now the argument, by which the replacement of Fig. 1 by Fig. 2 was shown to be equivalent to the replacement of γ_μ by L_μ, can be used also when a more complicated vertex part is substituted for the vertex in Fig. 1. If G is any graph with a vertex x_1 as shown in Fig. 1, and G' is obtained from G by substituting for x_1 any vertex part V, and if M and M' are elements of $U(\infty)$ formed analogously from G and G', then M' can be obtained from M by replacing an operator γ_μ by an operator

$$\Lambda_\mu=\Lambda_\mu(V,t^1,t^2), \tag{27}$$

dependent only on V and the 4 vectors t^1, t^2 and independent of G.

To summarize the results of this section, it has been shown that the S matrix formalism allows a wide variety of higher order radiative processes to be calculated in the form of operators in momentum space. Such operators appear as radiative corrections to the fundamental interaction between the photon and electron-positron fields, and need only to be calculated once to be applicable to the various special problems of electrodynamics.

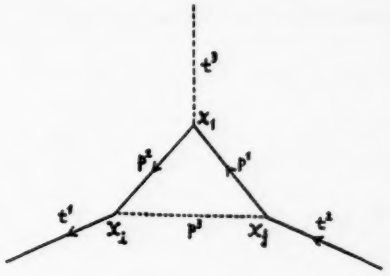

FIG. 2.

IV. FURTHER REDUCTION OF THE S MATRIX

It was shown in Section VII of I that, for the one-electron processes there considered, only connected graphs needed to be taken into account. In constructing the S matrix in general, this is no longer the case; disconnected graphs give matrix elements of $U(\infty)$ representing two or more collision processes occurring simultaneously among separate groups of particles, and such processes have physical reality. It is only permissable to omit a disconnected graph when one of its connected components is entirely lacking in external lines; such a component without external lines will give rise only to a constant multiplicative phase factor in every matrix element of $U(\infty)$ and is therefore devoid of physical significance.

On the other hand, the treatment in Section VII of I of graphs with "self-energy parts" applies almost without change to the general S matrix formalism. A "self-energy part" of a graph is a connected part, consisting of vertices and internal lines only, which can be inserted into the middle of a single line of a graph G so as to give a meaningful graph G'. In Fig. 3 is shown an example of such an insertion made in one of the lines of Fig. 1. Let M and M' be expressions derived in the manner of the previous section from the graphs G and G' of which parts are shown in Figs. 1 and 3. Suppose for definiteness that the line labelled t^1 is an internal line of G; then according to (22) it will contribute a factor $S_F(t^1)$ in M. By an argument similar to that leading to (26), it can be shown that M' may now be obtained from M by replacing $S_F(t^1)$ by

$$S_F(t^1)N(t^1)S_F(t^1)$$

$$=S_F(t^1)2\alpha\int dp[\gamma_\lambda(+i\gamma_\rho(p_\rho+t_\rho^1)-\kappa_0)\gamma_\lambda]$$

$$\times\delta_+((p+t^1)^2+\kappa_0^2)\delta_+(p^2)S_F(t^1). \quad (28)$$

In the same way, if G' were obtained from G by inserting in the t^1 line any self-energy part W, then M' would be obtained from M by replacing $S_F(t^1)$ by

$$S_F(t^1)\Sigma(W,t^1)S_F(t^1), \quad (29)$$

where Σ is an operator dependent only on W and t^1 and not on G. Moreover, if the t^1 line were an external line of G, then M' would be obtained from M by replacing a factor $\bar{\psi}(t^1)$ by

$$\bar{\psi}(t^1)\Sigma(W,t^1)S_F(t^1). \quad (30)$$

As a special case, W may consist of a single point; then at this point it is the term in δm of the interaction (8) which is operating, and Σ reduces to a constant,

$$\Sigma(W,t^1)=-2\pi i(\delta mc/\hbar)=-2\pi i\delta\kappa_0. \quad (31)$$

The operator $N(t^1)$ in (28) describes in a general way the second-order contribution to the electron self-energy and to the phenomenon called "vacuum polarization of the second kind" in Section VIII of I. The self-energy contribution is supposed to be cancelled by (31); the constant $\delta\kappa_0$ being a power series in α, the linear term only is required to cancel the self-energy part of (28), and the higher terms are available for the cancellation of self-energy effects from operators $\Sigma(W,t^1)$ of higher order. The S matrix formalism makes clear the important fact that, since the operators $\Sigma(W,t^1)$ are universal operators independent of the graph G, the electron self-energy effects will be formally cancelled by a constant $\delta\kappa_0$ independent of the physical situation in which the effects occur.

When a self-energy part W' is inserted into a photon line of a graph G, for example the line labelled t^3 in Fig. 1, then the modification produced in M may be again described by a function $\Pi(W',t^3)$ independent of G. Specifically, if the t^3 line in G is internal, M' is obtained from M by replacing a factor $D_F(t^3)$ by

$$D_F(t^3)\Pi(W',t^3)D_F(t^3). \quad (32)$$

If the t^3 line is external, the replacement is of a factor $A_\mu(t^3)$ by

$$A_\mu(t^3)\Pi(W',t^3)D_F(t^3). \quad (33)$$

In addition to terms of the form (33), there will appear terms such as

$$A_\nu(t^3)t_\nu^3t_\mu^3\Pi'(W',t^3)D_F(t^3); \quad (34)$$

these however are zero in consequence of the gauge condition satisfied by A_ν. Similar terms in $t_\nu^3t_\mu^3$ will also appear with the expression (32); in this case the extra terms can be shown to vanish in consequence of the equation of conservation of charge satisfied by the electron-positron field. The functions $\Pi(W',t^3)$ describe the phenomenon of photon self-energy and the "vacuum polarization of the first kind" of Section VIII of I. Following Schwinger, one does not explicitly subtract away the divergent photon self-energy effects from the $\Pi(W',t^3)$, but one asserts that these effects are zero as a consequence of the gauge invariance of electrodynamics.

In Section VII of I, it was shown how self-energy parts could be systematically eliminated from all

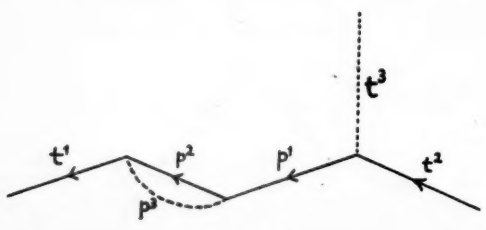

FIG. 3.

graphs, and their effects described by suitably modifying the functions D_F and S_F. The analysis was carried out in configuration space, and was confined to the one-electron problem. We are now in a position to extend this method to the whole S matrix formalism, working in momentum space, and furthermore to eliminate not only self-energy parts but also the "vertex parts" defined in the last section.

Every graph G has a uniquely defined "skeleton" G_0, which is the graph obtained by omitting all self-energy parts and vertex parts from G. A graph which is its own skeleton is called "irreducible;" all of its vertices will be of the kind depicted in Fig. 1. From every irreducible G_0, the G of which it is the skeleton can be built by inserting pieces in all possible ways at all vertices and lines of G_0; these G form a well-defined class Γ. The term "proper vertex part" must here be introduced, denoting a vertex part which is not divisible into two pieces joined only by a single line; thus a vertex part which is not proper is essentially redundant, being a proper vertex part plus one or more self-energy parts. The graphs of Γ are then accurately enumerated by inserting at some or all of the vertices of G_0 a proper vertex part, and in some or all of the lines a self-energy part, these insertions being made independently in all possible combinations.

Suppose that M is a constituent of a matrix element of $U(\infty)$, obtained from G_0 as described in Section III. Then every graph G in Γ will yield additional contributions to the same matrix element of $U(\infty)$; the sum of all such contributions, including M, is denoted by M_S. As a result of the analysis leading to (27), (29), and (32), and in view of the statistical independence of the insertions made at the different vertices and lines of G_0, the sum M_S will be obtained from M by the following substitutions. For every internal electron line of G_0, a factor $S_F(p^i)$ of M is replaced by

$$S_F'(p^i)=S_F(p^i)+S_F(p^i)\Sigma(p^i)S_F(p^i), \quad (35)$$

where $\Sigma(p^i)$ is the sum of the $\Sigma(W, p^i)$ over all electron self-energy parts W. For every internal photon line, a factor $D_F(p^i)$ is replaced by

$$D_F'(p^i)=D_F(p^i)+D_F(p^i)\Pi(p^i)D_F(p^i), \quad (36)$$

where $\Pi(p^i)$ is the sum of the $\Pi(W', p^i)$ over all photon self-energy parts W'. For every external line, a factor $\psi(k^i)$ or $\bar{\psi}(k^i)$ or $A_\mu(k^i)$ is replaced by

$$\begin{aligned}\psi'(k^i)&=S_F(k^i)\Sigma(k^i)\psi(k^i)+\psi(k^i),\\ \bar{\psi}'(k^i)&=\bar{\psi}(k^i)\Sigma(k^i)S_F(k^i)+\bar{\psi}(k^i),\\ A_\mu'(k^i)&=A_\mu(k^i)\Pi(k^i)D_F(k^i)+A_\mu(k^i),\end{aligned} \quad (37)$$

respectively. For every vertex of G_0, where the incident lines carry momentum variables as shown in Fig. 1, an operator γ_μ is replaced by

$$\Gamma_\mu(t^1, t^2)=\gamma_\mu+\Lambda_\mu(t^1, t^2), \quad (38)$$

where $\Lambda_\mu(t^1, t^2)$ is the sum of the $\Lambda_\mu(V, t^1, t^2)$ over all proper vertex parts V. The matrix elements of $U(\infty)$ will be correctly calculated, if one includes contributions only from irreducible graphs, after making in each contribution the replacements (35), (36), (37), (38).

To calculate the operators Λ_μ, Σ and Π, it is necessary to write down explicitly the integrals in momentum space, examples being (26) and (28), corresponding to every self-energy part W or proper vertex part V. When considering effects of higher order than the second, the parts W and V will themselves often be reducible, containing in their interior self-energy and vertex parts. It will again be convenient to omit such reducible V and W, and to include their effects by making the substitutions (35)–(38) in the integrals corresponding to irreducible V and W. In this way one obtains in general not explicit formulas, but integral equations, for Λ_μ, Σ and Π. For example,

$$\Lambda_\mu=\alpha I_\mu(\Lambda, \Sigma, \Pi) \quad (39)$$

where I_μ is an integral in which Λ_μ, Σ and Π occur explicitly. Fortunately, the appearance of α on the right side of (39) makes it easy to solve such equations by a process of successive substitution, the forms of Λ_μ, Σ, and Π being obtained correct to order α^n when values correct to order α^{n-1} are substituted into the integrals.

The functions D_F' and S_F' of (35) and (36) are the Fourier transforms of the corresponding functions in I. The interpretation of these functions in Section VIII of I can be extended in an obvious way to include the operator Γ_μ. Since $\bar{\psi}\gamma_\mu\psi$ is the charge-current 4 vector of an electron without radiative corrections, $\bar{\psi}\Gamma_\mu\psi$ may be interpreted as an "effective current" carried by an electron, including the effects of exchange interactions between the electron and the electron-positron field around it.

An additional reduction in the number of graphs effectively contributing to $U(\infty)$ is obtained from a theorem of Furry.[6] The theorem was shown by Feynman to be an elegant consequence of his theory. In any graph G, a "closed loop" is a closed electron polygon, at the vertices of which a number p of photon lines originate; the loop is called odd or even according to the parity of p. If G contains a closed loop, then there will be another graph $\bar{G}$ also contributing to $U(\infty)$, obtained from G by reversing the sense of the electron lines in the loop. Now if M and $\bar{M}$ are contributions from G and $\bar{G}$, $\bar{M}$ is derived from M by interchanging the roles of electron and positron states in each of the interactions at the vertices of the loop; such an interchange is called "charge conjugation." It was shown by Schwinger that his theory is invariant under charge

[6] Wendell H. Furry, Phys. Rev. 51, 125 (1937).

conjugation, provided that the sign of e is at the same time reversed (this is the well-known charge symmetry of the Dirac hole theory). It is clear from (8) that the constant e appears once in M for each of the p loop vertices at which there is a photon line; at the remaining vertices only the constant δm is involved, and δm is an even function of e. Therefore the principle of charge-symmetry implies

$$\bar{M}=(-1)^p M. \tag{40}$$

Taking p odd in (40) gives Furry's theorem; all contributions to $U(\infty)$ from graphs with one or more odd closed loops vanish identically.

By an "odd part" of a graph is meant any part, consisting only of vertices and internal lines, which touches no electron lines, and only an odd number of photon lines, belonging to the rest of the graph. The simplest type of odd part which can occur is a single odd closed loop. Conversely, it is easy to see that every odd part must include within itself at least one odd closed loop. Therefore, Furry's theorem allows all graphs with odd parts to be omitted from consideration in calculating $U(\infty)$.

V. INVESTIGATION OF DIVERGENCES IN THE S MATRIX

The δ_+ function defined by (19) has the property that, if b is real and $f(a)$ is any function analytic in the neighborhood of b, then

$$\int f(a)\delta_+(a-b)da=(1/2\pi i)\int f(a)(1/(a-b))da, \tag{41}$$

where the first integral is along a stretch of the real axis including b, and the second integral is along the same stretch of the real axis but with a small detour into the complex plane passing underneath b. In the matrix elements of $U(\infty)$ there appear integrals of the form

$$\int dpF(p)\delta_+(p_1^2+p_2^2+p_3^2-p_0^2+c^2), \tag{42}$$

integrated over all real values of p_1, p_2, p_3, p_0. By (41), one may write (42) in the form

$$\frac{1}{2\pi i}\int dp\frac{F(p)}{(p_1^2+p_2^2+p_3^2-p_0^2+c^2)}, \tag{43}$$

in which it is understood that the integration is along the real axis for the variables p_1, p_2, p_3, and for p_0 is along the real axis with two small detours, one passing above the point $+(p_1^2+p_2^2+p_3^2+c^2)^{\frac{1}{2}}$, and one passing below the point $-(p_1^2+p_2^2+p_3^2+c^2)^{\frac{1}{2}}$. To equate (42) with (43) is certainly correct, when $F(p)$ is analytic at the critical values of p_0. In practice one has to deal with integrals (42) in which $F(p)$ itself involves δ_+ functions (see for example (26) and (28)); in these cases it is legitimate to replace each δ_+ function by a reciprocal, making a separate detour in the p_0 integration for each pole in the integrand, provided that no two poles coincide. Thus every constituent part M of $U(\infty)$ can be written as an integral of a rational algebraic function of momentum variables, by using instead of (21) and (22)

$$D_F(p^i)=\frac{1}{2\pi i(p^i)^2}, \tag{44}$$

$$S_F(p^i)=\frac{(ip_\mu{}^i\gamma_\mu-\kappa_0)}{2\pi i((p^i)^2+\kappa_0{}^2)}. \tag{45}$$

This representation of D_F and S_F as rational functions in momentum-space has been developed and extensively used by Feynman (unpublished).

There may appear in M infinities of three distinct kinds. These are (i) singularities caused by the coincidence of two or more poles of the integrand, (ii) divergences at small momenta caused by a factor (44) in the integrand, (iii) divergences at large momenta due to insufficiently rapid decrease of the whole integrand at infinity.

In this paper no attempt will be made to explore the singularities of type (i). Such singularities occur, for example, when a many-particle scattering process may for special values of the particle momenta be divided into independent processes involving separate groups of particles. It is probable that all singularities of type (i) have a similarly clear physical meaning; these singularities have long been known in the form of vanishing energy denominators in ordinary perturbation theory, and have never caused any serious trouble.

A divergence of type (ii) is the so-called "infra-red catastrophe," and is well known to be caused by the failure of an expansion in powers of α to describe correctly the radiation of low momentum quanta. It would presumably be possible to eliminate this divergence from the theory by a suitable adaptation of the standard Bloch-Nordsieck[7] treatment; we shall not do this here. From a practical point of view, one may avoid the difficulty by arbitrarily writing instead of (44)

$$D_F(p^i)=\frac{1}{2\pi i((p^i)^2+\lambda^2)}, \tag{46}$$

where λ is some non-zero momentum, smaller than any of the quantum momenta which are significant in the particular process under discussion.[8]

[7] F. Bloch and A. Nordsieck, Phys. Rev. **52**, 54 (1937).

[8] The device of introducing λ in order to avoid infra-red divergences must be used with circumspection. Schwinger (unpublished) has shown that a long standing discrepancy between two alternative calculations of the Lamb shift was due to careless use of λ in one of them.

It is the divergences of type (iii) which have always been the main obstacle to the construction of a consistent quantum electrodynamics, and which it is the purpose of the present theory to eliminate. In the following pages, attention will be confined to type (iii) divergences; when the word "convergent" is used, the proviso "except for possible singularities of types (i) and (ii)" should always be understood.

A divergent M is called "primitive" if, whenever one of the momentum 4 vectors in its integrand is held fixed, the integration over the remaining variables is convergent. Correspondingly, a primitive divergent graph is a connected graph G giving rise to divergent M, but such that, if any internal line is removed and replaced by two external lines, the modified G gives convergent M. To analyze the divergences of the theory, it is sufficient to enumerate the primitive divergent M and G and to examine their properties.

Let G be a primitive divergent graph, with n vertices, E external and F internal lines. A corresponding M will be an integral over F variable p^i of a product of F factors (44) and (45) and n factors (23). Since G is connected, the δ-functions (23) in the integrand enable $(n-1)$ of the variables p^i to be expressed in terms of the remaining $(F-n+1)$ p^i and the constants k^i, leaving one δ-function involving the k^i only and expressing conservation of momentum and energy for the whole system. An example of such integration over the δ-functions was the derivation of (26) from (25). After this, the integrations in M may be arranged as follows; the fourth components of the $(F-n+1)$ independent p^i are written

$$p_4{}^i = ip_0{}^i = i\alpha\pi_0{}^i, \tag{47}$$

and the integration over α is performed first; subsequently, integration is carried out over the $3(F-n+1)$ independent $p_1{}^i$, $p_2{}^i$, $p_3{}^i$, and over the $(F-n)$ ratios of the $\pi_0{}^i$. M then has the form

$$M = \int dp_1{}^i dp_2{}^i dp_3{}^i d\pi_0{}^i \int_{-\infty}^{\infty} R\alpha^{F-n} d\alpha, \tag{48}$$

where R is a rational function of α, the denominator of which is a product of F factors

$$(p_1{}^i)^2+(p_2{}^i)^2+(p_3{}^i)^2+\mu^2-(\alpha\pi_0{}^i+c^i)^2. \tag{49}$$

Here the constants $\pi_0{}^i$, c^i are defined by the condition that

$$p_4{}^j = ip_0{}^j = i(\alpha\pi_0{}^j+c^j), \quad j=1, 2, \cdots, F. \tag{50}$$

Thus the c^i corresponding to the $(F-n+1)$ independent p^i are zero by (47), and the remainder are linear combinations of the k^i; also $(n-1)$ of the $\pi_0{}^i$ are linear combinations of the independent $\pi_0{}^i$ defined in (47). In view of (43), we take the integration variables in (48) to be real variables, with the exception of α which is to be integrated along a contour C deviating from the real axis at each of the $2F$ poles of R. As a general rule, C will detour above the real axis for $\alpha>0$, and below it for $\alpha<0$; the reverse will only occur at certain of the poles corresponding to denominators (49) for which

$$(p_1{}^i)^2+(p_2{}^i)^2+(p_3{}^i)^2+\mu^2 \leqslant (c^i)^2. \tag{51}$$

Such poles will be called "displaced." The integration over α alone will always be absolutely convergent. Therefore the contour C may be rotated in a counter-clockwise direction until it lies along the imaginary axis, and the value of M will be unchanged except for residues at the displaced poles.

Regarded as a function of the parameters k^i describing the incoming and outgoing particles, M will have a complicated behavior; the behavior will change abruptly whenever one of the c^i has a critical value for which (51) begins to be soluble for $p_1{}^i$, $p_2{}^i$, $p_3{}^i$, and a new displaced pole comes into existence. This behavior is explained by observing that displaced poles appear whenever there is sufficient energy available for one of the virtual particles involved in M to be actually emitted as a real particle. It is to be expected that the behavior of M should change when the process described by M begins to be in competition with other real processes. It is a feature of standard perturbation theory, that when a process A involves an intermediate state I which is variable over a continuous range, and in this range occurs a state II which is the final state of a competing process, then the matrix element for A involves an integral over I which has a singularity at the position II. In standard perturbation theory, this improper integral is always to be evaluated as a Cauchy principal value, and does not introduce any real divergence into the matrix element. In the theory of the present paper, the displaced poles give rise to similar improper integrals; these come under the heading of singularities of type (i) and will not be discussed further.

If $p_1{}^i$, $p_2{}^i$, $p_3{}^i$ satisfying (51) are held fixed, then the value of $p_4{}^i$ at the corresponding displaced pole is fixed by (50). The contribution to M from the displaced pole is just the expression obtained by holding the 4-vector p^i fixed in the original integral M, apart from bounded factors; since M is primitive divergent, this expression is convergent. The total contribution to M from the i'th displaced pole is the integral of this expression over the finite sphere (51) and is therefore finite. Strictly speaking, this argument requires not only the convergence of the expression, but uniform convergence in a finite region; however, it will be seen that the convergent integrals in this theory are convergent for large

momenta by virtue of a sufficient preponderance of large denominators, and convergence produced in this way will always be uniform in a finite region.

M is thus, apart from finite parts, equal to the integral M' obtained by replacing α by $i\alpha$ in (48) and (49). Alternatively, M' is obtained from the original integral M by substituting for each $p_0{}^j$

$$ip_4{}^j+(1-i)c^j, \tag{52}$$

and then treating the $4(F-n+1)$ independent $p_\mu{}^j$, $\mu=1, 2, 3, 4$, as ordinary real variables. In M' the denominators of the integrand take the form

$$(p_1{}^i)^2+(p_2{}^i)^2+(p_3{}^i)^2+\mu^2+(p_4{}^i-(1+i)c^i)^2, \tag{53}$$

and are uniformly large for large values of $p_\mu{}^i$. The convergence of M' can now be estimated simply by counting powers of $p_\mu{}^i$ in numerator and denominator of the integrand. Since M' is known to converge whenever one of the p^i is held fixed and integration is carried out over the others, the convergence of the whole expression is assured provided that

$$K=2F-F_e-4[F-n+1]\geqslant 1. \tag{54}$$

Here $2F$ is the degree of the denominator, and F_e that of the numerator, which is by (44) and (45) equal to the number of internal electron lines in G. Let E_e and E_p be the numbers of external electron and photon lines in G, and let n_s be the number of vertices without photon lines incident. It follows from the structure of G that

$$2F=3n-n_s-E_e-E_p,$$
$$F_e=n-\tfrac{1}{2}E_e,$$

and so the convergence condition (52) is

$$K=\tfrac{3}{2}E_e+E_p+n_s-4\geqslant 1. \tag{55}$$

This gives the vital information that the only possible primitive divergent graphs are those with $E_e=2$, $E_p=0, 1$, and with $E_e=0$, $E_p=1, 2, 3, 4$. Further, the cases $E_e=0$, $E_p=1, 3$, do not arise, since these give graphs with odd parts which were shown to be harmless in Section IV. It should be observed that the course of the argument has been "if E_e and E_p do not have certain small values, then the integral M is convergent at infinity;" there is no objection to changing the order of integrations in M as was done in (48), since the argument requires that this be done only in cases when M is, in fact, absolutely convergent.

The possible primitive divergent graphs that have been found are all of a kind familiar to physicists. The case $E_e=2$, $E_p=0$ describes self-energy effects of a single electron; $E_e=0$, $E_p=2$ self-energy effects of a single photon; $E_e=2$, $E_p=1$ the scattering of a single electron in an electromagnetic field; and $E_e=0$, $E_p=4$ the "scattering of light by light" or the mutual scattering of two photons. Further, (55) shows that the divergence will never be more than logarithmic in the third and fourth cases, more than linear in the first, or more than quadratic in the second. Thus it appears that, however far quantum electrodynamics is developed in the discussion of many-particle interactions and higher order phenomena, no essentially new kinds of divergence will be encountered. This gives strong support to the view that "subtraction physics," of the kind used by Schwinger and Feynman, will be enough to make quantum electrodynamics into a consistent theory.

VI. SEPARATION OF DIVERGENCES IN THE S MATRIX

First it will be shown that the "scattering of light by light" does not in fact introduce any divergence into the theory. The possible primitive divergent M in the case $E_e=0$, $E_p=4$ will be of the form

$$\delta(k^1+k^2+k^3+k^4)A_\lambda(k^1)A_\mu(k^2)A_\nu(k^3)A_\rho(k^4)I_{\lambda\mu\nu\rho}, \tag{56}$$

where $I_{\lambda\mu\nu\rho}$ is an integral of the type

$$\int R_{\lambda\mu\nu\rho}(k^1, k^2, k^3, k^4, p^i)dp^i, \tag{57}$$

at most logarithmically divergent, and R is a certain rational function of the constant k^i and the variable p^i. In any physical situation where, for example, the $A(k)$ are the potentials corresponding to particular incident and outgoing photons, there will appear in $U(\infty)$ a matrix element which is the sum of (56) and the 23 similar expressions obtained by permuting the suffixes of $I_{\lambda\mu\nu\rho}$ in all possible ways. It may therefore be supposed that at the start $R_{\lambda\mu\nu\rho}$ has been symmetrized by summation over all permutations of suffixes; (56) is then a sum of contributions from 24 or fewer (according to the degree of symmetry existing) graphs G.

If, under the sign of integration in (57), the value $R(0)$ of R for $k^1=k^2=k^3=k^4=0$ is subtracted from R, the integrand acquires one extra power of $|p_\mu{}^i|^{-1}$ for large $|p_\mu{}^i|$, and the integral becomes absolutely convergent at infinity. Therefore

$$I_{\lambda\mu\nu\rho}=I_{\lambda\mu\nu\rho}(0)+J_{\lambda\mu\nu\rho}, \tag{58}$$

where $I(0)$ is a possibly divergent integral independent of the k^i, and J is a convergent integral vanishing when all k^i's are zero. To interpret this result physically, it is convenient to write (56) again in terms of space-time variables; this gives

$$M=\int I_{\lambda\mu\nu\rho}(0)A_\lambda(x)A_\mu(x)A_\nu(x)A_\rho(x)dx+N, \tag{59}$$

where N is a convergent expression involving derivatives of the $A(x)$ with respect to space and

time. Now the first term in (59) is physically inadmissable; it is not gauge-invariant, and implies for example a scattering of light by an electric field depending on the absolute magnitude of the scalar potential, which has no physical meaning. Therefore $I(0)$ must vanish identically, and the whole expression (56) is convergent.

The fact that the scattering of light by light is finite in the lowest order in which it occurs has long been known.[9] It has also been verified by Feynman by direct calculation, using his own theory as described in this paper. The graphs which give rise to the lowest order scattering are shown in Fig. 4. It is found that the divergent parts of the corresponding M exactly cancel when the three contributions are added, or, what comes to the same thing, when the function $R_{\lambda\mu\nu\rho}$ is symmetrized. It is probable that the absence of divergence in the scattering of light by light is in all cases due to a similar cancellation, and it should not be difficult to prove this by calculation and thus avoid making an appeal to gauge-invariance.

The three remaining types of primitive divergent M are, in fact, divergent. However, these are just the expressions which have been studied in Sections III and IV and shown to be completely described by the operators Λ_μ, Σ, and Π. More specifically, when $E_e=2$, $E_p=0$, M will be of the form

$$\bar{\psi}(k^1)\Sigma(W, k^1)\psi(k^1), \tag{60}$$

where W is some electron self-energy part of a graph. When $E_e=0$, $E_p=2$, M will be

$$A_\mu(k^1)\Pi(W', k^1)A_\mu(k^1), \tag{61}$$

with W' some photon self-energy part. When $E_e=2$, $E_p=1$, M will be

$$\bar{\psi}(k^1)\Lambda_\mu(V, k^1, k^2)\psi(k^2)A_\mu(k^1-k^2), \tag{62}$$

with V some vertex part. Therefore, if some means can be found for isolating and removing the divergent parts from Λ_μ, Σ, and Π, the "irreducible" graphs defined in Section IV will not introduce any fresh divergences into the theory, and the rules of Section IV will lead to a divergence-free S matrix.

In considering Λ_μ, Σ, and Π in Section IV it was found convenient to divide vertex and self-energy parts themselves into the categories reducible and irreducible. An irreducible self-energy part W is required not only to have no vertex and self-energy parts inside itself; it is also required to be "proper," that is to say, it is not to be divisible into two pieces joined by a single line. In Section IV it was shown that to avoid redundancy the operator Λ_μ should be defined as a sum over proper vertex parts V only. By the same argument, in order to make (35), (36), (37) correct, it is essential to define Σ and Π as sums over both proper and improper self-energy parts. However, it is possible to define S_F' and D_F' in terms of proper self-energy parts only, at the cost of replacing the explicit definitions (35), (36) by implicit definitions. Let $\Sigma^*(p^i)$ be defined as the sum of the $\Sigma(W, p^i)$ over proper electron self-energy parts W, and let $\Pi^*(p^i)$ be defined similarly. Every W is either proper, or else it is a proper W joined by a single electron line to another self-energy part which may be proper or improper. Therefore, using (35), S_F' may be expressed in the two equivalent forms

$$\begin{aligned} S_F'(p^i) &= S_F(p^i)+S_F(p^i)\Sigma^*(p^i)S_F'(p^i) \\ &= S_F(p^i)+S_F'(p^i)\Sigma^*(p^i)S_F(p^i). \end{aligned} \tag{63}$$

Similarly,

$$\begin{aligned} D_F'(p^i) &= D_F(p^i)+D_F(p^i)\Pi^*(p^i)D_F'(p^i) \\ &= D_F(p^i)+D_F'(p^i)\Pi^*(p^i)D_F(p^i). \end{aligned} \tag{64}$$

It is sometimes convenient to work with the Σ and Π in the starred form, and sometimes in the unstarred form.

Consider the contribution $\Sigma(W, t^1)$ to the operator Σ^*, arising from an electron self-energy part W. It is supposed that W is irreducible, and the effects of possible insertions of self-energy and vertex parts inside W are for the time being neglected. Also it is supposed that W is not a single point, of which the contribution is given by (31). Then W has an even number $2l$ of vertices, at each of which a photon line is incident; and $\Sigma(W, t^1)$ will be of the form

$$e^{2l}\int R(t^1, p^i)dp^i, \tag{65}$$

where R is a certain rational function of the t^1 and p^i, and the integral is at most linearly divergent. The integrand in (65) is now written in the form

$$\begin{aligned} R(t^1, p^i) &= R(0, p^i) \\ &\quad + t_\mu^1\left(\frac{\partial R}{\partial t_\mu^1}(0, p^i)\right)+R_c(t^1, p^i), \end{aligned} \tag{66}$$

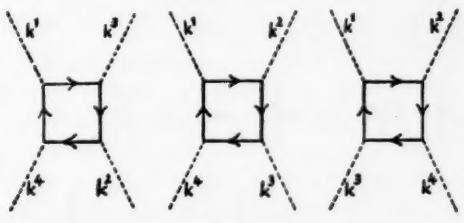

FIG. 4.

[9] H. Euler and B. Kockel, Naturwiss. **23**, 246 (1935); H. Euler, Ann. d. Phys. **26**, 398 (1936). In these early calculations of the scattering of light by light, the theory used is the Heisenberg electrodynamics, in which certain singularities are eliminated at the start by a procedure involving non-diagonal elements of the Dirac density matrix. In Feynman's calculation, on the other hand, a finite result is obtained without subtractions of any kind.

and for large values of the $|p_\mu{}^i|$ the remainder term R_c will tend to zero more rapidly by two powers of $|p_\mu{}^i|$ than R. Therefore, in complete analogy with (58),

$$\Sigma(W, t^1)=e^{2I}[A+B_\mu t_\mu{}^1+\Sigma_c(W, t^1)], \quad (67)$$

where A and B_μ are constant divergent operators, and $\Sigma_c(W, t^1)$ is defined by a covariant and absolutely convergent integral. $\Sigma_c(W, t^1)$ must, on grounds of covariance, be of the form

$$R_1((t^1)^2)+R_2((t^1)^2)t_\mu{}^1\gamma_\mu \quad (68)$$

with R_1 and R_2 particular functions of $(t^1)^2$; for the same reason, B_μ must be of the form $B\gamma_\mu$ with B a certain divergent integral. Now if t^1 happens to be the momentum-energy 4 vector of a free electron,

$$(t^1)^2=-\kappa_0{}^2, \quad t_\mu{}^1\gamma_\mu=i\kappa_0. \quad (69)$$

It is convenient to write

$$\Sigma_c(W, t^1)=A'+B'(t_\mu{}^1\gamma_\mu-i\kappa_0)+(t_\mu{}^1\gamma_\mu-i\kappa_0)S(W, t^1), \quad (70)$$

where $S(W, t^1)$ is zero for t^1 satisfying (69), and to include the first two terms in the constants A and B of (67); since all terms in (70) are finite, the separation of $S(W, t^1)$ is without ambiguity. Thus an equation of the form (67) is obtained, with

$$\Sigma_c(W, t^1)=(t_\mu{}^1\gamma_\mu-i\kappa_0)S(W, t^1). \quad (71)$$

Summing (67) over all irreducible W and including (31), gives for the operator Σ^*,

$$\Sigma^*(t^1)=A-2\pi i\delta\kappa_0+B(t_\mu{}^1\gamma_\mu-i\kappa_0)+(t_\mu{}^1\gamma_\mu-i\kappa_0)S_c(t^1). \quad (72)$$

Hence by (63) and (45)

$$S_F'(t^1)=(A-2\pi i\delta\kappa_0)S_F(t^1)S_F'(t^1)+\frac{1}{2\pi}BS_F'(t^1)+S_F(t^1)+\frac{1}{2\pi}S_c(t^1)S_F'(t^1). \quad (73)$$

In (72) and (73), A and B are infinite constants, and S_c a divergence-free operator which is zero when (69) holds; A, B, and S_c are power series in e starting with a term in e^2. In (72) and (73), however, effects of higher order corrections to the $\Sigma(W, t^1)$ themselves are not yet included.

A similar separation of divergent parts may be made for the $\Pi(W', t^1)$, when W' is an irreducible photon self-energy part. The integral (65) may now be quadratically divergent, and so it is necessary to use instead of (66)

$$R(t^1, p^i)=R(0, p^i)+t_\mu{}^1\left(\frac{\partial R}{\partial t_\mu{}^1}(0, p^i)\right)+\tfrac{1}{2}t_\mu{}^1t_\nu{}^1\left(\frac{\partial^2 R}{\partial t_\mu{}^1\partial t_\nu{}^1}(0, p^i)\right)+R_c(t^1, p^i),$$

and derive instead of (67)

$$\Pi(W', t^1)=e^{2I}[A+B_\mu t_\mu{}^1+C_{\mu\nu}t_\mu{}^1t_\nu{}^1+\Pi_c(W', t^1)]. \quad (74)$$

The A, B_μ, $C_{\mu\nu}$ are absolute constant numbers (not Dirac operators) and therefore covariance requires that $B_\mu=0$, $C_{\mu\nu}=C\delta_{\mu\nu}$. $\Pi_c(W', t^1)$ is defined by an absolutely convergent integral, and will be an invariant function of $(t^1)^2$ of a form

$$\Pi_c(W', t^1)=(t^1)^2D(W', t^1), \quad (75)$$

where $D(W', t^1)$ is zero for t^1 satisfying

$$(t^1)^2=0 \quad (76)$$

instead of (69). Summing (74) over all irreducible W''s will give

$$\Pi^*(t^1)=A'+C(t^1)^2+(t^1)^2D_c(t^1), \quad (77)$$

and hence by (64) and (44)

$$D_F'(t^1)=A'D_F(t^1)D_F'(t^1)+\frac{1}{2\pi i}CD_F'(t^1)+D_F(t^1)+\frac{1}{2\pi i}D_c(t^1)D_F'(t^1). \quad (78)$$

In (77) and (78), D_c is zero for t^1 satisfying (76), and is divergence free.

The constant A' in (77) is the quadratically divergent photon self-energy. It will give rise to matrix elements in $U(\infty)$ of the form

$$M=A'\int A_\mu(x)A_\mu(x)dx, \quad (79)$$

which are non-gauge invariant and inadmissable. Such matrix elements must be eliminated from the theory, as the first term of (59) was eliminated, by the statement that A' is zero. The verification of this statement, by direct calculation of the lowest order contribution to A', has been given by Schwinger.[3,10]

The separation of the divergent part of Λ_μ again follows the lines laid down for Σ^*. Since the integral analogous to (65) is now only logarithmically divergent, no derivative term is required in (66), and the analog of (67) is

$$\Lambda_\mu(V, t^1, t^2)=e^{2I}[L_\mu+\Lambda_{\mu c}(V, t^1, t^2)], \quad (80)$$

where L_μ is a constant divergent operator, and $\Lambda_{\mu c}$ is convergent and zero for $t^1=t^2=0$. In (80), L_μ can only be of the form $L\gamma_\mu$. Also, if $t^1=t^2$ and t^1 satisfies (69), $\Lambda_{\mu c}$ will reduce to a finite multiple of γ_μ which can be included in the term $L\gamma_\mu$. Therefore it may be supposed that $\Lambda_{\mu c}$ in (80) is zero not for $t^1=t^2=0$ but for $t^1=t^2$ satisfying (69). The meaning of this

[10] Gregor Wentzel, Phys. Rev. 74, 1070 (1948), presents the case against Schwinger's treatment of the photon self-energy.

physically is that $\Lambda_{\mu c}$ now gives zero contribution to the energy of a single electron in a constant electromagnetic potential, so that the whole measured static charge on an electron is included in the term $L\gamma_\mu$. Summing (80) over all irreducible vertex parts V, and using (38),

$$\Lambda_\mu(l^1, l^2) = L\gamma_\mu + \Lambda_{\mu c}(l^1, l^2), \tag{81}$$

$$\Gamma_\mu(l^1, l^2) = (1+L)\gamma_\mu + \Lambda_{\mu c}(l^1, l^2). \tag{82}$$

In (81) and (82), effects of higher order corrections to the $\Lambda_\mu(V, l^1, l^2)$ are again not yet included. Formally, (82) differs from (73) and (78) in not containing the unknown operator Γ_μ on both sides of the equation.

VII. REMOVAL OF DIVERGENCES FROM THE S MATRIX

The task remaining is to complete the formulas (73), (78), and (82), which show how the infinite parts can be separated from the operators Γ_μ, S_F', and D_F', and to include the corrections introduced into these operators by the radiative reactions which they themselves describe. In other words, we have to include radiative corrections to radiative corrections, and renormalizations of renormalizations, and so on *ad infinitum*. This task is not so formidable as it appears.

First, we observe that Λ_μ, Σ^*, and Π^* are defined by integral equations of the form (39), which will be referred to in the following pages as "the integral equations." More specifically, consider the contribution $\Lambda_\mu(V, l^1, l^2)$ to Λ_μ represented by (80), arising from a vertex part V with $(2l+1)$ vertices, l photon lines, and $2l$ electron lines. This contribution is defined by an integral analogous to (65), with an integrand which is a product of $(2l+1)$ operators γ_μ, l functions D_F, and $2l$ operators S_F. The exact $\Lambda_\mu(V, l^1, l^2)$ is to be obtained by replacing these factors, respectively, by Γ_μ, D_F', S_F', as described in Section IV. Now suppose that S_F' in the integrand is represented, to order e^{2n} say, by the sum of S_F and of a finite number of finite products of S_F with absolutely convergent operators $S(\bar{W}, l^1)$ such as appear in (71); similarly, let D_F' be represented by D_F plus a finite sum of finite products of D_F with functions $D(\bar{W}', l^1)$ appearing in (75); and let Γ_μ be represented by the sum of γ_μ and of a finite set of $\Lambda_{\mu c}(\bar{V}, l^1, l^2)$ from (80). Then the integral $\Lambda_\mu(V, l^1, l^2)$ will be determined to order e^{2n+2l}; and since the operators $S(\bar{W}, l^1)$, $D(\bar{W}', l^1)$, $\Lambda_{\mu c}(\bar{V}, l^1, l^2)$ always have a sufficiency of denominators for convergence, the theory of Section V can be applied to prove that this $\Lambda_\mu(V, l^1, l^2)$ will not be more than logarithmically divergent. Therefore the new $\Lambda_\mu(V, l^1, l^2)$ can be again separated into the form (80). The sum of these $\Lambda_\mu(V, l^1, l^2)$ will then be a $\Lambda_\mu(l^1, l^2)$ of the form (81), with constant L and convergent operator $\Lambda_{\mu c}$ determined to order e^{2n+2}. Thus (82) provides a new expression for Γ_μ, determined to order e^{2n+2}.

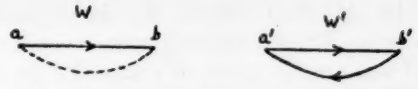

FIG. 5.

The above procedure describes the general method for separating out the finite part from the contribution to Γ_μ arising from a reducible vertex part V_R. First, V_R is broken down into an irreducible vertex part V plus various inserted parts $\bar{W}$, $\bar{W}'$, $\bar{V}$; the contribution to Γ_μ from V_R is an integral $M(V_R)$ which is not only divergent as a whole, but also diverges when integrated over the variables belonging to one of the insertions $\bar{W}$, $\bar{W}'$, $\bar{V}$, the remaining variables being held fixed. The divergences are to be removed from $M(V_R)$ in succession, beginning with those arising from the inserted parts, and ending with those arising from V itself. This successive removal of divergences is a well-defined procedure, because any two of the insertions made in V are either completely non-overlapping or else arranged so that one is completely contained in the other.

In calculating the contribution to Σ^* or Π^* from reducible self-energy parts, additional complications arise. There is in fact only one irreducible photon self-energy part, the one denoted by W' in Fig. 5; and there is, besides the self-energy part consisting of a single point, just one irreducible electron self-energy part, denoted by W in Fig. 5. All other self-energy parts may be obtained by making various insertions in W or W'. However, reducible self-energy parts are to be enumerated by inserting vertex parts at only one, and not both, of the vertices of W or W'; otherwise the same self-energy part would appear more than once in the enumeration. And the contribution $M(W_R)$ to Σ^* arising from a reducible part W_R will be, in general, an integral which involves simultaneously divergences corresponding to each of the ways in which W_R might have been built up by insertions of vertex parts at either or both vertices of W. This complication arises because, in the special case when two vertex parts are both contained in a self-energy part and each contains one end-vertex of the self-energy part (and in no other case), it is possible for the two vertex parts to overlap without either being completely contained in the other.

The finite part of $M(W_R)$ is to be separated out as follows. In a unique way, W_R is obtained from W by inserting a vertex part $\bar{V}_a$ at a, and self-energy parts $\bar{W}_a$ and $\bar{W}_a'$ in the two lines of W. From $M(W_R)$ there are subtracted all divergences arising from $\bar{V}_a$, $\bar{W}_a$, $\bar{W}_a'$; let the remainder after this sub-

traction be $M'(W_R)$. Next, W_R is considered as built up from W by inserting some vertex part $\bar{V}_b$ at b, and self-energy parts $\bar{W}_b$ and $\bar{W}_b'$ in the two lines of W. The integral $M'(W_R)$ will still contain divergences arising from $\bar{V}_b$ (but none from $\bar{W}_b$ and $\bar{W}_b'$), and these divergences are to be subtracted, leaving a remainder $M''(W_R)$. The finite part of $M''(W_R)$ can finally be separated by applying to the whole integral the method of Section VI, which gives for $M''(W_R)$ an expression of the form (67), with Σ_c given by (71). Therefore the finite part of $M(W_R)$ is a well-determined quantity, and is an operator of the form (71).

The behavior of the higher order contributions to Σ^* and Π^* having now been qualitatively explained, we may describe the precise rules for the calculation of Σ^* and Π^* by the same kind of inductive scheme as was given for Λ_μ in the second paragraph of this Section. Apart from the constant term $(-2\pi i\delta\kappa_0)$, Σ^* is just the contribution $\Sigma(W, t^1)$ from the W of Fig. 5; and $\Sigma(W, t^1)$ is represented by an integral of the form (65) with $l=1$. The integrand in (65) was a product of two operators γ_μ, one operator D_F, and one operator S_F. The exact $\Sigma(W, t^1)$ is to be obtained by replacing D_F by D_F', S_F by S_F', and one only of the factors γ_μ by Γ_μ, say the γ_μ corresponding to the vertex a of W. Suppose that S_F' in the integrand is represented, to order e^{2n}, by the sum of S_F and of a finite number of finite products of S_F with operators $S(\bar{W}, t^1)$ such as appear in (71); and suppose that D_F' and Γ_μ are similarly represented. Then $\Sigma(W, t^1)$ will be determined to order e^{2n+2}. The new $\Sigma(W, t^1)$ will be a sum of integrals like the $M'(W_R)$ of the previous paragraph, still containing divergences arising from vertex parts at the vertex b of W, in addition to divergences arising from the graph W_R as a whole. When all these divergences are dropped, we have a $\Sigma_c(W, t^1)$ which is finite; substituting this $\Sigma_c(W, t^1)$ for Σ^* in (63) gives an S_F' which is also finite and determined to the order e^{2n+2}.

The above procedures start from given S_F', D_F' and Γ_μ represented to order e^{2n} by, respectively, S_F plus S_F multiplied by a finite sum of products of $S(\bar{W}, t^1)$, D_F plus D_F multiplied by a finite sum of products of $D(\bar{W}', t^1)$, and γ_μ plus a finite sum of $\Lambda_{\mu c}(\bar{V}, t^1, t^2)$. From these there are obtained new expressions for S_F', D_F', Γ_μ. In the new expressions there appear new convergent operators $S(W, t^1)$, $D(W', t^1)$, $\Lambda_{\mu c}(V, t^1, t^2)$, determined to order e^{2n+2}; in the divergent terms which are separated out and dropped from the new expressions, there appear divergent coefficients A, B, C, L, such as occur in (73), (78), (82), also now determined to order e^{2n+2}. After the dropping of the divergent terms, the new Γ_μ by (82) is a sum of γ_μ and a finite set of $\Lambda_{\mu c}(V, t^1, t^2)$; the new S_F' by (73) is S_F plus S_F multiplied by a finite sum of products of $S(W, t^1)$; and the new D_F' by (78) is D_F plus D_F multiplied by a finite sum of products of $D(W', t^1)$. That is to say, the new Γ_μ, S_F', D_F' can be substituted back into the integrals of the form (65), and so a third set of operators Γ_μ, S_F', D_F' is obtained, determined to order e^{2n+4}, and again with finite and divergent parts separated. In this way, always dropping the divergent terms before substituting back into the integral equations, the finite parts of Γ_μ, S_F', D_F', may be calculated by a process of successive approximation, starting with the zero-order values γ_μ, S_F, D_F. After n substitutions, the finite parts of Γ_μ, S_F', D_F' will be determined to order e^{2n}.

It is necessary finally to justify the dropping of the divergent terms. This will be done by showing that the "true" Γ_μ, S_F', D_F', which are obtained if the divergent terms are not dropped, are only numerical multiples of those obtained by dropping divergences, and that the numerical multiples can themselves be eliminated from the theory by a consistent use of the ideas of mass and charge renormalization. Let $\Gamma_{\mu 1}(e)$, $S_{F1}'(e)$, $D_{F1}'(e)$ be the operators obtained by the process of substitution dropping divergent terms; these operators are power series in e with finite operator coefficients (to avoid raising the question of the convergence of these power-series, all quantities are supposed defined only up to some finite order e^{2N}). Then we shall show that the true operators Γ_μ, S_F', D_F' are of the form

$$\Gamma_\mu = Z_1^{-1}\Gamma_{\mu 1}(e_1), \tag{83}$$

$$S_F' = Z_2 S_{F1}'(e_1), \tag{84}$$

$$D_F' = Z_3 D_{F1}'(e_1), \tag{85}$$

where Z_1, Z_2, Z_3 are constants to be determined, and e_1 is given by

$$e_1 = Z_1^{-1} Z_2 Z_3^{\frac{1}{2}} e. \tag{86}$$

This e_1 will turn out to be the "true" electronic charge. It has to be proved that the result of substituting (83), (84), (85) into the integral equations defining Γ_μ, S_F', D_F', is to reproduce these expressions exactly, when Z_1, Z_2, Z_3, and $\delta\kappa_0$ are suitably chosen.

Concerning the $\Gamma_{\mu 1}(e)$, $S_{F1}'(e)$, $D_{F1}'(e)$, it is known that, when these operators are substituted into the integral equations, they reproduce themselves with the addition of certain divergent terms. The additional divergent terms consist partly of the terms involving A, B, C, L, which are displayed in (73), (78), (82), and partly of terms arising (in the case of S_F' and D_F' only) from the peculiar behavior of the vertices b, b' in Fig. 5. The terms arising from b and b' have been discussed earlier; they may be called for brevity b-divergences. Originally, of course, there is no asymmetry between the divergences arising in Σ^* from vertex parts inserted at

the two ends a and b of W; we have manufactured an asymmetry by including the divergences arising at a in the coefficient Z_1^{-1} of (83), while at b the operator γ_μ has not been replaced by Γ_μ and so the b divergences have not been so absorbed. It is thus to be expected that the effect of the b divergences, like that of the a divergences, will be merely to multiply all contributions to Σ^* by the constant Z_1^{-1}. Similarly, we expect that divergences at b' will multiply Π^* by the constant Z_1^{-1}. It can be shown, by a detailed argument too long to be given here, that these expectations are justified. (The interested reader is recommended to see for himself, by considering contributions to Σ^* arising from various self-energy parts, how it is that the finite terms of a given order are always reappearing in higher order multiplied by the same divergent coefficients.) Therefore, the complete expressions obtained by substituting $\Gamma_{\mu 1}(e)$, $S_{F1}'(e)$, $D_{F1}'(e)$, into the integral equations defining Λ_μ, Σ^*, Π^*, are

$$\Lambda_{\mu 1}(e)=\Lambda_{\mu c}(e)+L(e)\gamma_\mu, \tag{87}$$

$$S_F\Sigma_1^*(e)=-2\pi i\delta\kappa_0 S_F + Z_1^{-1}\left(A(e)S_F+\frac{1}{2\pi}B(e)+\frac{1}{2\pi}S_c(e)\right), \tag{88}$$

$$D_F\Pi_1^*(e)=Z_1^{-1}\left(\frac{1}{2\pi i}C(e)+\frac{1}{2\pi i}D_c(e)\right). \tag{89}$$

Here $A(e)$, $B(e)$, $C(e)$, $L(e)$ are well-defined power series in e, with coefficients which diverge never more strongly than as a power of a logarithm. The finite operators $\Lambda_{\mu c}(e)$, $S_c(e)$, $D_c(e)$, will, when all divergent terms are dropped, lead back to the $\Gamma_{\mu 1}(e)$, $S_{F1}'(e)$, $D_{F1}'(e)$, from which the substitution started; thus, according to (38), (63), (64),

$$\Gamma_{\mu 1}(e)=\gamma_\mu+\Lambda_{\mu c}(e), \tag{87'}$$

$$S_{F1}'(e)=S_F+\frac{1}{2\pi}S_c(e)S_{F1}'(e), \tag{88'}$$

$$D_{F1}'(e)=D_F+\frac{1}{2\pi i}D_c(e)D_{F1}'(e). \tag{89'}$$

Equations (87)–(89), (87′)–(89′), describe precisely the way in which the $\Gamma_{\mu 1}(e)$, $S_{F1}'(e)$, $D_{F1}'(e)$, when substituted into the integral equations, reproduce themselves with the addition of divergent terms. And from these results it is easy to deduce the self-reproducing property of the operators (83)–(85), when substituted into the same equations.

Consider for example the effect of substituting from (83)–(85) into the term $\Sigma(W, t^1)$, given by (65) with $l=1$. The integrand of (65) is a product of one factor Γ_μ, one γ_μ, one S_F', and one D_F'. Therefore the substitution gives

$$Z_1^{-1}Z_2Z_3\Sigma_0(W), \tag{90}$$

where $\Sigma_0(W)$ is the expression (65) obtained by substituting $\Gamma_{\mu 1}(e_1)$, $S_{F1}'(e_1)$, $D_{F1}'(e_1)$, without the Z factors. Now the Z factors in (90) combine with the e^2 of (65) to give

$$Z_1Z_2^{-1}e_1^2,$$

and the remaining factor of $\Sigma_0(W)$ is explicitly a function of e_1 and not of e. Therefore (90) is

$$Z_1Z_2^{-1}\Sigma_1(W, e_1),$$

where $\Sigma_1(W, e)$ is the expression obtained by substituting the operators $\Gamma_{\mu 1}(e)$, $S_{F1}'(e)$, $D_{F1}'(e)$ into $\Sigma(W, t^1)$. Thus the $\Sigma^*(t^1)$, obtained by substituting from (83)–(85) into (65), is identical with the result of substituting the operators $\Gamma_{\mu 1}(e)$, $S_{F1}'(e)$, $D_{F1}'(e)$, and afterwards changing e to e_1 and multiplying the whole expression (except for the constant term in $\delta\kappa_0$) by $Z_1Z_2^{-1}$. More exactly, using (88), one can say that the Σ^* obtained by substituting from (83)–(85) is given by

$$S_F\Sigma^*=-2\pi i\delta\kappa_0 S_F + Z_2^{-1}\left(A(e_1)S_F+\frac{1}{2\pi}B(e_1)+\frac{1}{2\pi}S_c(e_1)\right). \tag{91}$$

Further, the S_F' obtained by substituting from (83)–(85) into the integral equations is given by (91) and

$$S_F'=S_F+S_F\Sigma^*S_F'. \tag{92}$$

It is now easy to verify, using (88′), that S_F' given by (91) and (92) will be identical with (84), provided that

$$Z_2=1+\frac{1}{2\pi}B(e_1), \tag{93}$$

$$\delta\kappa_0=\frac{1}{2\pi i}Z_2^{-1}A(e_1). \tag{94}$$

In a similar way, the D_F' obtained by substituting from (83)–(85) into the integral equations can be related with the $\Pi_1^*(e)$ of (89). This D_F' will be identical with (85) provided that

$$Z_3=1+\frac{1}{2\pi i}C(e_1). \tag{95}$$

Finally, the Γ_μ obtained by substituting from (83)–(85) can be shown to be

$$\Gamma_\mu=\gamma_\mu+Z_1^{-1}\Lambda_{\mu 1}(e_1),$$

with $\Lambda_{\mu 1}(e)$ given by (87). Using (87′), this Γ_μ will

be identical with (83) provided that

$$Z_1=1-L(e_1). \tag{96}$$

Therefore, if Z_1, Z_2, Z_3, $\delta\kappa_0$ are defined by (96), (93), (95), (94), it is established that (83)–(85) give the correct forms of the operators Γ_μ, S_F', D_F', including all the effects of the radiative corrections which these operators introduce into themselves and into each other. The exact Eqs. (83)–(85) give a much simpler separation of the infinite from the finite parts of these operators than the approximate equations (73), (78), (82).

Consider now the result of using the exact operators (83)–(85) in calculating a constituent M of $U(\infty)$, where M is constructed from a certain irreducible graph G_0 according to the rules of Section IV. G_0 will have, say, F_e internal and E_e external electron lines, F_p internal and E_p external photon lines, and

$$n=F_e+\tfrac{1}{2}E_e=2F_p+E_p \tag{97}$$

vertices. In M there will be $\frac{1}{2}E_e$ factors $\psi'(k^i)$, $\frac{1}{2}E_e$ factors $\bar{\psi}'(k^i)$ and E_p factors $A_\mu'(k^i)$ given by (37). In $\psi'(k^i)$, k^i is the momentum-energy 4 vector of an electron, which satisfies (69), and the $S_c(k^i)$ in (73) are zero at every stage of the inductive definition of $S_{F1}'(e)$. Therefore (84), (35), (37) give in turn

$$\begin{aligned} &S_F'(k^i)=Z_2S_F(k^i),\\ &\Sigma(k^i)=2\pi(Z_2-1)(k_\mu{}^i\gamma_\mu-i\kappa_0),\\ &\psi'(k^i)=\psi(k^i)+2\pi(Z_2-1)S_F(k^i)(k_\mu{}^i\gamma_\mu-i\kappa_0)\psi(k^i). \end{aligned} \tag{98}$$

The expression (98) is indeterminate, since $(k_\mu{}^i\gamma_\mu-i\kappa_0)$ operating on $\psi(k^i)$ gives zero, while operating on $S_F(k^i)$ it gives the constant $(1/2\pi)$. Thus, according to the order in which the factors are evaluated, (98) will give for $\psi'(k^i)$ either the value $\psi(k^i)$ or the value $Z_2\psi(k^i)$. Similarly, $\bar{\psi}'(k^i)$ is indeterminate between $\bar{\psi}(k^i)$ and $Z_2\bar{\psi}(k^i)$, and, excluding for the moment $A_\mu(k^i)$ which are Fourier components of the external potential, $A_\mu'(k^i)$ is indeterminate between $A_\mu(k^i)$ and $Z_3A_\mu(k^i)$. In any case, considerations of covariance show that the $\psi'(k^i)$, $\bar{\psi}'(k^i)$, $A_\mu'(k^i)$ are numerical multiples of the $\psi(k^i)$, $\bar{\psi}(k^i)$, $A_\mu(k^i)$; thus the indeterminacy lies only in a constant factor multiplying the whole expression M.

There cannot be any indeterminacy in the magnitude of the matrix elements of $U(\infty)$, so long as this operator is restricted to be unitary. The indeterminacy in fact lies only in the normalization of the electron and photon wave functions $\psi(k^i)$, $\bar{\psi}(k^i)$, $A_\mu(k^i)$, which may or may not be regarded as altered by the continual interactions of these particles with the vacuum-fields around them. It can be shown that, if the wave functions are everywhere normalized in the usual way, the apparent indeterminacy is removed, and one must take

$$\begin{aligned} \psi'(k^i)&=Z_2{}^{\frac{1}{2}}\psi(k^i),\\ \bar{\psi}'(k^i)&=Z_2{}^{\frac{1}{2}}\bar{\psi}(k^i),\\ A_\mu'(k^i)&=Z_3{}^{\frac{1}{2}}A_\mu(k^i). \end{aligned} \tag{99}$$

It will be seen that (99) gives just the geometric mean of the two alternative values of $\psi'(k^i)$ obtained from (98).

When $A_\mu(k^i)$ is a Fourier component of the external potential, then in general $(k^i)^2\neq 0$, and $A_\mu'(k^i)$ is not indeterminate but is given by (37) and (85) in the form

$$A_\mu'(k^i)=2\pi iZ_3D_{F1}'(e_1)(k^i)^2A_\mu(k^i). \tag{100}$$

However, the unit in which external potentials are measured is defined by the dynamical effects which the potentials produce on known charges; and these dynamical effects are just the matrix elements of $U(\infty)$ in which (100) appears. Therefore the factor Z_3 in (100) has no physical significance, and will be changed when A_μ is measured in practical units. The correct constant which appears when practical units are used is $Z_3{}^{\frac{1}{2}}$; this is because the photon potentials A_μ in (99) were normalized in terms of practical units; and (100) should reduce to (99) when $(k^i)^2\to 0$, if the external A_μ and the photon A_μ are measured in the same units. Therefore the correct formula for A_μ', covering the cases both of photon and of external potentials, is

$$\left.\begin{aligned} &A_\mu'(k^i)=2\pi iZ_3{}^{\frac{1}{2}}D_{F1}'(e_1)(k^i)^2A_\mu(k^i), \quad (k^i)^2\neq 0,\\ &A_\mu'(k^i)=Z_3{}^{\frac{1}{2}}A_\mu(k^i), \quad (k^i)^2=0. \end{aligned}\right\} \tag{101}$$

In M there will appear F_e factors S_F', F_p factors D_F', and n factors Γ_μ, in addition to the factors of the type (99), (101). Hence by (97) the Z factors will occur in M only as the constant multiplier

$$Z_1{}^{-n}Z_2{}^nZ_3{}^{\frac{1}{2}n}.$$

By (86), this multiplier is exactly sufficient to convert the factor e^n, remaining in M from the original interaction (8), into a factor $e_1{}^n$. Thereby, both e and Z factors disappear from M, leaving only their combination e_1 in the operators $\Gamma_{\mu 1}(e_1)$, $S_{F1}'(e_1)$, $D_{F1}'(e_1)$, and in the factor $e_1{}^n$. If now e_1 is identified with the finite observed electronic charge, there no longer appear any divergent expressions in M. And since M is a completely general constituent of $U(\infty)$, the elimination of divergences from the S matrix is accomplished.

It hardly needs to be pointed out that the arguments of this section have involved extensive manipulations of infinite quantities. These manipulations have only a formal validity, and must be justified *a posteriori* by the fact that they ultimately lead to a clear separation of finite from infinite expressions. Such an *a posteriori* justification of dubious manipulations is an inevitable feature of

any theory which aims to extract meaningful results from not completely consistent premises.

We conclude with two disconnected remarks. First, it is probable that $Z_1=Z_2$ identically, though this has been proved so far only up to the order e^2. If this conjecture is correct, then all charge-renormalization effects arise according to (86) from the coefficient Z_3 alone, and the arguments of this paper can be somewhat simplified. Second, Eqs. (88′), (89′), which define the fundamental operators S_{F1}', D_{F1}', may be solved for these operators. Thus

$$S_{F1}'(e)=\left[1-\frac{1}{2\pi}S_c(e)\right]^{-1}S_F, \qquad (88'')$$

$$D_{F1}'(e)=\left[1-\frac{1}{2\pi i}D_c(e)\right]^{-1}D_F. \qquad (89'')$$

In electrodynamics, the S_c and D_c are small radiative corrections, and it will always be legitimate and convenient to expand (88″) and (89″) by the binomial theorem. If, however, the methods of the present paper are to be applied to meson fields, with coupling constants which are not small, then it will be desirable not to expand these expressions; in this way one may hope to escape partially from the limitations which the use of weak-coupling approximations imposes on the theory.

VIII. SUMMARY OF RESULTS

The results of the preceding sections divide themselves into two groups. On the one hand, there is a set of rules by which the element of the S matrix corresponding to any given scattering process may be calculated, without mentioning the divergent expressions occurring in the theory. On the other hand, there is the specification of the divergent expressions, and the interpretation of these expressions as mass and charge renormalization factors.

The first group of results may be summarized as follows. Given a particular scattering problem, with specified initial and final states, the corresponding matrix element of $U(\infty)$ is a sum of contributions from various graphs G as described in Section II. A particular contribution M from a particular G is to be written down as an integral over momentum variables according to the rules of Section III; the integrand is a product of factors $\psi(k^i)$, $\bar{\psi}(k^i)$, $A_\mu(k^i)$, $S_F(p^i)$, $D_F(p^i)$, $\delta(q_j)$, γ_μ, the factors corresponding in a prescribed way to the lines and vertices of G. According to Section IV, contributions M are only to be admitted from irreducible G; the effects of reducible graphs are included by replacing in M the factors ψ, $\bar{\psi}$, A_μ, S_F, D_F, γ_μ, by the corresponding expressions (37), (35), (36), (38). These replacements are then shown in Section VII to be equivalent to the following: each factor S_F in M is replaced by $S_{F1}'(e)$, each factor D_F by $D_{F1}'(e)$, each factor γ_μ by $\Gamma_{\mu 1}(e)$, each factor A_μ when it represents an external potential is replaced by

$$A_{\mu 1}(k^i)=2\pi i D_{F1}'(e)(k^i)^2 A_\mu(k^i), \qquad (102)$$

factors ψ, $\bar{\psi}$, A_μ representing particle wave-functions are left unchanged, and finally e wherever it occurs in M is replaced by e_1. The definition of M is completed by the specification of $S_{F1}'(e)$, $D_{F1}'(e)$, $\Gamma_{\mu 1}(e)$; it is in the calculation of these operators that the main difficulty of the theory lies. The method of obtaining these operators is the process of successive substitution and integration explained in the first part of Section VII; the operators so calculated are divergence-free, the divergent parts at every stage of the calculation being explicitly dropped after being separated from the finite parts by the method of Section VI.

The above rules determine each contribution M to $U(\infty)$ as a divergence-free expression, which is a function of the observed mass m and the observed charge e_1 of the electron, both of which quantities are taken to have their empirical values. The divergent parts of the theory are irrelevant to the calculation of $U(\infty)$, being absorbed into the unobservable constants δm and e occurring in (8). A place where some ambiguity might appear in M is in the calculation of the operators $S_{F1}'(e)$, $D_{F1}'(e)$, $\Gamma_{\mu 1}(e)$, when the method of Section VI is used to separate out the finite parts $S(W, t^1)$, $D(W', t^1)$, $\Lambda_{\mu c}(V, t^1, t^2)$, from the expressions (67), (74), (80). Even in this place the rules of Section VI give unambiguous directions for making the separation; only there is a question whether some alternative directions might be equally reasonable. For example, it is possible to separate out a finite part from $\Sigma(W, t^1)$ according to (67), and not to make the further step of using (70) to separate out a finite part $S(W, t^1)$ which vanishes when (69) holds. Actually it is easy to verify that such an alternative procedure will not change the value of M, but will only make its evaluation more complicated; it will lead to an expression for M in which one (infinite) part of the mass and charge renormalizations is absorbed into the constants δm and e, while other finite mass and charge renormalizations are left explicitly in the formulas. It is just these finite renormalization effects which the second step in the separation of $S(W, t^1)$ and $\Lambda_{\mu c}(V, t^1, t^2)$ is designed to avoid. Therefore it may be concluded that the rules of calculation of $U(\infty)$ are not only divergence-free but unambiguous.

As anyone acquainted with the history of the Lamb shift[11] knows, the utmost care is required

[11] H. A. Bethe, *Electromagnetic Shift of Energy Levels*, Report to Solvay Conference, Brussels (1948).

before it can be said that any particular rule of calculation is unambiguous. The rules given in this paper are unambiguous, in the sense that each quantity to be calculated is an integral in momentum-space which is absolutely convergent at infinity; such an integral has always a well-defined value. However, the rules would not be unambiguous if it were allowed to split the integrand into several parts and to evaluate the integral by integrating the parts separately and then adding the results; ambiguities would arise if ever the partial integrals were not absolutely convergent. A splitting of the integrals into conditionally convergent parts may seem unnatural in the context of the present paper, but occurs in a natural way when calculations are based upon a perturbation theory in which electron and positron states are considered separately from each other. The absolute convergence of the integrals in the present theory is essentially connected with the fact that the electron and positron parts of the electron-positron field are never separated; this finds its algebraic expression in the statement that the quadratic denominator in (45) is never to be separated into partial fractions. Therefore the absence of ambiguity in the rules of calculation of $U(\infty)$ is achieved by introducing into the theory what is really a new physical hypothesis, namely that the electron-positron field always acts as a unit and not as a combination of two separate fields. A similar hypothesis is made for the electromagnetic field, namely that this field also acts as a unit and not as a sum of one part representing photon emission and another part representing photon absorption.

Finally, it must be said that the proof of the finiteness and unambiguity of $U(\infty)$ given in this paper makes no pretence of being complete and rigorous. It is most desirable that these general arguments should as soon as possible be supplemented by an explicit calculation of at least one fourth-order radiative effect, to make sure that no unforeseen difficulties arise in that order.

The second group of results of the theory is the identification of δm and e by (94) and (86). Although these two equations are strictly meaningless, both sides being infinite, yet it is a satisfactory feature of the theory that it determines the unobservable constants δm and e formally as power series in the observable e_1, and not vice versa. There is thus no objection in principle to identifying e_1 with the observed electronic charge and writing

$$(e_1^2/4\pi\hbar c)=\alpha\doteq 1/137. \tag{103}$$

The constants appearing in (8) are then, by (94) and (86),

$$\delta m=m(A_1\alpha+A_2\alpha^2+\cdots), \tag{104}$$

$$e=e_1(1+B_1\alpha+B_2\alpha^2+\cdots), \tag{105}$$

where the A_i and B_i are logarithmically divergent numerical coefficients, independent of m and e_1.

IX. DISCUSSION OF FURTHER OUTLOOK

The surprising feature of the S matrix theory, as outlined in this paper, is its success in avoiding difficulties. Starting from the methods of Tomonaga, Schwinger and Feynman, and using no new ideas or techniques, one arrives at an S matrix from which the well-known divergences seem to have conspired to eliminate themselves. This automatic disappearance of divergences is an empirical fact, which must be given due weight in considering the future prospects of electrodynamics. Paradoxically opposed to the finiteness of the S matrix is the second fact, that the whole theory is built upon a Hamiltonian formalism with an interaction-function (8) which is infinite and therefore physically meaningless.

The arguments of this paper have been essentially mathematical in character, being concerned with the consequences of a particular mathematical formalism. In attempting to assess their significance for the future, one must pass from the language of mathematics to the language of physics. One must assume provisionally that the mathematical formalism corresponds to something existing in nature, and then enquire to what extent the paradoxical results of the formalism can be reconciled with such an assumption. In accordance with this program, we interpret the contrast between the divergent Hamiltonian formalism and the finite S matrix as a contrast between two pictures of the world, seen by two observers having a different choice of measuring equipment at their disposal. The first picture is of a collection of quantized fields with localizable interactions, and is seen by a fictitious observer whose apparatus has no atomic structure and whose measurements are limited in accuracy only by the existence of the fundamental constants c and h. This observer is able to make with complete freedom on a sub-microscopic scale the kind of observations which Bohr and Rosenfeld[12] employ in a more restricted domain in their classic discussion of the measurability of field-quantities; and he will be referred to in what follows as the "ideal" observer. The second picture is of a collection of observable quantities (in the terminology of Heisenberg), and is the picture seen by a real observer, whose apparatus consists of atoms and elementary particles and whose measurements are limited in accuracy not only by c and h but also by other constants such as α and m. The real observer

[12] N. Bohr and L. Rosenfeld, Kgl. Dansk. Vid. Sels. Math.-Phys. Medd. 12, No. 8 (1933). A second paper by Bohr and Rosenfeld is to be published later, and is abstracted in a booklet by A. Pais, *Developments in the Theory of the Electron* (Princeton University Press, Princeton, 1948).

makes spectroscopic observations, and performs experiments involving bombardments of atomic systems with various types of mutually interacting subatomic projectiles, but to the best of our knowledge he cannot measure the strength of a single field undisturbed by the interaction of that field with others. The ideal observer, utilizing his apparatus in the manner described in the analysis of the Hamiltonian formalism by Bohr and Rosenfeld,[12] makes measurements of precisely this last kind, and it is in terms of such measurements that the commutation-relations of the fields are interpreted. The interaction-function (8) will presumably always remain unobservable to the real observer, who is able to determine positions of particles only with limited accuracy, and who must always obtain finite results from his measurements. The ideal observer, however, using non-atomic apparatus whose location in space and time is known with infinite precision, is imagined to be able to disentangle a single field from its interactions with others, and to measure the interaction (8). In conformity with the Heisenberg uncertainty principle, it can perhaps be considered a physical consequence of the infinitely precise knowledge of location allowed to the ideal observer, that the value obtained by him when he measures (8) is infinite.

If the above analysis is correct, the divergences of electrodynamics are directly attributable to the fact that the Hamiltonian formalism is based upon an idealized conception of measurability. The paradoxical feature of the present situation does not then lie in the mere coexistence of a finite S matrix with an infinite interaction-function. The empirically found correlation, between expressions which are unobservable to a real observer and expressions which are infinite, is a physically intelligible and acceptable feature of the theory. The paradox is the fact that it is necessary in the present paper to start from the infinite expressions in order to deduce the finite ones. Accordingly, what is to be looked for in a future theory is not so much a modification of the present theory which will make all infinite quantities finite, but rather a turning-round of the theory so that the finite quantities shall become primary and the infinite quantities secondary.

One may expect that in the future a consistent formulation of electrodynamics will be possible, itself free from infinities and involving only the physical constants m and e_1, and such that a Hamiltonian formalism with interaction (8), with divergent coefficients δm and e, may in suitably idealized circumstances be deduced from it. The Hamiltonian formalism should appear as a limiting form of a description of the world as seen by a certain type of observer, the limit being approached more and more closely as the precision of measurement allowed to the observer tends to infinity.

The nature of a future theory is not a profitable subject for theoretical speculation. The future theory will be built, first of all upon the results of future experiments, and secondly upon an understanding of the interrelations between electrodynamics and mesonic and nucleonic phenomena. The purpose of the foregoing remarks is merely to point out that there is now no longer, as there has seemed to be in the past, a compelling necessity for a future theory to abandon some essential features of the present electrodynamics. The present electrodynamics is certainly incomplete, but is no longer certainly incorrect.

In conclusion, the author would like to express his profound indebtedness to Professor Feynman for many of the ideas upon which this paper is built, to Professor Oppenheimer for valuable discussions, and to the Commonwealth Fund of New York for financial support.

Short Range Alpha-Particles from Fluorine and Lithium Bombarded by Protons

W. E. Burcham and Joan M. Freeman
Cavendish Laboratory, Cambridge, England

April 18, 1949

In a recent paper Walker and McDaniel[1] report on measurements of the energy of the gamma-radiation emitted in the bombardment of fluorine and lithium by protons. The radiation from fluorine was found to consist of two lines of energies 6.13 ±0.06 and 6.98±0.07 Mev; similar results have been reported by Rasmussen, Hornyak, and Lauritsen.[2] The 6-Mev radiation has been shown to come from an excited O^{16} nucleus formed in the reaction:

$$F^{19}+H^1 \rightarrow O^{16*}+He^4,$$

and the alpha-particles (α_1) produced in this reaction have been detected.[3,4]

We have now observed alpha-particles (α_2) corresponding to the emission of the 7-Mev gamma-radiation. These particles were resolved magnetically from protons scattered from the target and were detected by a fluorescent screen and photoelectric multiplier. Figure 1 shows the number of alpha-particles observed from a thin calcium fluoride target as a function of analyzer magnet current. The magnetic analyzer was calibrated by means of the particles from the well-known reactions[5] $Be^9(p\alpha)Li^6$ and $Be^9(pd)Be^8$ and the Q values deduced for the alpha-particle groups from fluorine are shown in Table I, together with values obtained by range comparisons. The errors stated represent the uncertainty in setting the magnetic field and in the range determinations (0.05 Mev) together with an allowance of 0.03 Mev for possible systematic errors in calibration. The mean Q for the group α_1 (1.93±0.06 Mev) is higher than that found earlier,[4,6] but the sum of this value and the corresponding gamma-ray energy is 8.06±0.08 Mev which is consistent with the energy of 8.12±0.24 Mev available from the mass change.[7] The Q for the group α_1 is independent of proton energy, in agreement with previous work.[3,4]

The difference between the Q for the reaction $F^{19}(p\alpha_2,\gamma)O^{16*}$ at 867 kev and at the other tabulated resonances exceeds the experimental error. This suggests that the excited state in which the O^{16} nucleus is left in this reaction is not the same at all resonances; the results could be explained by the existence in the oxygen nucleus of levels at 6.94 and 7.15 Mev above the ground state, in addition to previously known levels at about 6.00 (pair emitting level) and 6.13 Mev.[2,6] If this is so, the energy of the gamma-radiation observed at the 932- and 665-kev resonances should be 7.15 Mev and that of the gamma-radiation at the 867-kev resonance should be 6.94 Mev. The thick target observations of Walker and McDaniel are not inconsistent with this hypothesis.[8]

The ratio of intensities α_1/α_2 of the two groups of alpha-particles (observed at 83° with the proton beam) is given in Table II for the more prominent resonances below 950 kev, together with the

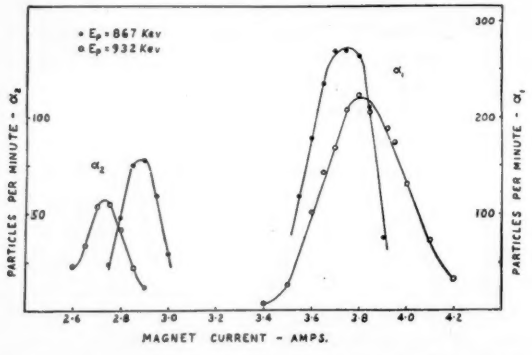

FIG. 1. Alpha-particles from the $F^{19}(p\alpha,\gamma)O^{16*}$ reaction for proton energies of 867 and 932 kev. Angle of observation = 104°.

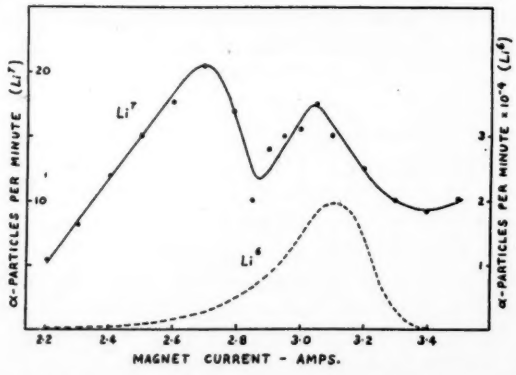

FIG. 2. Alpha-particles from lithium isotopes bombarded with 440-kev protons. Angle of observation = 104°.

[1] R. L. Walker and B. D. McDaniel, Phys. Rev. **74**, 315 (1948).
[2] Rasmussen, Hornyak, and Lauritsen, Phys. Rev. (to be published).
[3] W. E. Burcham and S. Devons, Proc. Roy. Soc. **A173**, 555 (1939).
[4] Becker, Fowler, and Lauritsen, Phys. Rev. **62**, 186 (1942).
[5] Tollestrup, Lauritsen, and Fowler, Phys. Rev. (to be published).
[6] J. M. Freeman and A. S. Baxter, Nature **162**, 696 (1948).
[7] H. A. Bethe, *Elementary Nuclear Theory* (John Wiley & Sons, Inc., New York, 1947).
[8] Measurements of the gamma-ray energies at the 867- and 932-kev resonances, kindly communicated to us by Professor Lauritsen, are also in agreement with the suggestion of a higher energy at the latter resonance.

TABLE I. Q values for the alpha-particle groups from fluorine.

Proton Energy (kev)	Group α_1 932	867	665	Group α_2 932	867	665
Q by magnetic deflection (Mev)	1.95	1.94	1.97	0.96	1.19	0.98
Q by range (Mev)	1.88	1.92	1.93	—	1.17	0.96
Mean Q (Mev)	1.92	1.93	1.95	0.96	1.18	0.97
Error (Mev)		±0.08			±0.08	

TABLE II. Ratio of the intensities ${}^{\alpha}1/\alpha_2$ of the two alpha-particle groups and the gamma-ray intensity ratio observed by Rasmussen, Hornyak, and Lauritsen.

Proton Energy (kev)	343	594	665	867	932
${}^{\alpha}1/\alpha_2$	50	>60	6	3.0	3.7
${}^{\gamma}1/\gamma_2$				2.5	3.3

gamma-ray intensity ratio observed by Rasmussen, Hornyak and Lauritsen.[2] The variation in ${}^{\alpha}1/\alpha_2$ with proton energy is predicted by the varying penetrability of the barrier of the O^{16*} nucleus for the two alpha-particle groups except in the case of the 594-kev resonance, for which the α_2 group could not be distinguished above background and appears to be forbidden.

In the work with lithium, Walker and McDaniel show that there are gamma-ray lines of energies 14.8 and 17.6 Mev, and give evidence that these lines correspond to transitions in the excited Be^8 nucleus formed in the reaction

$$Li^7+H^1\rightarrow Be^{8*}\rightarrow Be^8+\gamma.$$

The emission of a 17-Mev gamma-ray leaves the Be^8 nucleus in its ground state, while that of a 14-Mev gamma-ray could leave the nucleus in the well-known 2.8-Mev excited state, which has been observed in several other reactions and is known to break up into two alpha-particles.[9] We have observed these particles by bombarding a thick target of the Li^7 isotope (oxidized by exposure to air) with 440-kev protons. Figure 2 shows the distribution of alpha-particles emitted from this target, together with a curve taken with a Li^6 target under the same conditions. The alpha-particles from the excited state of Be^8 form a group centered at an energy of 1.38±0.08 Mev. This group was found to have an excitation function agreeing exactly with that of the gamma-radiation for proton energies between 350 and 700 kev. The energy of the excited state of Be^8 from these measurements is 2.6±0.2 Mev, and the width is 0.9±0.1 Mev. The higher energy group shown in Fig. 2 (Li^7) could be due to contamination of the target by Li^6 and check experiments showed that the number of particles in this group was only about twice that expected from the contamination; within the limits of accuracy of the comparison, the whole of the second group could be ascribed to the $Li^6(p\alpha)He^3$ reaction.

We wish to thank Sir John Cockcroft and Dr. W. D. Allen and members of his group at the Atomic Energy Research Establishment, Harwell, who provided the lithium targets used.

[9] Bonner, Evans, Malich, and Risser, Phys. Rev. **73**, 885 (1948).

PHYSICAL REVIEW VOLUME 75, NUMBER 11 JUNE 1, 1949

Photograph of a Shower Produced by a π-Meson and a π-μ-Decay

M. S. SINHA
Bose Institute, Calcutta, India
April 18, 1949

THE production of multiple heavy particles by the interaction of π-mesons with nuclei has been definitely established by the recent investigation with photographic plates by the Bristol school.[1] So far little evidence of such interactions has been obtained from Wilson Chamber photographs. We reproduce herewith a photograph of a shower which appears to be produced by the interaction of a π-meson with a nucleus; the particles emitted are not heavy in character, neither have they short ranges like the particles recorded in photographic emulsions (see Fig. 1). The photographs are stereoscopic and careful reprojection shows that the shower starts from a point in the gas of the chamber about 1.5 cm below the second lead plate (thickness 2.5 cm). Altogether seven particles are present in the shower and the two horizontal particles ejected towards the left start from the same point as the other five particles contained in the downward cone. These five particles pass out of the third lead plate (thickness 1 cm) with only one more secondary particle as the numbering of the tracks will show. The track No. 7 is an old track which is easily recognized from its diffused nature.

The first interesting point about the shower is its generation in the gas apparently from a point and the emission of the two particles toward the left without any apparent emission on the right

[1] Lattes, Occhialini, and Powell, Nature **160**, 486 (1947).

TABLE I. Range and energy of the particle P before entering the third lead plate of thickness one centimeter.

Nature of particle	m_0	β^2	E	Range in lead
π	1.6×10^8 ev	0.56	2.05×10^8 ev	1.01 cm
μ	1.0×10^8 ev	0.39	1.48×10^8 ev	1.96 cm

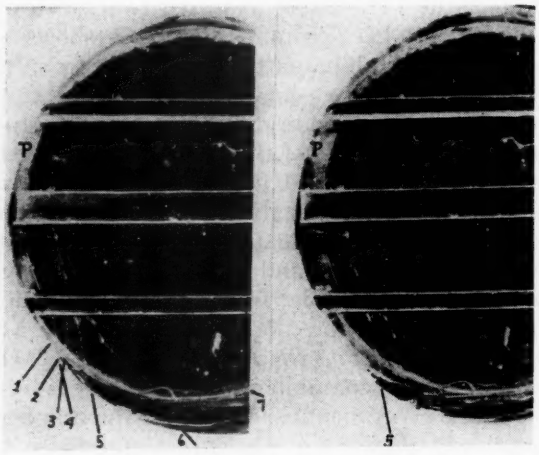

FIG. 1. Photograph of a shower which appears to be produced by the interaction of a π-meson with a nucleus.

side. If these are electrons they will carry negligible momentum, but otherwise conservation of momentum would require the emission of one or more neutral particles on the right side. Production of a pair of tracks in the gas of the chamber has been reported before by Rochester and Butler[2] but the present photograph is completely different from theirs.

Of the five particles contained in the downward cone, the fourth from the left (or second from the right) shows a large increase in ionization on passing out of the third lead plate (thickness 1 cm). This track is noted as No. 5 on emergence. It is clearly seen that track No. 5 has suddenly changed its direction and there is a considerable fall in ionization from the point at which it has changed its course. We shall see from the arguments given below that this particle is a π-meson and the sudden change in ionization and direction represents a π-μ-decay and not a μ-electron decay. Moreover, it is most probable that the shower has been produced by the interaction of this meson with a nucleus.

As there was no magnetic field in the chamber, the only method available for measuring the energy of the primary particle P is from the mean angle of scattering in the lead plates. The measurement of energy in this way is subject to the limitation that instead of determining the mean angle of scattering obtained from a large number of scattering observations, only the scattering angle in a single case is introduced in William's[3] equation. The discrepancy between the actual scattering angle (as observed) from the mean of a large number of similar observations will be small when the thickness of the scattering medium is fairly large. In our case the thickness is 1–2.5 cm of lead, which is large compared to the track length of multiply scattered particles observed in photographic plates.

The mean scattering angle of the incident particle in the second lead plate (thickness 2.5 cm) in the chamber is $0.7°\pm0.1$. This gives the total energy of the particle P as 2.04×10^9 ev, from William's formula.[3] The mean angle of scattering of track No. 5 (which we assume to be continuation of P) in the third lead plate (thickness 1 cm) in the chamber has been found to be $11°.3\pm0.3$ from which the total energy E of the particle *before entering this plate* comes out to be $E\beta^2=0.8\times10^8$ ev. This particle may be either a π- or a μ-meson. The value of β^2 was found out from the relation $E=m_0c^2/(1-\beta^2)^{\frac{1}{2}}$ and the above value of $E\beta^2$ for two values of m_0, those of π- and μ-mesons. The results, as obtained from Rossi and Griessen's curves, are given in Table I. From the values of the range it is evident that if the particle P were a μ-meson it would have sufficient kinetic energy to pass out of the chamber even after passing through 1 cm of lead, whereas if it were a π-meson it should stop just on emergence from the lead plate, and this is what has happened in our photograph. We may therefore conclude that the track P is that of a π-meson which has reached the end of its range and then decayed into a μ-meson. We believe this is the first cloud-chamber evidence of a π-μ-decay.

The next remarkable point is the scattering of track No. 6 in the gas. The scattering angle in the gas is about 16° and $2.9°\pm0.2$ in the lead plate above. The total energy of the particle before entering the plate is therefore 3.3×10^8 ev assuming its rest mass to be 10^8 ev. The particle is thus found to be too energetic to stop in the chamber and the sudden change in its direction must be attributed to nuclear scattering. No other particle has been emitted from the nucleus which is simply excited. One such case has been reported by Bhabha and Daniell[4] from photographic plate observation.

The particles constituting the shower do not appear to be electronic in nature as they do not multiply in the third lead plate. Moreover, the probability of emission of so many electrons in one single act from a point in the gas is negligibly small.

[2] G. D. Rochester and C. C. Butler, Nature **160**, 855 (1947).

[3] E. J. Williams, Proc. Roy. Soc. **169**, 531 (1939).

[4] H. J. Bhabha and R. R. Daniell, Nature **161**, 883 (1948).

The energy of the incident particle has been found to be 2.04×10^9 ev. We have assumed before that the π-meson referred to above (i.e., track No. 5) is the continuation of this incident particle. On this basis we find that the particle has lost an energy $(2.24\times10^9-2.05\times10^8)=1.835\times10^9$ ev in the interaction that has produced the shower. Excluding the incident particle there are then six particles in the shower and on an average, energy available for each is about 3.1×10^8 ev. We have seen that the total energy of one of the particles, i.e., particle No. 6 is 3.3×10^8 ev which gives support to our assumption. Though conservation of energy has been fulfilled, conservation of charge requires that three pairs of oppositely charged particles have been emitted, since it is very difficult to identify any of the tracks as due to a broken part of the nucleus. We therefore conclude that the shower is produced by a π-meson interacting with the nuclear field of another nucleus, the process being analogous to the phenomenon of scattering as visualized by Heitler and Peng[5] in which more than one meson can be emitted in a single interaction. The average total energy of each of the particles emitted in the process is about 3.1×10^8 ev. The ionization produced by a particle of this energy should be perceptibly more for a π-meson than for a μ-meson. Hence they appear to us to be more like μ-mesons than π-mesons as they produce less than the expected ionization for π-mesons. According to Occhialini and Powell,[6] however, π-mesons are first emitted in such an interaction, which then decay into μ-mesons. We cannot, however, exclude the possibility that they are π-mesons since the energy available for each of them is 3.1×10^8 ev, which is well above their rest mass.

The author is indebted to Professor D. M. Bose, Director, Bose Institute for very helpful and stimulating discussions.

[5] W. Heitler and H. W. Peng, Proc. Camb. Phil. Soc. **38**, 296 (1942).
[6] G. P. S. Occhialini and C. F. Powell, Nature **162**, 168 (1948).

PHYSICAL REVIEW VOLUME 75, NUMBER 11 JUNE 1, 1949

On the Origin of High Energy Photons

SATIO HAYAKAWA
Research Institute, Central Meteorological Observatory, Tokyo, Japan
April 14, 1949

RECENT experiments concerning mixed showers and extensive air showers suggest the simultaneous production of electronic and mesonic components by a nucleon-nucleon collision. The origin of such electronic component may, as pointed out by Oppenheimer,[1] be attributed to the disintegration photons of neutral mesons which are believed to have a very short life. But this interpretation, though of great interest, seems to lead to the following difficulties.

(1) The disintegration photons of the neutral mesons produced in a thick lead block at high altitude would give rise to cascade showers, but Schein *et al.*[2] observed only very few such showers in their high altitude experiment.[3] (2) Disintegration photons should have as large an angular divergence as mesons produced. But this expectation could be confirmed neither by the direct cloud-chamber observations, that the electron showers observed in mixed showers have always smaller angular divergence than mesons simultaneously produced,[4] nor by the analysis of extensive air showers that they have never multiple cores.[5] (3) The number of mesons produced in one collision is believed to be several or more and at least one-third of them should be neutral as concluded from the theory of nuclear forces. This would result in that *every* meson shower should be accompanied by multiple electron showers. Even when only one neutral meson is produced there would be two or more cores of electron showers since it disintegrates into at least two photons. The experiment by a cloud chamber operated with random expansion, however, shows that only one or two meson showers in several tens are accompanied by electron showers.[6] Even in a controlled chamber, which will certainly be favorable to mixed showers, not all meson showers contain cascade showers.[4,7] Further, almost all of them have a single core and only very few have double cores.[4]

Beside experimental evidences mentioned above,

[1] Lewis, Oppenheimer, and Wouthuysen, Phys. Rev. **73**, 127 (1948).
[2] Schein, Jesse, and Wollan, Phys. Rev. **59**, 615 (1941).
[3] M. Taketani, Symposium on Meson Theory (1943).
[4] H. Bridge and W. Hazen, Phys. Rev. **74**, 579 (1948).
[5] Robert W. Williams, Phys. Rev. **74**, 1689 (1948).
[6] Ralph P. Shutt, Phys. Rev. **69**, 261 (1946); Wilson M. Powell, Phys. Rev. **69**, 385 (1946).
[7] William B. Fretter, Phys. Rev. **73**, 41 (1948); C. Y. Chao, Phys. Rev. **74**, 962 (1948).

recent calculation on the life of the neutral meson shows that the life is so long that the simultaneous production of electronic component would hardly be observed in the cloud-chamber experiment.[8]

Now we must look for another cause of the production of the electron component appearing in mixed showers as well as extensive air showers. Tomonaga and the present author have once attempted to attribute this soft component production to the production of photons by the charge acceleration taking place in nucleon-nucleon collision.[9] The proposed mechanism is solely based on the electromagnetic interaction, the theory of which is trustworthy up to the region of extremely high energy. We concluded that, although other possibilities could not be excluded, at least a considerable part of air showers would have such an origin. When a charged particle with a velocity uc is stopped, photons with energy between ϵ and $\epsilon+d\epsilon$ are emitted by the acceleration. The probability for this emission can be estimated simply by picturing the phenomena in the following way: The Lorentz contracted Coulomb field attached to the particle is liberated as photons at the instant of the collision. This probability is found to be[10]

$$\frac{1}{137\pi}\left(\frac{1}{u}\ln\left(\frac{1+u}{1-u}\right)-2\right)\frac{d\epsilon}{\epsilon}$$

$$\approx\frac{1}{137\pi}\left(\ln 4\left(\frac{E}{Mc^2}\right)^2-2\right)\frac{d\epsilon}{\epsilon}, \quad (1)$$

where M and E mean the mass and energy of the incident particle. The same can be concluded also when a charge begins suddenly to move. Such a charge acceleration occurs also when an energetic proton or neutron converts into neutron or proton by the collision with a matter nucleus. The same effect will also be expected for each of newly produced mesons if the mesons are produced in the collision. In order that this simple picture be applicable, however, two conditions must be satisfied: (1) the process must take place sufficiently suddenly, and (2) there should be no interference between processes taking place at different nucleons in the collided nucleus. The first condition requires that the time of collision should be shorter than the period of the photon emitted. If the collision time is longer the process goes on adiabatically and no emission of light will take place. Denoting by r the impact parameter and by ξ the Lorentz factor for the particle, this condition requires that $r/\xi c<\hbar/\epsilon$, or $\epsilon<\xi\hbar c/r$ which gives the upper limit of the spectrum of the emitted photons. The second condition requires that the wave-length of the emitted photon should be shorter than the mean distance $\bar{r}$ between nucleons in the nucleus: $\epsilon>\hbar c/\bar{r}$, which limits the long wave side of the spectrum. The total probability of emission of photons in such a collision is now obtained by integrating (1) over ϵ from $\hbar c/\bar{r}$ to $\xi\hbar c/r$ and averaging over the impact parameter r. Assuming that $r_{\min}\approx\hbar/Mc$, $r_{\max}\approx\hbar/\mu c$, and $\bar{r}\approx\hbar/\mu c$, μ being the mass of the meson, we find the probability is approximately

$$\approx 4.7\times10^{-3}(\ln\xi)^2. \quad (2)$$

The emission of photons by newly produced mesons is improbable because the wave packet of the mesons produced multiply and cannot be smaller than $\hbar/\mu c$ so that the interference effect mentioned above cannot be neglected. The total probability of the emission of the photon in the nuclear collision is given by multiplying (2) by $A^{\frac{1}{3}}$, A being the atomic weight, and further by a factor k, the probability of the nuclear collision in which the proton→neutron or neutron→proton conversion takes place:

$$\approx kA^{\frac{1}{3}}\times4.7\times10^{-3}(\ln\xi)^2. \quad (3)$$

Though little is known about the factor k, we may suppose that it is not much smaller than unity. Then the value of (3) may be sufficient to explain the observed frequency of the accompaniment of electron showers by meson showers.

The above mechanism of soft-ray producing process can be responsible for the production of air showers and seems to be able to explain some experimental facts which could not be accounted for by the ordinary electron-primary hypothesis, e.g., the height of maximum shower frequency and the angular distribution.[11] A considerable part of the bursts under thick absorbers at high altitude will also be due to soft-rays produced by nucleons by the same mechanism, while at lower altitude they are mainly due to electromagnetic processes (e.g., bremsstrahlung and knock-on process) by mesons.[12] Because the nucleon component of the cosmic rays increases with altitude more rapidly than the meson component, the bursts produced by the former predominate over those by the latter at about 7-m water depth. The fact that the observed frequency-altitude relation of this phenomenon shows a much steeper increase at higher altitude than the increase of the meson component is accordance with this view.[13]

The author should like to express his sincerest thanks to Professor Tomonaga for his kind guidance.

[8] H. Fukuda and Y. Miyamoto, to be published.

[9] S. Hayakawa and S. Tomonaga, J. Sci. Research Inst. **43**, 67 (1948); Prog. Theor. Phys. **3**, 162 (1947).

[10] F. Bloch and A. Nordsieck, Phys. Rev. **52**, 54 (1937); Hayakawa, Miyamoto, and Tomonaga, J. Phys. Soc. Japan **2**, 172, 199 (1947).

[11] M. M. Mill, Phys. Rev. **74**, 1555 (1948).

[12] M. Schein and P. S. Gill, Rev. Mod. Phys. **11**, 267 (1939); R. E. Lapp, Phys. Rev. **69**, 321 (1946); E. F. Fahy and M. Schein, Phys. Rev. **75**, 207 (1949).

[13] Fujimoto, Hayakawa, and Yamaguchi, to be published.

Letters to the Editor

PUBLICATION of brief reports of important discoveries in physics may be secured by addressing them to this department. The closing date for this department is five weeks prior to the date of issue. No proof will be sent to the authors. The Board of Editors does not hold itself responsible for the opinions expressed by the correspondents. Communications should not exceed 600 words in length.

On the Measurement of Short-Lived Isomers of Nuclei*

F. K. McGowan, S. DeBenedetti,** J. E. Francis, Jr.
Oak Ridge National Laboratory, Oak Ridge, Tennessee
April 21, 1949

THE method of delayed coincidences between two anthracene scintillation counters has been extended to measure time intervals in the region 10^{-6} to 10^{-7} sec. The pulses from two 1*P*21 or 1*P*28 type multipliers are supplied to linear amplifiers[1] whose output signal has a rise time of approximately 1.5×10^{-7} sec. and whose pulse height selectors were replaced by circuits which minimize the variation in delay.[2] The maximum variation in delay was measured using pulses of different heights from a signal generator and was found to be 8×10^{-8} sec. After pulse height selection, the pulses are fed to a coincidence circuit through terminated coaxial cables which introduce a delay of 1.0-μ sec. per 24 ft. of line length (RG65/U; characteristic impedence 1000 ohms). The delay time can be varied from 0 to 2.0-μ sec. in discontinuous steps of 2×10^{-8} sec. The dependence of delay time on line length was measured with a synchroscope; all delays were found to be linear with the length of the coaxial cable. The resolving time of the coincidence circuit is 7×10^{-8} sec. and is kept constant. The clear anthracene crystals[3] and multiplier tubes are cooled to dry-ice temperature, and the tubes are operated at 60 volts per stage.

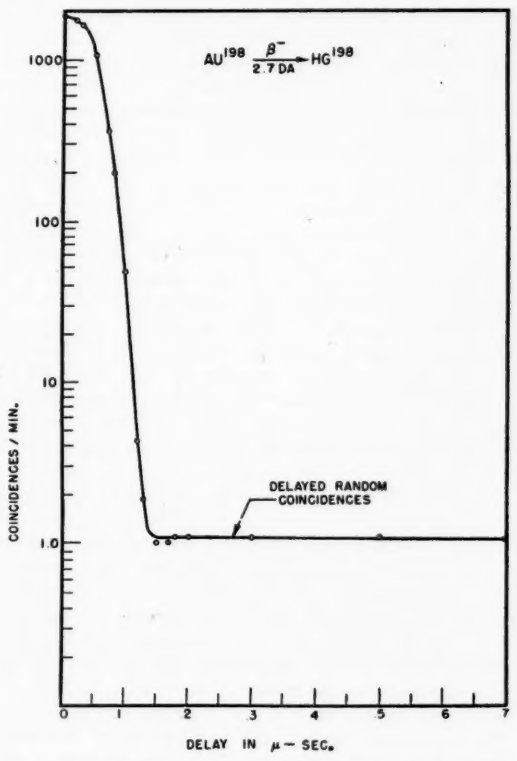

FIG. 1. Number of coincidences as a function of delay time.

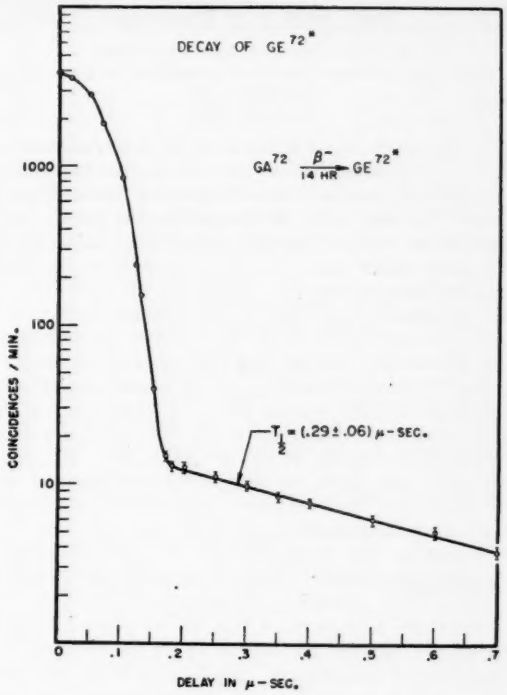

FIG. 2. Delayed coincidences as a function of delay time.

Figure 1 shows the number of coincidences as a function of delay time obtained with a source of Au^{198}. The majority of the sources used gave similar curves exhibiting a sharp break at 1.5×10^{-7} sec. The coincidences observed for shorter delays are mostly due to the scattering of β^--particles from one to the other detector. The width of the peak is just equal to the resolving time of the coincidence circuit plus the variation in delay introduced by the pulse height selectors. For delays larger than 1.5×10^{-7} sec. the number of coincidences is constant and equal to the computed random coincidence rate.

The present observations with Au^{198} are difficult to reconcile with the reported half-life of $(2 \text{ to } 3)\times10^{-7}$ sec.[4] for the state following the β^--decay of this isotope.

The existence of short-lived isomeric states of Re^{187*} [5] and Ge^{72*} [6] was confirmed. The value of the half-lives was found to be $(5.5\pm0.5)\times10^{-7}$ and $(2.9\pm0.6)\times10^{-7}$ sec., respectively. These values are somewhat different from those previously reported and probably more accurate. Figure 2 shows the delayed coincidence curve obtained with a source of Ga^{72} (decaying to Ge^{72*}) after subtraction of random coincidences. If the 0.41-Mev γ-rays following the β^--decay of Au^{198} had a half-life of $(2 \text{ to } 3)\times10^{-7}$ sec., they should contribute a number of delayed coincidences about ten times larger than those observed with Ge^{72*}.

* This document is based on work performed under Contract No. W-35-058, eng.-71 for the Atomic Energy Project at Oak Ridge National Laboratory.
** Present address: Washington University, Saint Louis, Missouri.
[1] W. H. Jordan and P. R. Bell, Rev. Sci. Inst. **18**, 703 (1947).
[2] Bell, DeBenedetti, Francis, Jr., Phys. Rev. **72**, 160 (1947).
[3] P. R. Bell, Phys. Rev. **73**, 1405 (1948).
[4] Leon Modansky and M. L. Wiedenbeck, Phys. Rev. **72**, 185 (1947).
[5] S. DeBenedetti and F. K. McGowan, Phys. Rev. **71**, 380 (1947).
[6] Bowe, Goldhaber, Hill, Meyerhof, and Sala, Phys. Rev. **73**, 1219 (1948).

Polarization of Electrons

KENICHI SHINOHARA AND NORIO RYU
Department of Physics, Faculty of Science, Kyushu University, Fukuoka, Japan
April 18, 1949

MANY experimental works have been carried out to find out the polarization of electrons by double scattering, and disagreeing results were obtained by various authors.[1] In view of the importance of the problem we have also made an experiment using a similar procedure but with slight modifications which might avoid the possible sources of error in the previous experiments.

The experimental arrangement is shown in Fig. 1. The electrons are accelerated by a high voltage equipment of the type of Cockcroft. The electrons suffer the first right angle scattering at the gold foil (the polarizer) placed at the transmission position. The second foil (the analyzer) was placed perpendicular to the incident electron beam and the electrons scattered approximately at 78° in the 0° and 180° azimuth, respectively, have been counted with two Geiger counters. This disposition of the analyzer foil avoids the difficulty of the so-called transmission-reflection effect[2] and also the possible error caused by the slight drift of the accelerating voltage during the measurement. Since the intensity of the electron beam scattered by a nucleus changes greatly with the energy of the electrons, a large error may be introduced by a slight change of the voltage. The foils used are beaten gold foils of the thickness of 5×10^{-6} cm. The slits defining the electron beam is made of aluminum, and also the inner surface of the scattering chamber was coated with thin aluminum plates, to minimize stray electrons and the emission of secondary x-rays. Lead blocks and plates were placed at suitable places to eliminate the effect of x-rays on the counters (not shown in Fig. 1). It was found experimentally that the effect of the x-rays and of the stray electrons are almost negligible and no error can be introduced from such origin. The part containing two counters and the analyzer foil can be rotated as a whole about an axis a (Fig. 1), and the positions of the counters can be interchanged so that the difference of the counting efficiencies of the two counters and the possible slight difference of the geometry in this part of the apparatus can be eliminated.

The result is given in Table I, together with the theoretical predictions. The errors given are the statistical probable errors. It may be concluded that the result shows positively the existence of the polarization. Its magnitude agrees rather well with the theory and increases with the voltage in the range of energies we have measured. The somewhat smaller experimental values may be due to the smaller angle of the second scattering compared to 90° assumed in all the theories.

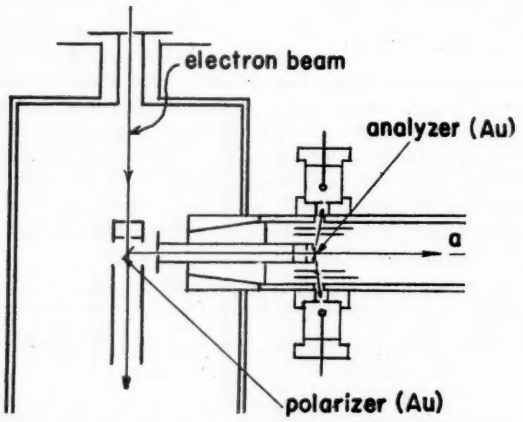

FIG. 1. Scattering foil and the counter arrangement.

TABLE I. Values of $2i\delta$.

Energy of electrons (kev)			45	60	70	90	92
	Experiment		3.6±1.4	4.2±2.2	6.8±1.0	9.0±1.0	9.1±1.4
$2i\delta$	Theory	Mott[3]	3.0	6.4	9.0	13.4	13.6
		Bartlett and Watson[4]	8.3	10.1	11.2	12.4	12.5
		Massey and Mohr[5]	6.6	10.4	12.5	15.8	16.0

A detailed account of the experimental method and the results will be published in the *Journal of the Physical Society of Japan.*

[1] E. G. Dymond, Proc. Roy. Soc. **A145**, 657 (1934); G. P. Thomson, Phil. Mag. **17**, 1058 (1934); H. Richter, Ann. d. Physik **28**, 533 (1937); K. Kikuchi, Proc. Phys. Math. Soc. Japan **22**, 805 (1940); Shull, Chase, and Myers, Phys. Rev. **63**, 29 (1943); E. Trounson and J. A. Simpson, Jr., Phys. Rev. **63**, 55 (1943).
[2] C. T. Chase and R. T. Cox, Phys. Rev. **58**, 243 (1940).
[3] N. F. Mott, Proc. Roy. Soc. **A135**, 429 (1932).
[4] J. H. Bartlett and R. E. Watson, Phys. Rev. **56**, 612 (1939).
[5] H. S. W. Massey and C. B. O. Mohr, Proc. Roy. Soc. **A177**, 341 (1941).

On the Energy Loss by Fission Fragments Along Their Path

N. O. LASSEN
Institute for Theoretical Physics, University of Copenhagen, Denmark
April 22, 1949

AS reported earlier,[1] the specific ionization by fission fragments in argon has been measured by means of a shallow ionization chamber. It is found to decrease along the path as would also be expected, since the charge of the fragments due to electron capture decreases with decreasing velocity. The ionization-range curves for the two groups of fragments are found to be different, the curve for the heavy group being the steeper and that for the light group being more flat at the beginning of the path.

Later, similar measurements have been performed in various other gases. The main features of the ionization-range curves are the same in all gases, but on close investigation the shapes of the curves are found to be slightly different in the light and in the heavy gases. Since the ionization decreases almost linearly over the last section of the range interval covered by the measurements, the so-called extrapolated ranges R_{ex} may be determined simply by linear extrapolation Fig. 1). They are found, especially in hydrogen, to be considerably smaller than the ranges as measured in a cloud-chamber by Bøggild, Arrøe, and Sigurgeirsson.[2]

This result is consistent with theoretical considerations.[3] At the beginning of the path the fragment will be slowed down almost entirely by energy transfer to the electrons in the atoms of the stopping gas, the atoms consequently being ionized or excited. As the ionization by such electronic encounters is proportional to the square of the fragment charge, it decreases along the path corresponding to the decreasing charge. When the fragments are slowed down to a velocity of the order of $v_0=e^2/\hbar$, they will be almost completely neutralized and, hence, the electronic stopping will become very small. This state is reached when the fragments have traversed a distance approximately equal to R_{ex}, but due to their large masses the fragments still have a considerable energy and will proceed in their motion. Over the remaining part of the range the fragments lose energy mainly by collisions with nuclei.

The ionization measurements only refer to the first part of the range; for the last part of the range the energy loss per cm and the ionization per cm are too low to be measured as compared with the background ionization. However, for the end of the path the energy loss, supposed to be due entirely to

nuclear collisions, may be calculated by means of the stopping formula given by Bohr.[3] The calculation is done for two fragments; the (z, m)-values of these are chosen to be (39, 95) and (53, 139), corresponding to the most frequent values of the light and heavy group of fragments, respectively. As an example hydrogen may be considered. Curve a in Fig. 1 gives the calculated energy loss for the heavy fragment; it is obtained only as a function of differences of the abscissae and, hence, in the figure the end-point for curve a is chosen in accordance with the total range of the heavy group as given by Bøggild, Arrøe, and Sigurgeirsson. Combining curve a with the measured ionization curve, we obtain the fulldrawn curve representing the specific energy loss along the whole range. The curve for the light fragment is obtained in a similar manner.

The ionization values which were measured only on a relative scale have been normalized so as to give an initial energy of the light fragment of 86 Mev. The ratio of the energy of the light and heavy fragment is found to be 1.53, in agreement with the measured value.[4] The fact that the curves in H_2 and D_2 coincide over the first part of the range proves the insignificance of nuclear collisions for the corresponding rather high velocities of the fragments. For smaller velocities the different magnitude of the nuclear stopping in H_2 and D_2 is demonstrated by the splitting up of the curves. Of course, the assumption that the electronic stopping becomes zero just for $v<v_0$ and that nuclear stopping is negligible for $v>v_0$ is somewhat arbitrary; nevertheless, it leads to differences between the total ranges in D_2 and H_2 of 0.7 and 0.5 cm for the light and heavy fragment, respectively, which are in good agreement with the experiments.

When given in cm normal air, the extrapolated ranges in various gases are, in contrast to the total ranges, found to increase monotonically with the atomic number of the stopping gas. Corresponding to the smaller values of R_{ex}^{air} the initial specific ionization by the fragments relative to that by α-particles is higher in the light than in the heavy gases. This result is in close agreement with the theoretical expectations when the initial charge of the fragments is assumed to be the same in all gases. Still, on careful consideration, the ionization in H_2 is found to be a little higher than should be expected on this assumption. The measurements thus seem to indicate a slightly higher charge in H_2 than in other gases, which may also be anticipated from the exceptionally low cross section for electron capture in H_2.

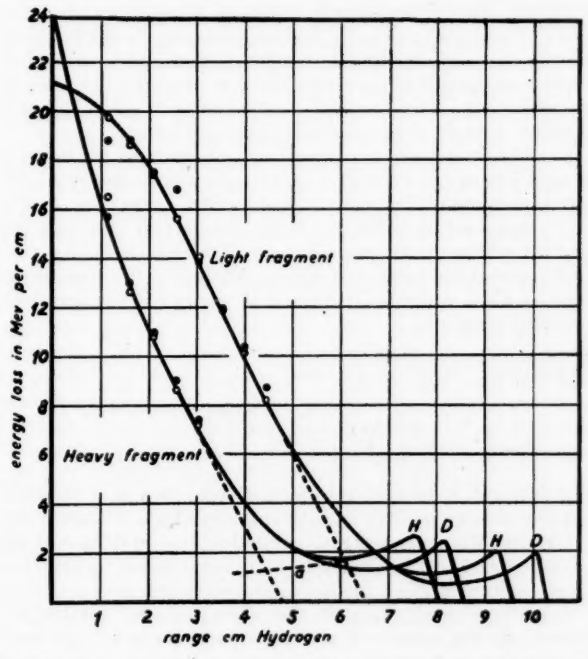

FIG. 1. The open circles give the result of measurements of the specific ionization in hydrogen. The full circles correspond to deuterium.

From the dE/dx-curves the energy and the velocity, as functions of the distance traversed, can be derived. Good agreement is obtained with the velocity-range relation found for argon by Bøggild, Brostrøm, and Lauritsen.[5] By means of the stopping formula the effective charge of the fragments can be calculated; the result agrees fairly well with the direct measurements of the total charge and its variation along range.[6]

A more detailed account of the present work will be published in the Communications of the Copenhagen Academy of Science.

[1] N. O. Lassen, Phys. Rev. **70**, 577 (1946).
[2] Bøggild, Arrøe, and Sigurgeirsson, Phys. Rev. **71**, 281 (1947).
[3] N. Bohr, Kgl. Danske Vid. Sels. Math.-Fys. Medd. **18**, No. 8 (1948).
[4] Flammersfeld, Gentner, and Jensen, Zeits. f. Physik **120**, 450 (1943). W. Jentschke, Zeits. f. Physik **120**, 165 (1943).
[5] Bøggild, Brostrøm, and Lauritsen, Kgl. Danske Vid. Sels. Math.-Fys. Medd. **18**, No. 4 (1946); Phys. Rev. **58**, 839 (1940).
[6] N. O. Lassen, Kgl. Danske Vid. Sels. Math.-Fys. Medd. **23**, No. 2, (1945); Phys. Rev. **68**, 142 (1945); Phys. Rev. **69**, 137 (1946).

The Distribution of Arc-Chord Differences in Scattered Particle Tracks*

W. T. SCOTT
Brookhaven National Laboratory, Upton, Long Island, New York
April 11, 1949

IN a previous letter,[1] it was suggested that the scattering of particle tracks in emulsions might be readily measured by the difference between the actual length of track and the chord joining the two ends. In fact, an approximate expression for the average value of this difference was given, which was quite similar to the corresponding expression for the usual measure of scattering.

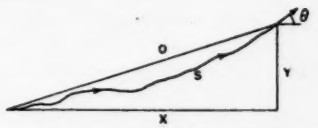

FIG. 1. A scattered track of arc length s, chord D, projection on the initial direction x, lateral displacement y, and angular deviation θ.

It is to be expected, however, that the statistical distributions in the two quantities should be qualitatively different. The arc-chord difference should be subject to relatively large fluctuations. A given, fairly large angle of scattering near the middle of the track will affect the entire measurement although a similar scattering near one end will have a much smaller effect. On the other hand, the sum of the squares of successive chord angles will not be greatly affected if one of the angles is large, and in fact the distribution of this quantity will certainly get narrower as the number of chords is increased. It is the object of this note to report on calculations of these two distributions that partially bear out these expectations.

The calculations are made for the case of constant energy which, of course, does not obtain in photographic emulsions, but which allows an explicit result that will serve to compare the two methods. We start with a diffusion equation for the combined distribution W of u, y and θ as functions of s. In these expressions, u stands for the difference between the arc length s and the projection x of the track along its initial direction; y is the lateral displacement from the x axis, and θ gives the direction of the track (Fig. 1). We have, assuming all angles to be small,

$$\frac{\partial W}{\partial s}+\frac{\theta^2}{2}\frac{\partial W}{\partial u}+\theta\frac{\partial W}{\partial y}=\frac{1}{\lambda}\frac{\partial^2 W}{\partial \theta^2}, \qquad (1)$$

where λ represents a "scattering length"; $2/\lambda$ is the mean square projected scattering angle per unit path length.[3] This equation may be solved by assuming an exponential-type solution (LaPlace transform) in the variables u, y, and s, solving the resulting ordinary differential equation in θ, in terms of Hermite functions. The condition of convergence in θ yields an expression for the exponential coefficient of s and a $\delta(\theta)$ boundary condition yields a solution in the form of a double integral over the transformed variables for u and y with an infinite series of the Hermite functions for θ.

The series may readily be summed. The coefficient of the double integral is determined in the following manner: $W(u, y, \theta, s)$ is written in terms of the dimensionless variables $\xi=u\lambda/s^2$, $\nu=y(\lambda/s^3)^{\frac{1}{2}}$, and $\eta=\theta(\lambda/s)^{\frac{1}{2}}$. It may be shown from Eq. (1) that the resulting distribution is independent of s, which implies that the shape of the distribution is constant, the scale factors changing as s changes. Hence, a normalized distribution of this form yields for $s=0$, $W=\delta(u)\delta(y)\delta(\theta)$. There is a unique coefficient in the double integral which yields this behavior. Two further checks are that integration over y yields a solution to the diffusion equation for u, θ, and s as it should, and integration over u yields Fermi's distribution function in y and θ (Eq. (1) of reference 2).

To get the distribution in $v=s-D=s-(x^2+y^2)^{\frac{1}{2}}\leqq u-y^2/2s$, we change variables from u to v, integrate the solution over ν and η, and using the dimensionless variable $\omega=v\lambda/s^2$ we arrive finally at the desired distribution

$$F(\omega)d\omega=\frac{d\omega}{2\pi i}\int_{a-i\infty}^{a+i\infty} z^{\frac{1}{2}}\sinh^{-\frac{1}{2}}z\exp(\tfrac{1}{2}z^2\omega)dz. \qquad (2)$$

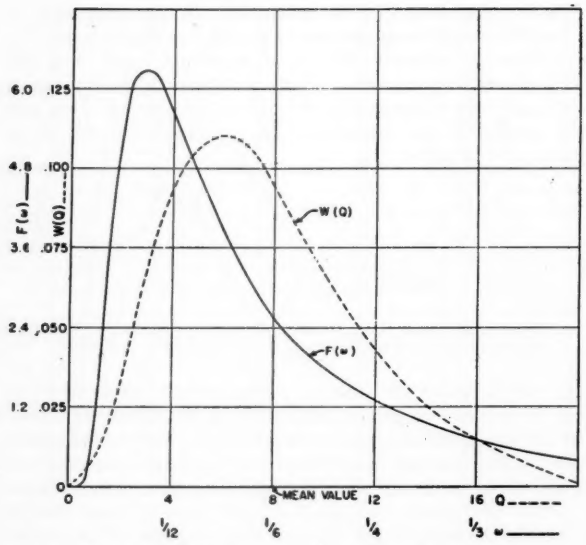

FIG. 2. $F(\omega)$, the distribution function for arc-chord differences, as a function of $\omega=\lambda(s-D)/s^2$ and $W(Q)$, the distribution function for the sum of squares of chord angles, as a function of $Q=(3\lambda/4s)\Sigma\alpha_k^2$ (calculated for nine chords).

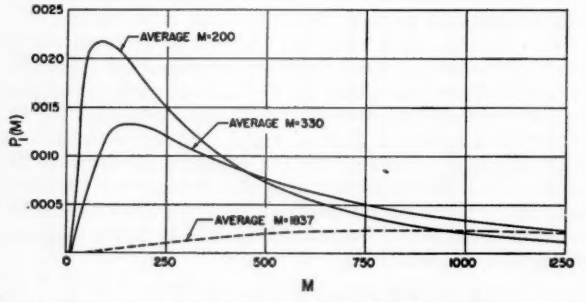

FIG. 3. $P_1(M)$, the arc-chord difference distribution, as a function of the apparent mass M.

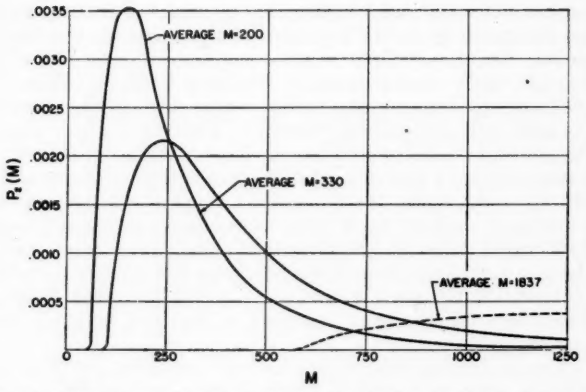

FIG. 4. $P_2(M)$ the sum-of-squares distribution for nine chords, as a function of the apparent mass M.

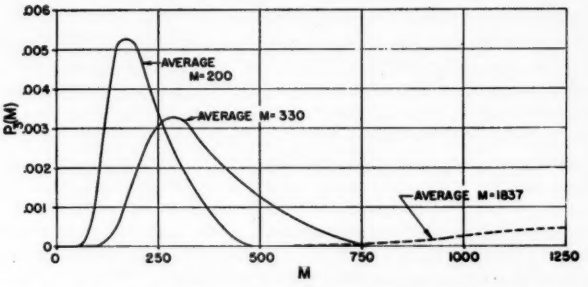

FIG. 5. $P_3(M)$ the sum-of-squares distribution (uncorrelated), for twenty-one chords, as a function of the apparent mass M.

The moments of the distribution are readily calculated: $\langle\omega\rangle_{Av}=\frac{1}{6}$; $\langle\omega^2\rangle_{Av}=1/20$; $[\langle\omega^2\rangle_{Av}-\langle\omega\rangle_{Av}^2]^{\frac{1}{2}}=0.89\langle\omega\rangle_{Av}$. The distribution itself may be calculated by expanding $\sinh^{-\frac{1}{2}}z$ in powers of e^{-z}; the kth term of the sum yields on integration an expression involving the parabolic cylinder function $D_{3/2}[(4k+1)/2\omega^{\frac{1}{2}}]$. These functions are expressible in terms of tabulated Toronto functions;[3] the final result of the computation is shown in Fig. 2. The skewness of this curve is quite apparent, the most probable value of ω being about $\frac{3}{8}$ the mean. The most important feature, however, is the long tail on the curve, indicating large fluctuations. (The skewness itself disappears if log ω instead of ω is used as a measure of scattering, e.g., for reasons of constant relative error. But, the nearly symmetrical curve obtained is very broad.)

The distribution in $q=(E^2/e)\Sigma\alpha_k^2$, the sum of the squares of angles between successive chords, may be found from the correlated probability for N such angles (reference 2, Eq. (31)). Standard probability calculus is used; we give here the result for nine track segments or eight chord angles (the improvement for more segments varies as $N^{\frac{1}{2}}$), in terms of the dimensionless variable $Q=3\lambda qe/4sE^2$ where s is the length of one path segment:

$$W(Q)dQ=\frac{[\beta_1\beta_2\cdots\beta_8]^{\frac{1}{2}}}{2\pi i}\int_{-i\infty}^{i\infty}dte^{Qt}\times[(t+\beta_1)(t+\beta_2)\cdots(t+\beta_8)]^{-\frac{1}{2}}, \qquad (3)$$

$$\beta_k=\left(2-\cos\frac{kT\psi}{9}\right)^{-1}.$$

The integral is readily transformed into two real integrals suitable for numerical calculation, and Fig. 2 shows this curve also. Moments are readily found: $\langle Q\rangle_{Av}=8$; $\langle Q^2\rangle_{Av}=81.75$; $[\langle Q^2\rangle_{Av}-\langle Q\rangle_{Av}^2]=0.53\langle Q\rangle_{Av}$. While the curve is not as broad or skew as that for $F(\omega)$, the fluctuations are still large.

A better representation of the efficacy of each method for estimating the masses of scattered particles is to plot each distribution as a function $P(M)$ of the "apparent mass" M which is the mass of a particle for which the given value of

ω or Q is the mean value. In this way, considerations of range and energy do not need to be explicitly included. Figure 3 shows $P_1(M)$ for the arc-chord differences, for three different average values of M; M is in units of the electron mass. Figure 4 shows $P_2(M)$ for the sums of squares of chord angles. Figure 5 shows $P_3(M)$ calculated for the *uncorrelated* probability for 20 chord angles with 21 segments. The result will be slightly broader if the correlation were taken into account.

The arc-chord difference is certainly a less precise measure of the scattering. However, the overlap of the curves in each graph shows the difficulty in using multiple scattering as an indication of the mass of the particle, and indicates the extent to which especially large or small observed values of ω or Q can eliminate, respectively, a large or small mass value from consideration. The separate chord-angle method can serve to distinguish between protons and mesons in most, but not all cases, which the arc-chord difference cannot do as well. Neither method has any reliability for distinguishing meson masses closer even than the values used in preparation of the figures.

* Research carried out at Brookhaven National Laboratory under the auspices of the AEC, while the author was on summer leave from Smith College.

[1] S. A. Goudsmit and W. T. Scott, Phys. Rev. **74**, 1537 (1948).
[2] W. T. Scott, Phys. Rev. (to be published).
[3] A. H. Heatley, Trans. Roy. Soc. Canada **37**, 13 (1943).

Scattering of Slow Neutrons by Deuterium Gas

J. A. SPIERS
National Research Council Laboratories, Chalk River, Ontario, Canada
April 12, 1949

PHYSICAL intuition is often considered of little use as a guide to the outcome of computations based on quantum-mechanical formulas. Here is an instance of an elaborate computation which finally led to results very similar to those obtained from a simple picture, a fact probably not to be surmised from inspection of the original formulas.

It is well known that slow neutron scattering experiments in deuterium gas can give information on the neutron-deuteron interaction.[1]

Only the total cross section has been considered so far as the calculation of the differential cross section requires involved transformations from the center of mass systems to the laboratory system, owing to the thermal velocities of the molecules.

A relatively simple method of calculation in which this effect is accurately taken into account has been devised by the writer, and is being used to compute the angular distribution in the laboratory system of monokinetic neutrons of energy 0.07 ev scattered by deuterium gas at a temperature of 90°K.

Two points of general interest have arisen as a result of these computations:

(1) Although $kT \sim \frac{1}{10}$th of the incident neutron energy for the figures quoted, the assumption of molecules initially at rest would lead to relatively small errors in the computed differential cross section ($\sim$1 to 7 percent, although percentage corrections to individual transitions may be large), according to the results obtained so far, which are for angles of scattering in the laboratory of 30° to 120°.

(2) The computed curves closely resemble those obtained from a semi-classical picture in which the incident neutron is scattered by two deuterons at a fixed distance (0.74A) apart on an axis with fixed but random orientation,[2] provided relative changes of phase on scattering by the two scatterers of (i) 0 and (ii) π-radians are assumed. Thus, it was found that for each initial molecular rotational quantum number J (the computations covered $J=0, 1, 2, 3$), the contribution to the differential cross section due to all transitions to final states of the same parity, had the form of curve (i), while for parity change the contribution had the form of curve (ii).

The respective quantum-mechanical curves follow closely the semi-classical curves for angles of observation (lab. system) around 30°, but fall off from the latter with increasing angle of observation to approximately $\frac{2}{3}$ of the semi-classical value at 180°.

Analytically, the quantum-mechanical formulas become identical with the semi-classical ones described above if the energy lost or gained by the neutron in the various molecular transition is treated as negligible, which, in fact, of course, is far from being the case. The same result is not obtained by neglecting the mass of the neutron compared with that of the molecule, since if we do this there is no recoil of the deuterium molecule, and the results then differ widely from the correct quantum-mechanical results.

The two methods of calculation (quantum and semi-classical) would however be expected to yield identical results for those diatomic molecules whose masses are, in fact, large compared to that of the neutron,[3] but the relatively good agreement for deuterium is perhaps surprising.

These calculations, together with graphs exhibiting the dependence of the various partial cross sections on angle of scattering, will be published in due course by the National Research Council of Canada.

[1] M. Hamermesh and J. Schwinger, Phys. Rev. **69**, 145 (1946).
[2] See Section 4 of the paper by E. Fermi and L. Marshall, Phys. Rev. **71**, 666 (1947).
[3] N. Z. Alcock and D. G. Hurst, Phys. Rev. **75**, 1609 (1949).

Observations on the Blood of Cyclotron Workers

M. INGRAM AND S. W. BARNES
Departments of Radiation Biology and Physics, The University of Rochester, Rochester, New York
April 20, 1949

ATTENTION is called to the finding of two types of unusual cells in the blood of personnel of the 130-in. cyclotron at Rochester, New York. These, are, respectively, very early mononuclear cells and cells which appear to be lymphocytes with bilobed or double nuclei. These cells, particularly the latter, occur in very small numbers, and it has been necessary to inspect several thousand leukocytes from each person in order to be assured of the finding. The "early mononuclear cells" are large (approximately 18–20μ in diameter), peroxidase negative, have deeply basophilic cytoplasm, and no nucleoli. The "lymphocytes with bilobed nuclei" tend to be somewhat larger than typical large lymphocytes. The nuclei stain slightly lighter than the nuclei of the other lymphocytes but are similar in consistency and have no nucleoli. The cytoplasm is clear, basophilic, peroxidase negative, and commonly contains a few typical azurophilic granules.

Both kinds of cells have been found in individuals not associated with the cyclotron who have abnormal blood smears due to infections, specifically in several cases of infectious mononucleosis and in one case of acute pharyngitis due to Hemolytic H. Influenza. There is, however, no indication that the findings in cyclotron personnel are due to infections.

Early mononuclear cells are occasionally found in routine films of "normal blood," however, lymphocytes with bilobed nuclei have not, to our knowledge, been described previously, and it is felt that they represent a true departure from the usual or normal blood picture. Although it is not possible to draw any conclusions relative to the significance of these cells as indicators of radiation damage, the findings may conceivably have such significance, and are presented at this time so that they may come to the attention of responsible individuals associated with cyclotrons in other institutions.

This work was supported by the joint program of the ONR and AEC.

Total Reflection of Neutrons on Cobalt

MORTON HAMERMESH
Argonne National Laboratory, Chicago, Illinois
April 13, 1949

ATTENTION has recently been called to the possibility of producing polarized neutron beams by reflection from magnetized iron mirrors.[1] The indices of refraction differ for the two neutron spin states, since their magnetic scattering amplitudes are opposite in sign. The resultant difference in critical angle of total reflection can be used to separate the spin components.

For Fe, the coherent nuclear amplitude exceeds the magnetic amplitude, so that the index of refraction is less than one for both spin states, and both are capable of total reflection. Since the critical angle is proportional to neutron wavelength, two wave-lengths (one for each spin state) will overlap. This circumstance prevents attainment of complete polarization, since intensity requirements dictate the use of a fairly broad band of neutron energies.

It is interesting to note that by reflecting neutrons from a cobalt mirror magnetized along the beam direction one can obtain an exact analog of the Nicol prism. The coherent scattering cross section of Co is ~ 1.8 barns[2] compared to 10.3 barns for Fe. At the same time, the magnetic amplitude for Co is $\sim 4.6\times 10^{-13}$ cm, which is only slightly below the value 6.0×10^{-13} for Fe, so that for Co the magnetic amplitude *exceeds* the nuclear amplitude. Consequently, the refractive indices for the two spin states lie on opposite sides of unity for *all* wave-lengths, and only one of the spin components is capable of undergoing total reflection. With an arbitrarily broad spectrum of incident neutrons, the mirror will reflect a completely polarized beam.

D. J. Hughes and his associates are now conducting reflection experiments with Fe and Co.

[1] O. Halpern, Phys. Rev. **75**, 343 (1949).
[2] C. G. Shull and E. O. Wollan, unpublished.

On the "Magic Numbers" in Nuclear Structure

OTTO HAXEL
Max Planck Institut, Göttingen
J. HANS D. JENSEN
Institut f. theor. Physik, Heidelberg
AND
HANS E. SUESS
Inst. f. phys. Chemie, Hamburg
April 18, 1949

A SIMPLE explanation of the "magic numbers" 14, 28, 50, 82, 126 follows at once from the oscillator model of the nucleus,[1] if one assumes that the spin-orbit coupling in the Yukawa field theory of nuclear forces leads to a strong splitting of a term with angular momentum l into two distinct terms $j=l\pm\frac{1}{2}$.

If, as a first approximation, one describes the field potential of the nucleons already present, acting on the last one added, as that due to an isotropic oscillator, then the energy levels are characterized by a single quantum number $r=r_1+r_2+r_3$, where r_1, r_2, r_3 are the quantum numbers of the oscillator in 3 orthogonal directions. Table I, column 2 shows the multiplicity of a term with a given value of r, column 3 the sum of all multiplicities up to and including r. Isotropic anharmonicity of the potential field leads to a splitting of each r-term according to the orbital angular momenta l (l even when r is odd, and vice versa), as in Table I, column 4. Finally, spin-orbit coupling leads to the l-term splitting into $j=l\pm\frac{1}{2}$, columns 5 and 6, whose multiplicities are listed in column 7.

The "magic numbers" (column 8) follow at once on the assumption of a particularly marked splitting of the term with the highest angular momentum, resulting in a "closed shell structure" for each completed r-group, together with the highest j-term of the next succeeding r-group. This classification of states is in good agreement with the spins and magnetic moments of the nuclei with odd mass number, so far as they are known at present. The anharmonic oscillator model seems to us preferable to the potential well model,[2] since the range of the nuclear forces is not notably smaller than the nuclear radius.

A more detailed account will appear in three communications to Naturwissenschaften.[3]

TABLE I. Classification of nuclear states.

1 Oscillator-quantum number r	2 Multiplicity	3 Sum of all multiplicities	4 Orbital momentum l	5 Total angular momentum j	6 l_j-symbol	7 Multiplicities	8 Magic numbers
1	2	2	0	1/2	$s_{1/2}$	2	
2			1	3/2	$p_{3/2}$	4	
	6	8		1/2	$p_{1/2}$	2	
3			2	5/2	$d_{5/2}$	6	14
				3/2	$d_{3/2}$	4	
	12	20	0	1/2	$s_{1/2}$	2	
4			3	7/2	$f_{7/2}$	8	28
				5/2	$f_{5/2}$	6	
			1	3/2	$p_{3/2}$	4	
	20	40		1/2	$p_{1/2}$	2	
5			4	9/2	$g_{9/2}$	10	50
				7/2	$g_{7/2}$	8	
			2	5/2	$d_{5/2}$	6	
				3/2	$d_{3/2}$	4	
	30	70	0	1/2	$s_{1/2}$	2	
6			5	11/2	$h_{11/2}$	12	82
				9/2	$h_{9/2}$	10	
			3	7/2	$f_{7/2}$	8	
				5/2	$f_{5/2}$	6	
			1	3/2	$p_{3/2}$	4	
	42	112		1/2	$p_{1/2}$	2	
7			6	13/2	$i_{13/2}$	14	126
				11/2	$i_{11/2}$	12	
			4	9/2	$g_{9/2}$	10	

[1] See, e.g., H. A. Bethe and R. Bacher, Rev. Mod. Phys. **8**, 82 (1937), pars. 32–34.
[2] Which anyhow does not lead to a very different term-sequence compared with that of an anharmonic oscillator, see reference 1.
[3] (a) Haxel, Jensen, and Suess, Naturwiss. (in press). (b) Suess, Haxel, and Jensen, Naturwiss. (in press). (c) Jensen, Suess, and Haxel, Naturwiss. (in press).

Concerning the Abundance of Atmospheric Carbon Monoxide

ARTHUR ADEL
Arizona State College, Flagstaff, Arizona
April 19, 1949

IN October of 1941 the 4.7-micron region of the solar spectrum was examined by the author at the Lowell Observatory, Flagstaff, for evidence of the carbon monoxide fundamental. The observation was made with a 2400-lines/inch grating in an $f/5$-Pfund type spectrometer of focal length 30 inches. Galvanometer deflections were recorded photographically. The solar spectrum was compared with laboratory observations,[1] but no conclusive evidence could be deduced for the existence of spectroscopically detectable quantities of carbon monoxide in the atmosphere above the observatory. The adequacy of the solar spectrum can be judged from the fact that carbon dioxide fine structure (some of it since traced to ν_3 of $C^{13}O_2^{16}$), which is twice as difficult to resolve as carbon monoxide fine structure, was abundantly present and clearly resolved.

One notes with interest, therefore, Migeotte's recent observation of the carbon monoxide fundamental as a prominent feature in the solar spectrum at Columbus, Ohio.[2]

The purely local nature of atmospheric abundance of carbon monoxide is emphasized by its absence over Flagstaff,

and further emphasized by the extremly large variations in the amount over Columbus as reported by Migeotte. There is a temptation to regard the presence of carbon monoxide in the air as a consequence of its nature as a product of incomplete combustion. It would be most instructive to follow the course of carbon monoxide above Columbus as a function of fuel consumption and local weather.

Amongst the minor constituents of the atmosphere, carbon monoxide must be regarded as a local manifestation, unlike nitrous oxide, for example, which was recently shown to be world wide in an essentially constant amount.[3]

[1] S. E. Whitcomb and R. T. Lagemann, Phys. Rev. **55**, 181 (1939).
[2] M. V. Migeotte, Phys. Rev. **75**, 1108 (1949).
[3] Arthur Adel, Astrophys. J. **90**, 627 (1939); **93**, 509 (1941); Shaw, Sutherland, and Wormell, Phys. Rev. **74**, 978 (1948).

On the Excited States of Li^7

S. S. Hanna and D. R. Inglis
Department of Physics, Johns Hopkins University, Baltimore, Maryland
April 20, 1949

THE ground state of Li^7 has nuclear spin $I=3/2$, and the possibility[1] that the 480-kev excited state is the other state of the doublet, $^2P_{\frac{1}{2}}$, is favored[2] by the existence of a transition[3] to this state by K-capture in Be^7. However, when thermal neutrons impinge on B^{10}, which[4] has $I=3$, the transition by alpha-emission leads[5] almost entirely (93 percent) to the excited state of Li^7, and this strong preference seems to demand[6] a selection rule based on a large angular momentum associated with the excited level, considerably larger than the value $I=1/2$. In keeping with the assumption of spherically symmetric exchange interactions, which have been used[7] fairly successfully to correlate nuclear stability properties, it was suggested[6] that the excited level of Li^7 might be the two states of an unresolved ^2F, having $I=7/2$ and $5/2$. In the light of recent observations[8] which display the energy groups as sharp peaks and agree quite closely on the excitation energy (and barring a pervasive selection rule), this would require very small spin-orbit coupling (<10 kev).

The objection to this latter scheme[9] is that it leaves the total orbital angular momentum L too nearly a good quantum number, and the Be^7 K-capture to the excited level would be forbidden with $\Delta L=2$. Retention of L as a quantum number is perhaps an oversimplification. It is noteworthy that agreement could be obtained both with the Be^7 K-capture and the $B^{10}(n,\alpha)Li^7$ transitions to the excited state by the assumption that this excited state is single and simply has $I=5/2$. This assumption is also compatible with the observed lifetime[10] of the excited state, which may be attributed to a magnetic dipole transition moment of plausible magnitude,[10] but requires an electric quadrupole transition moment considerably larger than estimated from nuclear dimensions. It agrees as well with the observed angular distribution[11] of the reaction $Li^6(d,p)Li^7$ at low energies, wherein the spherical symmetry of the long-range protons and a term as high as $\cos^4\theta$ in the short-range protons may be explained, only if the excited state has $I\geq 5/2$, in which case the explanation involves compound states 0^+, 2^+ (both competing with alphas[12]) and 5^-. Since $I=5/2$ seems to be the only single value compatible with all the observations, the problem is to make this assumption theoretically plausible.

The shell structure apparent as "magic numbers" in nuclear stability has been correlated by Mayer[13] with the trend of nuclear spins and magnetic moments by postulating $j-j$ coupling for the individual nucleons, which requires strong spin-orbit coupling in most nuclei. There are sufficiently few exceptions to the general experimental agreement[13,14] that the scheme has a strong empirical appeal in spite of its sharp divergence from previous concepts.[7] Perhaps the most serious discrepancy is found in Li^6, where two nucleons each with $j=3/2$ would be expected[14] to combine to make $I=3$, rather than 1 as observed, but there might be exceptionally small spin-orbit coupling in this nucleus because of the exceptionally weak binding of these nucleons. Then Li^7 might also be expected to have somewhat weaker spin-orbit coupling than normal for p orbits, and a 480-kev doublet splitting would seem ample to be compatible with a splitting of 2 Mev or more in heavier nuclei as might be required to have an influence on shell structure. This would leave the excited state a $^2P_{\frac{1}{2}}$. Because this is incompatible with the $B^{10}(n,\alpha)Li^7$ and the $Li^6(d,p)Li^7$ data, we wish also to consider the possibility of stronger spin-orbit coupling in Li^7.

In extreme $j-j$ coupling, one obtains the low states by coupling three vectors $j=3/2$. Because of the exclusion principle, the two neutron vectors make $J_p=0$ in the ground state, and $J_p=2$ combining with j_p to make $I=7/2$, $5/2$, $3/2$, $1/2$ in the simplest description of the next higher states, and we may expect that some acceptable choice of nucleon interactions would make their energies ascend in this order. Enumeration of the higher states with various nucleons having $j=1/2$ rather than $3/2$ shows that there are in all two states with $7/2$, five states with $5/2$, eight with $3/2$, and six with $1/2$. In a second-order calculation departing from extreme $j-j$ coupling, one might expect very roughly that the extent of depression of the lowest state with a given I, due to the familiar second-order "repulsion" in energy, would be greatest for the value of I which characterizes the greatest number of states. By this criterion, the first-order ground state would be depressed most and remain the ground state, and $I=5/2$ would be depressed more than $I=7/2$, which does indeed make it a fairly plausible first excited state. Unfortunately, in an approach to the intermediate coupling situation from the opposite extreme of $L-S$ coupling with the ^2P assumed lowest in first order as in earlier calculations,[7] the same plausibility argument favors $I=1/2$ as the first excited state. This suggests that the interactions which one assumes to provide the $j-j$ coupling scheme may have to deviate from previous concepts so severely as to alter the order of the multiplets calculated by neglecting spin-orbit coupling. Another difficulty is that recent observations[15] fail to detect further excited states in Li^7 up to about 1.6 Mev, and this qualitative discussion unfortunately does not suffice to explain this gap.

[1] D. R. Inglis, Phys. Rev. **50**, 783 (1936); G. Breit and J. R. Stehn, Phys. Rev. **53**, 459 (1938).
[2] G. Breit and J. K. Knipp, Phys. Rev. **54**, 652 (1938).
[3] N. P. Heydenburg and G. L. Locher, Phys. Rev. **53**, 1016 (1938); unpublished data of H. T. Richards and R. M. Williamson (12 percent to excited state).
[4] Gordy, Ring, and Burg, Phys. Rev. **74**, 1191 (1948).
[5] J. K. Bøggild, Kgl. Danske Vid. Sels. Math.-fys. Medd. **23**, 4, 26 (1945).
[6] D. R. Inglis, Phys. Rev. **74**, 1876 (1948).
[7] E. Feenberg and E. Wigner, Phys. Rev. **51**, 95 (1937); E. Feenberg and M. Phillips, Phys. Rev. **51**, 597 (1937), *et al.*
[8] Buechner, Strait, Stergiopoulos, and Sperduto, Phys. Rev. **74**, 1569 (1948); Rubin, Snyder, Lauritsen, and Fowler, Phys. Rev. **74**, 1564 (1948).
[9] As discussed by Wigner, Primakoff, and Feenberg, Feld, and others.
[10] L. C. Elliott and R. E. Bell, Phys. Rev. **74**, 1869 (1948); Rasmussen, Lauritsen, and Lauritsen, Phys. Rev. **75**, 199 (1948).
[11] Krone, Hanna, and Inglis, Phys. Rev. **75**, 335 (1949).
[12] R. Resnick and D. R. Inglis, Phys. Rev. **75**, 1291 (1949).
[13] M. G. Mayer, Phys. Rev. (to be published).
[14] E. Feenberg and K. C. Hammack, Phys. Rev. (to be published).
[15] Unpublished observations of Buechner and co-workers on $Be^9(d,\alpha)Li^7$ and $Li^6(d,p)Li^7$, of Heydenburg and Inglis on $Li^6(d,p)Li^7$, and of Resnick and Hanna and of Inglis on $Be^9(d,\alpha)Li^7$.

Meson Exchange and Spin-Orbit Coupling in Nuclei

D. R. Inglis
Department of Physics, Johns Hopkins University, Baltimore, Maryland
April 20, 1949

THE single-nucleon spin-orbit coupling required by recent conjectures[1-3] concerning the prevalence of a $j-j$ coupling scheme in most nuclei is too strong a coupling to be

entirely accounted for by the simple theory based on a Thomas precession

$$\omega_T = a \times v/2c^2, \quad (1)$$

proportional to the acceleration a and velocity v of a nucleon endowed with an intrinsic spin.[4-6] The analysis of the magnetic moments of the three-nucleon nuclei involves the graphic concept of exchange currents[7] representing the transport of charged mesons responsible for some of the inter-nucleon interactions. Certain types of mesons which may be responsible for nuclear forces (π-mesons with spin 1) are carriers of spin as well as of charge, and one may anticipate on the basis of similar graphic concepts that the process of meson exchange which binds a circulating nucleon to the rest of the nucleus involves a predominantly centripetal acceleration of the meson momentarily associated with the circulating nucleon. This meson acceleration is expected to be much greater than the centripetal acceleration of the nucleon, since the exchange process may be expected in effect to take place many times per revolution. Although one does not have at hand a sufficiently complete analysis of the energetics of meson fields, it seems plausible to suppose that this large acceleration a of the meson, together with the tangential component of v which the meson would have in common with the circulating nucleon, should give rise to a Thomas precession of the meson spin much more rapid than that of the intrinsic nucleon spin previously derived from (1). Even if somewhat suppressed by a weighting factor representing the ephemeral association of the meson and nucleon (as enters, for example, in the interpretation of anomalous nucleon magnetic moments),[8] this might still give a spin-orbit coupling $\sigma \cdot \omega_T$ much larger than that arising from precession of the nucleon spin alone. (A factor of ten or more seems to be needed by the empirical conjectures.) During the meson's fleeting association as part of the circulating nucleon, the meson spin has the direction of the nucleon spin of which it is a part (that is, a nucleon with spin up is part of the time a nucleon with spin down and a meson with spin up), and the directions of a and v are the same as before, so the sign of the coupling is the same as that arising from a Thomas precession of an intrinsic nucleon spin, which is satisfactory. From these graphic considerations, it seems more likely that a spin-orbit coupling belonging to each individual nucleon would arise from this second-order relativistic effect than from the second-order perturbation theory with a tensor interaction, as treated by Dancoff[6] in the simple case of He^5 with only one circulating nucleon.

[1] M. G. Mayer, Phys. Rev. (to be published).
[2] E. Feenberg and K. C. Hammack, Phys. Rev. (to be published).
[3] S. S. Hanna and D. R. Inglis, Phys. Rev. **75**, 1767 (1949).
[4] D. R. Inglis, Phys. Rev. **50**, 783 (1936); W. H. Furry, Phys. Rev. **50**, 784 (1936); G. Breit and J. R. Stehn, Phys. Rev. **53**, 459 (1938).
[5] D. R. Inglis, Phys. Rev. **74**, 1878 (1948).
[6] S. Dancoff, Phys. Rev. **58**, 326 (1940).
[7] S. T. Ma and F. C. Wu, Phys. Rev. **62**, 118 (1942); F. Villars, Phys. Rev. **72**, 256 (1947); A. Thelling and F. Villars, Phys. Rev. **73**, 925 (1948).
[8] Fröhlich, Heitler, and Kemmer, Proc. Roy. Soc. **A166**, 127 (1938); J. M. Jauch, Phys. Rev. **63**, 344 (1943).

The Interpretation of the K^{42} Radioactivity*

FRANKLIN B. SHULL AND EUGENE FEENBERG
Wayman Crow Laboratory, Washington University, St. Louis, Missouri
April 20, 1949

A NUMBER of recent studies have been concerned with the occurrence of a characteristic forbidden type of energy distribution in several well-known beta-radioactive transitions. The necessary theoretical conditions[1] are

(1) Gamow-Teller selection rules govern the beta-process,
(2) the transition is first-forbidden, with $\Delta I = \pm 2$ and a change in parity.

For this situation the beta-spectrum differs from the allowed shape by a factor G, which, if Z is small, has the approximate form $G \sim (W_0 - W)^2 + W^2 - 1$. Here W is the electron energy

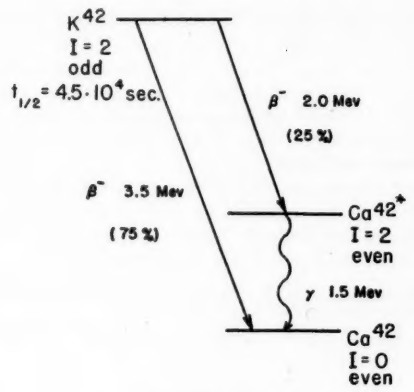

FIG. 1. Decay scheme of K^{42}.

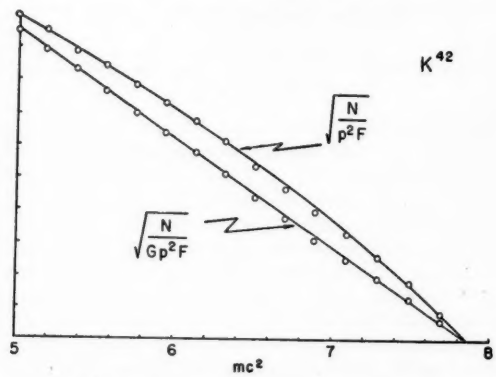

FIG. 2. FK plots for K^{42}, using data due to Siegbahn. Upper curve "allowed" plot, lower is "forbidden" plot.

and W_0 is the total energy release, both in units mc^2. The factor G emphasizes the relative number of high-energy particles and may also emphasize low-energy particles if $W_0 \geqq 2$. The FK (Fermi-Kurie) plot (computed as though the transition were allowed) tends to bulge upward at high energy, and may also curve upward at low energy, thus producing an S-shaped plot.

Beta-distributions of the type described above have been measured for Y^{91} by Langer and Price[2] and by Osoba,[3] for Cs^{137} by Mitchell and Peacock[4] and by Osoba,[3] for Y^{90} and Sr^{90} by Braden, Slack, and Shull,[5] and for Rb^{86} by Mitchell.[6]

The product ft provides a means of classifying transitions as allowed or forbidden to various degrees.[7] Here t is the half-life and f is the integral of the allowed probability function $P(W)$ over the available energy range. For the first-forbidden transitions discussed above $P(W)$ is modified by the factor G; consequently in this case the product $(W_0^2-1)ft$ should be more nearly constant than ft.

Using the shell model[8] as a guide, it is possible to select a group of beta-transitions between ground states wherein a change of parity is likely and for which the ft product is characteristic of first- or second-forbiddenness according to the empirical scheme of Konopinski. When these are reclassified according to the magnitude of $(W_0^2-1)ft$, it is found that the isotopes Y^{91}, Cs^{137}, Y^{90}, Sr^{90}, and Rb^{86}, for which the forbidden shape has already been observed, fall into a select category. For these isotopes, the product $(W_0^2-1)ft$ has values close to 10^{10}, whereas it is smaller by a factor of 10 or more for other transitions marked by a change in parity (according to the shell model). This suggests that $(W_0^2-1)ft \sim 10^{10}$ provides a rough criterion whereby one can pre-select the first-forbidden transitions for which $\Delta I = \pm 2$.

Nucleus	Cl^{38}	A^{41}	K^{42}	Br^{84}	Rb^{86}	Sr^{89}
$(W_0^2-1)ft \times 10^{10}$	0.5	1.4	0.7	0.8	0.8	0.7

Nucleus	Sr^{90}	Sr^{91}	Y^{90}	Y^{91}	Sb^{125}	Cs^{137}
$(W_0^2-1)ft\times10^{10}$	0.4	0.7	0.3	0.8	1.1	1.8

The criterion fits Sr^{89} and K^{42}; in both cases shell model considerations support the assignment $\Delta I=\pm2$ and change in parity. An excellent measurement of K^{42} has already been made by Siegbahn.[9] It disintegrates (Fig. 1) by negatron emission to the ground state of Ca^{42} and also to an excited state followed by a gamma-ray. We have analyzed Siegbahn's data for the high energy component with results shown in Fig. 2 both for an allowed FK plot and again as a forbidden FK plot wherein the factor G is included. The bulging curvature of the one and the near-straightness of the other confirm the above-stated criterion as well as those aspects of the shell model and of the Fermi theory of beta-decay which are involved in this example.

The shell model associates the odd configuration $(3d)^{-1}(4f)^3$ with the ground state of K^{42}. Similarly the even configuration $(4f)^2$ may be associated with the ground state of Ca^{42} (probably $I=0$) and with low excited states ($I=2$, 4, and 6). We suggest $I=2$ and even parity for the excited state of Ca^{42} observed in the K^{42} decay. The low energy transition is thus interpreted as first-forbidden with $\Delta I=0$.

* Assisted by the joint program of the ONR and the AEC.
[1] E. J. Konopinski and G. E. Uhlenbeck, Phys. Rev. **60**, 308 (1941).
[2] L. M. Langer and H. C. Price, Jr., Phys. Rev. **75**, 1109 (1949).
[3] J. S. Osoba, to be published.
[4] A. C. G. Mitchell and C. L. Peacock, to be published in Phys. Rev. (private communication).
[5] C. H. Braden, L. Slack, and F. B. Shull, to be published. Also L. J. Laslett and E. Jensen (private communication).
[6] A. C. G. Mitchell (private communication); also Zaffarano, Kern, and Mitchell, Phys. Rev. **74**, 682 (1948), particularly Fig. 4.
[7] E. J. Konopinski, Rev. Mod. Phys. **15**, 209 (1943).
[8] E. Feenberg and K. Hammack, Phys. Rev., to be published.
[9] K. Siegbahn, Arkiv. f. Mat., Astr. o. Fys. 34B, No. 4 (1946).

The Magnetic Moment of Be^9 *

W. C. Dickinson and T. F. Wimett
Research Laboratory of Electronics, Massachusetts Institute of Technology, Cambridge, Massachusetts
April 14, 1949

THE ratio of the frequency of the nuclear magnetic resonance of Be^9 to that of the proton has been measured at 7000 gauss by the magnetic-resonance-absorption method of Pound, Purcell, and Torrey.[1] The magnet and radiofrequency bridges employed were those used by both Bitter[2] and Poss[3] in their recent nuclear-magnetic-moment determinations. However, the accuracy of the present measurement exceeds that of previous measurements with this equipment by about a factor of ten. This was accomplished by taking advantage of the almost integral ratio of the two frequencies and heterodyning the seventh harmonic of the Be^9 frequency with the fundamental of the proton frequency.

Both the proton and Be^9 resonances were obtained from a single sample consisting of an aqueous solution of beryllium fluoride. The sample container was a cylindrical section $\frac{1}{2}$-in. long and $\frac{1}{2}$ in. in diameter. The coil for the 4.2-Mc (Be^9 resonant frequency) bridge was wound around the cylinder, and the coil for the 30-Mc (proton resonant frequency) bridge was wound at right angles over the first. This technique has previously been used by F. Bitter and assures that the external magnetic field seen by the two types of nuclei is the same. The two resonances were traced on separate recording milliammeters as the magnetic field was slowly varied. The frequencies were adjusted so that the resonances occurred nearly simultaneously. From a calibration of the rate of change of magnetic field, a correction was made, when necessary, to take into account the small field differences separating the two resonances. This correction never exceeded 0.003 percent of the observed frequency ratio.

A total of ten determinations was made. From these the following value for the ratio of the resonant frequencies in the same magnetic field was obtained:

$$\nu(Be^9)/\nu(H^1)=0.1405187\pm0.000002.$$

All ten values fall well within the above limits which were determined entirely by the uncertainty in locating the exact centers of the resonance curves.

Applying the Lamb[4] diamagnetic correction, and using the Millman and Kusch[5] value of the proton moment (2.7896 ±0.0008) μ_N, the Be^9 magnetic moment is found to be

$$\mu(Be^9)=(-)(1.17619\pm0.00034)\mu_N.$$

If, in agreement with more recent experiments, the more accurate value[6] of $(2.7926\pm0.0006)\mu_N$, is taken for the proton moment, the following value is obtained:

$$\mu(Be^9)=(-)(1.17747\pm0.00027)\mu_N.$$

It is to be noted that the uncertainties indicated for the Be^9 magnetic moment are determined by the uncertainty in the proton moment and not by that of the above frequency ratio.

* This work has been supported in part by the Signal Corps, the Air Materiel Command, and the ONR.
[1] Pound, Purcell, and Torrey, Phys. Rev. **69**, 681 (1946).
[2] F. Bitter, Phys. Rev. **75**, 1326 (1949).
[3] H. L. Poss, Phys. Rev. **75**, 600 (1949).
[4] W. E. Lamb, Jr., Phys. Rev. **60**, 817 (1941).
[5] S. Millman and P. Kusch, Phys. Rev. **60**, 91 (1941).
[6] This value was calculated using the absolute value of the proton gyromagnetic ratio given by Thomas, Driscoll, and Hipple, Phys. Rev. **75**, 902 (1949), and the physical constants e, M_p, and c taken from J. W. Dumond and E. R. Cohen, Rev. Mod. Phys. **20**, 82 (1948). The proton moment calculated in this way agrees very well with the value given by Millman and Kusch if the latter is corrected for the magnetic moment of the electron as suggested by J. Schwinger, Phys. Rev. **73**, 416 (1948). However, the small uncertainty in the absolute value of the proton gyromagnetic ratio cannot be carried over to the proton moment in units of the nuclear magneton because of the larger uncertainty in the values of e and M_p.

Paramagnetic Resonance Absorption in Crystals Colored by Irradiation

Clyde A. Hutchison, Jr.
*Institute for Nuclear Studies, University of Chicago** and *Argonne National Laboratory, Chicago, Illinois*
April 19, 1949

PARAMAGNETIC resonance absorption at 9350 mc produced by the irradiation of LiF with neutrons has been observed. Single crystals of LiF, which showed no resonance, were irradiated in a flux of approximately 10^{12} neutrons cm^{-2} for periods of time varying from 1 to 24 hrs. After irradiation, these crystals showed the resonance absorption described in Fig. 1, when placed at the midpoint of a resonant section of

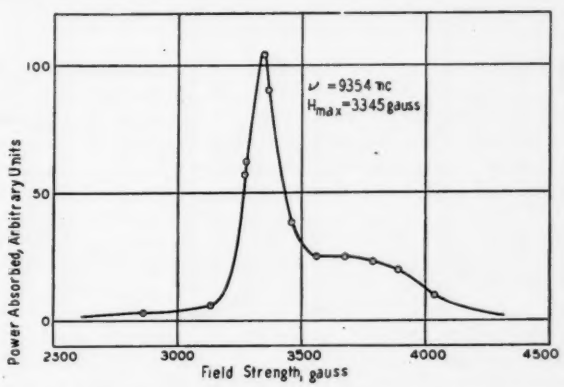

FIG. 1. Resonance absorption of LiF crystals after irradiation with neutrons.

rectangular wave guide oscillating in the $TE_{0,1,2}$ mode and the external field applied perpendicular to the wider dimension of the guide. The intensity of the effect observed after 24-hr. irradiation was less than that observed in an equal weight and volume of $CuSO_4 \cdot 5H_2O$ [1] by a factor of approximately 10. After 1-hr. irradiation, the effect was just slightly above the limits of observability. The width at half maximum absorption is approximately 160 gauss, and the absorption is asymmetric about the maximum. The maximum absorption occurred at a ratio of frequency to field strength identical with that for $MnSO_4 \cdot 2H_2O$ [1] within the error of measurement which is approximately 0.5 percent. Independent calibrations of the magnetic field and wave meter give the value, 2.00, for the ratio $h\nu/\beta H_{max} = g$. When the colored crystals were bleached by heating at 500°C, the paramagnetic resonance absorption disappeared completely. The effect has also been observed in KCl; the intensity is much less than in the LiF.

Attempts to correlate the growth and decay of the paramagnetic resonance absorption on irradiating and heating with the corresponding effects on the optical spectra encounter difficulties due to the intense colorations. E.g., the optical F band[2,3] at 2750A, supposedly due to trapped electrons, is so intense after irradiation times required for observation of the resonance that it cannot be measured in the thinnest crystals so far obtained.

The observed resonance is consistent with prevalent theories[4] of the trapping of electrons in negative ion vacancies to produce F centers. Other possible sources of such resonance are electrons trapped in other types of structure defects, free Li atoms, and free F atoms, all of which are quite probable consequences of the release of 4.6 Mev[5] per disintegration produced in the crystal. The problem of radiation-produced paramagnetic resonance is being investigated in some detail and a more complete account will be presented in the future.

The suggestion by O. C. Simpson of the possibility of observing the resonance, and the assistance and advice of P. Pringsheim and R. Casler of the Argonne National Laboratory, and of W. E. Good of the Westinghouse Research Laboratories are gratefully acknowledged.

* Assisted by the ONR.

[1] Cummerow, Halliday, and Moore, Phys. Rev. **72**, 1233 (1947).
[2] M. Burton, MDDC Document No. 17 War Department, Corps of Engineers, Office of the District Engineer, Manhattan District, Oak Ridge, Tennessee.
[3] H. F. Ivey, Phys. Rev. **72**, 341 (1947).
[4] F. Seitz, Rev. Mod. Phys. **18**, 384 (1946).
[5] M. S. Livingston and J. G. Hoffman, Phys. Rev. **50**, 401 (1936).

Neutron Capture γ-Rays from Cd*

C. D. Moak and J. W. T. Dabbs
Oak Ridge National Laboratory, Oak Ridge, Tennessee
April 15, 1949

THE neutron capture γ-rays from Cd^{113} have been studied by the cloud-chamber method in an attempt to determine the γ-ray energy distribution. A Cd target was placed in a neutron beam from the Oak Ridge National Laboratory pile; some of the resulting γ-rays entered a cloud chamber placed in a 1400-gauss magnetic field, where they struck a 0.0083 cm Pb foil and produced positron-electron pairs. Stereoscopic photographs were taken of the tracks and energy measurements were made by reconstructing the helical tracks through the optical system used in taking the pictures. For each pair of tracks measured an estimate was made of the various errors involved, namely: (1) multiple scattering error, (2) magnetic field error, (3) error due to electron energy loss in the Pb foil, and (4) errors of measurement due to finite track width, etc.

Each γ-ray measurement was then plotted as an appropriate error function of unit area so that when all measurements were completed the best estimate of the number of γ-rays found in any energy interval could be obtained by adding up all the area found in the interval. The energy interval widths were adjusted to give a constant probable counting error of 13 percent except at the ends of the distribution where the interval width was allowed to shrink to zero at $E_{max}+\Delta E_{max}$ and $E_{min}-\Delta E_{min}$ where the ΔE's are the resolution half-widths. This method of plotting, which allows both the counting errors and the resolution errors to dictate the amount of detail one is justified in seeing in the final distribution, will be described in more detail later.

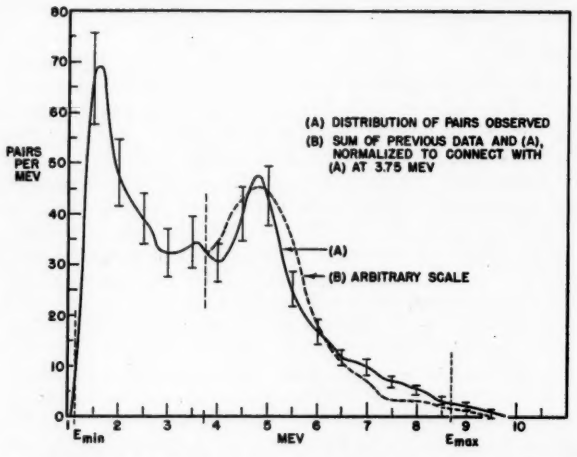

FIG. 1. (a) Distribution of pairs observed. (b) Sum of previous data and (a), normalized to connect with (a) at 3.75 Mev.

The first run** of pictures was taken under unfavorable background conditions which introduced many extraneous γ-rays from sources other than the Cd; a study of these background data showed that no reliable information could be obtained from the pictures for energies below 3.75 Mev. It was suspected that fast neutron effects were affecting the upper end of the distribution. For the second run the shielding against spurious γ-rays was improved and a set of background pictures was obtained in which every fifth picture was taken with a boron shutter placed in front of the neutron beam. This shutter allowed fast neutrons and pile γ-rays to pass through but stopped the slow neutrons. Thus every fifth picture showed the effect of all but slow neutron capture γ-rays from Cd. In this run No. 2, 8000 run-pictures and 2000 background-pictures were taken; 208 pairs were found in the run-pictures and no pairs were found in the background pictures. The energy distribution of the 208 pairs found is shown in Fig. 1(a) with the vertical lines shown in a few places to give a picture of the counting uncertainties. The highest energy measured in this run is noted on the curve as E_{max}. Run No. 1 in which background difficulties made the distribution uncertain below 3.75 Mev has been added to the part of 1(a) which lies above that energy. The result has been area-normalized and connected with the lower section of 1(a) and is shown as the dotted line of Fig. 1(b). Probable counting errors for 1(b) are 9½ percent. An analysis of the average asymmetry in the division of the γ-ray energy between positrons and electrons has shown that in all energy intervals except 1–2 Mev the average splitting is roughly equal. Below 2 Mev the data are probably not as reliable since at these energies the probability may be appreciable that a low energy Compton electron ejected from the foil will curve back into the foil and be backscattered into the chamber giving a spurious "pair." If this occurs frequently the average splitting of the energy of the γ-rays will be toward the positron side. This asymmetry was observed below 2 Mev.

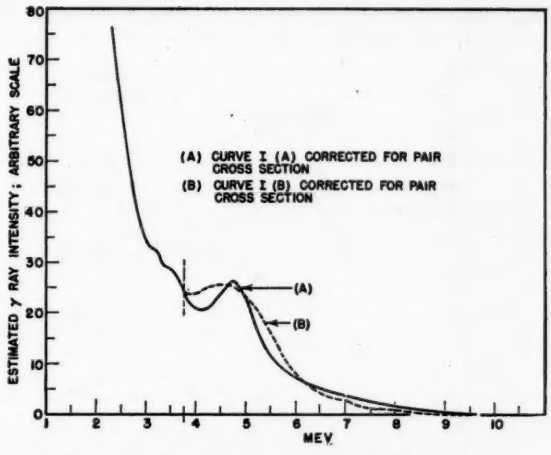
ESTIMATED γ RAY INTENSITY; ARBITRARY SCALE
(A) CURVE I (A) CORRECTED FOR PAIR CROSS SECTION
(B) CURVE I (B) CORRECTED FOR PAIR CROSS SECTION
(A)
(B)
MEV

FIG. 2. (a) Curve 1(a) corrected for pair cross section. (b) Curve 1(b) corrected for pair cross section.

Compensation for pair-production cross section of the curves of Fig. 1(a) and 1(b) gives the curves of Figs. 2(a) and 2(b), respectively, plotted to an arbitrary scale.

It is observed that the high energy tail of the gamma-ray distribution extends to 8.7 Mev (±0.6 Mev). Some significance should ge given to this value of E_{max} since in the run 8 pairs were observed with energies above 7.0 Mev while in $\frac{1}{4}$ as many background pictures which include the effects of the high energy neutrons in the beam no high energy gamma-rays were found.

* This document is based on work performed under Contract No. W-7405, eng. 26, for the Atomic Energy Project at Oak Ridge National Laboratory.

** Data of this run were reported in paper Z-6 at the Washington meeting of the American Physical Society, April 29, 1948. C. D. Moak and J. W. T. Dabbs, Phys. Rev. **74**, 1249 (1948).

New Ferroelectric Crystals

B. T. MATTHIAS
Bell Telephone Laboratories, Murray Hill, New Jersey
April 18, 1949

THREE different groups of crystals are known which show an anomalous dielectric behavior somewhat analogous in their phenomenological aspects to ferromagnetism. The crystal groups are: Rochelle salts; KH_2PO_4 and the corresponding isomorphous crystals; and barium titanate and its solid solutions with the strontium and lead salts.

The mechanism responsible for the high dielectric constant in the first two groups is generally considered to be associated with hydrogen bonds, whereas in $BaTiO_3$ the high polarizability of the TiO_6 octahedras combined with the polarizability of BaO is thought to be responsible for the occurrence of a spontaneous polarization.[1] The latter assumption is reasonable in view of the high dielectric constants of rutile and BaO.

As expressed previously[2] the occurrence of ferroelectricity in Rochelle salt and $BaTiO_3$ seems to be of an accidental nature, insofar as none of their isomorphous crystals are ferroelectric. In the case of $BaTiO_3$ it was thought probable that crystals would be ferroelectric, regardless of valency, if the metal-oxygen octahedra were of identical size and of similar electronic configuration to the Ti-O_6 octahedra in $BaTiO_3$. From this point of view the metals columbium and tantalum appeared to be of interest. Both the Cb^{+5} and Ta^{+5} ions have a noble gas configuration similar to Ti^{+4} and have the same octahedral radii. In the fourth row of the periodic table Ga^{+3} might be considered, though it is slightly smaller and its electronic core, although having closed shells, has not a noble gas configuration. The compounds of the foregoing metals which have a perovskite structure are $KCbO_3$, $NaCbO_3$, $KTaO_3$, $NaTaO_3$ and $LaGaO_3$.

Verification of the ferroelectric behavior of the alkali columbates and tantalates has recently been reported.[3] These crystals are piezoelectric, show a dielectric hysteresis loop and go through one or more polymorphic transitions below their Curie points. Their c/a ratios, as determined from powder pictures (under the assumption of a tetragonal symmetry) at room temperature, are between 0.98 and 0.99 for the columbates. For the tantalates they are even closer to 1, but remain *below* this value.

$NaCbO_3$, $KCbO_3$, $NaTaO_3$, and $KTaO_3$ have been obtained in clear crystals of 1 to 2-mm cube edge. The Curie points can be observed either by dielectric measurements or by optical observation, since at this point the crystals go from an anisotropic state to an isotropic one. The peak of the dielectric constant at the Curie point can be well observed as long as this temperature is not too high (Fig. 1). At higher temperatures, however, the dielectric tests become sowmheat more difficult due to the increase in conductivity. While the Curie point of $NaTaO_3$ around 475°C is the highest so far

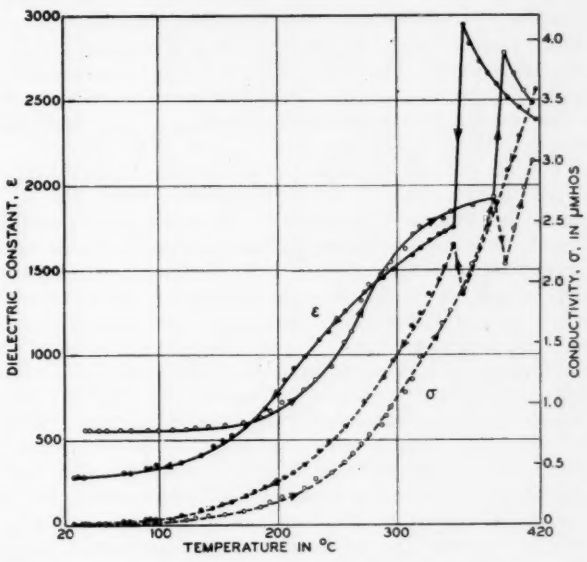

FIG. 1. Dielectric constant and loss of a $NaCbO_3$ crystal.

observed, that of $KTaO_3$ is even lower than reported previously[3] and comes close to room temperature.

It is expected that crystals of $LaGaO_3$ and $LaFeO_3$ may exhibit similar polymorphic transitions. Though the powder picture hardly indicates deviations from the cubic system for $LaFeO_3$, the crystals appear optically anisotropic. With increase of temperature their birefringence gradually decreases until, near 200°C, they are quite isotropic. For $LaGaO_3$, x-rays show a (tetragonal, $c/a>1$) deviation from the cubic system. The crystals undergo a marked optical transition between 90° and 100°C. Below this temperature they show parallel and 45° extinction, but above the transition they show only 45° extinction.

The dielectric constant of $LaGaO_3$ shows a discontinuity at its transition temperature. $LaFeO_3$ could not be tested dielectrically because of its high conductivity.

The x-ray investigation of these compounds and the optical investigation were carried out by Elizabeth A. Wood. The writer wishes to express his appreciation for her assistance.

[1] G. H. Jonker and J. H. van Santen, Chemisch Weekblad **43**, 672 (1947).
[2] Phase Transition meeting of the NRC, Cornell (1948).
[3] Bull. Am. Phys. Soc. **24**, No. 4, April 28-30, 1949, abstract L6.

Isotope Shift in the Helium Spectrum

MARK FRED, FRANK S. TOMKINS, AND JAMES K. BRODY
Argonne National Laboratory, Chicago, Illinois
April 14, 1949

THE availability of pure He^3 in this laboratory has made it possible to measure the He^3-He^4 shifts of a number of lines in the spectrum. The gas was diluted to about 55 percent He^3 with He^4 and sealed off in Pyrex tubes at 5 mm Hg pressure. The tubes were immersed in liquid nitrogen and excited by an electrodeless discharge. The spectrum was photographed directly in high orders of a Baird 3-meter Eagle mounting spectrograph, and with a Fabry-Perot interferometer and a 21-foot Jarrell-Ash Wadsworth mounting spectrograph. The direct shifts and the interferometer patterns were measured with a Leeds and Northrup recording microphotometer and also with a comparator, the latter giving much more accurate results except for some of the wide triplet lines.

The observed shifts $\Delta\nu$ in cm^{-1} are listed in Table I. Shifts have previously been reported on samples enriched in He^3 from natural sources to approximately one percent by Bradley and Kuhn[1] for 5015 ($\Delta\nu=-0.83\pm0.03$ cm^{-1}) and by Andrew and Carter[2] for 6678 ($\Delta\nu=-1.045\pm0.010$ cm^{-1}). The present samples are considerably more favorable, especially for the triplet lines, for which the isotope shift is of the same order as the fine structure. The triplet shifts in Table I were measured on the strong component ($^3P_1+^3P_2$); measurements on the single weak $^3P_0$ component gave discordant results, apparently due to a 15 percent increase in the triplet width for He^3.

The line shifts $\Delta\nu$ are equal to the difference in the shifts ΔT in the term values of the corresponding levels. The ΔT's cannot be determined uniquely by the combination principle but can only be compared with theory. The theory has been worked out by Hughes and Eckart[3] who showed that, neglecting electron spin energy, all levels are shifted by $\Delta T=(\Delta\mu/m)T$, where $\Delta\mu$ is the difference between the two reduced masses, m is the electron mass, and T is the absolute term value of the level. In addition to the reduced mass effect there is a further shift, upward for singlets and downward for triplets, which requires explicit expressions for the wave functions in order to be evaluated. Hughes and Eckart give a general formula based on approximate one-electron product functions with effective nuclear charges as determined independently by the variational procedure. This expression gives a contribution only for P terms. The theoretical shifts, using effective charges as determined by Eckart,[4] are also given in Table I, and finally the difference between the observed and calculated shifts.

TABLE I. Isotope shifts in the helium spectrum.

Transition	Wave-length	$-\Delta\nu$, Obs.	$-\Delta\nu$, Calc.	Difference
$2\,^3P-3\,^3S$	7065 A	(0)	0.083	—
4	4713	0.278	0.406	−0.128
5	4120	0.440	0.545	−0.105
6	3867	0.522	0.618	−0.096
7	3732	0.591	0.660	−0.069
$2\,^3P-3\,^3D$	5875	(0)	0.214	—
4	4471	0.343	0.458	−0.115
5	4026	0.471	0.571	−0.100
6	3819	0.555	0.632	−0.077
7	3705	0.605	0.670	−0.065
$2\,^1P-3\,^1S$	7281	1.045	0.999	0.046
4	5047	1.314	1.277	0.037
5	4437	1.442	1.402	0.040
$2\,^1P-3\,^1D$	6678	1.118	1.056	0.062
4	4921	1.336	1.300	0.036
5	4387	1.445	1.413	0.032
6	4143	1.496	1.474	0.022
7	4009	1.524	1.512	0.012
$2\,^3S-2\,^3P$	10830	0.975	0.986	−0.011
3	3888	1.378	1.351	0.027
$2\,^1S-3\,^1P$	5015	0.850	0.780	0.070
4	3964	1.158	1.102	0.056

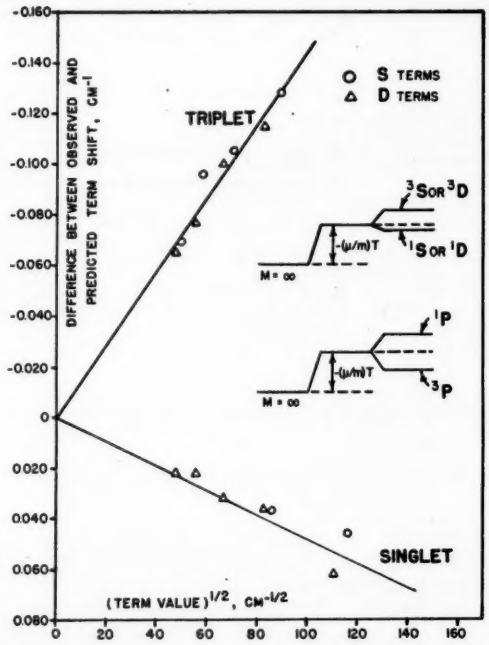

FIG. 1. Difference between observed and predicted term shifts plotted against the square root of the term value. (*Note:* The terms above which appear in parentheses should read $[1-(\mu/m)]$ and should *not* be preceded by minus signs. Also, the triangle at the extreme left of the lower curve should be above the line rather than on it.)

It will be observed that the deviations are much larger than the estimated errors, which are in general about ±0.005 cm^{-1}. It is unlikely that the choice of wave functions is at fault since a change of nuclear charge of 0.01 shifts the P levels by about 0.01 cm^{-1}, so that the observed deviations are much larger than corresponds to the known errors in the functions. More-

TABLE II. Isotope shifts of helium term values.

Term	$-\Delta T$, Obs.	$-\Delta T$, Calc.	Difference	T	$T^{\frac{1}{2}}$	Diff./$T^{\frac{1}{2}}$
$2\,^3S$	1.747	1.758	+0.011	38455	196.7	$+0.056\times10^3$
3	—	0.689	—	15074	122.8	—
4	0.494	0.366	−0.128	8013	89.5	−1.43
5	0.332	0.277	−0.105	4964	70.4	−1.49
6	0.250	0.154	−0.096	3375	58.1	−1.65
7	0.181	0.112	−0.069	2242	49.4	−1.40
$3\,^3D$	—	0.558	—	12209	110.5	—
4	0.429	0.314	−0.115	6866	82.8	−1.39
5	0.301	0.201	−0.100	4394	66.2	−1.66
6	0.217	0.140	−0.077	3051	55.2	−1.40
7	0.167	0.102	−0.065	2241	47.3	−1.38
$2\,^1S$	1.534	1.464	−0.070	32033	174.2	−0.40
3	0.569	0.615	0.046	13446	116.0	0.40
4	0.300	0.337	0.037	7371	85.8	0.43
5	0.17	0.212	0.04	4647	68.2	0.6
6	—	0.146	—	3196	56.5	—
$3\,^1D$	0.496	0.558	0.062	12205	110.5	0.56
4	0.278	0.314	0.036	6864	82.8	0.43
5	0.169	0.201	0.032	4393	66.2	0.48
6	0.118	0.140	0.022	3050	55.2	0.40
7	0.090	0.102	0.012	2241	47.3	0.46
$2\,^3P$	(0.772)	0.772	0.000*	29224	170.9	(0)
3	0.387	0.407	−0.020	12746	113.0	−0.018
4	0.220	0.230	−0.020	7094	84.2	−0.034
$2\,^1P$	(1.614)	1.614	0.000*	27176	164.8	(0)
3	(0.684)	0.684	0.000*	12102	110.0	(0)
4	0.376	0.362	−0.012	6818	82.6	−0.015

* Assumption.

over, different Z's for the $2P$ level would be required to explain the shifts for different lines if the theoretical shifts for the S and D levels are assumed correct. On the other hand it will be noted that the deviations for successive series members decreases and appears to approach zero at the limit, suggesting that the calculated P shifts are valid and that the S and D shifts are incorrect. On this basis the S and D shifts can be determined by subtracting the observed $\Delta\nu$'s from the calculated P shifts. These "observed" term shifts are given in Table II, together with the calculated shifts and the differences. The differences appear to be proportional to $T^{\frac{1}{2}}$ as shown in Fig. 1.

The following facts may be noted:

1. The shifts $\Delta T=T^{(4)}-T^{(3)}$ of the S and D levels may be represented by

$$\Delta T=(\Delta\mu/m)T\pm 4.77\times 10^{-4}(2S+1)T^{\frac{1}{2}},$$

where the plus sign applies to the triplets and the minus sign to the singlets.
2. The distinction between the triplets and singlets in the $T^{\frac{1}{2}}$ correction indicates that it is associated with electron spin. The ordinary reduced mass effect gives the center of gravity of the "spin" isotope effect. No difference can be distinguished between S and D terms.
3. The $T^{\frac{1}{2}}$ correction evidently does not apply to P terms or to the $2S$ term, but it is not of the form of a perturbation due to these low terms.
4. The fine structure of the $2\,^3P$ term seems to be about 15 percent greater for He^3.

Further measurements are in progress.

We are indebted to Mr. J. C. McGuire of the Chemical Engineering Division for the preparation of the sample tubes, and to the Ryerson Physical Laboratory of the University of Chicago for permission to use its comparator.

[1] L. C. Bradley and H. Kuhn, Nature **162**, 412 (1948).
[2] Alan Andrew and W. W. Carter, Phys. Rev. **74**, 838 (1948).
[3] D. S. Hughes and Carl Eckart, Phys. Rev. **36**, 694 (1930).
[4] Carl Eckart, Phys. Rev. **36**, 878 (1930).

Relativistic Treatment of Neutron-Proton Elastic Scattering in the Born Approximation

F. E. ALZOFON*
Radiation Laboratory, Department of Physics, University of California, Berkeley, California
April 18, 1949

AT a kinetic energy of 90 Mev, a neutron or proton (we assume both to have the same rest mass: $M=938$ Mev) has a total energy: $E'=1028$ Mev, $(v'/c)=\beta'=0.409$ and $\gamma'=(1-\beta'^2)^{-\frac{1}{2}}=1.10$, all in the laboratory system. The magnitude of β' indicates the necessity of a relativistic treatment of $n-p$ scattering, taking into account the retardation of the meson field through which the $n-p$ interaction is assumed to take place.

We have calculated the $n-p$ cross section for elastic scattering in the Born approximation, assuming a pseudoscalar coupling with exchange of both charged and neutral mesons. The interaction Hamiltonian has been given by N. Kemmer.[1]

The calculations were performed for the center of mass system (indicated by unprimed symbols). Transformation from the laboratory to the center of mass system is effected by means of the relations:

$$\beta_{cm}=(E'/Mc^2-1/E'/Mc^2+1)^{\frac{1}{2}}, \tag{1}$$

$$\tan\theta/2=\gamma_{cm}\tan\theta', \tag{2}$$

$$\beta=(\beta'-\beta_{cm})/(1-\beta'\beta_{cm}), \tag{2a}$$

where $\beta_{cm}=v_{cm}/c$ and v_{cm} denotes the speed of the center of relative to the laboratory system. For example, if $E'=1028$ Mev, then $\beta_{cm}=0.214$, $\beta'=0.409$, and $\beta=0.213$; also:

$$(\beta_{cm}-\beta'/2)/\beta'/2=4.4 \text{ percent}$$

and

$$(\beta-\beta'/2)/\beta'/2=3.9 \text{ percent}.$$

For a neutron incident with momentum $p=\beta\gamma Mc$ and a proton scattered into solid angle $2\pi\sin\theta d\theta$, we find the differential cross section:

$$\left(\frac{\sigma}{\sigma_0}\right)_r=\beta^4\gamma^2\Bigg\{\left[\cos^4\theta/2+\left(\frac{\sin^2\theta/2}{\mu^2/4M^2+\beta^2\gamma^2\sin^2\theta/2}\right)^2\right]+\left[\sin^4\theta/2+\left(\frac{\cos^2\theta/2}{\mu^2/4M^2+\beta^2\gamma^2\cos^2\theta/2}\right)^2\right]-\Bigg[\sin^2\theta/2\cos^2\theta/2+\frac{\sin^4\theta/2}{\mu^2/4M^2+\beta^2\gamma^2\sin^2\theta/2}+\frac{\cos^4\theta/2}{\mu^2/4M^2+\beta^2\gamma^2\cos^2\theta/2}+\frac{\sin^2\theta/2\cos^2\theta/2}{(\mu^2/4M^2+\beta^2\gamma^2\sin^2\theta/2)(\mu^2/4M^2+\beta^2\gamma^2\cos^2\theta/2)}\Bigg]\Bigg\}, \tag{3}$$

with $\sigma_0=[4(M/\mu)(\hbar/\mu c)(g^2/\hbar c)]^2$. The first two terms arise from the exchange of charged and neutral mesons, respectively, the third from the interference of these effects. The coupling constants between nucleon and meson fields were chosen with a view toward obtaining a cross section symmetric about the angle $\theta=90°$;[2] thus if g denotes the charged meson-nucleon coupling constant, and g', g'' the coupling constants for neutral mesons, we choose $g^2=-g'g''$.

The total cross section corresponding to Eq. (3) is:

$$\frac{1}{4\pi\sigma_0\beta^2}\Sigma_r=\frac{(\beta\gamma)^2}{2}-\frac{1}{(\beta\gamma)^2}+\frac{2}{(\beta\gamma)^4}\Bigg[\frac{\mu^2}{4M^2}+(\beta\gamma)^2-\frac{(\mu^2/4M^2)^2}{\mu^2/4M^2+(\beta\gamma)^2}-(\beta\gamma)^2\frac{2(\mu^2/4M^2)+(\beta\gamma)^2}{2}+2(\beta\gamma)^2\frac{\mu^2}{4M^2}+\frac{\mu^2}{4M^2}\left(2+\frac{\mu^2}{4M^2}-\frac{\mu^2/4M^2+(\beta\gamma)^2}{2\mu^2/4M^2+(\beta\gamma)^2}\ln\frac{\mu^2/4M^2}{\mu^2/4M^2+(\beta\gamma)^2}\right)\Bigg]. \tag{4}$$

The non-relativistic limits of Eqs. (3) and (4) were obtained by comparing states of the same momentum, with the assumption that $\beta\ll 1$ in the non-relativistic case. We find:

$$\left(\frac{\sigma}{\sigma_0}\right)_{nr}=\beta^4\gamma^2\Bigg[\left(\frac{\sin^2\theta/2}{\mu^2/4M^2+\beta^2\gamma^2\sin^2\theta/2}\right)^2-\frac{\sin^2\theta/2\cos^2\theta/2}{(\mu^2/4M^2+\beta^2\gamma^2\sin^2\theta/2)(\mu^2/4M^2+\beta^2\gamma^2\cos^2\theta/2)}+\left(\frac{\cos^2\theta/2}{\mu^2/4M^2+\beta^2\gamma^2\cos^2\theta/2}\right)^2\Bigg]. \tag{5}$$

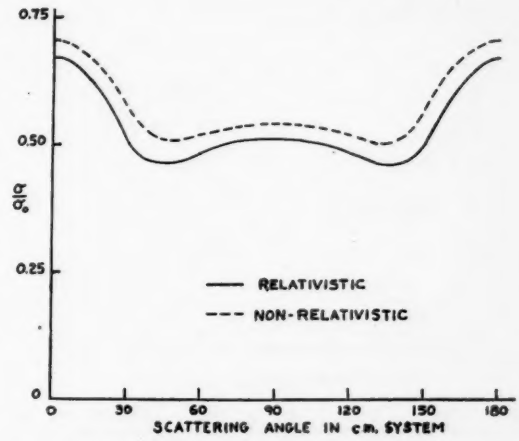

FIG. 1. Relativistic differential scattering cross section as a function of the scattering angle θ. Born approximation.

$$\frac{1}{4\pi\sigma_0}\Sigma_{nr}=\left(3\frac{\mu^2}{4M^2}+\beta^2\gamma^2\right)\left[\frac{1}{\mu^2/4M^2+\beta^2\gamma^2}+\frac{2\mu^2/4M^2}{2\mu^2/4M^2+\beta^2\gamma^2}\ln\frac{\mu^2/4M^2}{\mu^2/4M^2+\beta^2\gamma^2}\right]. \quad (6)$$

For $\mu=326m_e$, we obtain the curves shown in Fig. 1. The strong influence of the interference terms is to be noted.

The dependence of the potential energy on the separation $r=|\mathbf{r}'-\mathbf{r}^2|$, of the nucleons can be shown to have the form (in the Born approximation):

$$V(r)=(g/\kappa)^2(1+P_\tau)(i\gamma_5'((\kappa)^2-\Delta)^{\frac{1}{2}}-\boldsymbol{\sigma}'\cdot\boldsymbol{\nabla})\times(i\gamma_5^2((\kappa)^2-\Delta)^{\frac{1}{2}}-\boldsymbol{\sigma}^2\cdot\boldsymbol{\nabla})e^{-\kappa r}/r, \quad (7)$$

with $P_\tau=\frac{1}{2}(1+\boldsymbol{\tau}'\cdot\boldsymbol{\tau}^2)$. Relation (7) may be simplified.[3]

The author wishes to thank Professor R. Serber for suggesting the problem and for valuable discussion.

This work was performed under the auspices of the AEC.

* Now at North American Aviation, Inc., Los Angles, California.
[1] N. Kemmer, Proc. Roy. Soc. 166A, 127 (1938).
[2] Hadley, Kelly, Leith, Segré, Wiegand, and York, Phys. Rev. 75, 351 (1949).
[3] F. J. Dyson, Phys. Rev. 73, 929 (1948). E. C. Nelson, Phys. Rev. 60, 830 (1941).

A Suggested Slow Neutron Crystal Counter*

K. A. YAMAKAWA**
Palmer Physical Laboratory, Princeton University, Princeton, New Jersey
April 15, 1949

A SINGLE mixed crystal of lithium and silver bromide when annealed and cooled to liquid nitrogen temperature has been found to count ionizing radiation and neutrons. The crystal, grown by Bridgman's method, was 0.75 cm in thickness and 1.2 cm² in area and contained approximately four times as many silver atoms as lithium atoms.

In the experiment a field of 2700 volts/cm was maintained across the crystal. The radiation was provided by a 25-millicurie radium-beryllium source imbedded in an eight-inch cube of paraffin and shielded by four inches of lead. A $\frac{1}{32}$-in. sheet of cadmium placed between the lead and the paraffin was used as a shutter for slow neutrons.

Differential pulse-size distribution curves as shown in Fig. 1 were obtained with and without the cadmium shutter. The difference between the upper two curves gives the contribution from slow neutrons. For comparison, a similar curve (not shown) was taken for gamma-rays from a 0.1-millicurie radium source. The maximum pulse height for these gamma-rays was estimated to be about 70 volts. Thus, the pulses due to neutrons are seen to extend considerably beyond those due to gamma-rays from radium.

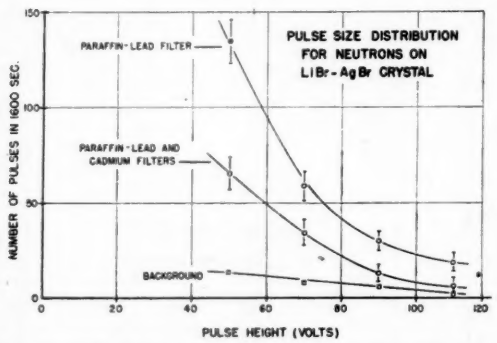

FIG. 1. Pulse height distribution for lithium bromide-silver bromide crystal counter irradiated by neutrons from a radium-beryllium source. Top curve: source filtered by paraffin—lead. Middle curve: source filtered by paraffin—lead and cadmium. Bottom curve: background with source absent.

The energy of the particles released in the neutron capture by Li^6 is 4.7 Mev, while the maximum energy of the gamma-rays from the radium is 2.4 Mev. Since the neutron pulses seem to have a high energy tail in the region where the gamma-ray pulses fall to zero, it would appear that the value of energy per ion pair for heavy particles (namely H^3 and He^4) released within the crystal is not more than twice, and may well be equal, to the value for beta-particles. This observation is to be contrasted with a result of Van Heerden[1] with silver chloride that the energy per ion pair for alpha-particles from an external source is four to six times the energy per ion pair for beta-particles. It is possible that the discrepancy is due to surface effects.

The slow neutron capture cross sections for naturally occurring lithium and silver are approximately equal.[2] Thus, in the crystal studied only one-fifth of the slow neutrons are captured by Li^6 nuclei, and four-fifths by silver nuclei. These latter decay quickly to give beta-rays with maximum energy about the same as that for the gamma-rays from radium.

The present counter of natural isotopes and of 0.75-cm thickness has an efficiency of the order of 5 percent for slow neutron detection. The efficiency and selectivity can be considerably improved by using a thicker crystal of lithium enriched in Li^6. It would then be expected that a crystal one- or two-centimeters thick with the same proportion of lithium to silver would have an efficiency of the order of 70 percent.

This work was performed as part of a Ph.D. thesis at Princeton University. The author is grateful to Professor R. Hofstadter for his continued encouragement and assistance.

* Supported in part by the Joint Program of the ONR and the AEC.
** Now at Ballistic Research Laboratories, Aberdeen Proving Ground, Maryland.
[1] P. J. Van Heerden, *The Crystal Counter*, Thesis, Utrecht (1945).
[2] Goldsmith, Ibser, and Feld, Rev. Mod. Phys. 19, 259 (1947).

Microwave Spectrum of Formaldehyde

J. K. BRAGG* AND A. H. SHARBAUGH
General Electric Research Laboratory, Schenectady, New York
April 14, 1949

FIVE lines of the pure rotation spectrum of formaldehyde have been observed in the region 18,300–27,500 megacycles. Comparison of the observed spectrum with that calculated for a wide range of the molecular parameters, and the resolution of the Stark pattern of the $9_{2,8}\rightarrow 9_{2,7}$ transition, permits an unambiguous identification of four of the lines. The analysis was facilitated by the fact that only transitions between the two components of "K-doublets" are expected in the region surveyed; this is a result of the small moments of inertia.

The observed spectrum is given in Table I; listed for comparison are the calculated frequencies, and the centrifugal distortion corrections which were applied. The rigid rotor frequencies were calculated by the method of Golden.[1] Wang[2] has given a simple expression for the splitting of K-type doublets which was useful for preliminary analysis but not sufficiently accurate for precise calculations. In the final calculation of the spectrum with $\kappa=-0.9612$, the continued fraction method[3] was used to provide precise values of the rigid rotor frequencies.

The corrections for centrifugal distortion were obtained by a method due to Golden,[4] based on the theory of Wilson.[5] Necessary values of the valence-type force constants were taken from Ebers and Nielsen.[6] The uncertainty in these cor-

TABLE I. The observed microwave spectrum of formaldehyde.

Transition	Observed freq. (mc/sec.)	Calculated (mc/sec.)	Centrifugal distortion correction	Temperature* coefficient of intensity	Intensity
$25_{4,22}\rightarrow25_{4,21}$	19595.23	19,593	−305	1/5	*m*
	20736.64			1/2	*w*
$9_{2,8}\rightarrow9_{2,7}$	22,965.71	22,966	− 30	2	*s*
$17_{3,15}\rightarrow17_{3,14}$	24,068.31	24,036	−147	1/3	*m*
$26_{4,23}\rightarrow26_{4,22}$	26,358.70	26,390	−396	1/5	*w*

*Approximately, $I(-78°C)/I(25°C)$.

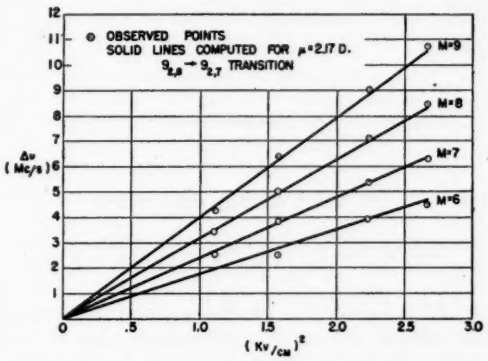

FIG. 1. Stark effect of formaldehyde absorption line at 22965.71 Mc/sec.

rections is rather large, since the results of calculation represent differences in large numbers, in which inadequacies in the assumptions made, or small discrepancies in the force constants, may be magnified. It is possible, for example, to change the correction to the $26_{4,23}\rightarrow26_{4,22}$ transition by 10 megacycles simply by varying the HCO bending force constant within the limits of uncertainty quoted by Ebers and Nielsen. The magnitude of these corrections is due to the small moment of inertia about the twofold axis.

Four Stark components of the $9_{2,8}\rightarrow9_{2,7}$ transition were resolved (see Fig. 1): their behavior as a function of frequency served to establish the identity of the line. The dipole moment in the ground vibrational state was calculated to be 2.17 ± 0.02 Debye units, using asymmetric rotor theory.[7] As far as we know, the only previously reported value is[8] 2.27, measured at 420–520°K.

The identity of the line at 20,737 is not known: it cannot be identified with any pure rotational transition below $J=35$ on the basis of the present assignment. Nevertheless, one cannot interpret even three lines of the spectrum on the basis of any other choice of rotational constants. The present assignment predicts that the strong $3_{1,3}\rightarrow3_{1,2}$ transition should fall at $29{,}058\pm50$ megacycles.

Further work is planned on the identification of the 20,737 line, and on refinement of the centrifugal distortion corrections, with the eventual object of providing close estimates of the limits of accuracy of the present theory of the semirigid rotor. It is hoped the work will lead to an independent set of force constants, which may then be compared with those determined from vibrational spectra.

The values of the effective molecular parameters on which the calculated spectrum is based are $\kappa=-0.9612\pm0.0001$ $\times(a-c)/2=1.2482\times10^5\pm0.006\times10^5$ megacycles. These are in essential agreement with the values -0.9623 and 1.2391 10^5 calculated from the results of the ultraviolet spectrum.[9] The value of κ can be given rather precisely because the frequency of the high J transitions is extremely sensitive to the parameters; there is a corresponding large uncertainty in the value of $(a-c)/2$. Observation of the $3_{1,3}\rightarrow3_{1,2}$ transition would suffice to determine the latter parameter with precision.

We wish to acknowledge the numerical calculations carried out by Miss Sally Thomas and Warren Thayer.

* Present address, Chemistry Department, Cornell University, Ithaca, New York.

[1] S. Golden, J. Chem. Phys. **16**, 78 (1948).
[2] S. C. Wang, Phys. Rev. **34**, 243 (1929).
[3] King, Hainer, and Cross, J. Chem. Phys. **11**, 27 (1943).
[4] S. Golden, J. Chem. Phys. **16**, 250 (1948).
[5] E. Bright Wilson, Jr., J. Chem. Phys. **5**, 617 (1937).
[6] E. S. Ebers and H. H. Nielsen, J. Chem. Phys. **6**, 311 (1938).
[7] S. Golden and E. B. Wilson, Jr., J. Chem. Phys. **16**, 669 (1948).
[8] E. C. Hurdis and C. P. Smyth, J. Am. Chem. Soc. **65**, 89 (1941).
[9] G. H. Diecke and G. B. Kistiakowsky, Phys. Rev. **45**, 4 (1934).

The Emission of Protons from Boron and Argon on Bombardment with Po α-Particles

R. R. ROY
King's College, University of London, London, England
April 18, 1949

BORON.—Earlier reports on the reaction $B^{10}(\alpha,p)C^{13}$ show that the compound nucleus $_7N^{14*}$ may decay with the emission of a proton leaving the final nucleus in the ground state or one of its excited states. The ground state transition ($Q=4.14$ Mev) escaped observation for a long time because of its feeble intensity. However, Brubaker and Pollard's[1] experiments gave a Q value of 4.7 ± 0.5 Mev for the protons emitted from the ground state. Later this result was confirmed by other workers. Jentshke[2] and Merhaut[3] obtained the values 3.86 and 3.85 Mev, and Joliot and Zlotowski[4] 4.3 Mev for protons of the longest range group.

The Q valves corresponding to the protons which are emitted from the compound nucleus, leaving the final nucleus C^{13} in an excited state are 3.3, 0.5, 0.1, −0.78, and −1.86 Mev.

The present experiment, utilizing a cloud chamber was chiefly concerned with the investigation of the angular distribution of the protons arising from the various states. The polonium source, strength 5 mc, was deposited on a silver foil 2 mm×2 mm and the beam of α-particles was canalized through a slit arrangement before striking the target, the thickness of which was 0.8 cm air equivalent.

In the course of over 700 photographs 86 protons were obtained. Figure 1 shows the variation of the yield of protons with the incident α-particle energy. The curve does not indicate a well defined level. From considerations of the barrier

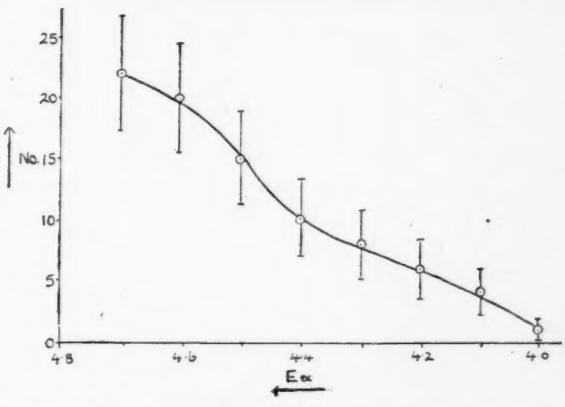

FIG. 1. The variation of the yield of protons with the incident α-particle energy.

TABLE I. Q values calculated from the energies of the emitted protons and incident α-particles.

No. of protons observed	Corresponding Q values in Mev
12	3.1
30	0.42
44	0.09

height of the B^{10} nucleus, it was estimated that the α-particle penetrated the nucleus through the top of the barrier and this could explain the absence of any peak in the curve.

The Q values calculated from the energies of the emitted protons and incident α-particles are given in Table I. These values are in close agreement with those reported by previous workers.

Owing to their feeble intensity there was no indication in this experiment of the longest range group of protons. No attempt was made to observe the protons from the still higher excited states because of their short ranges.

Miller, Duncanson, and May[5] reported a resonance level of the compound nucleus $_7N^{14*}$ corresponding to the incident α-particle energy of 2.9 Mev but no evidence of this level was obtained in the present experiment.

It should be remembered that B^{10} is present to the extent of only 20 percent of the total, B^{11} constituting the remaining 80 percent. The reaction $B^{11}(\alpha,p)C^{14}$ gives a Q value of 0.88 Mev for the longest range group of protons. On comparison with Table I it may be seen that the protons corresponding to the Q value 3.1 Mev were from the reaction $B^{10}(\alpha,p)C^{13}$. In the remaining two groups (Q values 0.42 and 0.09 Mev) it is likely that B^{11} may also have contributed to the total yield, in which case the protons emitted came from such transitions as left the final nucleus C^{14} in the excited state. In the reaction $B^{11}(\alpha,p)C^{14}$ Pollard[6] did not observe any protons from the excited states, but only the long range group attributed to the ground state transition.

The angular distribution of the protons of Q values 0.42 and 0.09 Mev have been plotted (Fig. 2). The abscissa, θ, is in the C.M. system. These distributions appear to have broad maximums between 30°–65° for $Q=0.09$ Mev and between 45°–65° for $Q=0.42$ Mev, but it is more reasonable to assume the distributions in both cases to be isotropic within the limits of statistical fluctuation. Also the distribution for $Q=3.1$ Mev (not shown in Fig. 2) indicates no definite maximum in any direction. It should be noted that only 12 protons were observed and therefore no definite conclusions can be drawn.

For the second and third excited states, however, as the distributions are isotropic it can be said that the angular momentum of the incident α-particle is $l=0$ and consequently only an S-wave is involved in this interaction.

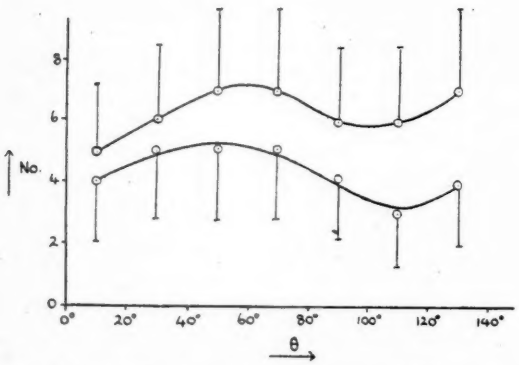

FIG. 2. The angular distribution of the protons of Q values 0.42 and 0.09 Mev.

Argon.—The investigation of Pollard and Brasefield[7] failed to detect any protons from the reaction $A^{40}(\alpha,p)Sc^{43}$. Using a cloud chamber and a strong α-particle source of $E\alpha=4.7$ Mev this reaction was studied in the present experiment.

In the course of 300 photographs, no protons were observed, which supports the findings of the previous workers. The isotropic masses of A^{40} and Sc^{43} are known.[8] It is also known that Sc^{43} is a positron emitter with a half-life of 4 hours. The Q value calculated from the mass-data is 3.71 Mev indicating that the reaction is energetically possible.

[1] G. Brubaker and E. Pollard, Phys. Rev. **51**, 1013 (1937).
[2] W. Jentshke, Physik. Zeits. **41**, 524 (1940).
[3] O. Merhaut, Physik. Zeits. **41**, 528 (1940).
[4] F. Joliot and I. Zlotowski, J. de phys. et rad. **9**, 393 (1938).
[5] Miller, Duncanson, and May, Proc. Camb. Phil. Soc. **30**, 549 (1934).
[6] E. Pollard, Phys. Rev. **56**, 1168 (1939).
[7] E. Pollard and C. J. Brasefield, Phys. Rev. **51**, 8 (1937).
[8] R. Grégóire, *Constantes Selectionnées Physique Nucléaire* (Hermann and Cie, Paris, 1948).

On the Cosmic-Ray Stars

Y. FUJIMOTO AND Y. YAMAGUCHI
Physical Institute, Tokyo University, Tokyo, Japan
April 14, 1949

BURSTS in thin-walled chambers show the same altitude dependence as stars in emulsions, so that both may be considered as being the same events. In fact, it was experimentally confirmed,[1] that most of such bursts were due to stars from the chamber wall. Meanwhile, Carmichael published his experimental data on bursts and analyzed them.[2] He thought that most of his "fragmentation" bursts were caused by single α-particles with rather high energy. But it is unlikely that such a high energy α-particle is frequently emitted in stars, so we reanalyzed his data and showed that these bursts could be explained by the ordinary star.[3]

The agents of these cosmic-ray stars are considered to be moderate energy nucleons (perhaps several hundred Mev), most of which are neutrons. These nucleons may be created in penetrating showers together with several mesotrons. We have calculated roughly the moderate energy nucleon intensity under the proton primary hypothesis.[4] If 1.6 such nucleons are produced in one penetrating shower in the average, we can obtain the correct intensity in the order of magnitude.

We can explain the most part of energy distribution curve of star particles according to the evaporation theory of nuclear physics.[5, 6] Figure 1 shows the experimental data of Perkins[7] and Weisskopf's distribution with the mean temperature of nuclei $\bar{T}=2.5$ Mev, which corresponds to the mean excitation energy $E_0\sim 300$ Mev, and the barrier height $V=7$ Mev. Most of these stars seem to be originated form heavy nuclei in emulsion, such as Ag or Br, thus these $\bar{T}$ and V should certainly be reasonable. From this curve, we see that many more protons are emitted in high ($\gtrsim 30$ Mev) as well as in low ($<V=7$ Mev) energy region than expected from the evaporation theory. As is well known, high energy protons are ejected from nuclei by a direct collision, not through the evaporation process. Thus, actually these protons must be added to evaporated ones. In order to explain the low energy protons, we are compelled to suppose either the nuclei are so enormously swelled out that barrier height decreases to a small fraction of its usual value,[6] or the protons penetrate the potential barrier by the tunnel effect. Since the compressibility of nuclear matter has a large value,[8] the former possibility will be too radical. Thus we may adopt the latter one.

The high energy nuclear reaction ($_{33}As^{75}+190$ Mev $_1D^2$) caused by Berkley cyclotron[9] throws the new light on our problem. From the yield of this reaction, we see that the number of emitted neutrons is about twice that of protons.

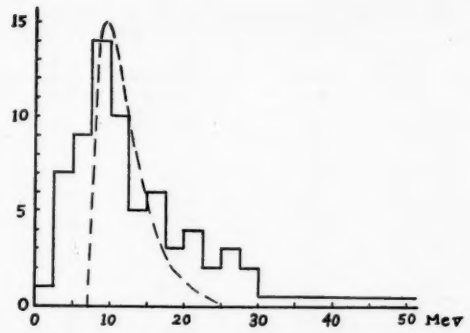

FIG. 1. Energy distribution of protons. The solid line represents the experimental data of Perkins. The dashed line is Weisskopf's distribution.

We may suppose the same circumstances will occur also in the cosmic-ray stars. This seems probable since the proton must go over the barrier. So after the evaporation process, the residual nucleus will be highly unstable, i.e., largely proton excessive. Under these circumstances it may be expected that a proton-decay will occur, analogous to the α-decay of heavy nuclei.

Assuming Geiger-Nuttal's law also to hold for the proton-decay, the lifetime of this new type of decay is estimated to be $10^{-15}-10^{-3}$ sec. for $A=100$ and proton energy $3-1.5$ Mev. This lifetime is much shorter than that of the β^+-decay. α- or γ-decay needs not to be considered because it does not improve the proton-excessive state. Finally, it is unlikely that the fission-like processes suggested by Bragge[6] occur in these nuclear states, because Bohr-Wheeler theory[10] shows that the threshold energy of fission has in our case a very large value (~40 Mev).

Thus we may conclude that the proton-decay predominates over other evaporation processes, and this will explain the appearance of low energy protons in stars. Also the cloud-chamber picture of Powell[11] seems to support the existence of this new type of decay; i.e., his picture Fig. 7a shows the heavy particle (proton) was emitted a few thousandths of a second after the evaporation process.

The detailed account will be published soon in *Progress of Theoretical Physics*. We should like to express our gratitude to Professor Tomonaga and Mr. Hayakawa for their kind interest taken in this work.

[1] Bridge, Hazen, Rossi, and Williams, Phys. Rev. **74**, 1083 (1948).
[2] H. Carmichael, Phys. Rev. **74**, 1667 (1948).
[3] Y. Fujimoto and Y. Yamaguchi, Prog. Theor. Phys., to appear shortly.
[4] Y. Fujimoto and Y. Yamaguchi, Prog. Theor. Phys., to appear shortly.
[5] V. Weisskopf, Phys. Rev. **52**, 293 (1937).
[6] E. Bragge, Ann. d. Physik **39**, 512 (1941).
[7] D. H. Perkins, Nature **160**, 299 (1947).
[8] E. Feenberg, Rev. Mod. Phys. **19**, 239 (1947).
[9] H. H. Hopkins and B. B. Cunningham, Phys. Rev. **73**, 1406 (1948).
[10] N. Bohr and J. A. Wheeler, Phys. Rev. **56**, 426 (1939).
[11] W. M. Powell, Phys. Rev. **69**, 385 (1946).

Pressure Change of Resistance of Tellurium

J. BARDEEN
Bell Telephone Laboratories, Murray Hill, New Jersey
April 21, 1949

BRIDGMAN[1] has observed that the resistivity of tellurium decreases by a factor of more than 600 at a pressure of 30,000 kg/cm². He interprets this large change as a result of the tellurium becoming more metallic with increase in pressure. As shown particularly by work at Purdue University,[2] tellurium is a typical semiconductor with an energy gap between the filled band and the conduction band of about 0.38 ev.

TABLE I. Relative resistance and calculated energy gap in tellerium at a function of pressure.

I	II	III	IV	V
P kg/cm²	$\log_{10}R/R_0$ 23.5° from axis	86° from axis		E_G ev
	30°C	30°C	75°C	
0	0	0	−0.311	0.29 (0.38
2500	−0.280	−0.384	−0.696	0.29 (0.33)
5000	−0.722	−0.739	−1.035	0.275 (0.29)
7500	−1.027	−1.066	−1.330	0.246
10,000	−1.302	−1.360	−1.590	0.214
12,500	−1.547	−1.622	−1.818	0.182
15,000	−1.761	−1.855	−2.020	0.154
17,500	−1.945	−2.063	−2.197	0.125
20,000	−2.110	−2.246	−2.353	0.100
22,500	−2.257	−2.408	−2.490	0.076
25,000	−2.386	−2.552	−2.610	0.054
27,500	−2.499	−2.679	−2.715	0.034
30,000	−2.599	−2.790	−2.806	0.015

The purpose of this note is to point out that the large change of resistivity with pressure is a result of a decrease in the energy gap, the gap becoming very small at 30,000 kg/cm². At a somewhat higher pressure (45,000 kg/cm²) Te undergoes a phase transition.[3] The high pressure modification may well be a true metallic phase.

Shown in the first four columns of Table I are Bridgman's measurements of the pressure change of resistance of a single crystal of tellurium. Measurements were made in two directions making angles of 23.5° and 86° to the axis of the crystal. In the 86° orientation measurements were made at 30°C and 75°C. Bridgman gives values of $\log_{10}R/R_0$, where R_0 is the resistance at 30°C at atmospheric pressure.

Very pure samples of Te are in the intrinsic conductivity range at room temperature, the resistance varying as

$$R=R_\infty \exp(E_G/2kT), \tag{1}$$

where T is the absolute temperature. The energy gap can be estimated from resistance measurements, R_1 and R_2, made at two different temperatures T_1 and T_2.

$$E_G=2k\log(R_1/R_2)/[1/T_1-1/T_2]. \tag{2}$$

Using Bridgman's data for the 86° orientation at the two temperatures, values of E_G in ev have been calculated from

$$E_G=0.93[\log_{10}R(30°\text{C})-\log_{10}R(75°\text{C})]. \tag{3}$$

The values are listed in column V of Table I and are plotted in Fig. 1. The sample is not entirely in the intrinsic range at pressures below 7500 kg/cm², at least at the lower temperature. An extrapolation of E_G from Bridgman's data obtained above 7500 kg/cm² to Miss Johnson's value of 0.38 ev at zero pressure is shown by the dotted line. Extrapolated values are given in parentheses in the table.

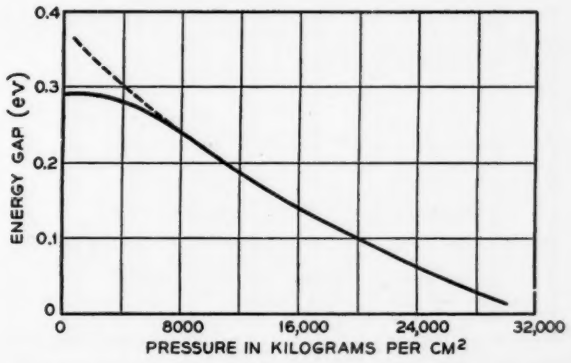

FIG. 1. Energy gap in tellurium as determined from variation of resistance with temperature at different pressures. Solid line; from Bridgman's data. Dotted line; extrapolation to $E_G=0.38$ ev at zero pressure.

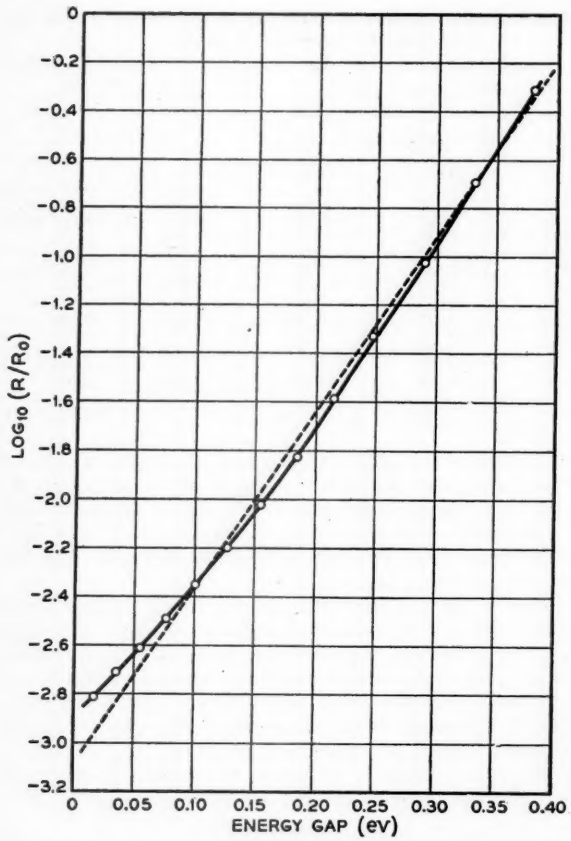

FIG. 2. Relative resistance of tellurium as a function of the energy gap. The dotted line gives the resistance change expected from the change in energy gap alone, other factors remaining constant with pressure.

As may be seen from Eq. (1), a decrease in E_G results in a decrease in R with pressure. When evaluated for $T=348°K$ (75°C), Eq. (1) may be written in the form

$$\log_{10}(R/R_0)=\log_{10}(R_\infty/R_0)+7.3E_G. \quad (4)$$

In Fig. 2 we have plotted $\log_{10}(R/R_0)$ from Bridgman's measurements as a function of E_G, using the extrapolated values of E_G at low pressures, and have shown for comparison a line of slope 7.3. It can be seen that the major cause of the pressure change of resistance is the decrease in the energy gap, E_G, and that changes in R_∞ with pressure are of secondary importance.

[1] P. W. Bridgman, Proc. Am. Acad. Sci. **72**, 159 (1938). Earlier measurements to 12,000 kg/cm² which cover a larger temperature range are given by the same author in Proc. Am. Acad. Sci. **68**, 95 (1933).
[2] V. E. Bottom, Phys. Rev. **74**, 1218(A) (1948), V. A. Johnson, Phys. Rev. **74**, 1255(A) (1948). Miss Johnson gives a value of 0.38 ev for the energy gap.
[3] P. W. Bridgman, Proc. Am. Acad. Sci. **74**, 21 (1940).

Gamma-Rays from Tantalum 182

J. M. CORK, H. B. KELLER, J. SAZYNSKI, W. C. RUTLEDGE, AND A. E. STODDARD
University of Michigan, Ann Arbor, Michigan
April 15, 1949

IN an earlier investigation[1] it was found that pure tantalum oxide irradiated in the Oak Ridge pile formed the radioactive tantalum isotope of mass 182, which emitted a profusion of electron groups due to several internally converted gamma-rays. With the increased absolute accuracy and sensitivity now available with our photographic beta-spectrometers this emitter has been reexamined and found to yield several previously unobserved gamma-rays, all fitting into a logical decay scheme. In all, 48 electron lines are observed as shown collectively in column 1, Table I.

TABLE I. Electron energies with their identification.

Electron energy	Possible interpretation	Gamma-energy	Electron energy	Possible interpretation	Gamma-energy
30.2 kev	K_9	99.5	90.0 kev	M_8	92.8
34.1	L_1	46.2		or K_{18}	159.3
37.7	K_{10}	107.0	96.1	M_9	98.9
40.0	K_{11}	109.3	98.2	N_9	98.8
43.3	M_1	46.1	100.0	L_{13}	112.1
	or K_{12}	112.6	102.2	K_{19}	171.5
46.4	L_2	58.5	108.3	K_{20}	177.6
48.4	K_{13}	117.7	109.2	M_{12}	112.0
52.7	L_3	64.8	127.1	K_{21}	196.4
53.4	K_{14}	122.7	137.8	L_{16}	149.9
54.7	L_4	66.8	142.2	K_{22}	211.5
55.3	M_2	58.1	147.2	M_{16}	150.0
56.7	L_5	68.8		or L_{18}	159.3
61.7	M_3	64.5	150.4	K_{23}	219.7
64.1	N_3	64.7	157.7	K_{24}	227.0
	or M_4	66.9	165.3	L_{20}	177.4
	or L_6	76.2	174.2	M_{20}	177.0
66.1	M_5	68.9	176.8	N_{20}	177.4
	or N_4	66.7	184.7	L_{21}	196.8
69.1	K_{15}	138.4	191.3	K_{25}	260.6
71.5	L_7	83.6	208.6	L_{23}	220.7
73.2	M_6	76.0	215.6	L_{24}	227.7
81.2	M_7	84.0	216.7	M_{23}	219.5
	or L_8	93.3	224.0	M_{24}	226.8
	or K_{16}	150.5	232.3	K_{26}	301.6
87.1	L_9	99.2	237.9	K_{27}	307.2
88.6	K_{17}	157.9	250.3	L_{25}	262.4
			259.1	K_{28}	328.4

On applying the K–L–M differences characteristic of tungsten ($Z=74$) following beta-emission from tantalum ($Z=73$), the electron lines give evidence for the existence of 28 gamma-rays, as shown in column 3, Table I, and summarized in Table II. Some of the electron lines as shown in column 2 are subject to alternate or dual interpretation. The subscripts for the number of the gamma-ray are arbitrarily assigned in the order of increasing energy.

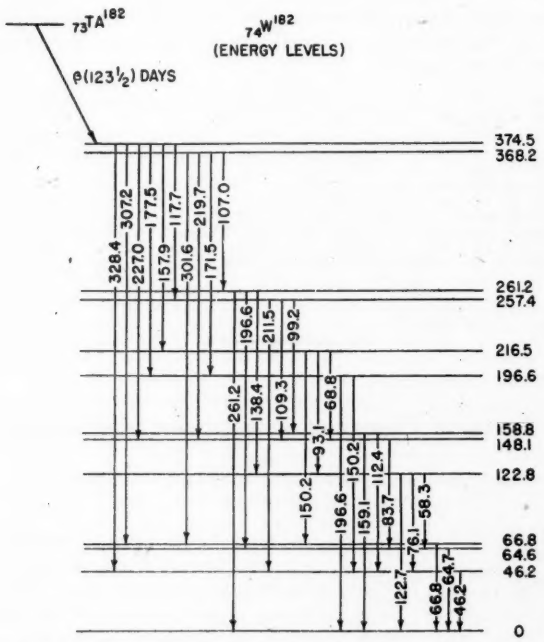

FIG. 1. Energy levels in tungsten 182 following beta-emission from tantalum.

TABLE II. Energy of gamma-rays.

Number	Gamma-energy	Number	Gamma-energy
1	46.2 kev	15	138.4
2	58.3	16	150.2
3	64.7	17	157.9
4	66.8	18	159.1
5	68.8	19	171.5
6	76.1	20	177.5
7	83.7	21	196.6
8	93.1	22	211.5
9	99.2	23	219.7
10	107.0	24	227.0
11	109.3	25	261.2
12	112.4	26	301.6
13	117.7	27	307.2
14	122.7	28	328.4

It can be noted that a great many numerical identities exist between mathematical combinations of the gamma-energies. For example, ten distinct combinations are observed to add to 374.5 kev. This suggests the possibility of a nuclear level scheme as shown in Fig. 1. While this proposal is undoubtedly not unique, it is remarkable that the 13 levels account completely for the 28 observed gamma-rays. In only a few cases do the gamma-energies deviate from the level differences by as much as 0.3 kev.

The decay of the tantalum shows the presence of activities of half-lives 3.5 days and 123.5 days. The radiations from the short-lived emitter have not been determined. This investigation was made possible by the support of the AEC and the ONR.

[1] J. M. Cork, Phys. Rev. **72**, 581 (1947).

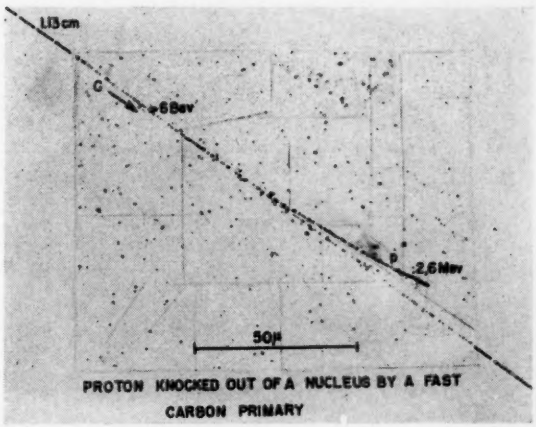

PROTON KNOCKED OUT OF A NUCLEUS BY A FAST CARBON PRIMARY

FIG. 1. Proton knocked out of a nucleus by a fast carbon primary (E_{kin} ~10 Bev). The track of the heavy ion in the emulsion was 1.13 cm long and the charge $Z=6$ was determined both by grain counting and δ-ray counting. The energy of the secondary proton is $E_p=2.6$ Mev and the angle between the track of the carbon ion and the proton track is $\vartheta=20°$ ($\vartheta_{proj}=5°$). Hence the collision could not have been an elastic collision (Ilford C-2 emulsion).

Nuclear Collisions of Heavy Cosmic-Ray Primaries

H. L. BRADT AND B. PETERS
University of Rochester, Rochester, New York
April 13, 1949

HEAVY primary cosmic-ray ions, predicted by Alfven[1] and later discovered at high altitudes in photographic plates and cloud chambers,[2] are absorbed in the upper layer of the atmosphere mainly as a result of nuclear collisions. One may classify these collisions according to their effect on the bombarding nucleus as follows:

(a) The incoming nucleus can proceed almost undeflected with undiminished charge. In this case a few nucleons may be ejected from the target nucleus. An example of such a collision is given in Fig. 1.
(b) The incoming nucleus may be completely destroyed in a large nuclear explosion. An example of such an event was published earlier.[3]
(c) Part of the incoming nucleus may be sheared off in the collision. The remaining nuclear matter proceeds with its original momentum either as a compact nucleus of reduced charge or partially or completely dissociated. This type of collision results therefore in a *narrow penetrating shower* consisting in general of relativistic protons, α-particles and heavy fragments.

We have so far observed eight narrow showers of relativistic particles. Most of these were observed in a $3''\times10''$ stack of 25 electron sensitive Eastman NTB3 plates flown for 6 hours at an altitude of 92,000 ft. off the coast of Cuba ($\lambda=29\frac{1}{2}°$N magn.). In the three cases where the incoming nucleus belonged to the carbon, nitrogen, oxygen group the shower contains only protons or a mixture of α-particles and protons. An example of such a shower is shown in Fig. 2.

In the remaining five cases where the bombarding nuclei have charges $Z=14$, 19, 20, 26, and 26 the shower contained in each case one heavy fragment of charge $Z=10$, 11, 10, 10, and 20, respectively. One example is shown in Fig. 3. The picture shows two sections of the same track in two adjacent photographic plates. The collision occurred in the glass between the emulsions.

The frequency of these showers is comparable (though perhaps smaller) to the number of collisions leading to total destruction of the incoming particle. They have not been observed earlier because all the lighter shower particles being in the relativistic range will only be recorded in electron sensitive emulsions, such as the Eastman NTB3 plates.

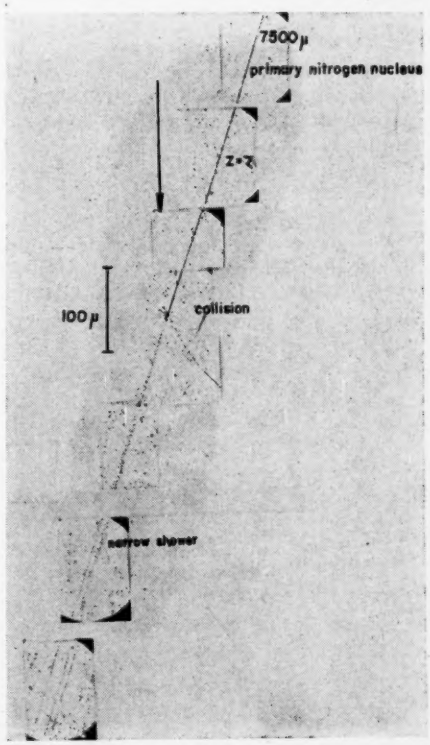

FIG. 2. Narrow shower of protons and α-particles resulting from the collision of a primary nitrogen nucleus. One of the α-particles has a path length of 5 cm in the emulsion. The projected angles between the tracks are 0.033, 0.077, and 0.110 degrees, respectively. (Eastman NTB3 emulsion.)

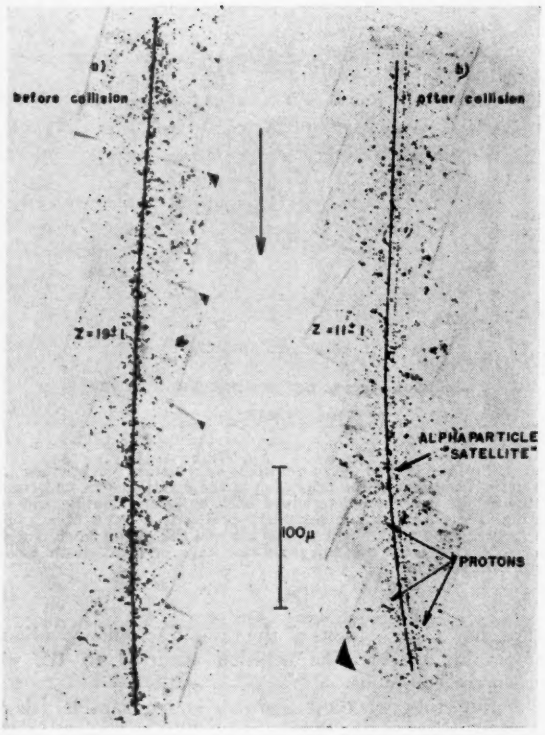

FIG. 3. Figure 3a shows the track of the nucleus of charge $Z=19$ as it appears in three plates before the collision occurs. Figure 3b shows the narrow shower emerging from the glass plate in which the collision occurred. It consists of a heavy fragment of $Z=11$, one α-particle, and 6 protons. The α-particle and 3 protons can be seen in the photograph. The apparent curvature of the tracks is the result of a distortion of the emulsion (Eastman NTB3 emulsion).

Since the tracks can be frequently followed through a whole stack of plates, the angles between the shower particles can be measured with very high precision and can therefore be used to estimate the energy of the incoming particle.

One may expect angles of the order of

$$\vartheta=\langle p_\perp\rangle_{Av}/p_0\approx(2Mc^2\langle E_\perp\rangle_{Av})^{\frac{1}{2}}/E_0,$$

where $\langle p_\perp\rangle_{Av}$ is the average transverse momentum of the nucleons inside the incoming particle (the corresponding energy is $\langle E_\perp\rangle_{Av}\approx(2/3)(3/5)\cdot 20$ Mev$=8$ Mev) and p_0 is the longitudinal momentum per nucleon.

In the shower illustrated in Fig. 3 we have an incoming nucleus of $Z=19\pm1$ and a shower consisting of 6 protons, 1 α-particle, and 1 nuclear fragment of charge $Z=11\pm1$. The angles between the light particles and the heavy fragment projected on the plane of the emulsion vary from 0.0050 to 0.0292 radian, the average projected angle ($\vartheta'=\vartheta/\sqrt{2}$) being 0.017 radian. The deviation of the angles obtained by measuring the change in separation in successive pairs of plates show that the scattering, although measurable, is less than 0.001 radian/cm of glass and therefore does not affect the argument. Hence we estimate that the incoming particle had an energy of the order of 5 Bev/nucleon.

A similar shower produced by an iron nucleus and consisting of 3 α-particles, probably some unobserved protons, and a heavy fragment of $Z\sim10$ has been observed in a stack of plates flown at Minnesota. It leads to an estimate for the total kinetic energy of the primary particle of 0.5×10^{12} ev.

Since most of the collisions occur in the glass only collisions of class (b) and (c) will in general be observed. If we define collisions as events where the charge of the incoming particle is reduced by at least two units we obtain from 40 collisions in an over-all path length of 520 cm of glass a mean free path $\lambda=33$ g/cm^2 for nuclei of $6\leqslant Z\leqslant 8$, and from 26 collisions in 255 cm of glass a mean free path of $\lambda=23.5$ g/cm^2 for nuclei of $10\leqslant Z\leqslant 18$. The corresponding collision cross section agrees for both groups with the one calculated for glass, assuming for all nuclei involved an effective collision radius equal to the geometrical nuclear radius $R_g=1.45\cdot A^{\frac{1}{3}}\cdot10^{-13}$ cm diminished by a constant decrement $\Delta R=0.8\times10^{-13}$ cm.

Since as many as 3 nuclear collisions may be required to reduce the charge of an iron nucleus to $Z\sim6$, it may be possible to observe such narrow showers even at low altitude. The appearance of these showers in a cloud-chamber photograph should be similar to the showers of parallel tracks of positive particles reported by Rochester and Butler,[4] for which no satisfactory explanation has thus far been found.

We are greatly indebted to Dr. John Spence of Eastman Kodak Company for preparing the large stack of very sensitive plates used in this investigation, to Dr. E. O. Salant and Dr. J. Hornbostel of Brookhaven National Laboratory for making many of the arrangements for the balloon flight and to the ONR for organizing the flight.

We are also grateful to Mr. R. Rickard and R. Brent who did much of the necessary surveying.

This work was carried out under the joint program of the ONR and the AEC.

[1] H. Alfven, Nature **143**, 435 (1939).
[2] Freier, Lofgren, Ney, Oppenheimer, Bradt and Peters, Phys. Rev. **74**, 213 (1948).
[3] H. L. Bradt and B. Peters, Phys. Rev. **74**, 1828 (1948).
[4] G. D. Rochester and C. C. Butler, Proc. Phys. Soc. **61**, 535 (1948).

THE AMERICAN INSTITUTE OF PHYSICS

INCORPORATED

57 East 55th Street, New York 22, N.Y.

MEMBER SOCIETIES:

American Physical Society
Karl K. Darrow, *Secretary*, Columbia University, New York 27, New York

Optical Society of America
Arthur C. Hardy, *Secretary*, Massachusetts Institute of Technology, Cambridge, Massachusetts

Acoustical Society of America
Wallace Waterfall, *Secretary*, 57 East 55th Street, New York 22, New York

Society of Rheology
Earl K. Walton, *Secretary*, Institute of Textile Technology, Charlottesville, Virginia

American Association of Physics Teachers
R. F. Paton, *Secretary*, University of Illinois, Urbana, Illinois

AFFILIATED SOCIETIES:

American Society for X-Ray and Electron Diffraction
Electron Microscope Society of America
Physicist Society of Pittsburgh
Physics Club of Chicago
Physics Club of Philadelphia
Cleveland Physics Society
Physics Club of the Lehigh Valley

ASSOCIATES:

Over seventy leading industrial corporations and other institutions which contribute to the support of the Institute.

JOURNALS:

The Physical Review
John T. Tate, *Editor*, University of Minnesota, Minneapolis, Minnesota

Reviews of Modern Physics
J. W. Buchta, *Editor*, University of Minnesota, Minneapolis, Minnesota

Journal of the Optical Society of America
George W. Stewart, *Editor*, Massachusetts Institute of Technology, Cambridge, Massachusetts

The Journal of the Acoustical Society of America
Floyd R. Watkins, *Editor*, 3318 Connecticut Street, N.W., Washington, D. C.

American Journal of Physics
Thomas H. Osgood, *Editor*, Michigan State College, East Lansing, Michigan

The Review of Scientific Instruments
Gaylord P. Harnwell, *Editor*, Randal Morgan Laboratory of Physics, University of Pennsylvania, Philadelphia, Pennsylvania

The Journal of Chemical Physics
Joseph E. Mayer, *Editor*, Kent Chemical Laboratory, University of Chicago, Chicago 37, Illinois

Journal of Applied Physics
Elmer Hutchisson, *Editor*, Case Institute of Technology, Cleveland 6, Ohio

Physics Today
David L. Webster, *Editor*, American Institute of Physics, 57 East 55 Street, New York 22, New York

OFFICERS

George B. Harrison, *Chairman*
Massachusetts Institute of Technology

Wallace Waterfall, *Secretary*
The Celotex Corporation

George B. Pegram, *Treasurer*
Columbia University

John T. Tate,
Adviser on Publications
University of Minnesota

GOVERNING BOARD

Luis W. Alvarez
J. W. Beams
Wallace R. Brode
E. U. Condon
W. F. Fair, Jr.
Harvey Fletcher
George R. Harrison
W. V. Houston
Paul Kirkpatrick
Paul E. Klopsteg
F. W. Loomis
Philip M. Morse
J. R. Oppenheimer
George B. Pegram
Harold K. Schilling
John T. Tate
Wallace Waterfall
M. W. White
A. G. Worthing

Consultant on Printing
Melvin Loos

ADMINISTRATIVE STAFF

Henry A. Barton, *Director*

Theodore Vorburger,
Business Manager

Ruth F. Bryans,
Publication Manager

Irene Hofstadter, *Office Manager*

Eileen B. Neuberger,
Circulation Manager

THE American Institute of Physics was founded in 1931 as a federation of leading societies in the field of Physics. It combines into one operating agency those functions on behalf of physics which can best be done by the Societies jointly. Its purposes is the advancement and diffusion of physics and its applications to human welfare. To this end it publishes for itself or the Societies the nine journals listed on this page; promotes unity and effectiveness of effort among all who are interested in physics; renders numerous direct services to physicists and to the public; and cooperates with government agencies, national associations, educational institutions, technical industries, and others in such manner as to realize the opportunities and fulfill the responsibilities of physics as an important and constructive human activity.

THE PHYSICAL REVIEW

On the Analysis of
. . . . . .
Charge Density and
. . . . . .
Theory of Proposed
Analysis of Neutron-
Scattering of Deuteron
. . . . J. M
Symmetrical Meson
Radioactive Isotopes
. . . . . .
Columbium 96 . . .
Radioactive Scandium
Three-Photon Annih
Measurements of A
. . . . . .
Optical Constants of
. . . . . .
Continuous X-Ray
Mass of Cosmic-Ray
Properties of Cosmic
On the Origin of Cos
On the Solar Origin
β Matrix in Quantu
Short Range Alpha-
. . . . . .
Photograph of a Show
On the Origin of Hig
Letters to the Editor:
On the Measu
. . . .
Polarization of
On the Energy
Distribution of
Scattering of
Observations on
Total Reflection
On the "Magic
. . . .
Concerning the
On the Excited
Meson Exchang
Interpretation of
Magnetic Mom
Paramagnetic
Neutron Capture
New Ferroelectric
Isotope Shift in
Relativistic Tre
. . . .
Suggested Slow
Microwave Spec
Emission of Pro
On the Cosmic-
Pressure Chang
Gamma-Rays fr
. . . .
Nuclear Collisio